

TECHNISCHE UNIVERSITÄT MÜNCHEN

Lehrstuhl für Entwicklungsgenetik

Genetic analysis of Glycogen Synthase Kinase-3
in the adult mouse brain

Patricia M. Steuber-Buchberger

Vollständiger Abdruck der von der Fakultät Wissenschaftszentrum Weihenstephan für Ernährung, Landnutzung und Umwelt der Technischen Universität München zur Erlangung des akademischen Grades eines

Doktors der Naturwissenschaften

genehmigten Dissertation.

Vorsitzender: Univ.-Prof. Dr. E. Grill
Prüfer der Dissertation: 1. Univ.-Prof. Dr. W. Wurst
2. Univ.-Prof. A. Schnieke, Ph.D

Die Dissertation wurde am 11.06.2008 bei der Technischen Universität München eingereicht und durch die Fakultät Wissenschaftszentrum Weihenstephan für Ernährung, Landnutzung und Umwelt am 10.12.2008 angenommen.

Danksagung

An erster Stelle gilt mein Dank Herrn Prof. Dr. Wolfgang Wurst für die Aufnahme an seinem Institut und die Möglichkeit meine Promotionsarbeit dort durchzuführen. Sowohl sein Ideenreichtum als auch seine konstruktive Kritik und seine Begeisterungsfähigkeit waren mir Motivation und haben meine Arbeit vorangetrieben. Die gewährten Freiräume in der Gestaltung und Durchführung meiner Forschungsarbeit förderten mein selbstständiges Denken und Handeln, sowie meine Kreativität.

Meinem direkten Betreuer Herr Dr. Ralf Kühn möchte ich ganz besonders danken für seine große Unterstützung, seine immer vorhandene Verfügbarkeit und seine Motivationsfähigkeit. Mit seinem fundierten Wissen und seiner Bereitschaft für zahlreiche Diskussionen schärfte er mein wissenschaftliches Denken und Verständnis maßgeblich.

Mein Dank richtet sich besonders an Frau Prof. Dr. Schnieke und Herrn Prof. Dr. Grill für ihre Bereitschaft meine Dissertation zu begutachten und die Promotionsprüfung durchzuführen.

Frau Dr. Daniela Vogt Weisenhorn möchte ich danken für ihre wissenschaftliche Unterstützung bei histologischen Fragen und für ihre Hilfe bei vielen Fragen anderer Art. Als ständige Ansprechpartnerin bei Verhaltensfragen in Bezug auf Mäuse verdient Frau Dr. Sabine Hölter-Koch ein besonderes Dankeschön. Auch meinen Kooperationspartnern im GMC, insbesondere Dr. Helmut Fuchs, Dr. Valerie Gailus-Durner, Dr. Anja Schrewe und Dr. Ilona Moßbrugger, danke ich für ihre unbürokratische und wertvolle Hilfe bei der Analyse meiner Mauslinien. Mein aufrichtiger Dank geht auch an unsere Tierpfleger in der DoBe und im C-Streifen für ihre Mithilfe und Aufmerksamkeit bei der Betreuung meiner Mäuse.

Für technische und private Unterstützung sowie eine tolle Arbeitsatmosphäre danke ich ganz besonders herzlich unseren technischen Assistentinnen Regina Kneuttinger, Katrin Angermüller, Stefanie Greppmair, Adrienne Tasdemir, Susi Weidemann und Annerose Kurz-Drexler. Dank ihrer tatkräftigen Hilfe und ihrem Rat konnte ich viel erreichen. Auch meinen Kollegen, insbesondere Benedikt Wefers, gilt mein Dank für die gute Zusammenarbeit und gegenseitige Hilfe im Labor, die vieles

erleichtert und noch mehr ermöglicht hat. Allen Mitarbeitern im Institut danke ich für ihre kollegiale Hilfsbereitschaft in vielen Fällen und die angenehme Arbeitsatmosphäre.

Christiane, Anne, Cordula, Regina und Katie danke ich für ihre Freundschaft, ihre Unterstützung und Verständnis, sowie ihr offenes Ohr für alle Lebenslagen. Ohne Euch wäre diese Zeit nicht dieselbe gewesen!

Mein liebster Dank und Respekt gilt meinem Mann und meinen Eltern für ihre unendliche Geduld, die zahllosen Gespräche und die grenzenlose Unterstützung während des Studiums und der Promotionszeit. Ohne Euch hätte ich es nicht bis hierher geschafft. Danke, dass ihr immer an meiner Seite seid!

Die Wissenschaft fängt eigentlich erst da an interessant zu werden, wo sie aufhört.

Justus von Liebig (1803-1873)

Content

1	SUMMARY	1
2	INTRODUCTION	3
2.1	GLYCOGEN SYNTHASE KINASE 3 – A MULTIFUNCTIONAL KEY REGULATOR	3
2.1.1	Regulation of GSK-3	3
2.1.2	The <i>Gsk-3</i> knockout mice	7
2.1.3	Functions of GSK-3 in the regulatory network of the cell	8
2.1.4	Linkage of GSK-3 to human diseases	10
2.2	THE WORLD OF RNA INTERFERENCE	12
2.2.1	The RNAi pathway	12
2.2.2	Application of RNAi in mice	14
2.3	AIM OF THE THESIS	15
3	MATERIALS	17
3.1	INSTRUMENTS	17
3.2	CHEMICALS	18
3.3	CONSUMABLES AND OTHERS	21
3.4	COMMON AND STOCK SOLUTIONS	22
3.5	MOLECULAR BIOLOGY	23
3.5.1	Kits	23
3.5.2	Work with bacteria	23
3.5.2.1	<i>E.coli</i> strains	23
3.5.2.2	Solutions	24
3.5.3	Southern blot analysis	24
3.5.4	Northern blot analysis	25
3.5.4.1	Solutions	25
3.5.4.2	Oligonucleotide probes	25
3.5.5	Western blot analysis	25
3.5.5.1	Solutions	25
3.5.5.2	Antibodies	26
3.5.6	Enzymes	26
3.5.7	Vectors and plasmids	27
3.5.8	Oligonucleotides	27
3.5.8.1	Oligonucleotides for genotyping	27
3.5.8.2	Oligonucleotides for PCR amplification	28
3.5.8.3	Oligonucleotides for sequencing	28

3.5.8.4	<i>Oligonucleotides for cloning</i>	29
3.6	HISTOLOGICAL METHODS	30
3.6.1	Kits	30
3.6.2	Solutions for RNA <i>in situ</i> hybridization on paraffin sections	30
3.6.3	Solutions for DIG labeled <i>in situ</i> hybridization	30
3.6.4	Antibodies for histology	32
3.6.5	LacZ staining solutions	32
3.6.6	Staining solutions	32
3.7	EMBRYONIC STEM CELL CULTURE	33
3.7.1	ES cell lines	33
3.7.2	Culture medium	33
3.8	MOUSE STRAINS	34
3.8.1	Wild type and other used mouse strains	34
3.8.2	Generated mouse lines	34
4	METHODS	35
4.1	MOLECULAR BIOLOGY	35
4.1.1	Cloning and work with plasmid DNA	35
4.1.1.1	<i>Production and transformation of competent bacteria</i>	35
4.1.1.2	<i>Preparation of plasmid DNA</i>	36
4.1.1.3	<i>Restriction digest of plasmid DNA</i>	36
4.1.1.4	<i>Isolation of DNA fragments</i>	36
4.1.1.5	<i>Ligation of DNA fragments</i>	37
4.1.1.6	<i>Sequencing</i>	37
4.1.2	Analysis of genomic DNA	38
4.1.2.1	<i>Isolation of genomic DNA</i>	38
4.1.2.2	<i>Southern Blot analysis</i>	38
4.1.2.3	<i>Polymerase Chain Reaction (PCR)</i>	39
4.1.3	Analysis of RNA	40
4.1.3.1	<i>Sample preparation and isolation of RNA</i>	40
4.1.3.2	<i>Reverse transcription of mRNA into cDNA</i>	41
4.1.3.3	<i>Anchored PCR (5' RACE)</i>	41
4.1.3.4	<i>Northern blot analysis</i>	41
4.1.4	Analysis of protein samples	43
4.1.4.1	<i>Preparation of protein samples</i>	43
4.1.4.2	<i>Western blot analysis</i>	43
4.2	EMBRYONIC STEM CELL CULTURE	44

4.2.1	Preparation of mouse fibroblasts (feeder cells)	45
4.2.2	Expansion of ES cells	45
4.2.3	Storage and thawing of ES cells	46
4.2.4	Introduction of DNA into ES cells using FuGENE transfection	47
4.2.5	β -Gal reporter gene assay	47
4.2.6	Introduction of DNA into ES cells via electroporation	48
4.2.7	Isolation and screening of stably transfected ES cell clones	48
4.3	MOUSE HUSBANDRY	49
4.3.1	Housing	49
4.3.2	Generation of mice from ES cells	50
4.3.3	Establishment of new mouse lines	51
4.4	HISTOLOGY	51
4.4.1	Perfusion and dissection of adult mice	51
4.4.2	Preparation of paraffin sections	52
4.4.3	Preparation of frozen sections	53
4.4.4	Radioactive <i>in situ</i> hybridization on paraffin sections	53
4.4.5	DIG labeled <i>in situ</i> hybridization on paraffin sections	55
4.4.6	Nissl staining (cresyl violet)	58
4.4.7	Immunohistochemistry (DAB-staining)	59
4.4.8	LacZ staining in mouse tissues	60
4.5	GERMAN MOUSE CLINIC	61
4.5.1	Behavioral testing	61
4.5.1.1	<i>Modified Hole Board test</i>	62
4.5.1.2	<i>Light-dark box</i>	63
4.5.1.3	<i>Accelerating rotarod</i>	63
4.5.1.4	<i>Forced swim test</i>	64
4.5.2	Cardiovascular analysis	64
4.5.3	Pathological analysis	65
5	RESULTS	67
5.1	EXPRESSION OF <i>GSK-3</i> DURING DEVELOPMENT AND IN THE ADULT MOUSE BRAIN	67
5.1.1	Construction of ISH probes	67
5.1.2	Expression of <i>Gsk-3</i> during embryonic development	68
5.1.3	Expression of <i>Gsk-3</i> in the adult mouse brain	69
5.2	TARGETING OF THE <i>GSK-3A</i> LOCUS BY A GENE TRAP VECTOR	70
5.2.1	The gene trap strategy	70
5.2.2	Confirmation of the <i>Gsk-3α</i> gene trap clone	71

5.2.3	Generation of homozygous gene trap mice	72
5.2.4	Analysis of the <i>Gsk-3α</i> gene trap mice	73
5.3	GENERATION OF CONDITIONAL KNOCKDOWN MICE BY RNA INTERFERENCE	74
5.3.1	Cloning of shRNA vectors	75
5.3.2	Cloning of conditional shRNA vectors	77
5.3.3	Cre mediated recombination of conditional shRNA vectors	78
5.3.4	Tests for knockdown efficiency of shRNAs	78
5.3.4.1	<i>Real-time qRT-PCR of transfected ES cells</i>	78
5.3.4.2	<i>pScreeniTTM system of Invitrogen</i>	79
5.3.4.3	<i>Knockdown of GSK-3 in transfected ES cells</i>	83
5.3.5	Simultaneous conditional knockdown of two genes in mice	85
5.3.6	Integration of shRNAs into ES cells by RMCE	86
5.3.7	Transfer of shRNAs into ES cells	89
5.3.8	Generation of conditional knockdown mice	90
5.4	CHARACTERIZATION OF USED CRE MOUSE LINES	92
5.4.1	The <i>Nestin-cre</i> mouse line	92
5.4.2	The <i>CamKII-cre</i> mouse line	94
5.5	SILENCING OF <i>GSK-3</i> GENES IN MICE	95
5.5.1	Breeding of <i>Gsk-3</i> knockdown mice	96
5.5.2	Analysis of knockdown efficiency in <i>Gsk-3/Nestin-cre</i> mice	97
5.5.2.1	<i>Activation of the shRNAs in the adult brain</i>	97
5.5.2.2	<i>Cre recombination efficiency in mice</i>	99
5.5.2.3	<i>Reduction of Gsk-3 mRNA in the adult brain</i>	100
5.5.2.4	<i>Knockdown of GSK-3 proteins in the adult brain</i>	103
5.5.3	General analysis of <i>Gsk-3</i> knockdown mice	103
5.5.4	Viability of <i>Gsk-3/Nestin-cre</i> knockdown mice	106
5.5.5	Analysis of brain morphology in <i>Gsk-3</i> knockdown mice	107
5.5.5.1	<i>Gsk-3/Nestin-cre knockdown mice</i>	108
5.5.5.2	<i>Gsk-3/CamKII-cre knockdown mice</i>	109
5.5.5.3	<i>Influence of Gsk-3 silencing on apoptosis</i>	110
5.5.6	Phenotypic analysis in the German Mouse Clinic	110
5.5.6.1	<i>Behavioral analysis of Gsk-3/Nestin-cre knockdown mice</i>	111
5.5.6.2	<i>Behavioral analysis of Gsk-3/CamKII-cre knockdown mice</i>	113
5.5.6.3	<i>Influence of Gsk-3 silencing on blood pressure</i>	118
5.5.6.4	<i>Analysis of myelin in the central nervous system</i>	120

6	DISCUSSION	125
6.1	GENERATION OF <i>GSK-3A</i> KNOCKOUT MICE BY GENE TRAPPING	125
6.2	COMPARISON OF KNOCKDOWN EFFICIENCY OF shRNAs <i>IN VITRO</i> AND <i>IN VIVO</i>	126
6.3	THE CRE RECOMBINASE EXPRESSION PATTERN IN TRANSGENIC CRE MICE	129
6.4	GENE SILENCING IN MICE VIA RNAi	130
6.4.1	Simultaneous gene silencing of two genes in mice	131
6.4.2	Mouse lines based on the <i>Gsk-3β-sh2</i> shRNA	133
6.5	REDUNDANCY OF GSK-3 ISOFORMS	135
6.5.1	The role of GSK-3 in the Wnt signaling pathway	135
6.5.2	The role of GSK-3 in neurogenesis	136
6.6	PHENOTYPIC CHANGES IN <i>GSK-3</i> KNOCKDOWN MICE	137
6.6.1	CNS unrelated phenotypes of <i>Gsk-3/Nestin-cre</i> knockdown mice	138
6.6.1.1	<i>Systemic defects</i>	138
6.6.1.2	<i>Hypotension of Gsk-3 knockdown mice</i>	140
6.6.2	Alterations in ventricle size in <i>Gsk-3/Nestin-cre</i> knockdown mice	141
6.6.3	Influence of <i>Gsk-3</i> silencing on myelination	142
6.6.3.1	<i>OPC development</i>	143
6.6.3.2	<i>Oligodendrocyte maturation</i>	144
6.6.3.3	<i>Myelination in the PNS</i>	145
6.6.3.4	<i>Remyelination</i>	146
6.6.4	Behavior alterations induced by <i>Gsk-3</i> silencing in the brain	146
6.6.4.1	<i>Silencing of Gsk-3 in the central nervous system</i>	147
6.6.4.2	<i>Silencing of Gsk-3 in forebrain neurons</i>	148
6.6.4.3	<i>GSK-3 and lithium in depression and anxiety</i>	149
6.7	CONCLUSION	150
7	LITERATURE	152
8	APPENDIX	162
8.1	ABBREVIATIONS	162
8.2	INDEX OF FIGURES AND TABLES	166
8.3	MEASURED PARAMETERS IN THE BEHAVIOR TESTS	167
8.3.1	Modified Hole Board test	167
8.3.2	Light-dark box	168
8.3.3	Accelerating rotarod	168
8.3.4	Forced swim test	168

1 SUMMARY

Glycogen synthase kinase 3 (GSK-3) is a fascinating enzyme and key regulator in multiple signaling pathways. Through its involvement in the signaling network of the cell, GSK-3 is functionally linked to a variety of human diseases, like non-insulin-dependent diabetes, cancer, Alzheimer's disease, schizophrenia, and bipolar mood disorder. Although various genetic and inhibitor based approaches have been made to elucidate the complex functions of GSK-3 α and GSK-3 β , none of these studies was able to model the effects of sustained GSK-3 inhibition in the brain. In this work I used conditional RNA interference for the tissue-specific silencing of GSK-3 isoforms in mice. For this purpose, shRNA transgenic mouse lines were generated that silence specifically one or both isoforms of GSK-3 in forebrain neurons or the whole central nervous system.

These knockdown mice exhibit a number of distinct phenotypic changes at a reduction of *Gsk-3 α* mRNA by 60% and of *Gsk-3 β* mRNA by 55%. In brain-wide *Gsk-3* knockdown mice infertility, hypotension, and defects in brain morphology were observed, besides reduced body weight and size. The severe loss of myelin sheaths in the brain of knockdown mice, link GSK-3 for the first time to the myelination process and associated oligodendrocyte function. Forebrain neuron specific *Gsk-3* knockdown mice gave an insight into its tight controlled functions in the complex regulation of behavior in mood disorders. Further detailed research with these mice could allow specifying the distinct roles of GSK-3 α and GSK-3 β in psychiatric diseases.

The *Gsk-3* knockdown mice enable the analysis of gradual and long term GSK-3 inhibition, similar to the sustained inhibition of GSK-3 by drug administration in humans, and can serve as a new and flexible model of pharmacological intervention.

ZUSAMMENFASSUNG

Das multifunktionale Enzym Glykogen Synthase Kinase-3 (GSK-3) nimmt im Signaltransduktionsnetzwerk der Zelle eine Schlüsselposition in unterschiedlichen Signalwegen ein. Dadurch konnte es funktionell mit einer Vielzahl von menschlichen Erkrankungen in Verbindung gebracht werden. Dazu gehören insbesondere Diabetes mellitus Typ II, Krebs, Alzheimer, Schizophrenie und Bipolare Störungen. Obwohl unterschiedliche genetische und Inhibitor-basierende Ansätze verfolgt wurden um die komplexen Funktionen von GSK-3 α und GSK-3 β aufzuklären, konnte bisher keine dieser Studien die Effekte von anhaltender GSK-3 Inhibition im Gehirn darstellen. Für die gewebespezifische Reduktion von GSK-3 Isoformen in Mäusen habe ich in dieser Arbeit die Methode der konditionalen RNA Interferenz angewendet. Unterschiedliche transgene Mausstämmen wurden produziert um eine oder beide GSK-3 Isoformen spezifisch in Vorderhirnneuronen oder dem zentralen Nervensystem der Maus auszuschalten.

Bei einer Reduktion von *Gsk-3 α* mRNA um 60% und von *Gsk-3 β* mRNA um 55% weisen diese Mäuse eine Anzahl von phänotypischen Veränderungen auf. Reduktion von *Gsk-3* im gesamten Gehirn der Maus führt zu Unfruchtbarkeit, Hypotension, morphologischen Defekten im Gehirn, sowie zu einer Verringerung der Körpergröße und des Körpergewichts. Der erstmalig beobachtete und gravierende Verlust von Myelin im Gehirn weist auf eine unbekannt Funktion von GSK-3 in der Myelinisierung hin. Knockdown-Mäuse mit einer Reduktion von *Gsk-3* in Vorderhirnneuronen ermöglichen einen Einblick in die streng regulierten Funktionen von GSK-3 in der komplexen Regulation des Verhaltens in Bipolaren Störungen. Weitere detaillierte Forschung mit diesen Mäusen führt möglicherweise zu einer Spezifizierung der Funktionen von GSK-3 α und GSK-3 β in anderen psychischen Erkrankungen.

Gsk-3 Knockdown-Mäuse ermöglichen die Untersuchung von gradueller und lang anhaltender GSK-3 Inhibition, vergleichbar mit der andauernden medikamentösen Inhibition von GSK-3 beim Menschen, und eignen sich daher als neues, flexibles Model für pharmakologische Intervention.

2 INTRODUCTION

2.1 Glycogen synthase kinase 3 – a multifunctional key regulator

Glycogen synthase kinase 3 (GSK-3) is a fascinating enzyme with a variety of functions in the signaling system of the cell. GSK-3 genes are highly conserved and have been identified in all investigated eukaryotes. They have been linked with fundamental functions including cell fate determination, metabolism, transcription control, and in mammals, oncogenesis and neurological diseases (Woodgett, 2001).

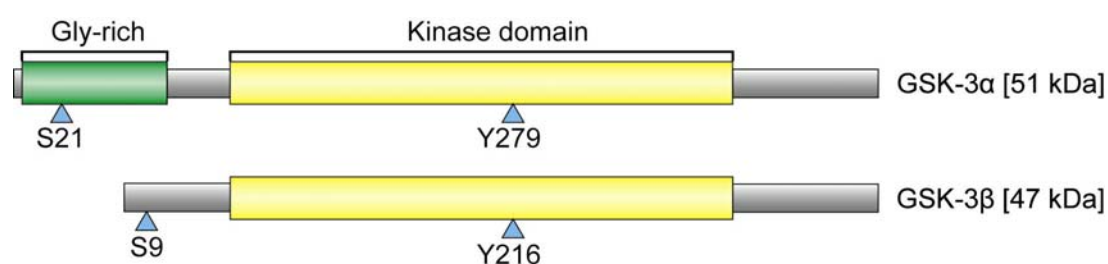


Fig. 1: Scheme of mammalian GSK-3 α and GSK-3 β . Blue arrowheads indicate the serine and tyrosine phosphorylation sites. The conserved kinase domain shared by both isoforms is marked in yellow. The glycine-rich N-terminal domain (green) is unique to GSK-3 α . Adapted from Doble and Woodgett (2003).

GSK-3 is a serine-threonine kinase and was first identified by its phosphorylation activity towards glycogen synthase, the rate limiting enzyme of glycogen metabolism. In mammals, two gene isoforms were identified in 1990, namely glycogen synthase kinase 3 alpha (*Gsk-3 α*) and beta (*Gsk-3 β*). The two genes share high similarity, which displays in 85% overall sequence identity and 93% identity in the catalytic domain (Ali et al., 2001). Both proteins are expressed during embryonic development in a variety of tissues and remain present in the adult stage, where they show especially a strong ubiquitous expression in the brain (Leroy and Brion, 1999; Takahashi et al., 2000; Yao et al., 2002). In the cell, their localization is membrane bound as well as cytosolic.

2.1.1 Regulation of GSK-3

Like other related protein kinases, for example CDK2, p38 γ and ERK2, GSK-3 is phosphorylated at tyrosine Y216 (GSK-3 β) and Y279 (GSK-3 α), which reside within a T-loop analogous to that required for activation of protein kinases of the MAPK family (Fig. 1). This might facilitate substrate phosphorylation, but is not strictly required for

kinase activity (Dajani et al., 2001). However, tyrosine phosphorylation correlates with increased activity as well as cellular apoptosis and in most cells GSK-3 is abundantly tyrosine phosphorylated (Woodgett, 2001).

GSK-3 prefers target proteins, which are already pre-phosphorylated by a priming kinase. The consensus sequence of these so called primed substrates is Ser/Thr-X-X-X-Ser-P/Thr-P, where the first Ser/Thr (serine/threonine) is the target residue, X can be any amino acid, and the last Ser-P/Thr-P is the site of priming phosphorylation (Doble and Woodgett, 2003). This ability of GSK-3 can be inhibited by phosphorylation of serine S9 (GSK-3 β) and S21 (GSK-3 α), which creates a primed pseudosubstrate that binds intramolecularly to the binding cleft. Therefore, the catalytic site is occupied and phosphorylation of primed substrates is blocked (Fig. 2). This inhibition is competitive and can be reversed by high concentrations of primed substrates (Doble and Woodgett, 2003). Due to the linkage of GSK-3 to multiple signaling pathways, there are many kinases like protein kinase B, protein kinase C, p70 S6 kinase or p90Rsk, which are able to phosphorylate and therefore regulate GSK-3 (Grimes and Jope, 2001).

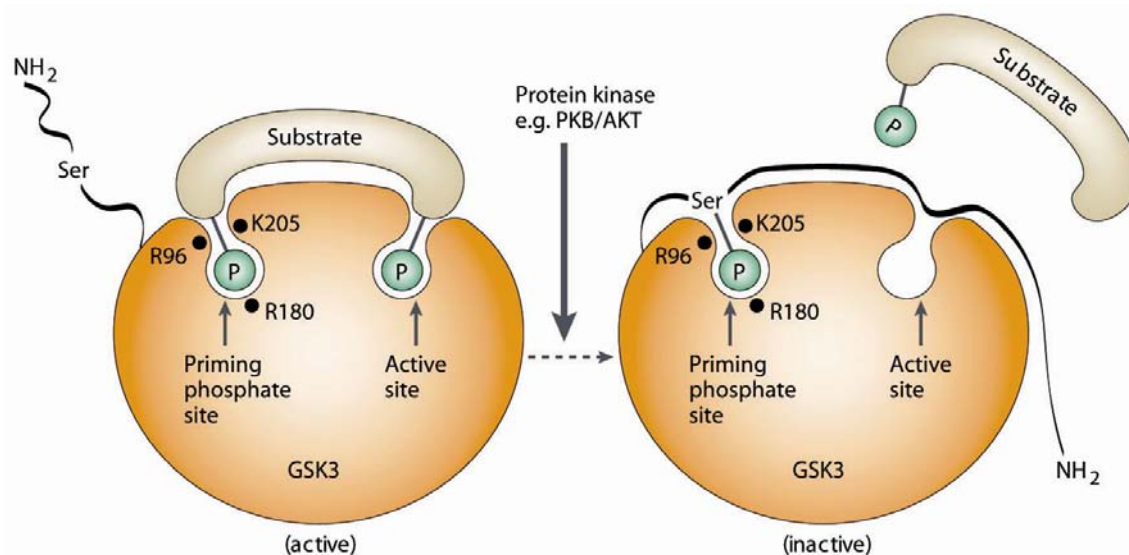


Fig. 2: Regulation of GSK-3 by phosphorylation of the regulatory serine residue. Active GSK-3 binds primed substrates via the priming phosphate site. This conformation situates a serine or threonine residue of the substrate in the active, catalytic site and the substrate is phosphorylated. To regulate GSK-3, an N-terminal serine (Ser) can be phosphorylated by regulatory protein kinases (PKB/AKT) and turns into a primed pseudosubstrate, occupying the priming phosphate site and blocking the catalytic site. In this state GSK-3 is inactivated and the phosphorylation of primed substrates is inhibited. Adapted from Cohen and Frame (2001). *PKB/AKT: protein kinase B, R96: arginine 96, R180: arginine 180, K205: lysine 205*

Besides its preference for primed substrates, GSK-3 also acts in protein complexes. In resting cells, GSK-3 is constitutively active and phosphorylates axin and APC (adenomatous polyposis coli), both components of the Wnt signaling pathway. Phosphorylation increases the binding of β -catenin to the Axin-APC-GSK-3 protein complex. In this combination β -catenin is phosphorylated by GSK-3 and subsequently degraded by the proteasome (Doble and Woodgett, 2003). In response to Wnt signaling, GSK-3 is not inhibited by serine phosphorylation, but by the binding of FRAT (frequently rearranged in advanced T-cell lymphomas) proteins. FRAT interacts with a key regulator of the Wnt pathway, called dishevelled (DVL), and together they disrupt the Axin-APC-GSK-3 complex. This step prevents the further phosphorylation of β -catenin and therefore facilitates its accumulation and translocation to the nucleus (Fig. 3). Although inhibited by FRAT, GSK-3 is still able to phosphorylate primed substrates (Frame and Cohen, 2001).

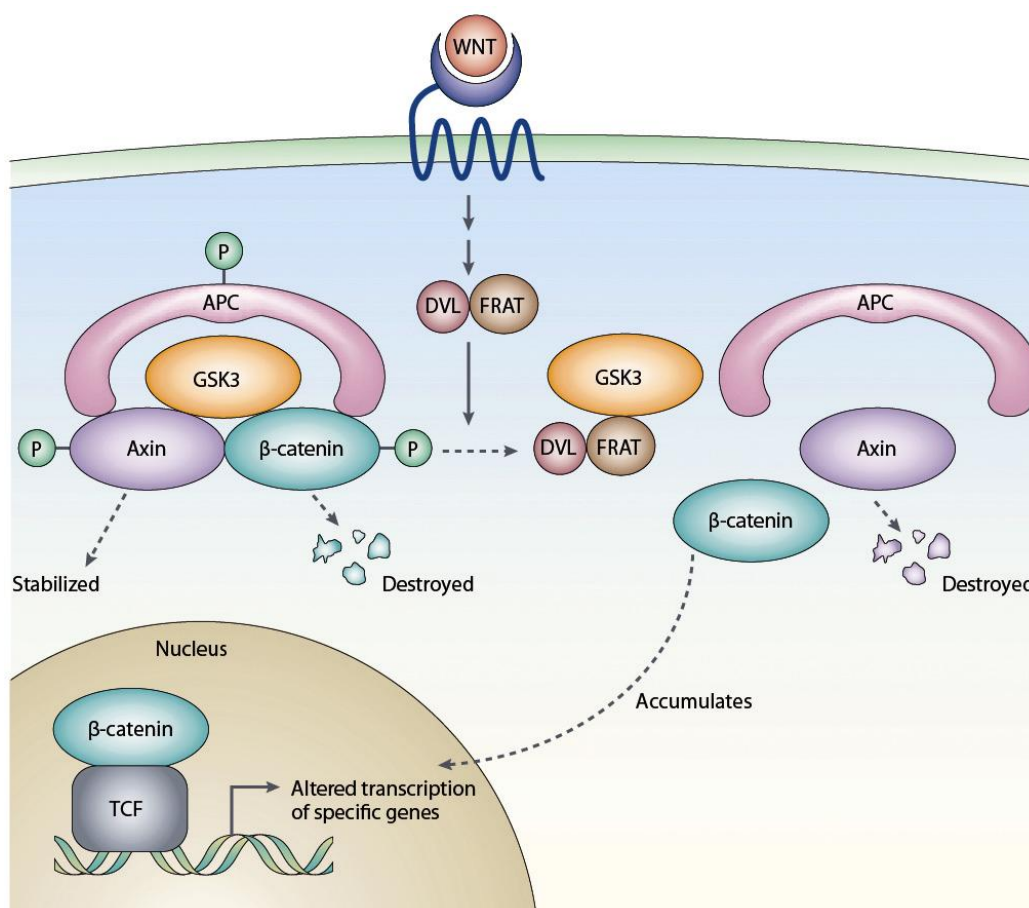


Fig. 3: Regulation of GSK-3 in the canonical Wnt signaling pathway. In the cell, a pool of GSK-3 is present in a multiprotein complex and phosphorylates its binding partners axin, APC, and β -catenin. Due to this phosphorylation, β -catenin is targeted for ubiquitylation and subsequent destruction. Upon activation of the Wnt signaling pathway, dishevelled (DVL) and FRAT (frequently rearranged in advanced T-cell

lymphomas) are recruited. This leads to destabilization of the multiprotein complex and the subsequent release of β -catenin, which accumulates and translocates into the nucleus to induce gene transcription. Adapted from Cohen and Frame (2001).

These versatile regulation possibilities enable GSK-3 to fulfill several regulatory functions and to take its center stage in the cell.

Because of its key regulatory functions in the cell, GSK-3 is a prominent target for inhibitory drugs. Four distinct regions of GSK-3 were targeted for inhibition: the ATP binding domain of the kinase, the separate magnesium (Mg^{2+}) binding region, the substrate binding site, and the FRAT/axin binding site. Most of the developed inhibitors compete with GSK-3 for ATP or magnesium by blocking the active phosphorylation site. But these competitors also inhibit a range of other kinases.

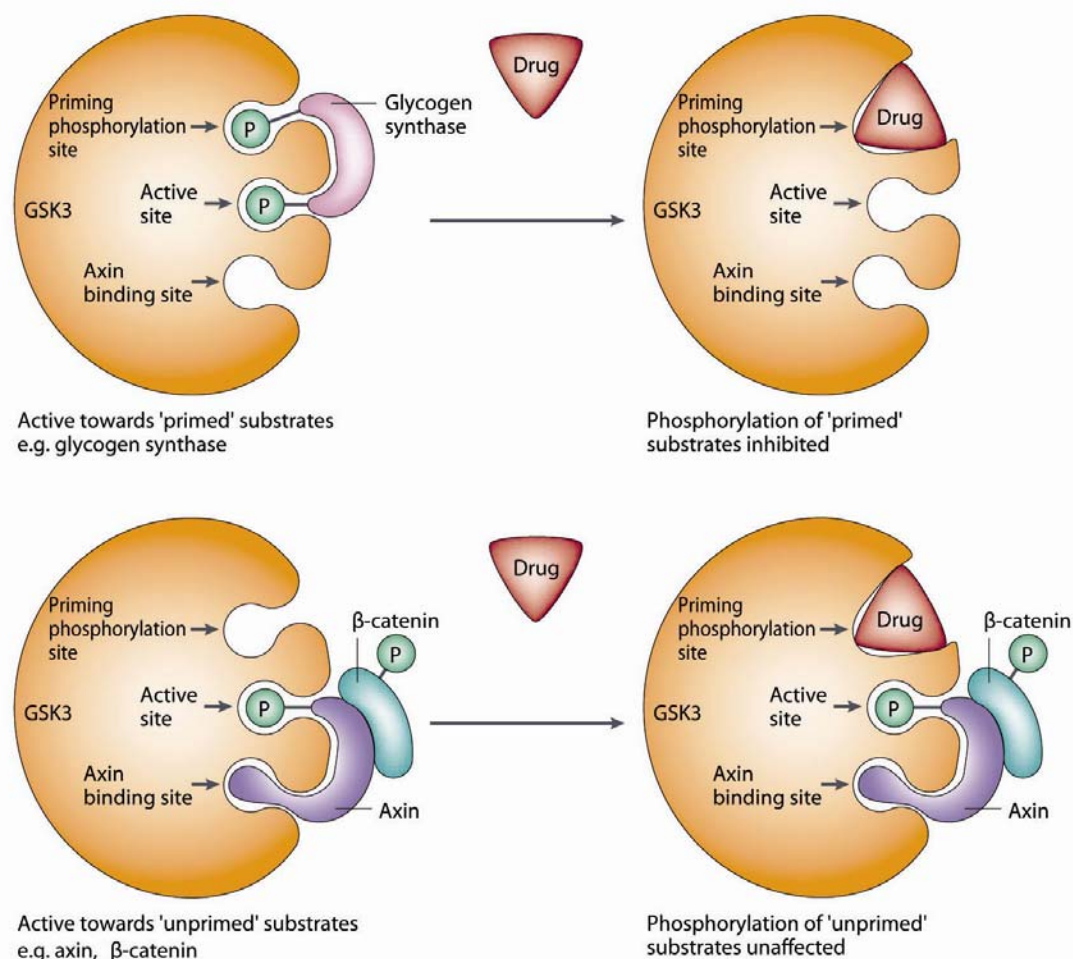


Fig. 4: Influence of inhibitors on GSK-3 activity. Most inhibitors target the active site of GSK-3 by competition for ATP or magnesium ions. In contrast, specially developed inhibitors target the priming phosphorylation site specifically, resulting in an inhibition of interaction with primed substrates, but leaving the phosphorylation of unprimed substrates, like axin, unaffected. Adapted from Cohen and Frame (2001).

More specific inhibitors are peptides mimicking primed substrates, which block the priming phosphorylation site (Forde and Dale, 2007). These pseudosubstrate peptides do not block the ability of GSK-3 to participate in multiprotein complexes. This specialty is useful to study the role of GSK-3 regarding its primed substrates, leaving its function in the Wnt signaling pathway intact (Fig. 4).

A prominent and frequently used inhibitor for GSK-3 is lithium. Lithium ions are competitive inhibitors for magnesium and therefore directly influence GSK-3 activity. But in addition, they affect the reactivation of the phosphorylated GSK-3 by inhibiting the function of the phosphatase that removes the phosphorylation of the inhibitory serine (Jope, 2003).

2.1.2 The *Gsk-3* knockout mice

Although GSK-3 was discovered over 20 years ago, little is known about the distinct functions of each isoform. Since all known inhibitors target both GSK-3 kinases, it is necessary to take genetic approaches to study the specific role of each *in vivo*. One way is the generation of knockout mice, where the gene coding sequence is disrupted on the genomic level.

The *Gsk-3 β* gene was targeted first and Hoeflich et al. published the knockout mouse in 2000. Mice lacking both copies of *Gsk-3 β* die during mid-gestation at the age of embryonic day (E) 13.5 to 16.5. At the age of E14.5 the embryos are pale, non-viable and display multifocal haemorrhagic degeneration in the liver; the hepatocytes are pyknotic and karyorrhectic, clearly undergoing apoptosis. But no evidence was found for a disturbance of Wnt signaling, cyclin D levels, β -catenin accumulation or glycogen metabolism (Hoeflich et al., 2000), indicating that *Gsk-3 α* might replace its functions. Apart from that, knockout mice display a hypersensitivity to TNF- α (tumor necrosis factor alpha). Homozygous *Gsk-3 β* null embryonic fibroblast cell lines treated with TNF- α undergo apoptosis, suggesting that *Gsk-3 β* is required for protection from TNF- α cytotoxicity. TNF- α induces apoptosis via the downstream transcription factor NF- κ B. The specific activation of NF- κ B by TNF- α treatment is reduced by more than 50% in the *Gsk-3 β* knockout cells. Hoeflich et al. could not elucidate where the intervention of GSK-3 β takes place in this pathway, but it is quite clear that GSK-3 β fulfills here a function that cannot be compensated by GSK-3 α .

Additionally, a variety of phenotypic aspects of *Gsk-3 β* null mice was published. Other researchers report that *Gsk-3 β* knockout mice survived until some hours after birth (Kim et al., 2006), did not display differences in the hypersensitivity to TNF- α (Stankunas et al., 2003), or any hepatic defects (Liu et al., 2007). Furthermore Liu et al. revealed recently the genetic requirement for GSK-3 β in midline development. The mutants show cleft palate, incomplete fusion of the ribs at the midline and bifid sternum as well as delayed sternal ossification. Another research group published conditional mice expressing a dominant negative GSK-3 β , driven by a postnatal neuron-specific promoter. They observed increased neuronal apoptosis and impaired motor coordination in mutants with reduced GSK-3 β activity in the striatum (Gomez-Sintes et al., 2007).

MacAulay et al. (2007) targeted the *Gsk-3 α* gene recently and showed that mice lacking GSK-3 α are viable, but display enhanced glucose and insulin sensitivity associated with a reduced fat mass. Since circulating leptin levels are directly proportional to total body fat mass, MacAulay et al. observed significantly reduced plasma leptin levels in fed *Gsk-3 α* knockout mice compared to wild type littermates. The most interesting finding in these mice is the significant enhancement of fasted and glucose-stimulated hepatic glycogen deposition. In contrast, the glycogen deposition in the muscle was not altered, suggesting a minimal role for GSK-3 α in this tissue. These findings indicate that GSK-3 α is the key regulator of hepatic glucose metabolism and that the two isoforms of GSK-3 exhibit divergent physiological roles in different tissues.

2.1.3 Functions of GSK-3 in the regulatory network of the cell

Various findings suggest that within the cell distinct populations of GSK-3 exist that are attentive to specific signals, but not to others (Ali et al., 2001). This allows GSK-3 to interact with multiple substrates and different pathways (Fig. 5).

One of the most prominent roles of GSK-3 is certainly in the insulin pathway. Its ability to phosphorylate glycogen synthase and insulin receptor substrate-1 (IRS-1), both important targets of insulin, was responsible for its identification in the 1980s. GSK-3 is inactivated due to insulin signaling and subsequently glycogen synthase is activated, which results in glycogen synthesis (Eldar-Finkelman and Krebs, 1997).

In the innate immune system, the activation of Toll-like receptors (TLRs) results in signaling of two distinct pathways, the MyD88/IRAK and the PI3K/GSK-3 pathway. In the PI3K pathway inhibition of GSK-3 increases the expression of interleukin 10 (IL-10) via CREB signaling and promotes an anti-inflammatory immune response. Since upon administration of a GSK-3 inhibitor, before a lethal dose of lipopolysaccharide (LPS) was given, just 70% of the mice died, compared to 100% in the control group, it was concluded that GSK-3 might have the ability to protect the organism against septic shock (Martin et al., 2005; Woodgett and Ohashi, 2005).

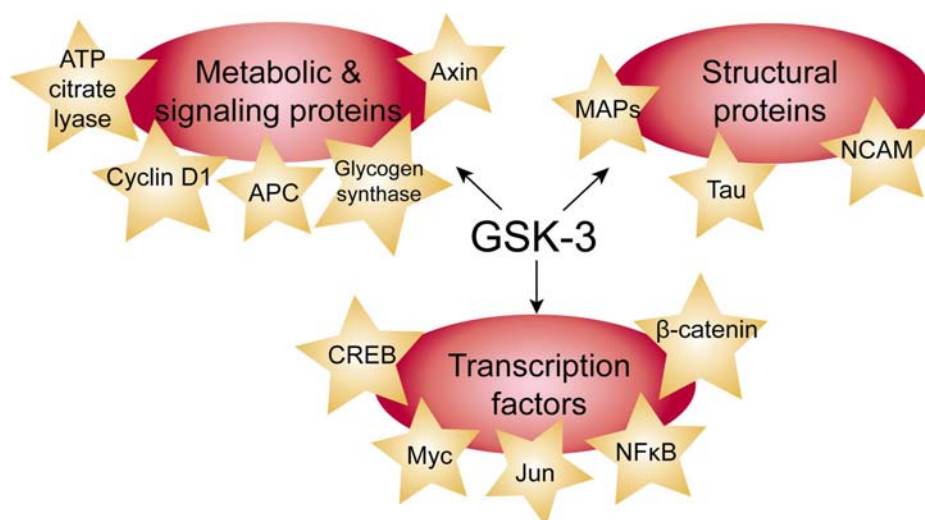


Fig. 5: Substrates of mammalian GSK-3. GSK-3 is able to phosphorylate many different types of substrates. Here, some of the most prominent targets are depicted.

In *Drosophila*, the GSK-3 homologue is essential for embryonic patterning as well as for mesoderm formation and cardiogenesis (Ali et al., 2001). In mammalian zygotes, GSK-3 is important for the proper and timely progression through the first mitotic division. Inhibition of GSK-3 at this point leads to abnormal chromatin segregation and failure to develop past the two-cell stage (Acevedo et al., 2007).

GSK-3 activity is also essential in the central nervous system (CNS), since different levels of inhibition cause morphological changes in axons, like growth retardation and branching initiation. *Gsk-3β* null mice show no gross morphology abnormalities in their nervous system, indicating the redundancy of both isoforms regarding the regulation of axon morphology (Kim et al., 2006). Additionally, it was shown that GSK-3 is involved in establishing and maintaining neuronal polarity. In polarized neurons, GSK-3 activity is increased in dendrites compared to axons. The

downstream signaling is mediated via CRMP-2 (Yoshimura et al., 2005) and inhibition of GSK-3 results in multiple axon formation with concomitant reduction of dendrite formation (Jiang et al., 2005).

These functions cover only a part of the regulatory network in which GSK-3 operates. Many other pathways are also related to GSK-3, like: cell division cycle and circadian clock (Cyclin D1), fatty acid synthesis (ATP citrate lyase), protein synthesis (eIF2B), and especially linked to GSK-3 α : regulation of bovine sperm motility (Vijayaraghavan et al., 2000) and keratinocyte migration (Koivisto et al., 2006).

2.1.4 Linkage of GSK-3 to human diseases

Since GSK-3 is involved in multiple pathways in the cell, it is not surprising that it is linked to a variety of human diseases.

One of them is diabetes mellitus type II or non-insulin-dependent diabetes, due to the function of GSK-3 in the insulin pathway. This type of diabetes, which accounts for approximate 90% of all cases, is characterized by insulin resistance. In these patients the tissue is not able to respond to the secreted insulin. In this context, increased activity of GSK-3 was observed in diabetes- and obesity-prone mice (Eldar-Finkelman et al., 1999). It was already shown that small inhibitors of GSK-3 are able to replace the regulatory function of insulin and activate glycogen synthase, stimulating the conversion of glucose to glycogen. Additionally, these inhibitors mimic another action of insulin, which is the ability to repress the transcription of rate-determining enzymes in the gluconeogenic pathway. This results in decreased blood glucose levels by inhibiting the production of glucose in the liver (Cohen and Frame, 2001).

Besides, GSK-3 takes a center stage in the canonical Wnt pathway. This signaling cascade directs many differentiation events during embryogenesis and it was shown that it regulates stem cell fate in adult organisms (Forde and Dale, 2007). The key transcription factor of this pathway is β -catenin and mutations at the phosphorylation sites of β -catenin targeted by GSK-3 have been found in numerous types of cancer, including colorectal cancer, melanoma, pilomatricoma, and hepatocellular and ovarian carcinoma (Patel et al., 2004). Although GSK-3 inhibition results in up-regulation of various proto-oncogenes (β -catenin, cyclin D1, c-Myc, c-Jun), it was

shown that reduction of GSK-3 activity by inhibitors attenuates the proliferation of human colon cancer cells in mice (Shakoori et al., 2007). The final involvement of GSK-3 in cancer is not yet elucidated and might be connected to the level of GSK-3 inhibition.

Another disease at the focus of scientific research and linked to GSK-3 is Alzheimer's disease (AD). In this context, the formation of amyloid plaques and neurofibrillary tangles takes place. Besides, the phosphorylation of Tau is another important factor in the pathology of AD. It was shown early that GSK-3 β phosphorylates Tau (Ishiguro et al., 1992), but until now the only evidence for its involvement in tauopathy is the colocalization of GSK-3 β with pathological structures *in vivo* (Muyllaert et al., 2008). Recently, especially GSK-3 α was linked to the formation of amyloid plaques by inhibitor studies (Phiel et al., 2003). Presently, GSK-3 is thought to be involved in many other pathological features of AD, including inflammation and memory defects. Further research will elucidate the functions of GSK-3 in this important disease.

Among neurological and mental disorders, schizophrenia and bipolar disorder (BPD) are influenced by GSK-3 activity through various pathways. BPD is characterized by maniac and depressed states, and lithium is a frequently used and potent therapeutic drug for the acute treatment of mania. Although the therapeutic mechanisms are still unclear, its target protein GSK-3 was supposed to be the mediator of the therapeutic effects and inhibition of GSK-3 in rodents produced antidepressant-like effects (Gould et al., 2004). These effects might be due to the role of GSK-3 in the Wnt signaling pathway, since transgenic mice overexpressing β -catenin phenocopy behaviors found in lithium treated mice (Gould et al., 2007). In addition, BPD patients suffer from circadian disturbances and GSK-3 has been observed to be an essential component of the *Drosophila* circadian clock. Studies in cell culture have demonstrated that loss of GSK-3 results in a significant delay in the periodicity of the mammalian endogenous clock mechanism (Kaladchibachi et al., 2007). Genes involved in the pathology of schizophrenia are also influenced by GSK-3 activity. These target genes are mainly related to the Wnt pathway and insulin signaling. Additionally, it was demonstrated that psychoactive substances and antipsychotic drugs signal through GSK-3 and that GSK-3 protein levels and activity are altered in the brain of schizophrenic patients (Lovestone et al., 2007).

Since its discovery, a plethora of GSK-3 functions was reported and now it is linked to a variety of signaling pathways and human diseases. These features make GSK-3 a central target of scientific research and connect different fields of interest to gain further insight into the functional networks of the body.

2.2 The world of RNA interference

In 2006, Craig Mello and Andrew Fire were awarded with the Nobel Prize in Physiology or Medicine for the discovery of the RNA interference (RNAi) mechanism in the nematode *Caenorhabditis elegans*. They discovered that injection of double stranded RNA (dsRNA) into worms silenced genes whose sequences were complementary to those of the introduced dsRNAs (Fire et al., 1998). At that time, dsRNA was thought to be a non-specific silencing agent that triggers the destruction of messenger RNA (mRNA) and suppresses the protein translation in mammalian cells. It was assumed that base pairing between mRNA and introduced antisense transcripts was responsible for the repression of translation and mRNA degradation. In 1995 a surprising observation was made: not only the antisense transcripts, but also sense transcripts induced silencing in *C. elegans*. So the mechanism known as antisense-mediated silencing was remodeled and over time the term RNAi was created (Mello and Conte, 2004). During the years, RNAi was described also in *Drosophila*, fungi, and plants, where it was known as posttranscriptional gene silencing (PTGS) or co-suppression since 1997 (Metzlaff et al., 1997). These findings confirmed that RNAi is an evolutionary conserved mechanism derived from a common ancestor of fungi, plants, and animals.

2.2.1 The RNAi pathway

Different types of RNA can trigger the RNAi pathway, but naturally, the RNAi pathway is used for posttranscriptional gene regulation via a large family of cell-autonomous short RNAs, the microRNAs (miRNAs). The precursors of these miRNAs are endogenous transcripts that contain complementary or near-complementary inverted repeats, which fold back on themselves to form double stranded RNA (dsRNA) hairpins. These primary RNAs (pri-miRNA) are processed in the nucleus into pre-miRNAs by Drosha, a dsRNA-specific RNase-III-type endonuclease. The pre-miRNAs are translocated into the cytoplasm via exportin 5,

a nuclear export receptor. Once in the cytoplasm, the pre-miRNAs are further processed by Dicer, which contains, additionally to its RNaseIII domain, a PAZ (piwi-argonaute-zwille) domain to recognize the 2-nucleotide 3' overhang of the precursor. Dicer finally produces the miRNAs with a length of 21 nucleotides.

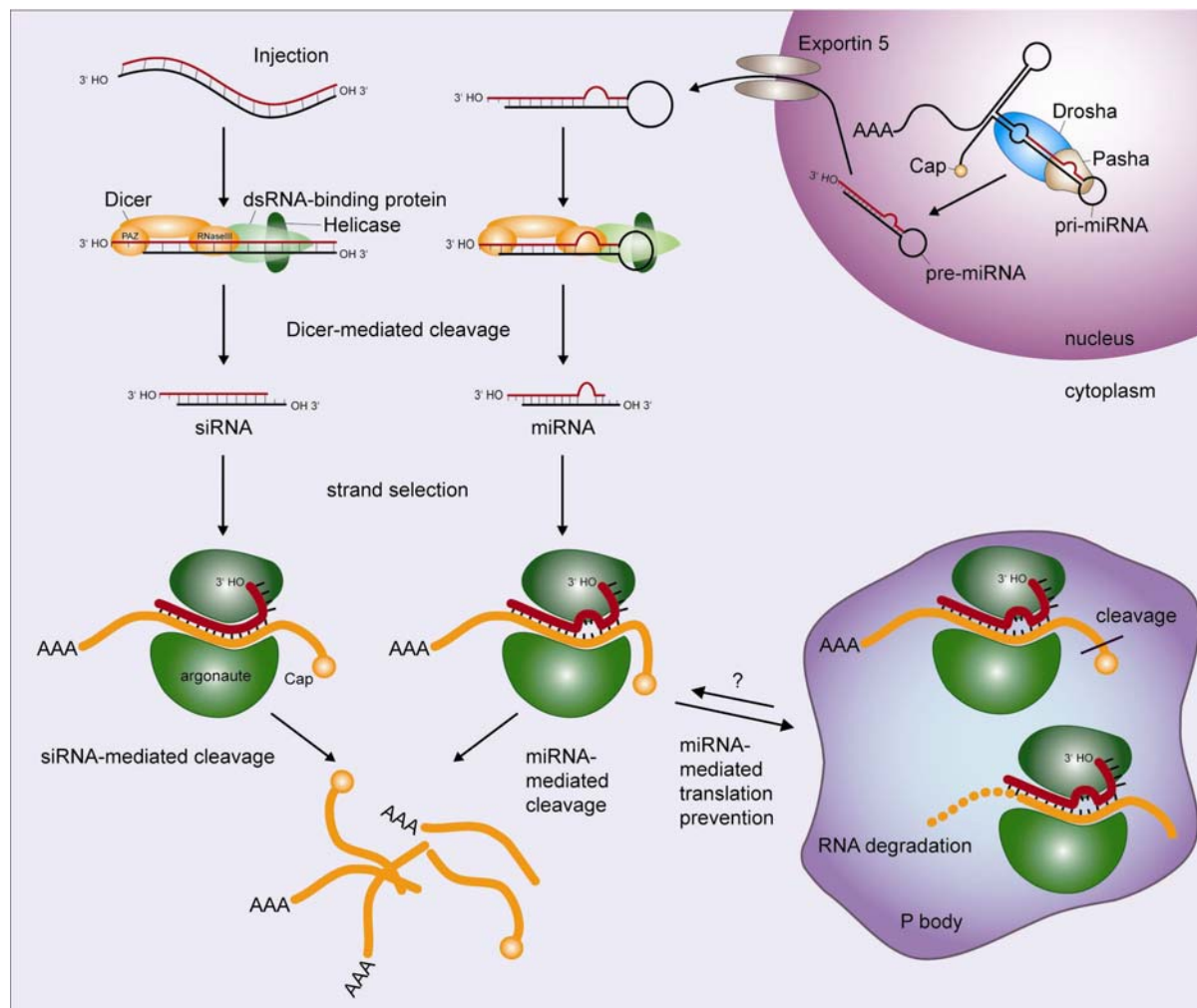


Fig. 6: The RNAi pathway in the cell. In the cell the RNAi pathway is used by a large family of cell-autonomous short RNAs, the so-called microRNAs (miRNAs). The precursors of the miRNAs, the primary miRNAs (pri-miRNAs), are transcribed in the nucleus and subsequently processed by Drosha and Pasha into pre-miRNAs, which are translocated to the cytoplasm. Here, the Dicer mediated cleavage of the pre-miRNAs takes place. The produced miRNAs are incorporated into the RISC complex and the double strands are unwound. If the miRNA has sufficient complementarity with the target mRNA, the endonuclease argonaute mediates the cleavage of the mRNA, resulting in gene silencing. Otherwise the repression of mRNA translation takes place, if the complementarity is not sufficient. These repressed mRNAs are translocated to so-called P-bodies, where they are stored or either degraded. If double stranded DNA is introduced into the cell, it is also processed by dicer into small interfering RNAs (siRNAs). The siRNAs can also enter the RISC complex and induce via perfect base pairing the cleavage and degradation of the target mRNAs. Adapted from Ketting (2005).

These enter now the multiprotein RNA-inducing silencing complex (RISC), and the strand selection takes place. The key rules for the strand selection are: first, the

strand with the most loosely base-paired 5' end enters the RISC complex and second, the 5' end must be phosphorylated. The duplex RNA is unwound, and the antisense strand guides the RISC complex to the complementary target mRNA. The main component of RISC is a member of the argonaute (Ago) protein family. Ago contains two conserved domains: the PAZ domain for recognition of the 2-nucleotide 3' overhang and the PIWI domain, which carries out the cleavage of the target mRNA at one single site in the center of the duplex region, ten nucleotides from the 5' end of the miRNA. The cleavage reaction induced by miRNAs only takes place if the seed region (nucleotides two to seven) of the miRNA is perfectly base paired with the target. Otherwise the mRNA is captured in the RISC complex and its translation is repressed. For degradation or storage, those captured mRNAs are recruited to so-called P-bodies (processing bodies), which are microscopically discrete foci in the cell with an accumulation of mRNA degradation enzymes and RNAi coenzymes (Fig. 6) (Dykxhoorn et al., 2003; Ketting, 2005; Meister and Tuschl, 2004).

But the RNAi pathway can also be induced by long dsRNA. Sources for dsRNA in the cell are viral RNAs, artificially introduced dsRNA, and genomic sense and antisense transcripts. Long dsRNA is processed by Dicer in the cytoplasm into various small interfering RNAs (siRNAs) of 21 to 23 nucleotides length, which enable effective silencing of gene expression. But the applicability of this approach is limited in mammals, because the introduction of dsRNA with more than 30 nucleotides induces a sequence-nonspecific interferon response, which triggers mRNA degradation and global inhibition of mRNA translation. Besides gene silencing, siRNAs can affect the chromatin structure of targeted genes and thereby induce transcriptional inhibition (Dykxhoorn et al., 2003; Ketting, 2005; Meister and Tuschl, 2004).

2.2.2 Application of RNAi in mice

To induce RNAi mediated gene silencing in animals like nematodes or flies, it is possible to soak the animals in dsRNA or to give food containing bacterially expressed dsRNA (Mello and Conte, 2004). In mammals, dsRNA can induce an interferon response and the methods to deliver the RNAi trigger had to be adjusted. A common way to induce RNAi in rodents is the use of vector-based systems, expressing short hairpin RNAs (shRNAs). It was observed that Dicer is able to mediate the cleavage of chemically synthesized shRNAs with 29-base-pair stems

and the necessary 2-nucleotide 3' overhangs into predictable homogenous siRNAs (Siolas et al., 2005). These shRNAs can be ubiquitously and stably transcribed by integration of shRNA expression vectors into the genome and mediate body-wide gene silencing (Seibler et al., 2005). This technique is now frequently used and it was shown that such knockdown mice can produce a similar phenotype as conventional knockout mice (Kunath et al., 2003). To gain further control over the time and spatial expression of the shRNAs, the vector based RNAi system can be combined with various regulatory techniques. A versatile tool is created by combination with the Cre/loxP recombination system. Cre is a site specific recombinase derived from the bacteriophage P1 that catalyzes DNA recombination between a pair of loxP recombination sites (Sternberg et al., 1986). By flanking a transcriptional stop element repressing the shRNA expression, with loxP sites, the expression pattern of the shRNA in the mouse is dependent on the presence of Cre recombinase in the tissue. At the moment, a variety of Cre recombinase transgenic mouse lines is available, each using a different promoter to achieve a specific time dependent and/or spatial Cre expression pattern (Gaveriaux-Ruff and Kieffer, 2007). This combination allows the controlled knockdown in specific cell types at different developmental stages.

2.3 Aim of the thesis

The central aim of this work was the characterization of GSK-3 function in the CNS.

Therefore, I used the RNAi technique for the generation of knockdown mice, specific for each GSK-3 isoform. Because the complete loss of *Gsk-3 β* is lethal, conditional knockdown mice were generated to study the functions of GSK-3 in adult animals. For this purpose, I combined the vector-based expression of shRNAs with the Cre/loxP recombination system. This conditional approach allowed me to restrict the GSK-3 knockdown to specific tissues by using mouse strains with a limited expression of Cre recombinase. In this work, I used transgenic Cre mice, which display Cre recombinase expression in the entire CNS (*Nestin-cre* mice) or only in excitatory neurons of the forebrain (*CamKII-cre* mice). Due to the diverse functions of GSK-3 in the organism, this was advantageous to avoid metabolic perturbations or changes of the physical constitution, which could interfere with behavioral tests. The

RNAi technique offered a quick and easy way to silence each GSK-3 isoform specifically in order to compare their functions in the brain.

In detail, I generated three different mouse lines. In the first, the *Gsk-3 α* gene was targeted, whereas in the second the *Gsk-3 β* gene was silenced. In addition, a third mouse line was generated, where the expression of both isoforms was reduced in the same strain. The conditional knockdown mice were bred to *Nestin-cre* or *CamKII-cre* transgenic strains and analyzed for changes in brain morphology and anxiety and depression related behavior. This allowed a new insight into the functions of this key regulatory protein.

3 MATERIALS

3.1 Instruments

autoclave	<i>Aigner, type 667-1ST</i>
balances	<i>Sartorius, LC6201S, LC220-S</i>
bottles for hybridization	<i>ThermoHybaid</i>
cassettes for autoradiography	<i>Amersham, Hypercassette</i>
centrifuges	<i>Sorvall, Evolution RC; Eppendorf, 5415D, 5417R; Heraeus, Varifuge 3.0R, Multifuge 3L-R</i>
chambers for electrophoresis (DNA)	<i>MWG Biotech; Peqlab</i>
cryostat	<i>Mikrom, HM560</i>
developing machine	<i>Agfa, Curix 60</i>
digital camera	<i>Zeiss, AxioCam MRc</i>
DNA sequencer	<i>Applied Biotech, DNA Analyzer 3730</i>
electric homogenizer	<i>IKA, Ultra-Turrax T25 basic</i>
freezer (-20°C)	<i>Liebherr</i>
freezer (-80°C)	<i>Heraeus HFU 686 Basic</i>
fridges (4°C)	<i>Liebherr</i>
gel documentation system	<i>Herolab, E.A.S.Y.</i>
gel-/blottingsystem "Criterion"	<i>BioRad</i>
gel-/blottingsystem "Xcell SureLock™ Mini-Cell"	<i>Invitrogen</i>
Genesis RSP 200 robot	<i>TECAN</i>
glass homogenizer (tissue grinder, 2 ml)	<i>KIMBLE / KONTES</i>
glass pipettes	<i>Hirschmann</i>
glassware	<i>Schott</i>
ice machine	<i>Scotsman, AF 30</i>
imaging analyzer	<i>Fuji, FLA-3000</i>
incubators (for bacteria)	<i>New Brunswick Scientific, innova 4230</i>
incubators (for ES cells)	<i>Heraeus</i>
laminar flow	<i>Nunc Microflow 2</i>
light source for microscopy	<i>Leica KL 1500</i>
liquid scintillation counter	<i>Hidex, Triathler</i>
luminometer	<i>Berthold, Orion I</i>
magnetic stirrer / heater	<i>Heidolph, MR3001</i>
microscope	<i>Zeiss Axioplan 2</i>
microwave oven	<i>Sharp R-937 IN</i>
Neubauer counting chamber	<i>Brand</i>
oven for hybridization	<i>Memmert, UM 400;</i>

paraffin embedding machine	MWG-Biotech, Mini 10; ThermoElectron, Shake'n'Stack Leica, EG1160
PCR machine	Eppendorf, MasterCycler Gradient
pH-meter	InoLab, pH Level 1
photometer	Eppendorf, Biophotometer 6131
pipetteboy	Eppendorf, Easypet; Hirschmann, Pipettus akku
pipettes	Gilson; Eppendorf
power supplies for electrophoresis	Consort, E443; Pharmacia Biotech, EPS200; Thermo, EC250-90, EC3000-90
radiation monitor	Berthold, LB122
rotating rod apparatus	Bioseb, Letica LE 8200
shaker	Heidolph, Promax 2020
slide warmer	Adamas instrument, BV SW 85
sonifier	Branson sonifier, cell disrupter B15
stereomicroscope	Zeiss, Stemi SV6
thermomixer	Eppendorf, comfort
ultramicrotom	Microm, HM 355S
UV-DNA/RNA-crosslinker	Scotlab, Crosslinker SL-8042; Stratagene, UV-Stratalinker 1800
UV-lamp	Benda, N-36
vortex	Scientific Industries, Vortex Genie 2
water bath	Lauda, ecoline RE 112; Leica, HI1210; Mettler, WB7
water conditioning system	Millipore, Milli-Q biocel

3.2 Chemicals

α - ³² P-dCTP	Amersham
α -thio ³⁵ S-UTP	Amersham
γ - ³² P-dATP	Amersham
3,3'-diaminobenzidine (DAB)	Sigma
4-NBT (Nitro blue tetrazolium)	Roche
acetic acid	Merck
acetic anhydride	Sigma
agarose (for gel electrophoresis)	Gibco Life Technologies, Biozym
aluminum potassium sulfate dodecahydrate	Sigma
ammonium acetate	Merck
ampicillin	Sigma

Ampuwa	<i>Fresenius</i>
β -Mercaptoethanol	<i>Sigma, Gibco</i>
bacto agar	<i>Difco</i>
bacto peptone	<i>BD Biosciences</i>
BCIP (5-bromo-4-chloro-3-indolyl phosphate)	<i>Roche</i>
bicine	<i>Fluka</i>
bis-tris	<i>Sigma</i>
Blocking reagent	<i>Roche</i>
Blocking reagent	<i>Perkin Elmer</i>
boric acid	<i>Merck</i>
bovine serum albumin (BSA, 20 mg/ml)	<i>NEB, Sigma</i>
bromphenol blue	<i>Sigma</i>
calcium chloride (CaCl ₂)	<i>Sigma</i>
carrier DNA	<i>Sigma</i>
chicken serum	<i>Perbio</i>
chloral hydrate	<i>Sigma</i>
chlorobutanol	<i>Sigma</i>
citric acid	<i>Sigma</i>
Complete® Mini (protease inhibitors)	<i>Roche</i>
cresyl violet acetate	<i>Sigma</i>
dextran sulphate	<i>Sigma</i>
dithiotreitol (DTT)	<i>Roche</i>
DMEM	<i>Gibco</i>
DMSO	<i>Sigma</i>
dNTP (100 mM dATP, dTTP, dCTP, dGTP)	<i>MBI</i>
EDTA	<i>Sigma</i>
EGTA	<i>Sigma</i>
Eosin Y	<i>Sigma</i>
ethanol absolute	<i>Merck</i>
ethidiumbromide	<i>Fluka</i>
ethylene glycol	<i>Sigma</i>
fetal calf serum (FCS)	<i>PAN, Hybond</i>
Ficoll 400	<i>Sigma</i>
formaldehyde	<i>Sigma</i>
formamide	<i>Sigma</i>
freezing medium	<i>Tissue Tek, OCT compound</i>
gelatin	<i>Sigma</i>
Glasgow MEM	<i>Gibco</i>
glucose	<i>Sigma</i>
glycerol	<i>Sigma</i>

hematoxylin	<i>Fluka</i>
Hepes	<i>Gibco</i>
human chorion gonadotropin (hCG/Ovogest)	<i>Intervet</i>
Hyb-mix	<i>Ambion</i>
hydrochloric acid (HCl)	<i>Merck</i>
hydrogen peroxide (30%)	<i>Sigma</i>
iodoacetamide	<i>Sigma</i>
isopropanol	<i>Merck</i>
kanamycin	<i>Sigma</i>
levamisol	<i>Sigma</i>
lithium carbonate	<i>Fluka</i>
luxol fast blue MBS	<i>CHROMA</i>
M2 medium	<i>Sigma</i>
magnesium chloride ($\text{MgCl}_2 \cdot 4\text{H}_2\text{O}$)	<i>Merck</i>
maleic acid	<i>Sigma</i>
MEM nonessential aminoacids	<i>Gibco</i>
MES hydrate	<i>Sigma</i>
methanol	<i>Merck</i>
mineral oil	<i>Sigma</i>
MOPS	<i>Sigma</i>
NeutrAvidine™ biotin-binding protein	<i>Pierce</i>
Nonidet P40 (NP-40)	<i>Fluka</i>
orange G	<i>Sigma</i>
paraformaldehyde	<i>Sigma</i>
PBS (for cell culture)	<i>Gibco</i>
Pertex mounting medium	<i>HDScientific</i>
PIPES	<i>Sigma</i>
polyvinylpyrrolidone 40 (PVP 40)	<i>Sigma</i>
potassium chloride (KCl)	<i>Merck</i>
potassium ferricyanid ($\text{K}_3\text{Fe}(\text{CN})_6$)	<i>Sigma</i>
potassium ferrocyanid ($\text{K}_4\text{Fe}(\text{CN})_6 \cdot 3\text{H}_2\text{O}$)	<i>Sigma</i>
potassium hydroxid (KOH)	<i>Sigma</i>
potassium phosphate ($\text{KH}_2\text{PO}_4 \cdot \text{H}_2\text{O}$, K_2HPO_4)	<i>Roth</i>
pregnant mare's serum gonadotropin (PMSG)	<i>Intervet</i>
RapidHyb buffer	<i>Amersham</i>
RNaseZAP®	<i>Sigma</i>
Roti-HistoKit® II	<i>Roth</i>
Roti-Histol®	<i>Roth</i>
salmon sperm DNA	<i>Fluka</i>
SB 216763 (GSK-3 inhibitor)	<i>Tocris</i>

sheep serum	<i>Gibco</i>
skim milk powder	<i>BD Biosciences</i>
sodium acetate (NaOAc)	<i>Merck, Sigma</i>
sodium chloride (NaCl)	<i>Merck</i>
sodium citrate	<i>Sigma</i>
sodium desoxycholate	<i>Sigma</i>
sodium dodecylsulfate (SDS)	<i>Merck</i>
sodium hydroxide (NaOH)	<i>Roth</i>
sodium iodate	<i>Sigma</i>
sodium phosphate (NaH ₂ PO ₄ ·H ₂ O, Na ₂ HPO ₄)	<i>Sigma</i>
spermidin	<i>Sigma</i>
sucrose	<i>Sigma</i>
triethanolamine	<i>Merck</i>
TriReagent	<i>Sigma</i>
Tris (Trizma-Base)	<i>Sigma</i>
Triton-X 100	<i>Biorad</i>
Trizol	<i>Invitrogen</i>
tRNA	<i>Roche</i>
trypsin	<i>Gibco</i>
tryptone	<i>BD Biosciences</i>
Tween 20	<i>Sigma</i>
xylol	<i>Fluka</i>
yeast extract	<i>Difco</i>

3.3 Consumables and others

1kb+ DNA Ladder	<i>Invitrogen</i>
cell culture dishes	<i>Nunc</i>
centrifuge tubes (15 ml, 50 ml)	<i>Falcon, Sarstedt</i>
coverslips (24 mm x 50 mm, 24 mm x 60 mm)	<i>Menzel Gläser</i>
Criterion™ XT Bis-Tris-gels, 10% (protein)	<i>BioRad</i>
cuvettes for electroporation (0.4 cm)	<i>Biorad</i>
developer (<i>in situ</i> hybridization)	<i>Kodak D19</i>
embedding pots	<i>Polysciences, Peel-A-Way</i>
films for autoradiography	<i>Kodak: Biomax MS, Biomax MR</i>
filter paper	<i>Whatman 3MM (Kat.-Nr.:3030 917)</i>
filter tips 10 µl, 20 µl, 200 µl, 1 ml	<i>Art, Starlab</i>
fixer (<i>in situ</i> hybridization)	<i>Kodak fixer (Kat.-Nr.: 197 1720)</i>
FuGENE 6 transfection reagent	<i>Roche</i>
gloves	<i>Kimberley-Clark, Safeskin PFE Safeskin, Nitrile</i>

Hybond N Plus (nylon membrane)	<i>Amersham</i>
Hyperfilm (chemiluminescence detection)	<i>Amersham</i>
MicroSpin S-300	<i>Amersham</i>
NuPAGE® Novex Bis-Tris gels, 10% (protein)	<i>Invitrogen</i>
one-way needles	<i>Terumo, Neolus 20G, 27G</i>
one-way syringes	<i>Terumo, 1ml, 10ml, 20ml</i>
Pasteur pipettes	<i>Brand</i>
PCR reaction tubes (0,2 ml), lids	<i>Biozym</i>
Phase Lock Gel™, heavy	<i>Eppendorf</i>
pipette tips	<i>Gilson</i>
plastic pipettes (1 ml, 5 ml, 10 ml, 25 ml)	<i>Greiner</i>
PVDF membrane (protein)	<i>Pall Biosciences</i>
reaction tubes (0.5 ml, 1.5 ml, 2 ml)	<i>Eppendorf</i>
SeeBlue® Plus2 Prestained protein ladder	<i>Invitrogen</i>
SmartLadder DNA marker	<i>Eurogentec</i>
Superfrost Plus slides	<i>Menzel Gläser</i>
TBE urea gels, 15% (RNA)	<i>Invitrogen</i>
TBE urea sample buffer (2x)	<i>Invitrogen</i>
tissue cassettes	<i>Merck</i>
tissue embedding molds	<i>Polysciences, Inc.</i>

3.4 Common and stock solutions

loading buffer for agarose gels	15%	Ficoll 400
	200 mM	EDTA
	1 - 2%	orange G
paraformaldehyde solution (PFA, 4%)	4%	PFA w/v in PBS
PBS (1x)	171 mM	NaCl
	3.4 mM	KCl
	10 mM	Na ₂ HPO ₄
	1.8 mM	KH ₂ PO ₄
		pH 7.4
SSC (saline sodium citrate, 20x)	3 M	NaCl
	0.3 M	sodium citrate
		pH 7.0
sucrose solution (20%)	20%	sucrose w/v in PBS
TAE (10x)	0.4 M	Tris base
	0.1 M	acetate
	0.01 M	EDTA

TBE (10x)	0.89 M	Tris base
	0.89 M	boric acid
	0.02 M	EDTA
TBS (10x)	0.25 M	Tris-HCl pH 7.6
	1.37 M	NaCl
TBS-T (1x)	1 x	TBS
	0.05%	Tween 20
TE (Tris-EDTA)	10 mM	Tris-HCl pH 7.4
	1 mM	EDTA
Tris-HCl	1 M	Tris base pH 7.5

3.5 Molecular biology

3.5.1 Kits

β -Gal reporter gene assay	<i>Roche</i>
5' RACE System for Rapid Amplification of cDNA Ends	<i>Invitrogen</i>
BCA™ protein assay kit	<i>Pierce</i>
DNA Highspeed Maxi Prep Kit	<i>Qiagen</i>
DNA Mini Prep Kit	<i>Qiagen</i>
ECL Detection Kit	<i>Amersham</i>
<i>mirVana</i> ™ miRNA Isolation Kit	<i>Ambion</i>
NorthernMax®-Gly Kit	<i>Ambion</i>
PCR Purification Kit	<i>Qiagen</i>
QIAquick Gel Extraction Kit	<i>Qiagen</i>
RediPrime™ II DNA Labeling Kit	<i>Amersham</i>
SuperScript™ First-Strand Synthesis System for RT-PCR	<i>Invitrogen</i>
TOPO® TA Cloning Kit	<i>Invitrogen</i>
Wizard Genomic DNA Purification Kit	<i>Promega</i>
Zero Blunt® TOPO® PCR Cloning Kit	<i>Invitrogen</i>

3.5.2 Work with bacteria

3.5.2.1 *E.coli* strains

DH5 α	Gibco Life Technologies
--------------	-------------------------

3.5.2.2 Solutions

CaCl ₂ solution	60 mM 15% 10 mM autoclave	CaCl ₂ glycerol PIPES pH 7.0 or filter sterile
LB agar	98,5% 1,5%	LB-Medium Bacto agar
Ampicillin selection agar		LB agar with 100 µg/ml ampicillin
Kanamycin selection agar		LB agar with 50 µg/ml kanamycin
LB medium (Luria-Bertani)	10 g 5 g 5 g ad 1 l	Bacto peptone yeast extract NaCl H ₂ O
Ampicillin selection medium		LB medium with 50 µg/ml ampicillin
Kanamycin selection medium		LB medium with 25 µg/ml kanamycin

3.5.3 Southern blot analysis

Lysis buffer for genomic DNA extraction	0.1 M 5 mM 0.2% 0.2 M 0.1 mg/ml	Tris pH 8.5 EDTA SDS NaCl Proteinase K
Church buffer	0.5 M 0.5 M 1% 7% 1 mM 0.1 mg/ml	Na ₂ HPO ₄ NaH ₂ PO ₄ BSA SDS EDTA pH 8,0 salmon sperm DNA
Denaturation solution	0.5 M 1.5 M	NaOH NaCl
Neutralizing solution	0.1 M 0.5 M	Tris - HCl pH 7.5 NaCl
Stripping solution	0.4 M	NaOH
Wash solution I	2 x 0.1%	SSC SDS

Wash solution II	0.2x	SSC
	0.1%	SDS

3.5.4 Northern blot analysis

3.5.4.1 Solutions

RNA storage solution	1mM	sodium citrate pH 6.4
Wash solution I	2 x	SSC
	0.1%	SDS
Wash solution II	0.2x	SSC
	0.1%	SDS

3.5.4.2 Oligonucleotide probes

Name	Sequence	remark
Gsk-3 β -sh2 sense	5'-GAC ACG AAA GTG ATT GGA AAT GG-3'	siNorthern probe for Gsk-3 β -sh2
Gsk-3 β -sh2 antisense	5'-CCA TTT CCA ATC ACT TTC GTG TC-3'	siNorthern positive control for Gsk-3 β -sh2 probe
Gsk-3 β -sh4 sense	5'-GCT GTG TGT TGG CTG AAT TGT-3'	siNorthern probe for Gsk-3 β -sh4
Gsk-3 β -sh4 antisense	5'-ACA ATT CAG CCA ACA CAC AGC-3'	siNorthern positive control for Gsk-3 β -sh4 probe
Gsk-3 α -sh1 sense	5'-GCT CAT TCG GAG TAG TAT ACC-3'	siNorthern probe for Gsk-3 α -sh2
Gsk-3 α -sh1 antisense	5'-GGT ATA CTA CTC CGA ATG AGC-3'	siNorthern positive control for Gsk-3 α -sh2 probe

3.5.5 Western blot analysis

3.5.5.1 Solutions

Blocking solution	4%	skim milk powder in TBS-T
Laemmli buffer (5x)	313 mM	Tris-HCl pH 6.8
	50%	glycerol
	10%	SDS
	0,05%	bromphenolblue
	25%	β -mercaptoethanol
MES running buffer	500 mM	MES

(10x, for NuPAGE gels)	500 mM	Tris
	1%	SDS
	10 mM	EDTA
		pH 7.2
MOPS running buffer	500 mM	MOPS
(10x, for Criterion gels)	500 mM	Tris
	1%	SDS
	10 mM	EDTA
		pH 7.7
NuPAGE transfer buffer	250 mM	bicine
(10x, for NuPAGE gels)	250 mM	bis-tris
	10 mM	EDTA
	0.05 mM	chlorobutanol
NuPAGE transfer buffer	10%	10x transfer buffer
(1x, for NuPAGE gels)	10%	Methanol
RIPA buffer	50 mM	Tris-HCl pH 7.4
	1%	NP-40
	0,25%	sodium desoxycholate
	150 mM	NaCl
	1 mM	EDTA
Tris glycine blotting buffer (10x)	0.25 M	Tris
	1.92 M	glycine
Tris glycine blotting buffer (1x)	10%	10x blotting buffer
	10%	methanol

3.5.5.2 Antibodies

Antibodies	Organism	Dilution	Company
Anti-GSK-3 α/β , monoclonal	mouse	1:10,000	Stressgen
Anti- β -Actin, monoclonal	mouse	1:100,000	Abcam
Anti- β -Catenin, antiserum	rabbit	1:6,000	Sigma
Anti-HPRT, polyclonal	rabbit	1:500	Santa Cruz Biotechnology
Anti-mouse, polyclonal, peroxidase-conjugated	goat	1:10,000	Jackson ImmunoResearch
Anti-rabbit, polyclonal, peroxidase-conjugated	goat	1:5,000	Dianova

3.5.6 Enzymes

Cre recombinase

NEB

DNase I (RNase-free)

Roche

Klenow fragment of DNA Polymerase I	NEB
PCR-Mastermix 5x	5 PRIME
polynucleotide kinase (PNK)	NEB
proteinase K	Roche
restriction enzymes	Roche, MBI, NEB
RNA polymerases (T7, SP6)	Roche
RNase A	Serva
RNasin RNase inhibitor	Roche
Shrimp alkaline phosphatase (SAP)	Roche
SuperScriptII™	Invitrogen
T4 DNA ligase	NEB

3.5.7 Vectors and plasmids

Name of plasmid	Construct from	Description
BQ884537, BU708039, and BU707880	Open Biosystems	Gsk-3 α cDNA EST clones
pIRAK p961P0751.1	RZPD	Contains Gsk-3 β cDNA
pCR®-Blunt II-TOPO®	Invitrogen	Blunt end TOPO cloning vector
pCR®II-TOPO®	Invitrogen	TOPO TA cloning vector
pScreeniT™	Invitrogen	Screening system for shRNA efficiency
pBluescript	R. Kühn	Contains human U6 promoter from pSHAG (Paddison et al., 2004)
pCAG-C31Int(NLS)-bpA	R. Kühn	Expression of C31Int driven by the CAG promoter
pCRII-Rosa5'probe	R. Kühn	Contains the Southern probe 5'Rosa locus
pgk-neo-bpa	R. Kühn	Contains a pgk promoter, a neomycin resistance gene and a polyA signal
pNEB-loxP-RLuc-loxP	R. Kühn	Contains wild type loxP sites
pRMCE	R. Kühn	Donor vector for RMCE

3.5.8 Oligonucleotides

3.5.8.1 Oligonucleotides for genotyping

Name	Sequence	Conditions	Size of product
U6-for	5'-GAG GGC CTA TTT CCC ATG AT-3'	95°C 60 sec	1370 bp (sh-mice, mutant allele)
Rosa3'HA-rev2	5'-ACT CCC GCC CAT CTT CTA G-3'	57°C 40 sec 30 x	
		72°C 80 sec	
Rosa5'HA-for	5'-CGT GTT CGT GCA AGT TGA GT-3'	95°C 60 sec	536 bp (sh-mice, wt allele)
Rosa3'HA-rev	5'-ACT CCC GCC CAT CTT CTA G-3'	57°C 40 sec 30 x	
		72°C 60 sec	

Name	Sequence	Conditions	Size of product
expgk3 exneo2	5'-CAC GCT TCA AAA GCG CAC GTC TG-3' 5'-GTT GTG CCC AGT CAT AGC CGA ATA G-3'	94°C 60 sec 65°C 60 sec 30 x 72°C 60 sec	280 bp (sh-mice, RMCE cells, mutant allele)
Hyg-1 Hyg-2	5'-GAA GAA TCT CGT GCT TTC AGC TTC GAT G-3' 5'-AAT GAC CGC TGT TAT GCG GCC ATT G-3'	94°C 60 sec 65°C 60 sec 30 x 72°C 60 sec	552 bp (RMCE cells, acceptor allele)
Cre1 Cre2	5'-ATG CCC AAG AAG AAG AGG AAG GT-3' 5'-GAA ATC AGT GCG TTC GAA CGC TAG A-3'	94°C 30 sec 55°C 40 sec 30 x 72°C 90 sec	447 bp (cre-mice, mutant allele)
Gsk-3 α -Ex2-1 Gsk-3 α -In2-1 lac2	5'-ACG GCT GGC AGA GAC GAG-3' 5'-TGA GCA CCT TAA GGG ATG GA-3' 5'-CAA GGC GAT TAA GTT GGG TAA CG-3'	94°C 60 sec 61°C 40 sec 30 x 72°C 90 sec	wt: 720 bp mut: 1100 bp (gene trap mice)
R26R-D1 R26R-R1 R26R-Mt	5'-CCA AAG TCG CTC TGA GTT GTT AT-3' 5'-CAC ACC AGG TTA GCC TTT AAG CC-3' 5'-GCG AAG AGT TTG TCC TCA ACC-3'	94°C 60 sec 57°C 60 sec 30 x 72°C 60 sec	wt: 254 bp mut: ~320 bp (R26R reporter mice)

3.5.8.2 Oligonucleotides for PCR amplification

Name	Sequence	Conditions	Size of product
Gsk-3 β -5'UTR Gsk-3 β -Ex2-2	5'-GTT GCC TGG TTC CCA TGT C-3' 5'-GTG GTT ACC TTG CTG CCA TC-3'	94°C 60 sec 55°C 60 sec 35 x 72°C 90 sec	729 bp (on cDNA, ISH probe for Gsk-3 β)
Gsk-3 α -In1-1 Gsk-3 α -Ex2-2	5'-AGT GCT CTG GCT GTG AGG AT-3' 5'-CTT GGC CTA CAG TGG CTA CC-3'	94°C 60 sec 56°C 60 sec 30 x 72°C 60 sec	531 bp (Southern blot probe, Gsk-3 α locus)
Gsk-3 α -Ex1-1 Gsk-3 α -Ex3-1	5'-AGC GTC AGT CGG GGC TAT-3' 5'-AAG TAC CGC AGC CTC ACA AT-3'	94°C 60 sec 55°C 60 sec 35 x 72°C 60 sec	384 bp (on cDNA, Gsk-3 α locus)
Gsk-3 α -Ex1-1 lac2	5'-AGC GTC AGT CGG GGC TAT-3' 5'-CAA GGC GAT TAA GTT GGG TAA CG-3'	94°C 60 sec 55°C 60 sec 35 x 72°C 60 sec	489 bp (on cDNA, gene trapped Gsk-3 α locus)

3.5.8.3 Oligonucleotides for sequencing

Name	Sequence	Temp.	Binding site in
bpA	5'-GGG AGG ATT GGG AAG ACA AT-3'	52°C	pRMCE
BQ884537int	5'-GCT TGG CCT ACA TCC AC-3'	55°C	Gsk-3 α EST clones
BU707880int	5'-CTA TAC GGA GTT CAA GTT CC-3'	57°C	Gsk-3 α EST clones
Gsk-3 α -Ex1-1	5'-AGC GTC AGT CGG GGC TAT-3'	52°C	Gsk-3 α Exon1
Irak-1	5'-ATC CAC GCT GTT TTG ACC TC-3'	52°C	Gsk-3 β cDNA clone
Irak-2	5'-GGA ATC TGC CAT CGA GAC AT-3'	51°C	Gsk-3 β cDNA clone
Irak-rev	5'-GCA AAA CTC TCA AGC AGC AA-3'	51°C	Gsk-3 β cDNA clone
M13 for	5'-GTA AAA CGA CGG CCA GT-3'	48°C	
M13 rev	5'-CAG GAA ACA GCT ATG AC-3'	46°C	
RMCE-rev	5'-CTA GTG GCC CCG CTA ACT TT-3'	61°C	pRMCE

Name	Sequence	Temp.	Binding site in
ScreeniT for	5'-CGG TCG CTA CCA TTA CCA GT-3'	52°C	pScreeniT™
ScreeniT forfirst	5'-TTC AAC ATC AGC CGC TAC AG-3'	52°C	pScreeniT™
ScreeniT rev	5'-AAC ACC CGT GCG TTT TAT TC-3'	52°C	pScreeniT™
SP6	5'-ATT TAG GTG ACA CTA TAG-3'	46°C	
StopK1-rev	5'-GGG CGA ATT CTT TCC AAA A-3'	60°C	stop cassette
T3	5'-AAT TAA CCC TCA CTA AAG GG-3'	52°C	
T7	5'-GTA ATA CGA CTC ACT ATA GGG C-3'	59°C	
U6-Profor	5'-CCG TAA CTT GAA AGT ATT TCG-3'	49°C	U6 promoter

3.5.8.4 Oligonucleotides for cloning

Name	Sequence
Gsk-3 α -sh1 A	5'-ctcattcggagtagtataccgaagcttgggtatactactccgaatgagctttttggaaa-3'
Gsk-3 α -sh1 B	5'-gatctttcaaaaaagctcattcggagtagtataccaagcttcggtatactactccgaatgagcg-3'
Gsk-3 α -sh2 A	5'-ctggaccactgcaatattgtgaagcttgacaatattgcagtggtccagctttttggaaa-3'
Gsk-3 α -sh2 B	5'-gatctttcaaaaaagctggaccactgcaatattgtcaagcttcacaatattgcagtggtccagcg-3'
Gsk-3 α -sh3 A	5'-ggaacaaatccgagagatgagaagctgtcatctcctcgattgttccctttttggaaa-3'
Gsk-3 α -sh3 B	5'-gatctttcaaaaaaggggaacaaatccgagagatgacaagcttctcatctcctcgattgttcccg-3'
Gsk-3 α -sh4 A	5'-gccagagcgttccaagaagaagcttgttctgggaacgctctgggctttttggaaa-3'
Gsk-3 α -sh4 B	5'-gatctttcaaaaaaggcccagagcgttccaagaacaagcttctctgggaacgctctgggccc-3'
Gsk-3 α -sh5 A	5'-acatcaagccccagaattgaagcttgaattctggggctgatgtctttttggaaa-3'
Gsk-3 α -sh5 B	5'-gatctttcaaaaaagacatcaagccccagaattcaagcttcaattctggggctgatgtcg-3'
Gsk-3 β -sh1 A	5'-tgattggaatggatcatgaagcttgatgatccattccaatcactttttggaaa-3'
Gsk-3 β -sh1 B	5'-gatctttcaaaaaagtgattggaatggatcatcaagcttcatgatccattccaatcacg-3'
Gsk-3 β -sh2 A	5'-acacgaaagtgattggaatgggaagcttgcattccaatcacttctgtctttttggaaa-3'
Gsk-3 β -sh2 B	5'-gatctttcaaaaaagacacgaaagtgattggaatggcaagcttcccattccaatcacttctgtcg-3'
Gsk-3 β -sh3 A	5'-gttccatcaagaaagtctgaagcttgagaacttcttgatggcaacctttttggaaa-3'
Gsk-3 β -sh3 B	5'-gatctttcaaaaaaggttgcatcaagaaagtctcaagcttcagaacttcttgatggcaaccg-3'
Gsk-3 β -sh4 A	5'-ctgtgtgtggctgaattgtgaagcttgacaattcagccaacacacagctttttggaaa-3'
Gsk-3 β -sh4 B	5'-gatctttcaaaaaagctgtgtgtggctgaattgtcaagcttcacaattcagccaacacacagcg-3'
Gsk-3 β -sh5 A	5'-aaccgagagctccagatcgaagcttggatctggagctctcggttctttttggaaa-3'
Gsk-3 β -sh5 B	5'-gatctttcaaaaaagaaccgagagctccagatccaagcttctgatctggagctctcggttcg-3'
lox2272 A	5'-ctaggagtcgactgataactctgataaggtatcctatacgaagttatggatccataactctgataaggtatcctatacgaagttatgactggactc-3'
lox2272 B	5'-aattgagtcagtcataactctgataaggtatcctatacgaagttatggatccataactctgataaggtatcctatacgaagttatcagtcgactc-3'

3.6 Histological methods

3.6.1 Kits

(Renaissance) Individual Indirect Tyramide reagent Pack	<i>Perkin Elmer</i>
DIG labeled control DNA	<i>Roche</i>
DIG RNA Labeling Mix	<i>Roche</i>
RNeasy Mini Kit	<i>Qiagen</i>
Vectastain Elite ABC Kit	<i>Vector Labs</i>

3.6.2 Solutions for RNA *in situ* hybridization on paraffin sections

ammonium acetate stock solution (10x)	3 M	NH ₄ OAc
chamber fluid	50% 2x	formamide SSC
hybridization mix	50% 20 mM 300 mM 5 mM 10% 0.02% 0.02% 0.02% 0.5 mg/ml 0.2 mg/ml 20 mM	formamide Tris-HCl, pH 8.0 NaCl EDTA, pH 8.0 dextrane sulphate Ficoll 400 PVP40 BSA tRNA carrier DNA, acid cleaved DTT
NTE buffer (5x)	0.5 M 10 mM 5 mM	NaCl Tris-HCl (pH 8.0) EDTA (pH 8.0) autoclave
proteinase K buffer (PK buffer)	50 mM 5 mM	Tris-HCl (pH 7.6) EDTA (pH 8.0) autoclave
triethanolamine solution	0.1 M	triethanolamine pH 8.0 (with HCl)

3.6.3 Solutions for DIG labeled *in situ* hybridization

Blocking buffer	1%	blocking reagent (Roche) in MWB filter before use (45 µm)
-----------------	----	---

iodoacetamide <i>prepare fresh, protect from light</i>	20 mM	iodoacetamide in NTE
Levamisol <i>store at -20°C</i>	200 mM	Levamisol in H ₂ O
Maleate wash buffer (MWB) <i>prepare fresh</i>	150 mM 100 mM	NaCl maleic acid pH 7.5
NBT-BCIP	0.4 µg/ml 0.15 µg/ml 0.5 mg/ml	NBT BCIP Levamisol in TMN
NTE buffer (5x)	2.5 M 50 mM 25 mM	NaCl Tris-HCl (pH 8.0) EDTA (pH 8.0) pH 7.6
PBT	0.05% in	Tween 20 PBS
Proteinase K buffer	100 mM 10 mM	Tris EDTA, pH 8.0
Sheep serum	4%	sheep serum in TNT filter before use (45 µm)
TMN <i>aliquot, store at -20°C</i>	0.1 M 0.1 M 0.05 M	Tris NaCl MgCl ₂ (6H ₂ O) pH 9.5
TN	1 M 1.5 M	Tris NaCl pH 7.6
TNB <i>aliquot, store at -20°C</i>	0.1 M 0.15 M 0.5%	Tris NaCl Blocking reagent (Perkin)
TNT	0.05% in	Tween 20 TN
Wash 1	2x 50%	SSC formamide

Mayer's hematoxylin	0.1%	hematoxylin
	0.02%	sodium iodate
	5%	aluminum potassium sulfate dodecahydrate
	5%	chloral hydrate
	0.1%	citric acid
	in	H ₂ O
		filter before use

3.7 Embryonic stem cell culture

3.7.1 ES cell lines

IDG3.2	R. Kühn (F1 cells, wt)
IDG3.2-26.10-3	R. Kühn (F1 cells, for RMCE)
RRK111 (E14TG2A.4)	BayGenomics (gene trap clone)

3.7.2 Culture medium

E14 medium (E14TG2A.4)	10%	FCS (Hybond)
	1 mM	Sodium Pyruvat
	1x	MEM nonessential AA
	0.1 mM	β-Mercaptoethanol
	1000 U/ml	LIF
	in	Glasgow MEM
F1 medium (IDG3.2)	15%	FCS (PAN)
	20 mM	Hepes
	1x	MEM nonessential AA
	0.1 mM	β-Mercaptoethanol
	1500 U/ml	LIF
	in	DMEM
feeder medium	10%	FCS
	in	DMEM
freezing medium (1x)	15%	FCS (PAN)
	10%	DMSO
	in	DMEM
gelatine solution	1%	gelatine
	in	H ₂ O
Luciferase assay buffer	25 mM	glycylglycine
	15 mM	K-phosphate pH 8.0
	4 mM	EGTA
	2 mM	ATP

	1 mM	DTT
	100 μ M	coenzyme A
	75 μ M	luciferin
		pH 8.0
Trypsin solution (E14)	0.05%	Trypsin
	0.5 mM	EDTA
	1%	chicken serum
	in	PBS
	aliquot	and store at -20°C

3.8 Mouse strains

3.8.1 Wild type and other used mouse strains

<i>C57Bl/6J</i>	Wild type mouse line
<i>C57Bl/6J-Tg(pPGKneobpA)3Ems/J</i>	Wild type mice containing a neo resistance vector (for feeder cells production).
<i>R26R</i> (Soriano, 1999)	Reporter mouse line, carrying a floxed lacZ gene in the <i>Rosa26</i> locus.
<i>Nestin-cre</i> (Tronche et al., 1999)	Mouse line expressing Cre recombinase under the control of the Nestin promoter and enhancer; active in the CNS and additional tissue starting E11.0.
<i>CamKII-cre</i> (Minichiello et al., 1999)	Mouse line expressing Cre recombinase under the control of the CaMKII α promoter; active in forebrain excitatory neurons and partially in further CNS areas starting P20.

3.8.2 Generated mouse lines

<i>RRK111</i>	Gene trap mouse line targeting <i>Gsk-3α</i>
<i>Gsk-3α-flox</i>	Mouse line expressing <i>Gsk-3α-sh1</i> conditionally
<i>Gsk-3β-sh</i>	Mouse line expressing <i>Gsk-3β-sh2</i>
<i>Gsk-3β-flox-sh1</i>	Mouse line expressing <i>Gsk-3β-sh2</i> conditionally
<i>Gsk-3β-flox-sh2</i>	Mouse line expressing <i>Gsk-3β-sh4</i> conditionally
<i>Gsk-3-flox-dh</i>	Mouse line expressing <i>Gsk-3β-sh2</i> and <i>Gsk-3α-sh1</i> conditionally
<i>Gsk-3-flox-dh2</i>	Mouse line expressing <i>Gsk-3β-sh4</i> and <i>Gsk-3α-sh1</i> conditionally
<i>Gsk-3α-flox^{Nes}</i>	<i>Gsk3α-flox</i> x <i>Nestin-cre</i>
<i>Gsk-3β-flox-sh1^{Nes}</i>	<i>Gsk3β-flox-sh1</i> x <i>Nestin-cre</i>
<i>Gsk-3β-flox-sh2^{Nes}</i>	<i>Gsk3β-flox-sh2</i> x <i>Nestin-cre</i>
<i>Gsk-3-flox-dh^{Nes}</i>	<i>Gsk3-flox-dh</i> x <i>Nestin-cre</i>
<i>Gsk-3-flox-dh2^{Nes}</i>	<i>Gsk3-flox-dh2</i> x <i>Nestin-cre</i>
<i>Gsk-3α-flox^{CamKII}</i>	<i>Gsk3α-flox</i> x <i>CamKII-cre</i>
<i>Gsk-3β-flox-sh2^{CamKII}</i>	<i>Gsk3β-flox-sh2</i> x <i>CamKII-cre</i>
<i>Gsk-3-flox-dh2^{CamKII}</i>	<i>Gsk3-flox-dh2</i> x <i>CamKII-cre</i>

4 METHODS

4.1 Molecular biology

4.1.1 Cloning and work with plasmid DNA

4.1.1.1 Production and transformation of competent bacteria

Cloning was performed in *E.coli* bacteria (DH5 α). For transformation chemically competent bacteria were produced. After overnight culture at 37°C on a LB agar plate without antibiotic selection, a single colony was inoculated in 5 ml LB medium and again incubated overnight. 4 ml of the preparatory culture were transferred to 400 ml LB medium and incubated on a shaker. During the incubation the absorption at 590 nm was checked regularly, until it reached 0.375. The extinction of the cell suspension should not exceed 0.4. In the following procedure the suspension was kept on ice. The bacteria were split to 50 ml tubes, chilled on ice for 5-10 min and centrifuged (1600x g, 7 min, 4°C). The pellets were carefully resuspended in 10 ml ice-cold CaCl₂ solution and centrifuged again (1600x g, 5 min, 4°C). The pellets were again carefully resuspended in 10 ml ice-cold CaCl₂ solution and incubated on ice for 30 min before centrifugation (1600x g, 5 min, 4°C). Each pellet was then resuspended in 2 ml ice-cold CaCl₂ solution and split into aliquots of 50, 100, 150, and 200 μ l. The transformation efficiency was determined and aliquots were stored at -80°C.

For one transformation a 50 μ l aliquot was slowly thawed on ice and 5 μ l of ligation product (approx. 25 ng of plasmid DNA) was added to the bacterial suspension. The sample was inverted carefully and incubated on ice for at least 10 min. The following heat shock for 90 sec at 42°C allows the DNA to enter the bacteria. 1 ml of LB medium was added and the sample was incubated at 37°C for 30-60 min. During this time the transformed bacteria express the plasmid based antibiotic resistance genes, used for selection. Afterwards the bacteria were plated on LB agar plates containing the appropriate antibiotic and incubated overnight at 37°C. In general, ampicillin (100 μ g/ml) or kanamycin (50 μ g/ml) were used for selection.

4.1.1.2 Preparation of plasmid DNA

To extract plasmid DNA the following Qiagen kits were used: DNA Highspeed Maxi Prep Kit and DNA Mini Prep Kit.

For mini-prep production, one colony was inoculated in 5 ml LB medium containing an appropriate antibiotic and incubated overnight. 1.5 ml of the culture was used for preparation following the manufacturer's instructions.

In case of maxi-prep production, 200 ml of LB medium with antibiotic were inoculated and incubated overnight. The whole culture was used for preparation following the manufacturer's instructions.

The concentration of DNA was determined by measuring the optical density (OD) in a photometer at the wavelength of 260 nm. One OD₂₆₀ corresponds to 50 µg double stranded DNA per ml and 33 µg single stranded DNA per ml.

4.1.1.3 Restriction digest of plasmid DNA

The amount of restriction enzyme was determined in relation to the amount of plasmid DNA used. For one µg of supercoiled DNA two units (U) of enzyme were used. The reaction conditions were adjusted to the manufacturer's instructions and requirements of the used enzyme(s). The restriction digest was incubated for one hour at least at the appropriate temperature of each used enzyme.

If blunt ends were required, 5 U of large (Klenow) fragment of *E.coli* DNA polymerase I and 25nMol dNTPs were added to the sample after the restriction digest and incubated at RT for 20 min. Klenow was inactivated by incubation for 15 min at 75°C.

To minimize the religation of an opened vector it is useful to remove the terminal phosphates of the DNA, which prevents DNA ligase from joining these ends. This dephosphorylation is performed by 0.1 U shrimp alkaline phosphatase (SAP). For sticky vector ends the sample was incubated for 15 min, blunt vector ends were dephosphorylated for 60 min. SAP was inactivated by incubation for 10 min at 75°C.

4.1.1.4 Isolation of DNA fragments

For cloning, the vector fragments were separated using gel electrophoresis. In general 1% agarose gels were used, containing ethidium bromide to visualize the DNA using ultraviolet light. The gels were run using 1x TAE buffer. The complete

restriction digest was applied to gels with 5x loading buffer and as length standard the 1kb+ ladder was used. After separation in the gel, the needed fragments were cut out with a clean scalpel. DNA was visualized just short-time using long wave UV radiation (366 nm) to avoid DNA damage.

The DNA fragments were isolated from the agarose using the Qiagen Gel Extraction Kit following manufacturer's instructions. The concentration of the DNA fragments was measured in the photometer (4.1.1.2).

4.1.1.5 Ligation of DNA fragments

For ligation the linearized vector and the insert DNA fragment were applied in a molar ratio of approximately 1:3. The vector and fragment DNA was mixed and T4 DNA ligase buffer was added to the sample. The reaction was performed at RT with 600 U T4 DNA ligase in a total of 15 µl. For sticky end ligation the reaction time was 15 min and for blunt ends 60 min. Subsequently, 5 µl of the ligation product were used for transformation (4.1.1.1).

In case of hindered restriction digest of the vector DNA, because of low enzyme efficiency, a special restriction technique was applied (3-fragment ligation). Therefore, the vector was cut one time in the backbone to distinguish undigested vector DNA from correct digested DNA. If it was necessary to linearize the vector with two different enzymes, the digest was split in two. Both samples were digested with the backbone cutter and one of the linearization enzymes. For the vector two fragments were isolated from the gel and ligation was performed with three fragments (two vector fragments, one insert). This ligation technique stands out due to high cloning efficiency.

For cloning of PCR fragments, I used the TOPO TA Cloning Kit. This kit contained a linearized vector conjugated with Topoisomerase I, which allowed subcloning without ligase. The reaction was done following manufacturer's instructions.

4.1.1.6 Sequencing

To verify the cloned vectors or amplified DNA fragments, they were analyzed using a DNA sequencer. A PCR reaction was performed, to incorporate labeled stop nucleotides and amplify the DNA for sequencing. 5 pmol of one specific primer were mixed with the DNA and a reaction mix containing Big dye, sequencing buffer was

added to a total of 5 μ l. After initial denaturation of the template DNA at 95°C, the PCR was performed for 25 cycles each consisting of the following steps: 30 sec of cyclic melting of the DNA at 95°C, 15 sec of annealing at a primer specific temperature, 4 min of primer elongation at 60 °C. In the end the samples were chilled at 4°C. To purify the fragments, the DNA was precipitated by 100% ethanol and resuspended in pure water (Ampuwa). The samples were loaded to a 96-well sequencer plate and analyzed by the sequencer. The data was verified using Vector NTI. Difficult templates like shRNA hairpin structures or long DNA fragments were analyzed by SequiServe, Vaterstetten, Germany.

4.1.2 Analysis of genomic DNA

4.1.2.1 Isolation of genomic DNA

Genomic DNA from ES cells and mouse tissues was isolated using the Wizard genomic DNA purification kit following manufacturer's instructions. Apart from the tail clips, mouse tissues were first homogenized in PBS using a glass homogenizer. A small part of the homogenate was then used in the DNA purification kit.

For large-scale DNA extraction the tissue was homogenized in lysis buffer and the genomic DNA was extracted using phenol/chloroform.

4.1.2.2 Southern Blot analysis

Approximately 20 μ g of genomic DNA were digested with an appropriate restriction enzyme (30 U) in a total of 30 μ l. Spermidine (3.3 mM) was added to the sample for better restriction accuracy and DNA was digested for 2 hours up to overnight at 37°C. Digested DNA was separated on a 0.8% agarose / TBE gel for 14 to 20 hours at 30 to 70 V, depending on the length of the expected bands. To increase the blotting efficiency of large DNA fragments, the gel was gently shaken in 0.25 M HCl for 30 min to depurinate the DNA. Afterwards the gel was rinsed in water, and the DNA was denatured for one hour in denaturing solution. Neutralization was performed by agitating the gel for one hour in neutralization solution. The now single stranded DNA was transferred overnight via capillary transfer using 20x SSC to a nylon membrane. After the transfer, the membrane was briefly washed with 2x SSC and crosslinked by UV radiation. If not used for immediate hybridization, the membrane was dried, put between whatman papers and stored at RT.

For hybridization 50 to 100 ng of DNA probe was radioactively labeled with α -³²P-dCTP using the Rediprime II labeling kit following manufacturer's instructions. To remove unincorporated radioactive nucleotides, Microspin S-300 columns were used. The labeling efficiency was determined by measuring 1 μ l of the probe in a liquid scintillation counter. For hybridization 300,000 to 600,000 cpm/ml Church buffer were applied. Unused probe was stored at -20°C for up to 2 weeks. Before hybridization, the membrane was incubated with Church buffer for at least one hour at 65°C in a hybridization bottle. For hybridization the labeled DNA probe was denatured at 95°C, chilled on ice, and added to the Church buffer. Finally, the membrane was hybridized at 65°C for 5 hours to overnight.

The membrane was incubated with wash solution I two times for 30 min at 65°C to eliminate unspecifically hybridized probe. If necessary, wash solution II was used to increase wash capacity. The washed membrane was covered in transparent foil and exposed to an autoradiography film for maximal three days at -80°C. To increase the intensity of weak signals, the Biomax MS film was used together with the Biomax screen. This combination intensified the signal six times compared to a conventional film without enhancer screen. Finally, the film was developed using a developing machine.

To detect the DNA on the membrane with another probe, the old signal was removed with stripping solution. The membrane was incubated for 20 min at RT in the stripping solution, rinsed with 2x SSC, and used for prehybridizing.

4.1.2.3 Polymerase Chain Reaction (PCR)

Polymerase chain reaction (PCR) was performed to amplify DNA fragments from genomic or vector DNA. For easy application, a 5x PCR Mastermix was used. In general, the reaction was performed in 25 μ l total volume.

After initial separation of the template DNA into single strands at 95°C, the PCR was performed for 25 to 30 cycles each consisting of the following steps:

- 60 sec of cyclic melting of the DNA at 95°C
- 60 sec of annealing at the primer pair specific temperature
- 60-90 sec of primer elongation at 72°C, depending on product size

After a final elongation phase for 10 min at 72°C, the samples were chilled at 4°C until processing. For optimal results, the cycle time and the annealing temperature were adjusted for each primer pair (3.5.8).

The PCR products were separated on a 1% agarose gel (4.1.1.4) and visualized on a UV desk with short wave UV radiation (254 nm).

4.1.3 Analysis of RNA

For the work with RNA just RNase free solutions, chemicals, and tubes were used. Pipetting was performed with cleaned pipettes using separate filter tips. Glass, plastic equipment, and the working place were cleaned with RNaseZAP® or 70% ethanol and fresh MilliQ water before use. Samples were kept on ice, handled with clean gloves and exposed to air as short as possible to prevent RNA degradation.

4.1.3.1 Sample preparation and isolation of RNA

For tissue preparation from mice, the single animal was asphyxiated with CO₂, decapitated, and the brain or other organs were rapidly dissected. The whole tissue or dissected parts were immediately frozen on dry ice or liquid nitrogen to prevent degradation of RNA. Tissue was processed directly by homogenization with TriReagent or Trizol in a glass homogenizer or stored at -80°C.

ES cell samples were detached from the cell culture dishes, washed with 1x PBS and the cell pellet was homogenized directly in TriReagent or Trizol. After homogenization the samples were processed or stored at -80°C for further use.

Total RNA was extracted following manufacturer's instructions. For higher purity and increased handling, Phase Lock Gel™ heavy was applied following manufacturer's instructions to separate the aqueous from the organic phase. Total RNA was resuspended in RNA storage solution and concentration was determined using a photometer, where an OD₂₆₀ of one corresponds to 40 µg RNA per ml. If not processed immediately, isolated RNA was stored at -80°C.

Short RNAs were prepared from half mouse brains with the mirVana miRNA isolation kit for the extraction of small RNAs following manufacturer's instructions. Using specific columns and binding conditions, RNA molecules between 10 and 200 nt can be highly enriched. Concentration was determined using a photometer, where an

OD₂₆₀ of one corresponds to 33 µg RNA per ml. As total RNA, small RNAs were stored at -80°C.

4.1.3.2 Reverse transcription of mRNA into cDNA

To generate cDNA, using mRNA templates, SuperScriptII™ (from Invitrogen), a reverse transcriptase, was used. For reverse transcription (RT-PCR) approximately 5 µg of total RNA were incubated with oligo(dt) primer, dNTPs, SuperScriptII™, and the corresponding buffers at 42°C following manufacturer's instructions. Subsequently, the RNA template was destroyed by RNase H incubation. Before the cDNA was used for further PCR reactions, the quality was checked on an agarose gel.

4.1.3.3 Anchored PCR (5' RACE)

Low-copy mRNA can be isolated and characterized using a so-called anchored PCR. Therefore first strand cDNA synthesis is performed by using a gene-specific antisense oligonucleotide (GSP1) primer. This allows the cDNA conversion of specific mRNA. Following cDNA synthesis the first strand product is purified and homopolymeric tails are added to the 3' end of the cDNA. The tailed product is amplified using a nested gene specific (GSP2) primer and a combination of a complementary homopolymer-containing anchor primer and corresponding adapter primer, which permit amplification from the homopolymeric tail. This allows amplification of unknown sequences between the GSP2 and the 5'-end of the mRNA. To perform anchored PCR, the 5' RACE system for rapid amplification of cDNA ends from Invitrogen was used. Amplified products were sequenced before cloning.

4.1.3.4 Northern blot analysis

The NorthernMax®-Gly Kit from Ambion was used for Northern blotting of total RNA. For electrophoresis, 15 µg of total brain RNA were mixed with loading buffer, and separated on a 1% agarose gel. The separated RNA was transferred to a nitrocellulose membrane, and the membrane was incubated with ULTRAhyb buffer in a hybridization bottle for at least 30 min at 65°C. The radioactive DNA probe (50 to 100 ng template DNA) was labeled with α-³²P-dCTP using the Rediprime II labeling kit following manufacturer's instructions. To remove unincorporated radioactive nucleotides, Microspin S-300 columns were used. The labeled probe was denatured

at 95°C, chilled on ice, and added to the ULTRAhyb buffer. Hybridization was performed overnight at 65°C. To remove unspecifically bound probe, the membrane was incubated with the wash solutions provided with the NorthernMax®-Gly Kit according to the manual. For normalization the β -Actin probe was used. Here, the prehybridization and hybridization was done at 42°C. For detection of the signal, the membrane was exposed to a Kodak BioMax MS film for several hours or overnight at -80°C, depending on the signal intensity. A developing machine was used to visualize the signal on the film. Finally, to quantify band intensities, the membrane was exposed to an Imaging Plate. This plate was scanned with the FLA-3000 imaging analyzer to detect the signals.

For Northern blotting of small RNAs precasted 15% TBE urea gels were used. For electrophoresis, 2 or 3 μ g of RNA were mixed with 2x TBE urea sample buffer (1:1), denatured at 70°C for 3 min, chilled on ice, and applied to the gel. Separation was performed at 180 V for 75 min. The Xcell II™ Blot Module was used to transfer the separated RNA to a nylon membrane. The transfer was done for one hour at 30 V and afterwards the RNA was fixed to the membrane by UV radiation. If not used subsequently for hybridization, the membrane was stored at -20°C. Before hybridization, the membrane was incubated with RapidHyb buffer for at least one hour at 40°C in a 50 ml plastic tube. The radioactively labeled oligonucleotide probe for hybridization was generated by labeling 10 pmol of the probe oligonucleotide with 70 μ Ci γ -³²P-dATP. The reaction was performed by incubation with 20 U polynucleotide kinase (PNK) at 37°C for 30 min. PNK was inactivated by denaturation at 65°C for 20 min. For hybridization the labeled probe was chilled on ice, added to the RapidHyb buffer, and incubated with the membrane overnight at 40°C. Unbound probe was removed by incubation of the membrane two times for 30 min with wash solution I, and one time for 15 min with wash solution II. For detection of the radioactive signal the membrane was exposed to a Kodak BioMax MR film for several hours or one day, depending on the intensity of the signal. Finally, the film was developed in a developing machine (Agfa).

4.1.4 Analysis of protein samples

To prevent the degradation of protein samples, they were kept on ice whenever possible, and suitable dilutions were prepared to circumvent repeated thaw/freezing cycles of the stock solutions. Additionally, a preparation buffer with proteinase inhibitor was used.

4.1.4.1 Preparation of protein samples

ES cell samples were detached from the cell culture dishes, washed with 1x PBS and the cell pellet was homogenized directly in RIPA buffer by pipetting. The cell debris in the homogenate was pelleted by centrifugation for 15 min at 4°C (13.000 rpm). The supernatant containing the protein was removed to a new tube and stored at -20°C.

For mouse brains, tissue was homogenized in RIPA buffer with a glass homogenizer. For a half brain approximately 1 ml of RIPA buffer was used. The homogenate was sonificated to shear the DNA and cell debris was pelleted by centrifugation. The supernatant containing the protein was removed to a new tube and stored at -20°C.

The protein concentration was determined with the BCA™ protein assay kit. Therefore, 1 µl of protein solution was diluted with 49 µl of RIPA buffer and 1 ml of BCA working reagent was added. A water bath with lid was used to incubate samples at 37°C for 30 min. After cooling of the samples to RT, the absorption was measured at 562 nm in a photometer. For each measurement a BSA standard curve was included, and used to correlate the absorption to the protein concentration.

4.1.4.2 Western blot analysis

For detection of proteins with specific antibodies, protein samples were applied to a SDS polyacrylamide gel for electrophoretic separation (SDS-PAGE) according to their size (Laemmli, 1970). For SDS-PAGE the precasted gel systems from Invitrogen (NuPAGE® Novex) and Biorad (Criterion™ XT) were used. The amount of protein used varied between 5 and 20 µg of total protein, depending on the used antibody. The needed protein was mixed 1:5 with 5x Laemmli buffer, denatured at 95°C for 3 to 5 min, chilled on ice and loaded onto the gel. The pre-stained SeeBlue® Plus2 standard was applied as molecular weight marker. Electrophoresis was performed at 200 V for one to one and a half hours. Afterwards the gel was blotted on a PVDF membrane, which has been rinsed in 100% methanol. Protein transfer

was performed at 30 V for one hour with the module from Invitrogen or at 50 V for at least two hours to overnight with the Biorad apparatus. If the transfer was done overnight, it was performed at 4°C, otherwise at RT.

Membranes were blocked with 4% skim milk or BSA in TBS-T for one hour (RT) to overnight (4°C) to prevent unspecific signals. Afterwards, the membrane was incubated with the first antibody for one hour in TBS-T. Unbound antibody was removed by washing three times for 10 min each with TBS-T. The membrane was incubated with the second horseradish-peroxidase-conjugated antibody for one hour in TBS-T and washed again. The proteins were detected with ECL detection reagent following manufacturer's instructions. The membrane with the substrate was exposed to a chemiluminescent film for different time periods (initially 30 sec), depending on the signal intensity. Films were developed using a developing machine (Agfa) and, if necessary, quantified by ImageJ (Abramoff et al., 2004).

4.2 Embryonic stem cell culture

Embryonic stem (ES) cells represent the inner cell mass of blastocysts and their pluripotency enables them to differentiate into divergent cell types *in vivo* as well as *in vitro*. Because they can contribute to all cell lineages in the embryo, including the germ cells, genetically modified ES cells can be injected into wild type blastocysts and modify the developing embryo. The modified blastocysts are implanted into pseudo-pregnant foster mothers, which give birth to genetically divergent pups, sharing more or less genetically information with the injected ES cells. These chimeras consist partly of cells derived from the wild type blastocyst and partly of cells derived from the injected ES cells. Bred to wild type mice, so called germline chimeras transmit the genetically modified information of the ES cells to the next generation, producing progeny consisting to 100% of the mutant cells. Additionally to producing chimeras, it is even possible to produce complete transgenic animals by tetraploid aggregation. In this special case, the modified ES cells are aggregated with fused, tetraploid blastomeres and build up the developing embryo on their own, just assisted by the tetraploid cells, which contribute to extraembryonic tissues.

The mouse ES cell line IDG3.2, used here, consists of F1 ES cells, obtained from crossing the mouse strains C57Bl/6J and 129SvEv/Tac. To keep them undifferentiated and pluripotent (Smith et al., 1988; Williams et al., 1988), the culture medium was supplemented with Leukemia inhibiting factor (LIF) and pretested fetal

calf serum (FCS). The ES cells for mouse production were grown on feeder cells (mouse fibroblasts, see 4.2.1) at 37°C and 5% CO₂. During expansion, ES cells were splitted regularly to avoid confluent growth and subsequent differentiation. ES cells used for test experiments, like the determination of shRNA efficiency, were grown on gelatine coated cell culture dishes without feeder cells. These dishes were coated by covering the surface briefly with 1% gelatine solution. The solution was removed before the ES cells were plated.

Additionally to the IDG3.2 ES cells, a genetrapp ES cell clone from Baygenomics was obtained. The E14TG2A.4 (E14) ES cell line differs in its morphology compared to IDG3.2 cells as well as in its cell culture needs. They were grown without feeder cells on gelatine coated dishes and splitted in high rates (1:8) using an adjusted trypsin solution and E14 ES cell medium.

4.2.1 Preparation of mouse fibroblasts (feeder cells)

Feeder cells are mouse fibroblast cells, which have been mitotically inactivated by treatment with Mitomycin C. They need to be resistant against the antibiotic used in later transfections. At the age of E14.5 to E16.5, embryos of the transgenic mouse strain C57Bl/6J-Tg(pPGKneobpA)3Ems/J were dissected under sterile conditions to obtain primary neomycin resistant fibroblasts. These cultivated primary fibroblasts were expanded for two passages and grown to confluence. They were inactivated by incubation with medium containing 10 µg/ml mitomycin c for two hours at 37°C. Mitomycin C was removed by multiple wash steps with PBS. Afterwards, the feeder cells were trypsinized and plated on a fresh culture dish or frozen at -80°C (in 1x freezing medium) for later use. For plating of ES cells, feeder cells were incubated at a density of 2 - 2.5 x 10⁴ cells/cm² for at least several hours.

4.2.2 Expansion of ES cells

For expansion, ES cells were splitted regularly every two days before they start growing confluent. At this time point the ES cells should form distinct, light breaking colonies. After visual control of the cells in the microscope, the medium was removed and the cells were washed with PBS. To detach them from the surface, they were treated with trypsin for a maximum of 5 min at 37°C. The trypsin was inactivated by adding an equal amount of medium to the cells, and the cells were separated carefully by pipetting up and down. The cell suspension was splitted on several fresh

culture dishes, depending on the desired amount of cells per dish. Since this procedure can harm the ES cells, it was always performed as careful and quick as possible.

The cell number was determined in a Neubauer counting chamber. Therefore, 10 μ l of cell suspension were loaded into the chamber and ES cells were counted. The number of cells in one ml cell suspension is calculated by multiplying the cell number of one quadrant by 10,000.

4.2.3 Storage and thawing of ES cells

For storage, ES cells were frozen in liquid nitrogen. They were trypsinized as described in 3.2.2, and centrifuged after stopping the reaction. The cell pellet was carefully resuspended in ice cold 1x freezing medium and splitted to an appropriate number of cryovials. For slow freezing, the vials were put in a freezing container at -80°C , which contained isopropanol to increase the freezing time. The next day, the vials were transferred to liquid nitrogen for long term storage or at -80°C for storage up to 3 months. Cells on a multi well plate were trypsinized and resuspended in an equal amount of medium to stop the reaction. Instead of centrifugation, 2x freezing medium was added in a ratio of 1:1 to achieve finally a 1x concentration of freezing medium in each well. To slow down the freezing, multi well plates were wrapped in cellulose and put in paperback boxes at -80°C .

Cells in cryovials were thawed in a water bath at 37°C and resuspended in 5 ml of prewarmed medium. To remove the freezing medium, cells were centrifuged, resuspended in fresh medium and plated on an appropriate number of cell culture dishes. ES cells frozen in multi-well dishes were placed in plastic foil, before thawing in a water bath at 37°C to prevent contamination. To dilute the freezing medium, prewarmed medium was added to each well up to the limit of the well size. The medium of freshly thawed cells was exchanged the next day to remove residual traces of DMSO.

4.2.4 Introduction of DNA into ES cells using FuGENE transfection

Several vehicles can be used to introduce foreign DNA into ES cells. Here, I used FuGENE 6, a multi-component lipid-based transfection reagent, that can complex with DNA, and transport it into cells. For transient transfection, DNA was used as circular plasmid and mostly a mixture of several plasmids was cotransfected.

First, for the use in ES cell culture, the DNA had to be sterilized by precipitation. Therefore, an appropriate amount of the DNA plasmid was precipitated with 0.1 Vol. 3M sodium acetate (NaOAc), pH 5.2, and 3 Vol. 100% ethanol. The liquid was mixed and incubated for one hour to overnight at -20°C to improve precipitation. The DNA was pelleted by centrifugation at 14000 x g for 10 min and washed with 70% ethanol. Decanting of the ethanol, drying, and dissolving of the DNA pellet in sterile water was performed under a laminar flow. A DNA concentration of 100 ng/μl was used for transient transfection of ES cells.

One day before transfection, ES cells were plated on a gelatin coated 24-well plate (approximate 40,000 cells per well). For each well, 2 μl FuGENE 6 were mixed with 66 μl DMEM, and incubated for 5 min at RT. The DNA was added, and the mixture was incubated for at least 15 min at RT. The medium of the ES cells was exchanged with 600 μl fresh F1 medium, the mixture, containing the FuGENE / DNA complex, was added, and incubated with the ES cells overnight at 37°C. The next day, the medium was changed to remove the FuGENE / DNA complex. Two days after transfection, the ES cells were harvested for analysis by Western blot or reporter assays.

4.2.5 β-Gal reporter gene assay

The β-Gal reporter gene assay kit was used to assess the activity of β-Galactosidase (LacZ) and firefly-luciferase (Luc) after transfection of the corresponding expression plasmids. Following the manufacturer's instructions, the cell lysates were prepared and the LacZ activity was measured. Thereby 100 μl of a LacZ substrate were added to 50 μl of the cell lysate, which resulted in light emission at 475 nm, initiated by the cleaved substrate after a shift of the pH value. To measure the intensity of the emitted light for 5 sec, a plate luminometer was used.

To detect the Luc activity, 20 μ l of each lysate were mixed with 100 μ l Luciferase assay buffer and measured for 5 sec in the luminometer. The assay buffer contained luciferin, which was oxidized by Luc and emitted light at 490 nm.

4.2.6 Introduction of DNA into ES cells via electroporation

Apart from transfection reagents, a physical method to bring foreign DNA into ES cells is electroporation. By short electrical impulses, the cell membranes are permeabilized transiently, so that DNA can enter the cell through the emerging pores. Linearized plasmids can be integrated into the genome, whereas circular plasmid DNA stays only transiently in the cells. Cotransfection of several plasmids is possible, too. A refined possibility to integrate DNA stably into the genome is the cotransfection of a specially designed circular plasmid together with an expression vector for an integrase. The expressed integrase catalyzes the integration of a defined fragment of the circular plasmid into the genome of the cell.

For each electroporation 10^6 - 10^7 ES cells have been used. ES cells were harvested by trypsination, centrifuged at 1200 rpm for 5 min, washed with PBS, and pelleted again. The cells were resuspended in 800 μ l PBS containing the DNA for electroporation. For 10^7 cells a maximum of 50 μ g of total DNA was used; for lower cell numbers the DNA amount was adjusted. The DNA containing suspension was transferred into an electroporation cuvette and electroporated with 300 V and 500 μ F for 2 ms. For a high transfection efficiency in transient transfections, a voltage of 320 V was used for 3 ms. The ES cells were allowed to rest for 5 min at RT after the transfection, before they were diluted in medium and plated on an appropriate number of culture dishes (10^7 cells on 4-5 10 cm dishes). For transient experiments gelatin coated plates were used, whereas for stable transfections dishes with feeder cells were needed. Cells were incubated for two days at 37°C, before they were harvested for analysis. Otherwise, the ES cells were incubated in selection medium.

4.2.7 Isolation and screening of stably transfected ES cell clones

To select clones, which stably integrated the electroporated vector, the specific antibiotic was added to the medium two days after the transfection. In general, selection was performed with the neomycin analog Geneticin (G418). The used vectors contained a neomycin resistance gene, which is expressed after stable integration into the genome. In medium supplemented with 140 μ g/ml G418, only

resistant ES cells are able to survive and form colonies, whereas cells with no integration die during selection. The selection was performed for five to seven days until round, light breaking, and prominent colonies could be identified and until most of the single cells died.

Colonies were picked from the culture dish containing PBS with a 20 μ l pipette into a 96-well plate containing 50 μ l trypsin in each well to dissociate the ES cell colony for a maximum of 20 min. Afterwards, 50 μ l medium were added to inactivate the trypsin and the picked colonies were resuspended. The separated ES cells were plated on a fresh 96-well plate with feeder cells in a total volume of 300 μ l medium. To remove dead cells and to decrease the trypsin concentration in the wells, the medium was changed the next day and cells were transferred to larger wells as soon as necessary. On 24-well plates, multiple copies of the clones were splitted onto several feeder and gelatin coated plates. For storage the cell copies on feeder coated plates were frozen at -80°C with 2x freezing medium or further expanded to 10 cm plates.

Screening of the clones was performed by PCR and positive tested clones were confirmed by Southern blot. Therefore, DNA was extracted from cell copies on gelatin coated plates to avoid extraction of feeder cell DNA. The ES cells were grown to confluence, washed with PBS, and used immediately for DNA extraction. Otherwise, the plates were stored dry at -20°C . Extraction of genomic DNA is described in 4.1.2.1.

4.3 Mouse husbandry

4.3.1 Housing

All mice at the HelmholtzZentrum München are bred in accordance with national and institutional guidelines. If not mentioned else, the mice were group housed with maximal five mice per cage. In general, they were kept in open cages and a light/dark cycle of 12 hours was maintained. Food and water were given *ad libitum*. The temperature in the animal facility was kept at $22 \pm 2^{\circ}\text{C}$ and at a relative humidity of $55 \pm 5\%$. In the German Mouse Clinic (GMC), the mice were housed in individually ventilated cages (IVC) due to hygienic reasons.

For breeding one male was paired with one or two females and pups were weaned at an age of three weeks. At weaning mice were separated according to their gender

and received earmarks for identification. In this process tail clips for genotyping were taken and stored at -20°C until DNA extraction.

4.3.2 Generation of mice from ES cells

Mice were generated by injection of ES cells into mouse blastocysts or by tetraploid embryo aggregation (Nagy et al., 1993).

Young female C57BL/6 mice were superovulated to increase the number of ovulated oocytes for the production of mouse blastocysts (E3.5). For superovulation, the females were injected intraperitoneally (i.p.) with analogs of the gonadotropins follicle-stimulating hormone and luteinizing hormone. Injections were performed at noon, starting with 7.5 I. E. of pregnant mare's serum gonadotropin (PMSG) to induce maturation of the follicles. After 48 hours, 7.5 I. E. of human chorion gonadotropin (hCG/Ovogest) were injected, which initiates the ovulation of the oocytes. Then female mice were mated overnight with one male of the same strain. Dissection of the uteri was performed three days *post coitum* and blastocysts were obtained by flushing the uteri with M2 medium. *In vitro*, 10 to 20 mutant ES cells were injected into the blastocoel of one isolated blastocyst, which was fixed with a capillary of the micromanipulator, to contribute to the inner cell mass.

For mouse generation via tetraploid embryo aggregation, late two-cell-stage embryos were collected from the superovulated females 46 h after treatment with hCG. One two-cell-stage embryo in M2 medium was placed between two electrodes (250 µm apart) and the blastomeres were fused by a short electric pulse (90 V, 100 µsec). The fused, tetraploid embryos were cultivated for 24 h until the four-cell-stage and afterwards the zona pellucida was removed. Two of these four-cell-stage embryos were aggregated overnight with 10 - 15 ES cells in-between and the next morning the aggregates were transferred into foster mothers.

For these two types of early embryos, pseudo-pregnant CD1 females were used as foster mothers. To obtain pseudo-pregnant foster mothers, the females were mated to sterile, vasectomized males. For embryo transfer, the females were given anesthesia dependent on their body weight. In general, 0.25 ml of 1% ketamine and 0.1% rompun in isotonic saline solution were used and during surgery the eyes were kept wet with 0.9% NaCl to prevent dehydration of the cornea. To dissect the ovaries and the uterus, the retroperitoneal cavity of the foster mother was opened. Up to ten

manipulated blastocysts were transferred into each side of the uterus via a thin cannula. Afterwards, the surgery field was closed with clips and the foster mothers were kept on warming plates to prevent loss of body temperature until awakening.

4.3.3 Establishment of new mouse lines

Chimeras were born 17 days after embryo transfer. Since the injected blastocysts were obtained from C57BL/6 females, the wild type ES cells coded for black fur color in the offspring. In combination with the used F1 ES cells, which gave agouti fur color, chimeric mice showed a mixture of black and agouti fur. A high contribution of mutant ES cells to the chimera leads to a complete or nearly complete brown mouse. In the opposite case, the chimera just shows some brown spots in its black fur.

Chimeras were mated to wild type C57Bl/6J mice to obtain germline transmission of the modified allele in the offspring. A first hint for positive germline transmission is the presence of brown pups in the offspring of the chimera, indicating that mutant ES cells have populated the gonads. But also black pups can carry the desired mutation, because of the heterozygous coded dominant agouti gene in the used F1 Es cells. Germline offspring, which inherited the modified allele from the chimera, were identified by PCR or Southern blot.

In the case of injection of E14 ES cells, all germline offspring of the chimeras display a brown fur color, because in these cells the agouti gene is present in a homozygous state. All black pups were sorted out immediately and just brown pups were genotyped.

4.4 Histology

4.4.1 Perfusion and dissection of adult mice

For perfusion the mice were asphyxiated with CO₂, fixed with their paws, and the thoracic cavity was dissected to gain access to the heart. Tail clips were taken for second genotyping. The left ventricle was cut and a blunt needle was inserted carefully into the ascending aorta and fixed with a clamp. Now, the pump was started to flush the blood vessels with PBS. To decrease the pressure on the system, the right atrium was opened. When the liver and the fluids became colorless, the pump was switched to 4% fresh diluted paraformaldehyde (PFA/PBS). The fixation of the hind paws was removed and, in general, small twitches, indicating the starting

fixation of the tissue, were detected. Perfusion was performed for approximate 5 min until the mice became stiff. To dissect the brain, the mice were decapitated and the skull bones were removed carefully. After dissection, the brains were kept in 4% PFA/PBS for several hours to overnight at 4°C for final fixation.

4.4.2 Preparation of paraffin sections

After final fixation, the brains were dehydrated in an ascending ethanol scale, equilibrated, and embedded in paraffin. Following, the steps for the automated embedding machine are given:

step	time [min]	solution	temp.	remarks
dehydration	90	30% ethanol	RT	
dehydration	90	50% ethanol	RT	
dehydration	90	75% ethanol	RT	
dehydration	90	85% ethanol	RT	
dehydration	90	95% ethanol	RT	
dehydration	90	100% ethanol	RT	
dehydration	60	100% ethanol	RT	under vacuum
clarification	60	Roti-Histol	RT	under vacuum
clarification	60	Roti-Histol	RT	under vacuum
paraffination	60	50% Roti-Histol / 50% paraffin	65°C	under vacuum
paraffination	60	paraffin	65°C	under vacuum
paraffination	480	paraffin	65°C	under vacuum
embedding		paraffin	65°C to RT	

The embedded tissue was stored at 4°C until cutting with the microtome.

To cut the embedded tissue on the microtome, it had to be fixed on a tissue cassette using paraffin. With the microtome, 8 µm thick sections were cut and transferred into a water bath (approximate 39°C) for flattening. From the water bath, the straightened sections were mounted on slides and dried first on a heating plate and later in an incubator at 37°C. Dry slides were stored at 4°C in special boxes or directly used.

4.4.3 Preparation of frozen sections

After final fixation, the brains were equilibrated in 20% sucrose solution overnight at 4°C. For longer storage 0.01% sodium azide was added to the sucrose. To produce frozen sections on the cryostat, the tissue was frozen on dry ice and fixed on an object holder with freezing medium. Slices of 30 µm to 50 µm were cut and collected free-floating in PBS. For longer storage the slices were kept in cryoprotection solution at -20°C.

For some purposes frozen sections were mounted directly on slides during cutting. The thickness of the slices varied from 16 µm to 30 µm, depending on the planned experiment. They were cut, mounted, and dried on the slides, which were kept at -20°C or -80°C (for longer storage).

4.4.4 Radioactive *in situ* hybridization on paraffin sections

Radioactive *in situ* hybridizations (ISH) were performed to detect mRNA expression in brain sections. To avoid degradation of the mRNA and the RNA probe, for the complete procedure RNase free solutions and materials were used.

To detect the mRNA of the desired gene, a probe containing cDNA information of the gene is labeled with radioactive sulfur (³⁵S). These radioactively labeled RNA probes were generated by *in vitro* transcription with an appropriate RNA polymerase (T7, SP6) in the presence of α-thio³⁵S-UTP. The template DNA was linearized after the cDNA sequence with an appropriate restriction enzyme, and the transcription reaction was set up as follows:

3 µl	10x transcription buffer
3 µl	dNTP mix (rATP/rCTP/rGTP 10mM each)
1 µl	0.5 M DTT
1 µl	RNasin (RNase inhibitor; 40 U/µl)
1,5 µg	linearized plasmid DNA template
3 µl	[α-thio- ³⁵ S]-UTP (12.5 mCi/mM)
ad 29 µl	RNase-free water
1 µl	RNA polymerase (T7 or SP6; 20 U/µl)

The reaction was performed at 37°C for 3 hours in total. After one hour, another 0.5 µl of RNA polymerase was added to increase the transcription. Finally, by adding 2 µl of RNase-free DNase I and incubation at 37°C for 15 min, the DNA template was destroyed. Purification was performed with the RNeasy Mini Kit following manufacturer's instructions and activity was measured in a liquid scintillation counter.

For hybridization the paraffin sections were dewaxed and pretreated as follows:

step	time	solution	remarks
dewaxing	2 x 15 min	Roti-Histol	
rehydration	2 x 5 min	100% ethanol	
rehydration	5 min	70% ethanol	
rehydration	3 min	H ₂ O	
fixation	20 min	4% PFA in PBS	on ice
wash	2 x 5 min	1x PBS	
permeabilization	7 min	20 µg/ml proteinase K in proteinase K buffer	
wash	5 min	1x PBS	
fixation	20 min	4% PFA in PBS	on ice
wash	5 min	1x PBS	
acetylation / denaturing of ribosomes	10 min	0.1 M triethanolamine-HCl	add 600µl acetic anhydride; rapidly stirring
wash	2 x 5 min	2x SSC	
dehydration	1 min	60% ethanol	
dehydration	1 min	70% ethanol	
dehydration	1 min	95% ethanol	
dehydration	1 min	100% ethanol	

Before hybridization the slides were dried dust free and prehybridized with hybridization mix for one hour at 57°C. Later, the labeled probe was used at a concentration of 70,000 cpm/µl in hybridization mix, whereas 100 µl of solution were applied per slide. First, the probe was added to an appropriate amount of hybridization mix. This mixture was incubated at 90°C for 2 min for denaturation of the probe. Second, the mixture was chilled on ice and applied to the prehybridized slides. To prevent dehydration, the slides were covered with coverslips and kept in a humid chamber with chamber fluid at 57°C overnight.

The next day, cover slips were removed and the slides were washed according to the following protocol:

step	time	solution	temp.
wash	4 x 5 min	4x SSC (radioactive waste)	RT
RNA digestion	20 min	20 µg/ml RNase A in 1x NTE buffer	37°C
wash	2 x 5 min	2x SSC / 1mM DTT	RT
wash	10 min	1x SSC / 1mM DTT	RT
wash	10 min	0.5x SSC / 1mM DTT	RT
wash	2 x 30 min	0.1x SSC / 1mM DTT	64°C
wash	2 x 10 min	0.1x SSC / 1mM DTT	RT
dehydration	1 min	30% ethanol in NH ₄ OAc solution (1x)	RT
dehydration	1 min	50% ethanol in NH ₄ OAc solution (1x)	RT
dehydration	1 min	70% ethanol in NH ₄ OAc solution (1x)	RT
dehydration	1 min	95% ethanol in NH ₄ OAc solution (1x)	RT
dehydration	2 x 1 min	100% ethanol in NH ₄ OAc solution (1x)	RT

Slides were air dried and exposed to an autoradiography film (BioMax MR) for two days to check for positive hybridization. Afterwards, the signal on the slides was developed. Therefore, the slides were covered with a photo emulsion (diluted 1:1 with water), dried, and stored at 4°C in the dark for an appropriate time depending on the signal intensity. The time period was estimated by the results of the film, in general the slides were stored for two to four weeks. For developing, slides were equilibrated to RT for at least one hour, developed for 5 min, rinsed in tap water and fixed for 7 min. Afterwards, the slides were washed for 25 min in cold floating tap water and remaining emulsion on the backside was removed with a razor blade. Finally, the slides were counterstained with cresyl violet (6.4.6).

4.4.5 DIG labeled *in situ* hybridization on paraffin sections

For the detection of neuronal markers non-radioactive DIG labeled *in situ* hybridization was performed.

The following markers were used for analysis:

probe	target mRNA	species	size
GAD2	glutamic acid decarboxylase 2	mus musculus	~ 1000 bp
Sert	Serotonin transporter	mus musculus	~ 500 bp
TH	Tyrosine hydroxylase	mus musculus	unknown
VACHT	vesicular acetylcholine transporter	rattus norvegicus	1594 bp

The probes were cloned from cDNA of the specific gene and inserted into appropriate vectors with RNA polymerase promoter sequences, e.g. T7, T3, and SP6. The vectors were linearized with a suitable restriction enzyme and the probe was amplified with the corresponding RNA polymerase.

During the whole procedure RNase free solutions and materials were used to avoid degradation of the mRNA. Probes were labeled with the DIG RNA Labeling Mix following the manufacturer's protocol. For cleaning of the probes the RNeasy Mini kit was used. The check for DIG integration and semi-quantitative determination was done by comparison with dilution of a standard DIG-labeled control RNA of known concentration (DIG-labeled control RNA).

Paraffin sections were dewaxed first according to the following protocol:

step	time	solution	remarks
dewaxing	2 x 20 min	Roti-Histol	
rehydration	2 x 5 min	100% ethanol	
rehydration	5 min	95% ethanol	
rehydration	5 min	70% ethanol	
rehydration	3 min	H ₂ O	
wash	3 min	1x PBS	
fixation	20 min	4% PFA in PBS	on ice
wash	2 x 5 min	1x PBS	
dehydration	2 min	60% ethanol	
dehydration	2 min	70% ethanol	
dehydration	2 min	95% ethanol	
dehydration	2 min	100% ethanol	

The whole procedure was performed using the Genesis RSP 200 robot from TECAN. For the processing in the robot all 1x solutions were supplemented with 0.05% Tween 20. The slides passed the following steps:

day one			
cycles	volume	time	reagent
5	350 µl	5 min	0.6 % H ₂ O ₂ / MeOH; @ 24°C
7	350 µl	5 min	1x PBS
2	350 µl	5 min	0.2 M HCl
4	350 µl	5 min	1x PBS
1	400 µl	5 min	proteinase K buffer
2	350 µl	10 min	0.5 µg/ml proteinase K in proteinase K buffer
7	350 µl	5 min	1x PBS
2	350 µl	10 min	4% PFA in PBT
7	350 µl	5 min	1x PBS
1	350 µl	15 min	Hyb-mix + 1.5 mg/ml DTT; @ 24°C
1	350 µl	30 min	Hyb-mix, heat to 64°C
1	350 µl	6 h	hybridization with DIG probes; @ 64°C
day two			
cycles	volume	time	reagent
5	350 µl	5 min	5x SSC (preheated to 62°C); @ 64°C
5	350 µl	10 min	Wash 1 @ 64°C
5	350 µl	12 min	Wash 2 @ 64°C
4	350 µl	8 min	0.1x SSC; @ 25°C
4	350 µl	5 min	NTE
4	350 µl	7 min	iodoacetamide
4	350 µl	5 min	NTE
2	350 µl	5 min	TNT
3	350 µl	10 min	sheep serum
4	350 µl	5 min	TNT
2	250 µl	10 min	TNB
2	350 µl	5 min	TNT
2	350 µl	5 min	Maleate wash buffer
2	350 µl	10 min	Blocking buffer
2	350 µl	5 min	Maleate wash buffer

cycles	volume	time	reagent
2	350 µl	5 min	TNT
3	350 µl	5 min	TMN
4	350 µl	5 min	TNT
2	350 µl	10 min	TNB
2	350 µl	30 min	Anti DIG-POD, 0.2924 U/ml in TNB
6	300 µl	5 min	TNT
1	300 µl	30 min	Tyramid-Biotin, 1:50 in TSA, prewarmed to 37°C
6	350 µl	5 min	MWB
2	350 µl	30 min	NeutrAvidin™ protein 2.85 µg/ml in blocking buffer
6	350 µl	5 min	MWB
4	350 µl	5 min	TNT
2	350 µl	5 min	TMN
2	350 µl	15 min	NBT-BCIP
4	400 µl	5 min	H ₂ O, 0.05% Tween 20
1	300 µl	5 min	NTE
1	200 µl	20 min	4% PFA in PBT
4	400 µl	5 min	H ₂ O, 0.05% Tween 20

The slides were embedded immediately in a water soluble matrix and dried.

4.4.6 Nissl staining (cresyl violet)

Staining of nuclei with cresyl violet was performed according to the following protocol:

step	time	solution	remarks
staining	1 - 5 min	cresyl violet staining solution	
rinse		H ₂ O	
differentiate	1 min	70% ethanol	until slide is clear
differentiate	10 - 60 sec	96% ethanol + 0.5% acetic acid	
dehydration	2 x 1 min	96% ethanol	
dehydration	2 x 2 min	100% ethanol	
embedding	2 x 10 min	Roti-Histol	

Slides were embedded in Roti-Histokitt II and dried overnight under the hood.

4.4.7 Immunohistochemistry (DAB-staining)

For IHC on Paraffin sections the slides were dewaxed first and heated according to the following protocol:

step	time	solution	remarks
dewaxing	min. 45 min	Roti-Histol	
rehydration	2 x 5 min	ethanol 100%	
rehydration	2 x 5 min	ethanol 96%	
rehydration	2 x 5 min	ethanol 70%	
rinse	10 min	H ₂ O	
wash	3 min	0.01 M sodium citrate	
antigen retrieval microwave at 100%	5 min	0.01 M sodium citrate	~ 900 watt
cooling down	10 min	0.01 M sodium citrate	
antigen retrieval microwave at 70%	3 min	0.01 M sodium citrate	~ 600 watt
cooling down	20 min	0.01 M sodium citrate	

For IHC on frozen sections, the slides were thawed in a precooled box at RT for one hour. Next, they were washed and fixed according to the following protocol:

step	time	solution	remarks
rinse	5 min	1x PBS	
fix	10 min	4% PFA in 1x PBS	
wash	2 x 5 min	1x PBS	

Afterwards the procedure for both types of sections was the same and they were treated according to the following protocol:

step	time	solution	remarks
wash	2 x 5 min	1x PBS	
destruction of endogenous peroxidases	5 min	0.1% H ₂ O ₂ / PBS	add H ₂ O ₂ directly before use
wash	2 x 5 min	1x PBS	
blocking	1 h	10% FCS, 0.05% Triton-X in PBS	RT, humid chamber (hc)
1 st antibody	Overnight	1 st antibody in 10% FCS / PBS	4°C, hc

step	time	solution	remarks
wash	3 x 5 min	1x PBS	
2 nd antibody	1 hr	2 nd antibody in 10% FCS / PBS	RT, hc
wash	3 x 5 min	1x PBS	
intensifying with ABC-solution	30 min	1:300 in 10% FCS / PBS preparation 30 min before use	RT, hc, keep dark
wash	2 x 5 min	1x PBS	
wash	5 min	0.1M Tris-HCl	
DAB-staining	max. 30 min	0.05% DAB, 0.02% H ₂ O ₂ in Tris-HCl	hc, keep dark
stop staining	2 x 5 min	1x PBS	
dehydration	2 x 5 min	70% ethanol	
dehydration	2 x 5 min	96% ethanol	
dehydration	2 x 5 min	100% ethanol	
embedding	2 x 5 min	Roti-Histol	

Slides were embedded in Roti-Histokitt II and dried overnight under the hood.

4.4.8 LacZ staining in mouse tissues

A common reporter in various applications is the lacZ gene. Its product the enzyme β -galactosidase (LacZ) converts X-gal to galactose and a blue water-insoluble indigo dye. For the detection of lacZ expression in mice, the following protocol was used. To maintain the activity of LacZ in the tissue, all solutions used for LacZ staining were substituted with MgCl₂ and EGTA, and the staining was performed as soon as possible for optimal results.

For fixation, the mice were perfused with LacZ fix, containing 4% PFA/PBS. The brain and other tissues were immediately stained or stored for cutting overnight at 4°C in 20% sucrose. During cutting, free-floating sections were stored in LacZ storage solution. Whole tissue or free-floating sections were washed in LacZ wash buffer for 15 min and transferred to freshly prepared LacZ staining solution. Staining was performed overnight at 37°C, protected from light. Staining was stopped by washing in PBS.

Mouse embryos for LacZ staining were dissected and frozen immediately on dry ice. They were cut on the cryostat and mounted on slides. The dried slides were washed two times in LacZ storage solution to remove freezing medium, fixed in LacZ

fix, washed two times in LacZ wash buffer and stained overnight, protected from light, at 37°C in fresh LacZ staining solution. Staining was stopped by washing in PBS. After post-fixing the slides in 4% PFA/PBS and washing in PBS, they were counterstained with Eosin-red according to the following protocol:

step	time	solution	remarks
staining	10 min	0.1% Eosin-red staining solution	overcolor slightly
rinse	1 min	tap water	
differentiate		80% ethanol	control intensity
dehydration	2 min	96% ethanol	
dehydration	2 min	100% ethanol	
embedding	10 min	Roti-Histol	

Stained slides were embedded in Roti-Histokitt II and dried overnight under the hood.

4.5 German Mouse Clinic

The German Mouse Clinic at the HelmholtzZentrum München offers a standardized phenotypic analysis. Two mouse lines, the *Gsk-3 β -flox-sh2^{Nes}* and the *Gsk-3 α -flox^{Nes}*, were tested in the complete primary screen to analyze their phenotype. For other lines, only an adjusted behavioral screening was performed. If necessary, single modules of the primary screen were done. All tests were performed as cited on the webpage of the GMC (<http://www.mouseclinic.de/info/publications.html>).

4.5.1 Behavioral testing

An enlarged behavioral screening was performed with all mice in the GMC by R. Kneutinger under the supervision of Dr. S. Hölter-Koch. Therefore, mice were transferred to the GMC at the age of eight to ten weeks. First tests started after a minimum of two weeks of habituation for the animals. All mouse lines, except the *Gsk-3-flox-dh2*, were tested in two combinations, crossed to the *Nestin-cre* and to the *CamKII-cre* mice. Each group of animals consisted of 10 to 15 mice for each sex and genotype (mutant or control) with a maximal difference in age of two weeks and underwent the following tests in the given order: modified Hole Board (mHB), light-dark box (LD), accelerating rotarod (Rota), and forced swim test (FST).

Obtained data were statistically analyzed using SPSS software. The significance level was set to $p < 0.05$.

4.5.1.1 Modified Hole Board test

The modified Hole Board test performed by the GMC is an improved version of the procedures described by Ohl et al. (2001). The apparatus was made of dark grey PVC to allow easy cleaning. The mHB box (150 x 50 x 50 cm) was divided into a test arena (100 x 50 cm) and a group compartment (50 x 50 cm) by a transparent PVC partition (50 x 50 x 0.5 cm) with 111 holes (1 cm diameter), staggered in twelve lines, to allow the test animal contact with the cage mates. In the middle of the test arena a board (60 x 20 x 2 cm) with 23 holes (1.5 x 0.5 cm), staggered in three lines and covered by individual movable lids, was placed. This central area of the test arena represented an open field. The surrounding area was divided into twelve similar sized quadrants by lines taped onto the floor of the box (see Ohl et al., 2001).

Before each trial, all lids were closed and two objects were placed into the test arena with a distance of 2 cm. The first object was a blue plastic tube lid considered as unfamiliar object. The second, familiar object was a metal cube of similar size, which was already introduced to the test animals three days before testing and which was removed from the home cage one day before the trial. The illumination level in the corners of the test arena was set to 150 lux, and the center of the arena was illuminated at 200 lux.

First, the animals of one cage were put into the group compartment of the mHB for 20 min to habituate and explore the test environment. Second, one test animal was placed in one corner of the test arena, next to the partition, facing the board diagonally. The two mentioned objects were placed in the corner diametrically to the starting point. The test animal was allowed to explore the test arena freely for 5 min. In this time period the cage mates stayed in the group compartment to measure group contact. During the trial, the behavior of the test animal was observed and measured by an experienced observer using a hand-held computer. Additionally, the track of the animal was recorded by a video camera, which was installed 1.2 m above the center of the test area. The locomotor path of the animal was analyzed too by a video-tracking system. Between the trials, the test arena was cleaned with a disinfectant. All measured parameters are given in the Appendix.

4.5.1.2 Light-dark box

The Light-dark box was divided into two compartments, connected by a small tunnel (4 x 6 x 9 cm). The smaller dark compartment (14 x 19 x 24 cm) was fabricated of black PVC and not separately illuminated (approximate 20 lux in the center), whereas the bigger lit compartment (29 x 19 x 24 cm) was made of white PVC and illuminated by cold light with an intensity of 650 lux in the center.

At the beginning of the trial, the test animal was placed in the center of the dark box and allowed to explore the environment freely for 5 min. During the trial, the behavior of the test animal was observed and measured by an experienced observer using a hand-held computer. Since the number of entries into the compartments was measured, an entry was defined as placement of all four paws into the compartment. All measured parameters are given in the Appendix. Additionally, the trial was recorded by a video camera, which was installed above the center of the lit compartment and the locomotor path was analyzed by a video-tracking system. Between the trials, the test arena was cleaned with a disinfectant.

4.5.1.3 Accelerating rotarod

The accelerating rotarod was performed to assess motor coordination and balance. The rod diameter of the rotating rod apparatus was approximate 4.5 cm and it was fabricated of hard plastic, covered by soft black rubber foam to enable the mice to run on it. The lane widths were 5 cm, which allowed the animals to turn on the rod.

The three trials of the test were interrupted by intertrial intervals (ITI) for 15 min each. At the beginning of a trial, three mice were marked at the tail with a pencil to ensure that the same animals are tested together in the following trials. Initially, the rod was rotating at a constant speed of 4 rpm to allow the placing of the mice. Now, the three mice were placed on the rod facing away from the observer, each with an empty lane to the next mouse. After all mice were positioned on the rod and getting along with the rotation, the test was started and the rod accelerated from 4 rpm to 40 rpm in 300 sec. When a mouse fell off, the actual speed of the rod and the time spent running was noted. Additionally, passive rotations were noted and considered as a fall off. For the 15 min of ITI the mice were put back to their home cage. Between the trials, the test arena was cleaned with a disinfectant.

4.5.1.4 Forced swim test

In the forced swim test, adapted from Ebner et al. (2002), the mice were forced to swim in a cylindrical 10 l glass tank with 24.5 cm in diameter. The water depth was 20 cm and the temperature was 25 °C (\pm 1°C). The illumination was about 30 lux.

The mouse was put into the tank and an experienced observer, using a hand-held computer, recorded the behavior for 6 min. The behavior was subdivided into three different sorts of possible movements. First, struggling was defined as movement of the animal during which the forelimbs broke the water surface. Second, swimming was defined as movement of all four limbs without breaking the water surface. And third, floating was defined as the minimal amount of using the limbs to keep the equilibrium, without any movement of the trunk. After each trial the water was exchanged and the mouse was dried with paper towels before put into a new cage.

4.5.2 Cardiovascular analysis

During the GMC primary screen, the mouse strains *Gsk-3 β -flox-sh2^{Nes}* and *Gsk-3 α -flox^{Nes}* were analyzed in the cardiovascular screen. Mainly responsible for the tests done, were Dr. B. Ivandic, Dr. A. Schrewe, S. Axtner and M. Backs. Information about procedures and analysis were taken from the obtained GMC report.

Blood pressure was measured in conscious mice with a non-invasive tail-cuff method using the MC4000 Blood Pressure Analysis Systems (Hatteras Instruments Inc., Cary, North Carolina, USA). Four animals were restrained on a pre-warmed metal platform in metal boxes. The tails were looped through a tail-cuff and fixed in a notch containing an optical path with a LED light and a photosensor. The blood pulse wave in the tail artery was detected as transformed optical pulse signal by measurement of light extinction. Pulse detection, cuff inflation, and pressure evaluation were automated by the system software. After five initial inflation runs for habituation, 12 measurement runs were performed for each animal in one session. Runs with movement artifacts were excluded. After one day of training, in which the animals were habituated to the apparatus and protocol, the measurements were performed on four consecutive days between 8:30 and 11:30 AM. For blood pressure analysis, at least 20 to 48 individual measurements were pooled to obtain a mean over the four measurement days for each animal.

ECG was performed in anesthetized (isoflurane/pressured air inhalation) mice by use of three metal bracelets that were put on the joints of the feet together with electrode gel. The complete setup was located in a faraday cage. The electrodes were positioned on the front-paws and the left hind-paw, resulting in the bipolar standard limb leads I, II and III and the augmented unipolar leads AVF, AVR, AVL. ECG was recorded for about seven minutes. A shape analysis of the ECG traces was performed with the software ECG-auto (EMKA technologies, Paris, France). For each animal, intervals and amplitudes were evaluated from five different sets of averaged beats (lead II). The parameter Q-T interval was also corrected for the RR interval. In addition, the recordings were screened for arrhythmias, including supraventricular and ventricular extrasystoles and conduction blockages. In the quantitative ECG analysis sets of five analyzed beats were averaged for one animal.

The data were analyzed statistically using Statistica. Analysis of variance (ANOVA) tests are used for multi-factorial analysis of sex and genotype. Post hoc analysis for multiple comparisons included a Duncan's Multiple Range Test & Critical Ranges.

4.5.3 Pathological analysis

Since the mouse strains *Gsk-3 β -flox-sh2^{Nes}* and *Gsk-3 α -flox^{Nes}* performed the whole GMC primary screen, they were finally analyzed in the pathology. Mainly responsible for the tests done, were PD Dr. L. Quintanilla-Fend, Dr. I. Moßbrugger, Dr. G. Hölzlwimmer, J. Müller, and E. Samson.

Mice were asphyxiated with CO₂ and the organs were dissected and stored in 4% buffered formalin. For cutting the tissue was embedded in paraffin and cut on a microtome in 4 μ m thin slices. For an overview the tissue was stained with hematoxylin and eosin (HE) and for differentiation the myelin in nervous tissue (brain, spinal cord) was stained with luxol fast blue according to the following protocol:

step	time	solution	remarks
dewaxing	10 min	xylol	
rehydration	2 x 5 min	100% ethanol	
rehydration	2 x 5 min	96% ethanol	
staining	overnight	luxol fast blue staining solution	@ 60°C, covered
rinse		96% ethanol	until color fades
rinse		H ₂ O	

step	time	solution	remarks
differentiate	3 x 5 sec	0.05% lithium carbonate solution	add fresh solution until it stays clear
differentiate	~ 25 sec	70% ethanol	add fresh solution until it stays clear
rinse		H ₂ O	
counterstaining	~ 2 min	Mayer's hematoxylin	
rinse	10 min	tap water	
dehydration	2 x 5 min	96% ethanol	
dehydration	2 x 5 min	100% ethanol	
embedding	10 min	xylol	

The steps with lithium carbonate and 70% ethanol had to be repeated until grey and white matter could be distinguished. In this procedure myelin sheets were stained with a clear blue color, whereas the grey matter was stained in aquamarine, and the nuclei were stained deep purple-blue. The slides were embedded in Pertex mounting medium.

5 RESULTS

5.1 Expression of *Gsk-3* during development and in the adult mouse brain

Most of the published studies for *Gsk-3* are derived from the rat (Leroy and Brion, 1999; Takahashi et al., 2000; Takahashi et al., 1994), and only a single study describes the expression pattern of *Gsk-3* in the mouse (Yao et al., 2002). To obtain detailed information about the expression pattern of *Gsk-3 α* and *Gsk-3 β* in the adult mouse brain and in the developing embryo, radioactive *in situ* hybridizations (ISH) were performed. The analysis was performed on adjacent sagittal and coronal paraffin sections with a thickness of 8 μ m to compare the expression of both genes in different brain regions.

5.1.1 Construction of ISH probes

The sequence identity of both *Gsk-3* genes is high and in the catalytic domain it reaches even 93% (Ali et al., 2001). Because of this homology, the probes for ISH were designed carefully. To avoid crossreactivity between the two probes, they were selected from the 5'UTR regions of the genes to avoid the complementary kinase domain. The *Gsk-3 α* probe was derived from the glycine-rich N-terminal domain, which is unique to the *Gsk-3 α* gene (Doble and Woodgett, 2003). For *Gsk-3 β* , the probe selection from the 5'UTR allowed the detection of both known *Gsk-3 β* splice variants, which differ in a 13-residue insert within the kinase domain (Mukai et al., 2002). No splice variants are known for *Gsk-3 α* .

The ISH probe for *Gsk-3 β* covered 729 nt from the 5' UTR up to the beginning of exon two of the *Gsk-3 β* cDNA. This probe was amplified with the primer pair *Gsk-3 β -5'UTR* and *Gsk-3 β -Ex2-2* from cDNA of IDG3.2 wild type cells, cloned into TOPO TA cloning vector (pCR®II-TOPO®), and sequenced with SP6 and T7 primers. For ISH, the vector was cut with BamHI 3' of the cDNA insert, and the riboprobe was amplified with T7 RNA polymerase.

The probe for *Gsk-3 α* could not be amplified by PCR, but was retrieved from an EST cDNA clone. The clone BQ884537 was cut using BamHI/BstEII and the fragment, covering 420 nt of the 5'UTR to the beginning of exon two, was purified by gel

electrophoresis and cloned into pCR®-Blunt II-TOPO® vector. The vector was sequenced with M13 rev primer. For ISH, the vector was cut with EcoRV 3' of the cDNA insert, and the riboprobe was amplified with SP6 RNA polymerase.

5.1.2 Expression of *Gsk-3* during embryonic development

Leroy and Brion (1999) detected expression of *Gsk-3 β* in rat during the developmental stages E10, E15, and E18. They reported *Gsk-3 β* expression in neurons in all studied developmental stages, including postnatal (P) days P0, P3, P10, and P20. Labeling of white matter tracts was strongest in the embryo (E18) and diminished during development. At P20, labeling of the white matter was not detected anymore. Yao et al. (2002) reported the expression of GSK-3 protein in brain, heart, liver, and skeletal muscle of P7 mice.

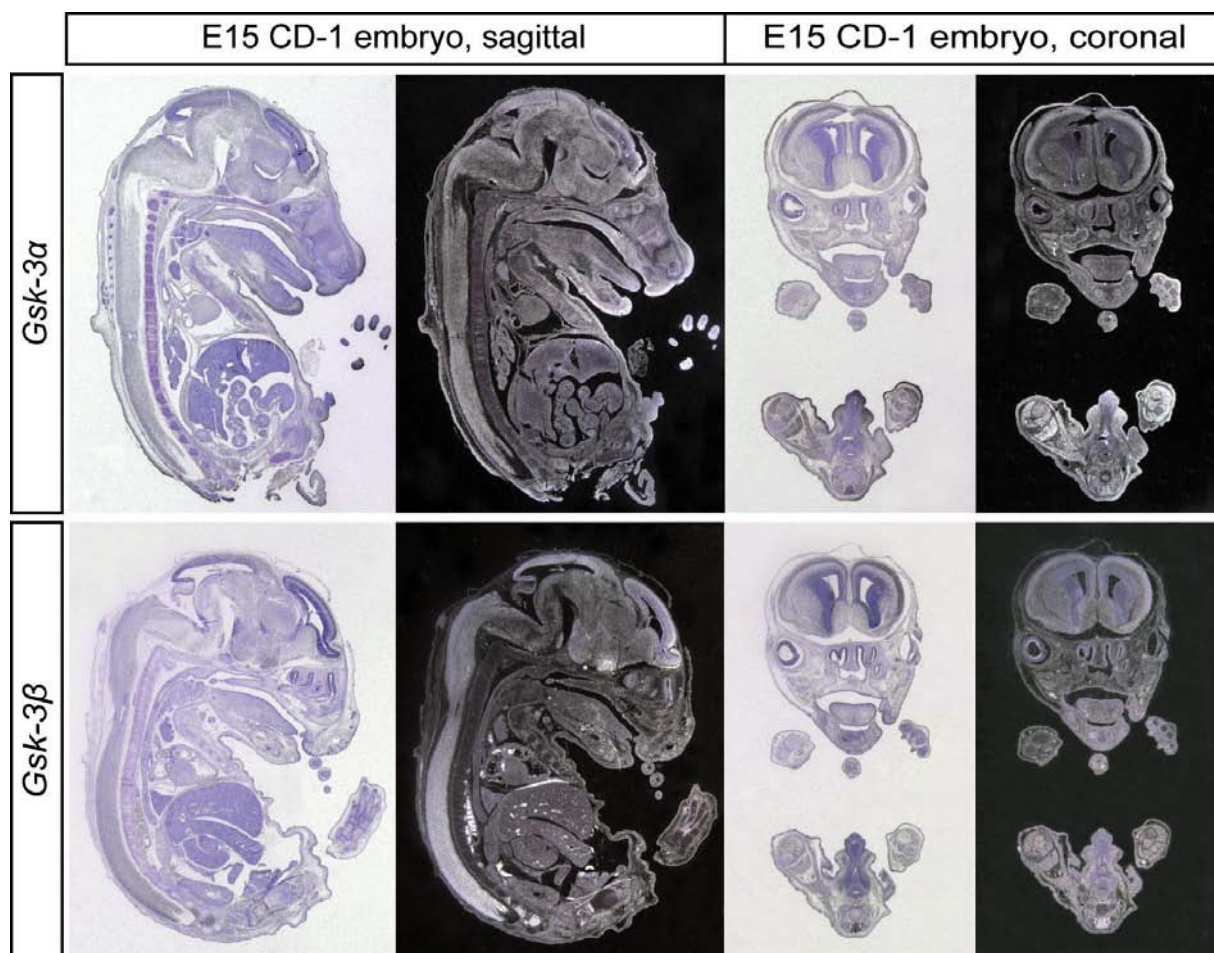


Fig. 7: Expression of *Gsk-3* mRNA in the embryo. A ubiquitous expression, which is weaker for *Gsk-3 β* , was detected in the whole embryo for both *Gsk-3* transcripts. Comparable was also the slight increase of expression in the developing cortex. The more refined expression pattern of *Gsk-3 β* to the CNS showed additionally an increased expression in the developing olfactory bulbs and in the anterior hypothalamus.

To take a more detailed look at the expression of *Gsk-3* mRNA during the development, the following embryonic stages were analyzed in CD-1 wild type embryos using ISH: E9, E10, E14, and E15. In all studied developmental stages *Gsk-3* mRNA was detected. Fig. 7 shows the expression pattern of an E15 embryo. *Gsk-3 α* expression was ubiquitous in the whole body and, as expected, also present in the central nervous system (CNS). A slight increase of expression was observed in the developing cortex. The pattern of *Gsk-3 β* was more refined to the CNS with a similar increase of expression in the forebrain. Other spots of high *Gsk-3 β* expression were the developing olfactory bulbs and the anterior hypothalamus. Like for *Gsk-3 α* , there was an overall, but weaker, expression in the rest of the body.

5.1.3 Expression of *Gsk-3* in the adult mouse brain

Like in the embryo, a strong neuronal expression of *Gsk-3* was observed in the brain of adult mice. As mentioned, the staining of white matter tracts faded until stage P20 and was undetectable in adult mice. This was confirmed by ISH (Fig. 8).

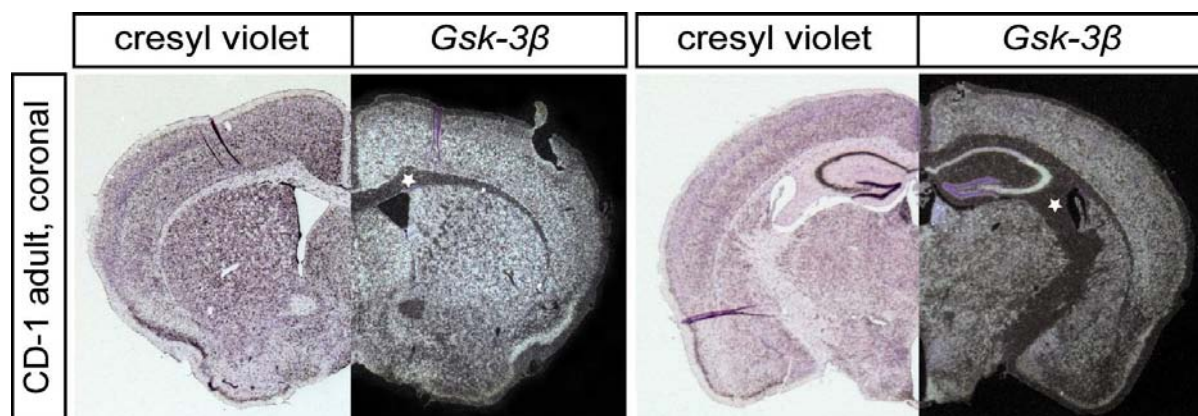


Fig. 8: Expression of *Gsk-3 β* mRNA in the adult mouse brain (coronal view). A distinct neuronal expression of *Gsk-3 β* was predominant in the whole adult mouse brain. The white matter tracts showed no expression of *Gsk-3 β* (asterisk).

Fig. 9 shows the ubiquitous expression of *Gsk-3* in the adult brain. All regions showed detectable signals; especially the hippocampus and the Purkinje cell layer of the cerebellum displayed strong expression. Both *Gsk-3* genes were comparably expressed in the adult brain, apparently in the same cell types and regions, which could enable the sharing of each others functions.

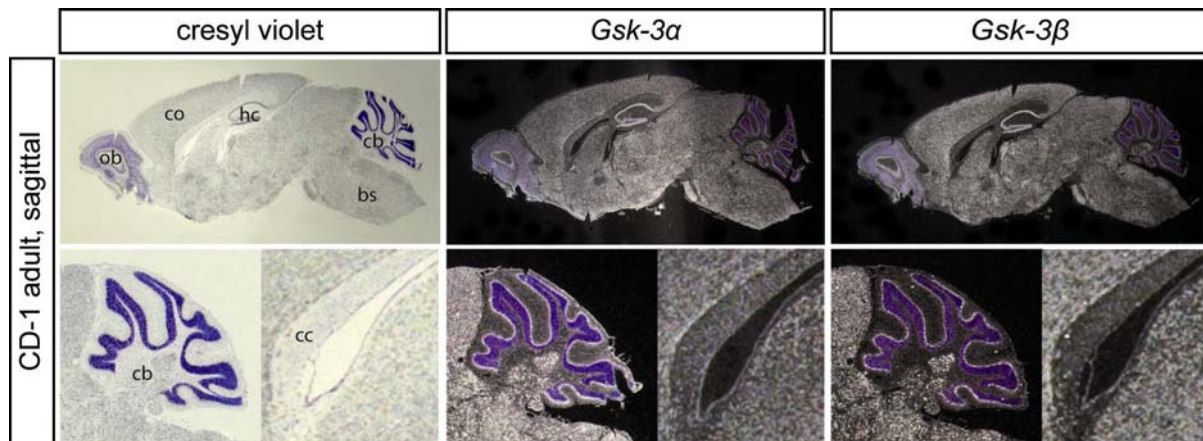


Fig. 9: Expression of *Gsk-3* mRNA in the adult mouse brain (sagittal view). Both *Gsk-3* genes displayed a ubiquitous neuronal expression all over the adult mouse brain. A strong signal was detected in the hippocampus (hc) and in the Purkinje cell layer of the cerebellum (cb). No expression was observed in the white matter tracts of the adult brain, as can be seen in the corpus callosum (cc). *ob*: olfactory bulbs, *co*: cortex, *hc*: hippocampus, *cb*: cerebellum, *bs*: brainstem

5.2 Targeting of the *Gsk-3 α* locus by a gene trap vector

At the time when the project started, knockout mice for the *Gsk-3 α* gene were not yet available. Since I could identify the trapped *Gsk-3 α* gene in a database for gene trap mice, I decided to generate knockout mice from this ES cell clone. These mice would be a useful comparison to the *Gsk-3 α* knockdown mice.

5.2.1 The gene trap strategy

Gene trapping is a method to generate random insertional mutations using gene trap vectors in ES cells. These vectors insert into intronic or coding region of genomic DNA. The insertion site is determined by 5'RACE using primer located in the trap cassette. These gene trap sequences are derived from cDNA or genomic DNA and are used to identify and annotate the trapped gene. In general, the insertion of the gene trap vector leads to a complete inactivation of the trapped gene, but in some cases the fusion protein still shows some rest activity or, in rare cases, the inactivation fails completely.

Gene trap vectors contain a splice acceptor, a trap cassette with a reporter construct, for example β -*geo*, and a polyadenylation signal. They utilize the splicing apparatus of the cell via the splice acceptor signal to combine the vector sequence with the mRNA. Thereby the downstream vector sequence is transcribed and a fusion transcript is generated, inactivating normal gene function. These conventional gene

trap vectors use the endogenous promoter of the trapped gene for expression and the polyadenylation signal at the 3' end causes the truncation of the targeted mRNA (Fig. 10), whereas the 5' region of the gene is left intact (Stanford et al., 2001).

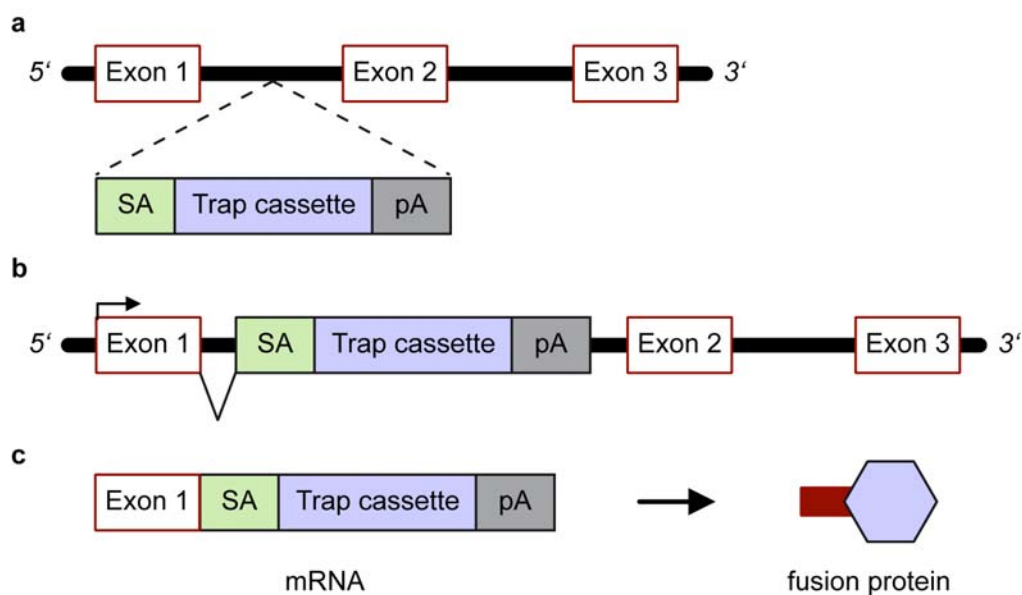


Fig. 10: Trapping of a gene with a conventional gene trap vector. The gene trap vector integrates randomly into a genomic locus (a). Transcription of a trapped gene fuses the vector sequence, via the integrated splice acceptor, to the 5' exon and the polyadenylation signal interrupts the endogenous splicing process (b). The resulting mRNA is truncated, and translates into a disrupted fusion protein carrying the reporter of the trap cassette (c). SA: splice acceptor, pA: polyadenylation signal

For the *Gsk-3 α* gene a gene trap ES cell clone was identified (RRK111) and obtained from the BayGenomics gene trap collection. This ES cell clone contained a conventional β -geo gene trap vector and after confirmation of the trapped gene it was subsequently injected into blastocysts to produce *Gsk-3 α* gene trap mice.

5.2.2 Confirmation of the *Gsk-3 α* gene trap clone

To verify the insertion of the gene trap vector into the *Gsk-3 α* locus, total RNA was extracted from the RRK111 ES cell clone and cDNA was produced. With the primer pair Gsk3 α -Ex1-1 and lac2 the gene trapped sequence was amplified and sequenced (Fig. 11). The sequence tag from BayGenomics was confirmed, as was the correct splicing of the gene trap vector. The vector sequence after the splice acceptor was unchanged, indicating a functional gene trap clone.

Next, the integration site of the vector into the genomic locus was determined. PCR using the primer pair Gsk3 α -Ex2-1 and lac2 was performed on genomic DNA of RRK111 cells. The product was cloned into TOPO TA cloning vector and sequencing

revealed that the gene trap vector integrated at base pair 32 of intron two. The first 654 bp of the vector were lost during integration, whereas the following 346 bp of the vector were unchanged, but the next 437 bp displayed some deleted and rearranged sequences. The last 100 bp of the *en2* splice acceptor and the following sequence were correct as far as sequenced.

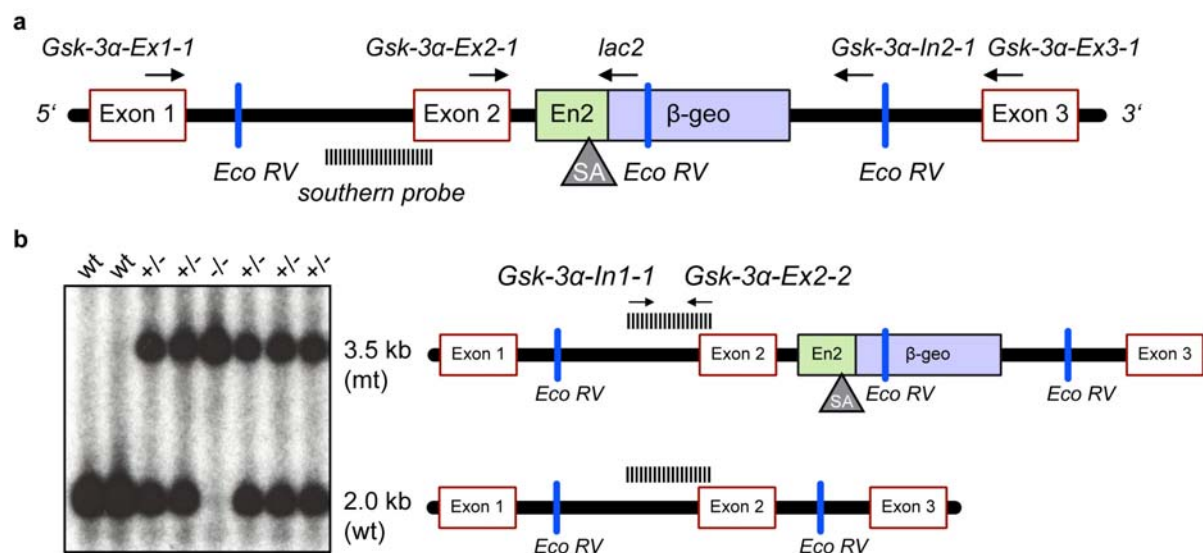


Fig. 11: Integration of the gene trap vector in the RRK111 ES cell clone. The gene trap vector was integrated at base pair 32 of intron two in the *Gsk-3α* locus (a). Gene trap mice were genotyped by Southern blot. After digestion of the genomic DNA with EcoRV, the wild type (wt) *Gsk-3α* locus was detected by a 2.0 kb band, whereas the mutant (mt) locus was detected by a band of 3.5 kb size (b). SA: splice acceptor, *En2*: engrailed 2, *β-geo*: *β*-galactosidase/neomycin

5.2.3 Generation of homozygous gene trap mice

After the correct splicing of the gene trap vector was confirmed, the RRK111 ES cell clone was injected into C57BL/6 blastocysts (4.3.2). The resulting chimeras were bred to C57BL/6 wild type females. The ES cell line E14TG2A.4 originates from 129/Ola mice and is homozygous for the agouti locus A3. This leads to agouti fur in germline offspring of the chimera and black fur in wild type pups.

ES cell derived agouti offspring was genotyped by triple PCR using the following primers: *Gsk3α-Ex2-1*, *Gsk3α-In2-1*, and *lac2*. The F1 generation was intercrossed to generate homozygous knockout mice. Since the PCR showed instability, a Southern blot probe was established via PCR amplification of tail DNA with the primer pair *Gsk-3α-In1-1* and *Gsk-3α-Ex2-2*. This probe was located in intron one, covering 531 bp, containing also the beginning of exon two. Cutting the genomic locus of wild type mice with EcoRV produced a band of 2.0 kb, whereas the gene trapped locus was cut in the vector sequence. This produced a 3.5 kb band and additional a

10.0 kB band derived from undigested DNA (Fig. 11b). The Southern blot analysis was able to detect the first homozygous mice. These could not be identified via PCR, because the wild type band was still amplified. A second PCR was set up to identify this problem, but also this primer pair still amplified the wild type band in the homozygous animals. Therefore, the PCR product was sequenced to ensure the amplification of the right locus. Since this was the case, further PCR genotyping was abandoned and transgenic mice were identified only by Southern blotting.

5.2.4 Analysis of the *Gsk-3 α* gene trap mice

The first homozygous mice were analyzed by Western blotting to check for the loss of GSK-3 α protein. Wild type, heterozygous, and homozygous mice were dissected and samples of the brain, heart, liver, spleen, and kidney were taken. Fig. 12a displays a Western blot of brain protein. There was obviously no protein reduction of *Gsk-3 α* in heterozygous or homozygous gene trap mice. In other organs analyzed, no loss of GSK-3 α protein was detected either.

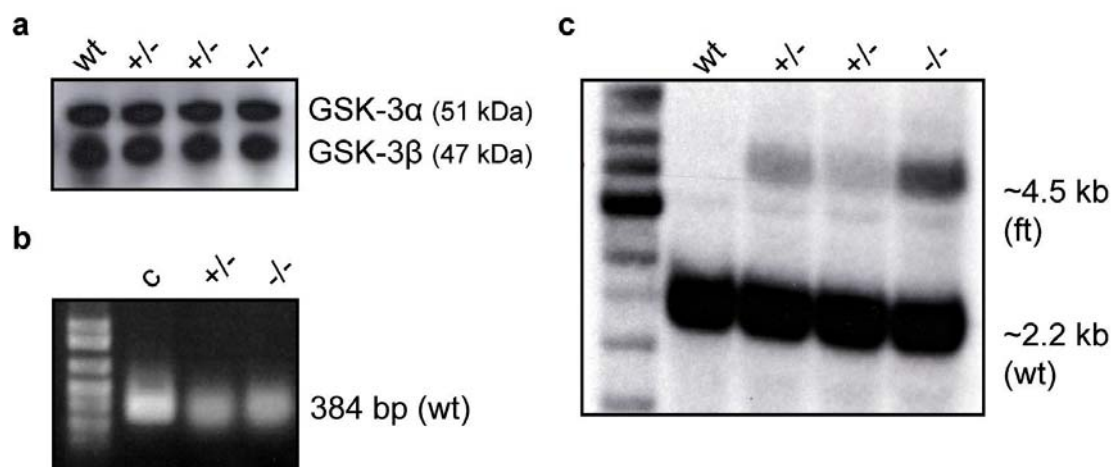


Fig. 12: Analysis of *Gsk-3 α* gene trap mice. In the Western blot of brain protein no reduction of GSK-3 α can be detected in the mutant (+/-; -/-) mice compared to the wild type (wt) mice (a). The *Gsk-3 α* transcript can also be detected by RT-PCR in homozygous (-/-) gene trap mice (b). The amount of fusion transcript (ft) in the mutant mice is very low, as quantified by Northern blot (c). In heterozygous (+/-) mice 3% and in homozygous (-/-) mice 14.5% of the mRNA belong to the fusion transcript. *c*: control cDNA

Further mice were dissected for LacZ staining to check for β -galactosidase (LacZ) activity of the gene trap vector. Whole mount staining of spleen, liver, and kidney of gene trap mice showed a red staining instead of the expected blue color. But an increased red staining was detected in homozygous mice. As positive control a part of wild type small intestine was used, which stained correctly blue. Even brain

sections of the gene trap mice displayed a red staining. Perhaps, this red dye represented the reduced form of the blue indigo dye, normally produced in this staining. This indicated that the function of the LacZ was compromised.

Although the correct splicing of the vector to the *Gsk-3 α* transcript was confirmed before producing the mice, there is still the possibility of splicing out the gene trap vector, which would result in wild type transcript in homozygous gene trap mice. To check for this possibility, a PCR, using the primer pair *Gsk-3 α -Ex1-1* and *Gsk-3 α -Ex3-1*, detecting the wild type transcript was performed on cDNA of mutant mice. Fig. 12b shows a detectable band of 384 bp in the cDNA of the homozygous gene trap mice. This indicated clearly that partially the gene trap vector was spliced out, so that the wild type *Gsk-3 α* transcript was detected.

To analyze the frequency of this event, Northern blot of brain RNA was performed. The ISH probe was used for the detection of *Gsk-3 α* mRNA (see 5.1.1). The fusion transcript of the gene trap vector (4.5 kb) was detected in the heterozygous and homozygous gene trap mice (Fig. 12c), but also the wild type transcript (2.2 kb) was still present at a high rate. Quantification in the homozygous mice showed that 85.5% of the *Gsk-3 α* transcript was wild type mRNA, whereas in the heterozygous mice it were even 97%. This explained why no GSK-3 α protein reduction was observed in the Western blot.

A Southern blot using a neo probe displayed several bands in genomic DNA of gene trap mice, which can be explained by multiple integrations of the gene trap vector into the *Gsk-3 α* locus. Taking all these results together, this could be the reason for the high efficiency of splicing out the gene trap vector. Since no further functional gene trap clones were available, the project was terminated.

5.3 Generation of conditional knockdown mice by RNA interference

Besides knockout mice, an alternative to study the function of a gene is the use of RNA interference. To produce knockdown mice, an expression cassette, containing a short hairpin construct driven by an RNA polymerase III promoter, is integrated into the mouse genome. The produced short hairpin RNAs (shRNAs) are processed by the RNAi machinery and the targeted gene mRNA is silenced (Dykxhoorn et al., 2003). Knockdown mice are comparable to knockout mice, as it was already shown

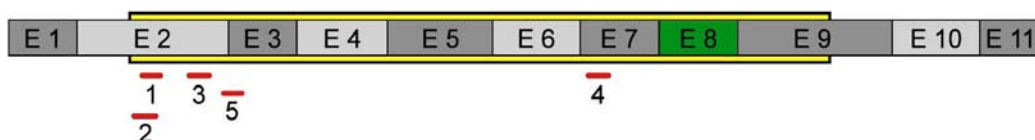
that they are able to produce a similar body wide knockdown phenotype (Kunath et al., 2003). But they also share some of the limitations known for the knockout technique. One problem is the deletion of developmentally essential genes, which may cause embryonic lethality. However, it is possible to apply the same technology used to circumvent this limitation in knockout mice, which is the application of conditional vectors. With this refinement, it is possible to study gene functions in a tissue- and/or time-specific manner (van der Neut, 1997).

For the knockdown mice generated here, the Cre/loxP recombination system was combined with the RNAi strategy. A transcriptional stop element, flanked by loxP sites, was inserted into the loop region of the shRNA. Upon Cre recombinase expression, the transcriptional stop element is cut out, leaving one loxP site behind and the shRNA is activated in the desired tissue (Hitz et al., 2007). To generate knockdown mice for GSK-3, the conditional expression cassette was integrated into the *Rosa26* locus by recombinase mediated cassette exchange (RMCE) to ensure a stable and ubiquitous expression of the shRNAs (Seibler et al., 2005).

5.3.1 Cloning of shRNA vectors

The generation of effective shRNAs is the first and most important step for effective gene silencing. A large number of publications discuss the key elements for effective siRNA and shRNA design, and many public internet tools use these algorithms and modifications to predict functionally effective target sequences (Mittal, 2004; Reynolds et al., 2004; Vermeulen et al., 2005).

Gsk-3 α mouse cDNA (1,473 bp)



Gsk-3 β mouse cDNA (1,260 bp)

Fig. 13: Location of shRNA target sequences in the corresponding *Gsk-3* cDNA. Both *Gsk-3* transcripts are separated in 11 exons. The target sequences for the selected shRNAs are depicted in the cDNA sequence. To silence all splice variants, *Gsk-3 β* exon 8 was avoided (green). Except one, all target sequences are located in the kinase domain (yellow) of GSK-3.

For each *Gsk-3* gene, five shRNA target sequences were chosen by using the following selection tools: Whitehead siRNA Selection Web Server (Yuan et al., 2004), siDirect (<http://genomics.jp/sidirect/>) and BLOCK-iT™ RNAi designer (Invitrogen, <https://rnaidesigner.invitrogen.com/rnaiexpress/>). One shRNA for *Gsk-3β* (*Gsk-3β*-sh5) was already published as functional and effective (Yu et al., 2003). The length of the siRNA core sequence varied from 19 to 23 nt. The target sequences were chosen to be specific for each *Gsk-3* gene and to target all splice variants of *Gsk-3β*, exon eight was excluded (Fig. 13). Detailed information is given in Tab. 1.

shRNA	target sequence	length	designed by	oligonucleotides
Gsk-3α-sh1	GCT CAT TCG GAG TAG TAT ACC	21 nt	BLOCK-iT™	Gsk-3α-sh1 A/B
Gsk-3α-sh2	GCT GGA CCA CTG CAA TAT TGT	21 nt	BLOCK-iT™	Gsk-3α-sh2 A/B
Gsk-3α-sh3	GGG AAC AAA TCC GAG AGA TGA	21 nt	BLOCK-iT™	Gsk-3α-sh3 A/B
Gsk-3α-sh4	GGC CCA GAG CGT TCC CAA GAA	21 nt	Whitehead siRNA SWS	Gsk-3α-sh4 A/B
Gsk-3α-sh5	GAC ATC AAG CCC CAG AAT T	19 nt	siDirect	Gsk-3α-sh5 A/B
Gsk-3β-sh1	GTG ATT GGA AAT GGA TCA T	19 nt	Whitehead siRNA SWS	Gsk-3β-sh1 A/B
Gsk-3β-sh2	GAC ACG AAA GTG ATT GGA AAT GG	23 nt	siDirect	Gsk-3β-sh2 A/B
Gsk-3β-sh3	GGT TGC CAT CAA GAA AGT TCT	21 nt	BLOCK-iT™	Gsk-3β-sh3 A/B
Gsk-3β-sh4	GCT GTG TGT TGG CTG AAT TGT	21 nt	BLOCK-iT™	Gsk-3β-sh4 A/B
Gsk-3β-sh5	GAA CCG AGA GCT CCA GAT C	19 nt	Yu et al. (2003)	Gsk-3β-sh5 A/B

Tab. 1: ShRNAs against *Gsk-3α* and *Gsk-3β*. For each shRNA, the target sequence, its length, the selection tool, and the oligonucleotides used for cloning are given. The sequences of the oligonucleotides are listed in the material section (3.5.8.4).

The oligonucleotides for cloning were designed that the annealing of oligonucleotide A and oligonucleotide B forms a stable double stranded DNA fragment with overhanging sticky ends. These DNA fragments were cloned into the pBluescript vector, containing the human U6 promoter. The H1 promoter is also able to drive the expression of shRNA constructs (Brummelkamp et al., 2002; Paddison et al., 2004), but Hitz et al. showed that for my purpose the human U6 promoter is the most effective one (Hitz et al., 2007). At the 3' end of the U6 promoter coding sequence a BseRI restriction site is located, which was used, together with a BamHI restriction site, to open the vector. The annealed oligonucleotides were ligated into the vector and the product was redigested with BamHI to increase cloning efficiency. The plasmids were transformed into DH5α competent bacteria, and ampicillin resistant

colonies were screened by digestion with PstI and HindIII restriction enzymes. Positive clones, containing the shRNA, displayed two fragments (300 bp and 3.0 kb) in the gel, whereas the empty vector showed one fragment (3.2 kb). Plasmids were sequenced with M13 for and rev primer and one clone each, with correct shRNA sequence, was used for further cloning.

5.3.2 Cloning of conditional shRNA vectors

To gain control over the expression of shRNA in a time- and tissue-specific manner, the Cre/loxP recombination system was combined with the RNAi strategy. Therefore, a transcriptional stop element, flanked by loxP sites, was inserted into the loop region of the shRNAs. It has been evaluated that this position was the best for controlling the shRNA and maintaining knockdown efficiency (Hitz et al., 2007). After insertion of the transcriptional stop element, the transcription of the shRNA is terminated after the loop region, producing an inactivated RNA consisting of the sense strand of the shRNA and parts of the stop element. After Cre mediated recombination, the stop element is deleted, leaving one of the loxP sites behind. The remaining loxP site enlarges the loop of the shRNA by 34 bp, but does not interfere with the function of the shRNA (see Fig. 16/17, 5.3.4.2). Thereby the Cre/loxP system allows to control shRNA activity in a time- and tissue-specific manner.

The 863 bp transcriptional stop element (stop cassette) consists of a 679 bp fragment of the neomycin coding region, which serves as stuffer DNA, flanked by wild type loxP sites (34 bp each) and contains three oligothymidine regions as transcriptional termination signals for RNA polymerase III. In addition, I used a modified version of this stop cassette containing mutant lox2272 sites instead of wild type loxP sites. The lox2272 sites are recombined by Cre recombinase like wild type sites, but are not recombined with loxP sites itself (Siegel et al., 2001). The use of two different stop cassettes offers the possibility of combining two shRNAs in one vector (Steuber-Buchberger et al., 2008; see also 5.3.5).

The loxP flanked stop cassette was cloned by opening pNEB-loxP-RLuc-loxP, a plasmid containing two wild type loxP sites, with EcoRI and NarI and ligation with a NarI and XbaI fragment from plasmid pgk-neo-bpa as spacer. The stop cassette was recovered as an 863 bp MlyI fragment for subsequent cloning. The lox2272 flanked stop cassette was cloned by ligating the lox2272 oligonucleotide pair into pBluescript, which has been opened with XbaI and EcoRI. The resulting plasmid was opened with

BamHI and ligated with a BamHI fragment of the basic loxP stop cassette vector containing the spacer. For subsequent cloning, the lox2272 stop cassette was isolated as 863 bp MlyI fragment.

The shRNA vectors were opened via the HindIII site in the loop region and blunt ends were created by large (Klenow) fragment of *E.coli* DNA polymerase I. The 863 bp MlyI fragment, containing the stop cassette, was ligated into the shRNA vector and positive clones displayed an 852 bp and a 3.3 kb fragment in the gel. In opposite orientation a 145 bp and 4.0 kb fragment were detected. The empty vector showed a single fragment of 3.3 kb. Clones were confirmed by sequencing with M13 for and rev primer and one clone each was used for further cloning.

5.3.3 Cre mediated recombination of conditional shRNA vectors

To test the efficiency of Cre mediated conditional shRNAs, the stop cassette was cut out *in vitro* using Cre recombinase protein. For this purpose the conditional shRNA vector was incubated with Cre enzyme for one hour at 37°C, before inactivation of the reaction at 70°C for 10 min. Afterwards the reaction was digested with EcoRI to linearize unrecombined vector. The plasmid was transformed into DH5α bacteria and clones were screened by digestion with XbaI. Recombined clones shifted the 1.3 kb band to 460 bp, showing both an additional band with ~2.8 kb. Correct excision was confirmed by sequencing.

5.3.4 Tests for knockdown efficiency of shRNAs

To achieve sufficient knockdown of the target gene, the identification of effective shRNAs is crucial. Public siRNA prediction programs were used to design functional shRNAs. Despite the use of such prediction programs, each shRNA construct has to be confirmed for functionality and its efficiency *in vitro*.

5.3.4.1 Real-time qRT-PCR of transfected ES cells

There are several ways of controlling the functionality of shRNAs. One approach is to check the reduction of the targeted mRNA by real-time qRT-PCR. This was performed by our cooperation partner Cenix BIOSCIENCE. For this purpose $3 \cdot 10^6$ IDG3.2 ES cells were transiently transfected with 20 µg shRNA plasmid DNA at 320 V for 3 ms. Cells were grown for two days, harvested and the lysed cell pellet was frozen at -80°C and sent to the cooperation partner. They measured each target

gene in triplicate and calculated the relative remaining mRNA for target versus 18S rRNA levels, comparing the samples versus the transfection vector controls. Fig. 14 shows the results for *Gsk-3 α* and *Gsk-3 β* mRNA reduction. All shRNAs against *Gsk-3 α* , except *Gsk-3 α -sh2*, resulted in mRNA levels below the given threshold of 30% remaining mRNA. Three shRNAs against *Gsk-3 β* reached this threshold: *Gsk-3 β -sh1*, *Gsk-3 β -sh2*, and *Gsk-3 β -sh4*. The other two shRNAs, especially *Gsk-3 β -sh3*, showed high variation and low mean knockdown efficiencies.

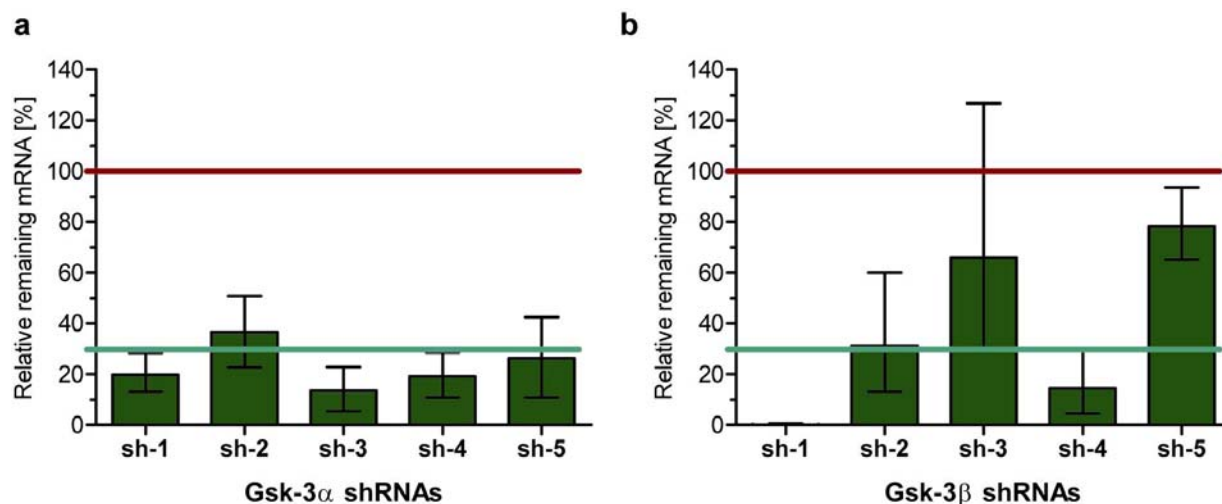


Fig. 14: Real-time qRT-PCR for *Gsk-3* shRNAs upon transfection into ES cells. IDG3.2 ES cells were transfected with shRNAs against *Gsk-3 α* and *Gsk-3 β* , respectively and real-time qRT-PCR was performed. In the left panel the results for *Gsk-3 α* are displayed. The shRNAs *Gsk-3 α -sh1*, *Gsk-3 α -sh3*, and *Gsk-3 α -sh4* showed the highest knockdown efficiency, reducing *Gsk-3 α mRNA* below the threshold of 30% (a). In the right panel the shRNAs *Gsk-3 β -sh1*, *Gsk-3 β -sh2* and *Gsk-3 β -sh4* achieved the best reduction of *Gsk-3 β mRNA*, whereas *Gsk-3 β -sh3* and *Gsk-3 β -sh5* performed poor (b).

Although the transfection efficiency by electroporation is approximate 90%, 10% of non-targeted cells remain, which negatively influence the overall knockdown results. Despite this fact it was possible to estimate that some of the selected shRNAs exhibit high capacity to knockdown the targeted genes.

5.3.4.2 pScreeniT™ system of Invitrogen

During this efficiency tests, another approach was used to test the function of shRNAs at the mRNA level. In a commercially available screening system from Invitrogen, the cDNA of the targeted gene is cloned in frame with the lacZ coding region to obtain a fusion transcript of lacZ and the targeted gene. The reduction of LacZ activity can be quantified as a measure of effective degradation of the fusion mRNA. The pScreeniT™ vector, containing lacZ, was modified by deleting an unnecessary fragment of 1.7 kb (PmeI/XhoI) and insertion of a 102 bp multiple

cloning site (MCS) from pBluescript (SacI/KpnI). Into this MCS, the cDNA of *Gsk-3 α* or *Gsk-3 β* was cloned in frame to the lacZ open reading frame (ORF).

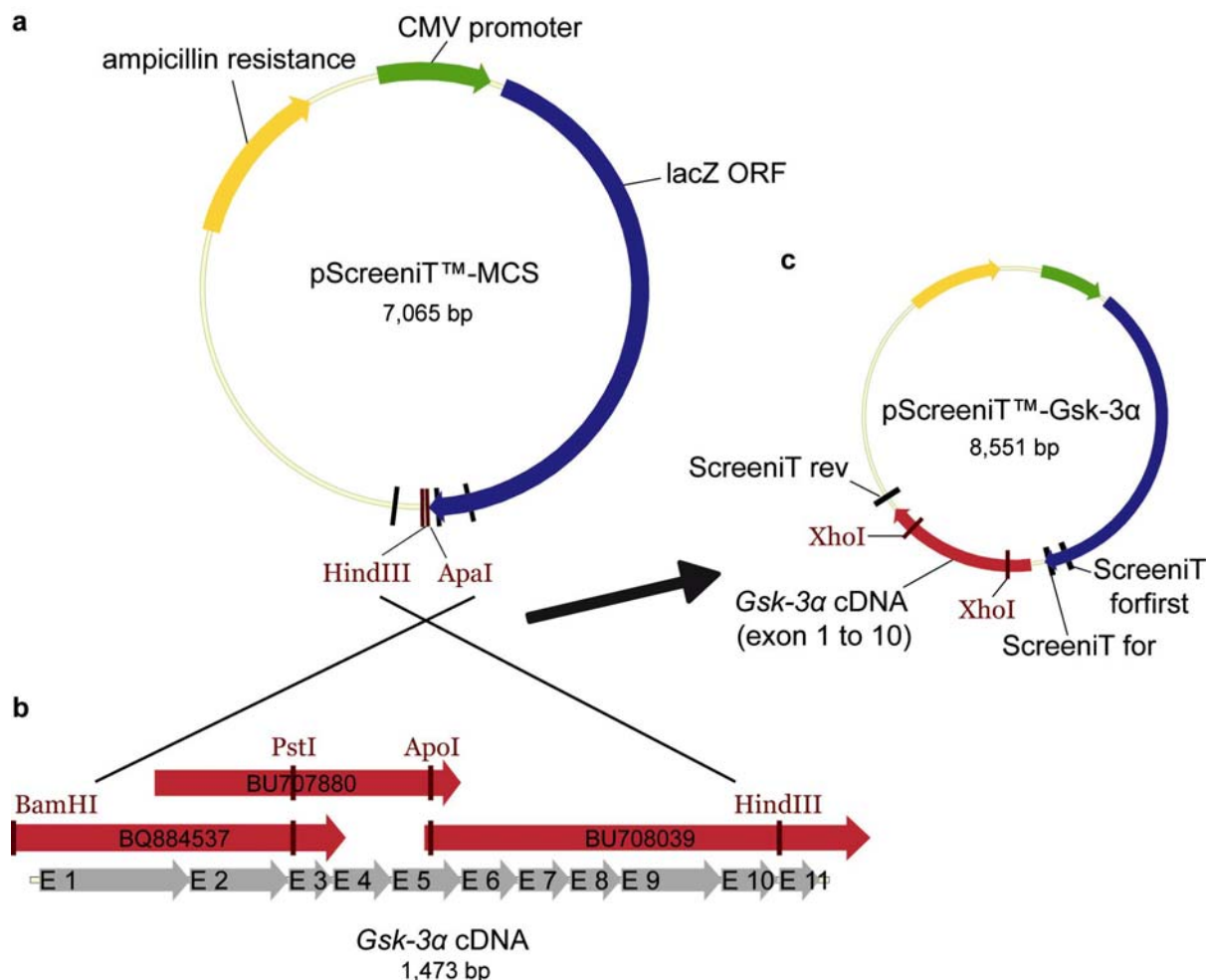


Fig. 15: Cloning of the pScreenIT™ *Gsk-3 α* cDNA vector. The *Gsk-3 α* cDNA was combined from three EST clones, covering the whole cDNA sequence. The pScreenIT™-MCS vector was opened with ApaI and HindIII (a) and ligated with the three EST fragments via the HindIII site and the filled BamHI/ApaI site (b). The created pScreenIT™ *Gsk-3 α* cDNA vector was checked by XhoI digest and was sequenced with ScreenIT for, ScreenIT forfirst, and ScreenIT rev (c).

The cDNA of *Gsk-3 β* (1.5 kb) was recovered from the plasmid pIRAK p961P0751.1 restriction digest with XbaI and SmaI. A cDNA vector for *Gsk-3 α* was not available, so the first 1,343 bp of the cDNA (exon 1 to 10) were combined from the three EST clones BQ884537, BU708039, and BU707880 (Fig. 15). The pScreenIT™ plasmid was opened with ApaI and the restriction site was filled with Klenow. After inactivation, the vector was further digested with HindIII and dephosphorylated. BQ884537 was digested with BamHI, filled with Klenow and digested further with PstI. BU708039 was digested with PstI and ApoI, and BU707880 with ApoI and HindIII. The final pScreenIT™ cDNA vectors were sequenced with ScreenIT for, ScreenIT forfirst and ScreenIT rev primers.

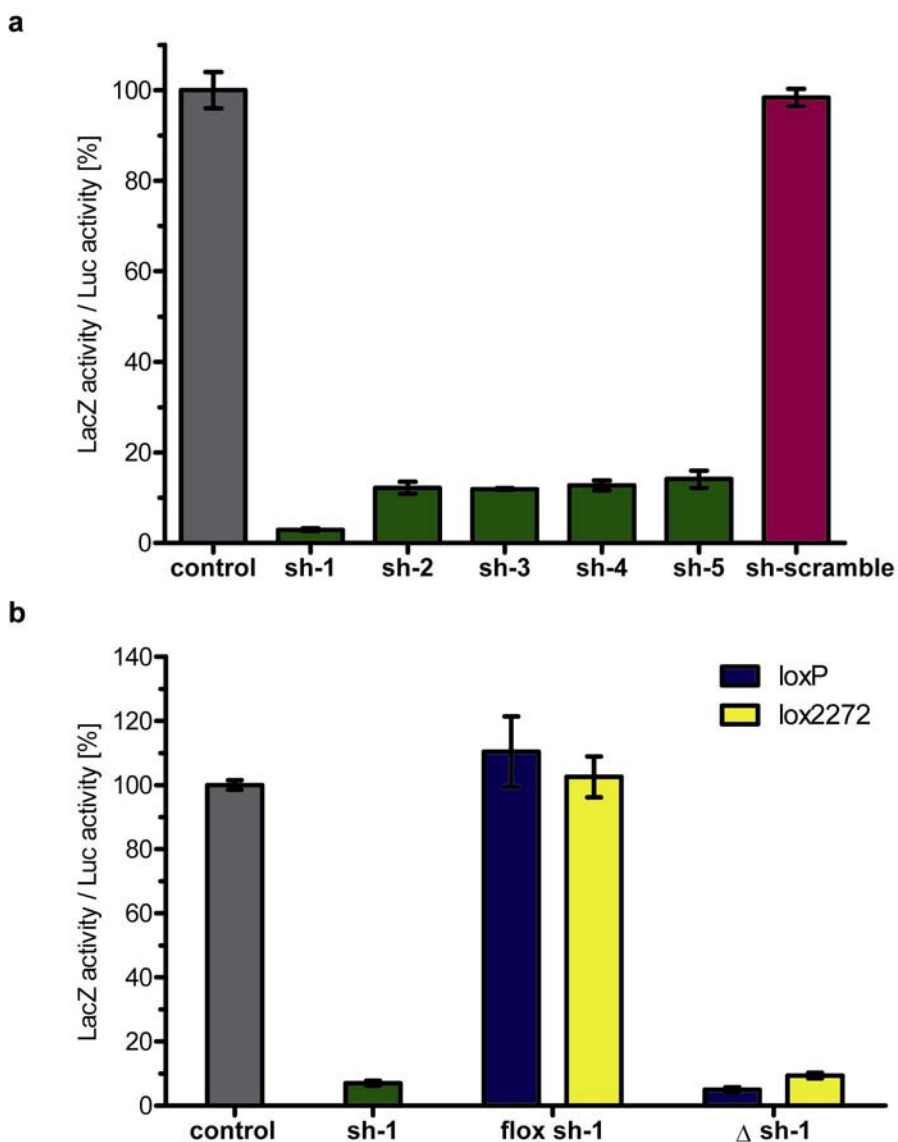


Fig. 16: ShRNA efficiency for *Gsk-3 α* in the pScreeniT™ system. IDG3.2 ES cells were transfected with shRNAs against *Gsk-3 α* and the *Gsk-3 α* cDNA pScreeniT™ vector. In the upper panel (a) the non-conditional shRNAs were tested and *Gsk-3 α* -sh1 was the most efficient (3% LacZ rest activity). The lower panel (b) displays the results of *Gsk-3 α* -sh1 with the integrated (flox) and deleted (Δ) stop cassette in comparison to the non-conditional situation. Error bars represent the SEM. control: IDG3.2 ES cells transfected with *Gsk-3 α* cDNA pScreeniT™ vector, sh-scramble: nonsense shRNA

ES cells were co-transfected with the pScreeniT™ cDNA vector, the corresponding shRNA vector, and a third plasmid containing a firefly-Luciferase gene (Luc) for normalization. The *lacZ-Gsk-3* fusion transcript should be targeted in ES cells by the transfected shRNA and the decrease of LacZ activity was measured after two days. The reduction of LacZ activity in cell lysates should indicate the knockdown efficiency of the shRNA. To normalize experimental variation, the activity of the co-transfected Luc was measured as well, and the data set was normalized with these values. Each transfection experiment was repeated three times to get reliable results.

The results for the *Gsk-3 α* shRNAs are depicted in Fig. 16. In comparison to a transfected nonsense shRNA (sh-scramble), the knockdown of the *lacZ-Gsk-3* fusion transcript worked quite well for all five *Gsk-3 α* specific shRNAs. *Gsk-3 α -sh1* was the most effective shRNA, achieving the maximum knockdown of 3% remaining LacZ activity. The other four shRNAs varied between 12 and 14% residual LacZ activity. Additionally, the *Gsk-3 α -sh1* shRNA was tested after the integration of the stop cassette into the loop region, and upon deletion of the stop cassette by Cre recombinase (Fig. 16b). As expected, the integration of the stop cassette inactivated the silencing of the fusion mRNA such that LacZ activity was unchanged compared to the control. Upon Cre mediated deletion of the stop cassette, the reactivated *Gsk-3 α -sh1* shRNA, containing the remaining loxP site in the loop region, silenced the fusion mRNA to the same extent as in the non-conditional state. The same results were obtained for the modified stop cassette flanked by lox2272.

In Fig. 17 the results for the *Gsk-3 β* shRNAs are shown. As positive control a shRNA against the *lacZ* transcript was transfected (sh-*lacZ*), which reduced LacZ activity by 95% compared to the pScreeniT™ cDNA vector. The reduction achieved by the *Gsk-3 β* shRNAs varied. *Gsk-3 β -sh1* reduced the activity of LacZ to 8%, whereas *Gsk-3 β -sh3* and *Gsk-3 β -sh5* reached only 51% and 37%, respectively. The two most promising shRNAs, *Gsk-3 β -sh2* and *Gsk-3 β -sh4*, reduced LacZ activity to 2%, achieving a knockdown of 98%. These shRNAs were further equipped with the loxP and the lox2272 stop cassettes (Fig. 17b). As seen for the *Gsk-3 α* shRNAs, the integration of the stop cassettes prevented the production of functional shRNAs and LacZ activity was unchanged compared to the control vector. After Cre mediated deletion of the inhibitory stop cassette, both shRNAs regained full activation of gene silencing.

The pScreeniT™ system is easy to handle and offers quick testing of shRNA function. The results of Real-time qRT-PCR could be partly confirmed, but the pScreeniT™ system has a certain disadvantage, because of the used fusion mRNA. The fusion transcript might display another secondary structure than the native *Gsk-3* mRNA, and this structural difference may expose the target sequences differentially to the shRNAs compared to the state *in vivo*. This difference could influence the efficiency of the tested shRNAs.

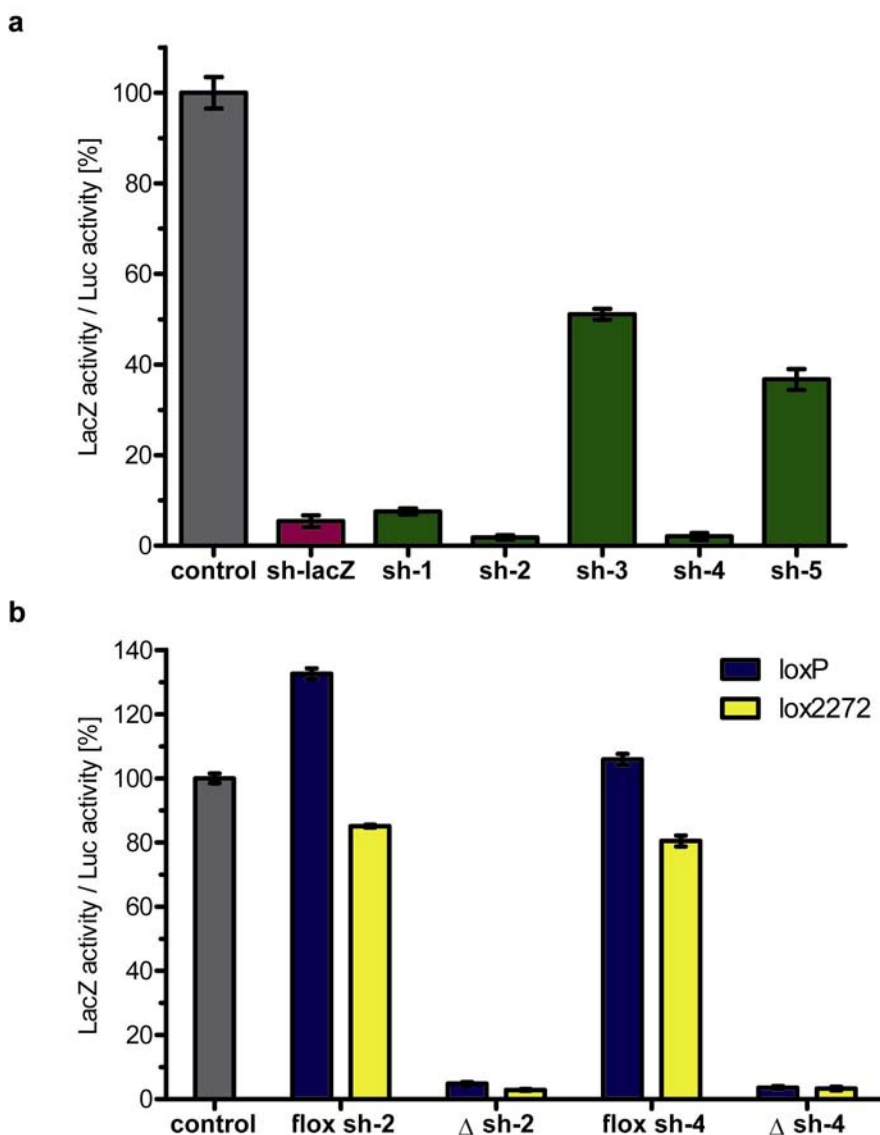


Fig. 17: ShRNA efficiency for *Gsk-3β* in the pScreeniT™ system. IDG3.2 ES cells were transfected with shRNAs against *Gsk-3β* and the *Gsk-3β* cDNA pScreeniT™ vector. In the upper panel (a) the non-conditional shRNAs were tested and *Gsk-3β*-sh2 and *Gsk-3β*-sh4 showed the highest efficiency (2% LacZ rest activity). The lower panel (b) displays the results of *Gsk-3β*-sh2 and *Gsk-3β*-sh4 with the integrated (flox) and deleted (Δ) stop cassette. Error bars represent the SEM. control: IDG3.2 ES cells transfected with *Gsk-3β* cDNA pScreeniT™ vector, sh-lacZ: shRNA against lacZ transcript

5.3.4.3 Knockdown of GSK-3 in transfected ES cells

Since the translation of mRNA into protein is not strictly correlated due to posttranscriptional and modifying processes, the knockdown efficiency of the shRNA should be confirmed on the protein level. To assess protein knockdown, $3 \cdot 10^6$ IDG3.2 ES cells were transiently transfected with 20 μ g shRNA plasmid DNA at 320 V for 3 ms. Transfected cells were further grown for two days, harvested and the cell pellet was lysed in RIPA protein buffer. The total amount of protein was measured and

10 µg were loaded to a SDS polyacrylamide gel and subsequently transferred to a PVDF membrane. GSK-3 proteins were detected with a specific antibody, visualizing a band of 51 kDa for GSK-3 α and a band of 47 kDa for GSK-3 β . An HPRT antibody was used as loading control. The GSK-3 signals were quantified by the ImageJ software (Abramoff et al., 2004) in relation to the HPRT signals.

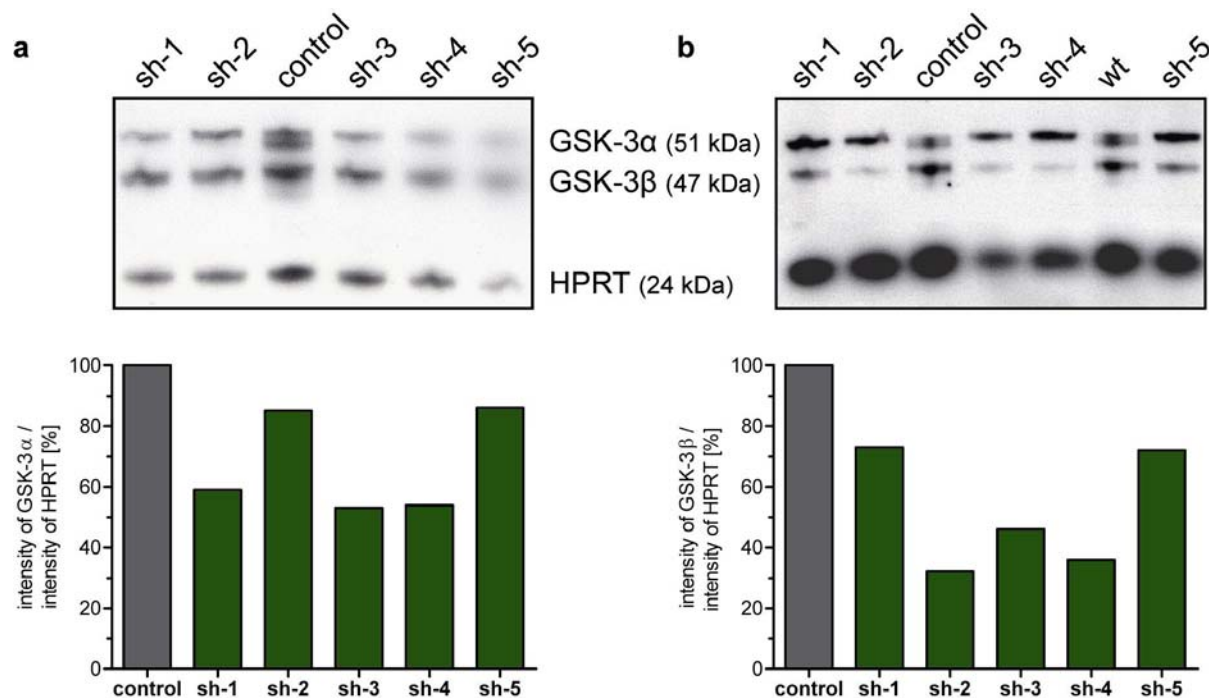


Fig. 18: Knockdown of GSK-3 proteins in the Western blot of shRNA transfected ES cells. IDG3.2 ES cells were transfected with shRNAs against GSK-3 α and GSK-3 β , respectively. In the left panel the results for GSK-3 α are displayed. The shRNAs Gsk-3 α -sh1, Gsk-3 α -sh3, and Gsk-3 α -sh4 showed the highest knockdown efficiency, reducing GSK-3 α to 59%, 53%, and 54% (a). In the right panel the shRNAs Gsk-3 β -sh2 and Gsk-3 β -sh4 achieved the best reduction of GSK-3 β protein to 32% and 36% (b). *control: not transfected IDG3.2 ES cells*

Quantification results and corresponding Western blot signals are depicted in Fig. 18. It is obvious that the knockdown on protein level was not as strong as seen at the mRNA level. One reason for this are the non-transfected ES cells, which remain in the culture and increase the experimental background due to normal GSK-3 levels. The shRNAs Gsk-3 α -sh1, Gsk-3 α -sh3, and Gsk-3 α -sh4 showed the highest knockdown efficiency, reducing GSK-3 α to 59%, 53%, and 54%. In case of GSK-3 β , the shRNAs Gsk-3 β -sh2 and Gsk-3 β -sh4 again showed the strongest reduction of GSK-3 β protein down to 32% and 36%, respectively.

Another important aspect of testing shRNA efficiency in Western blot analysis is the specific targeting of the selected gene. By co-detecting both Gsk-3 genes in the Western blot, I could exclude an influence of the corresponding shRNAs to the

non-targeted gene, which was clearly visible by the unaffected *Gsk-3 β* bands in Fig. 18a. The same result was found for *Gsk-3 α* , as showed in Fig. 18b.

5.3.5 Simultaneous conditional knockdown of two genes in mice

It has been already shown that shRNA vectors driven by the U6 promoter can be placed one after another without disrupting the RNAi mechanism (Jazag et al., 2005). Since the conditional aspect of the knockdown strategy was crucial for the purpose of the present work, I combined the use of multiple shRNAs with the Cre/loxP recombination system. I already introduced the necessary tool for this step in section 5.3.2. Mutated loxP sites are incompatible with the wild type loxP sites and therefore can be used in combination with the wild type sites without interrupting the correct function of the stop cassettes. These sites enable the simultaneous conditional knockdown of two genes (Steuber-Buchberger et al., 2008).

The principle of this strategy is shown in Fig. 19. As for single conditional shRNA vectors, the stop cassettes are cloned via the HindIII restriction site into the shRNA and the single conditional shRNA expression cassettes are combined into a pRMCE vector containing functions for recombinase mediated cassette exchange (RMCE). After integration of the two conditional shRNA expression cassettes into the target locus, both shRNAs remain inactive due to the inserted stop cassettes. Upon Cre expression in ES cells or tissue, both stop cassettes are deleted, each leaving one lox site behind. These remaining lox sites do not interfere with shRNA transcription, resulting in two active shRNAs both able to silence their target genes.

Two double shRNA vectors were constructed and the used shRNAs were selected based on the efficiency tests. The first vector contained *Gsk-3 β -sh2* combined with *Gsk-3 α -sh1*, and the second vektor combined *Gsk-3 β -sh4* with *Gsk-3 α -sh1*. The double shRNA vectors were handled the same way as single shRNA vectors, only for sequencing some modifications were necessary due to the increased plasmid size.

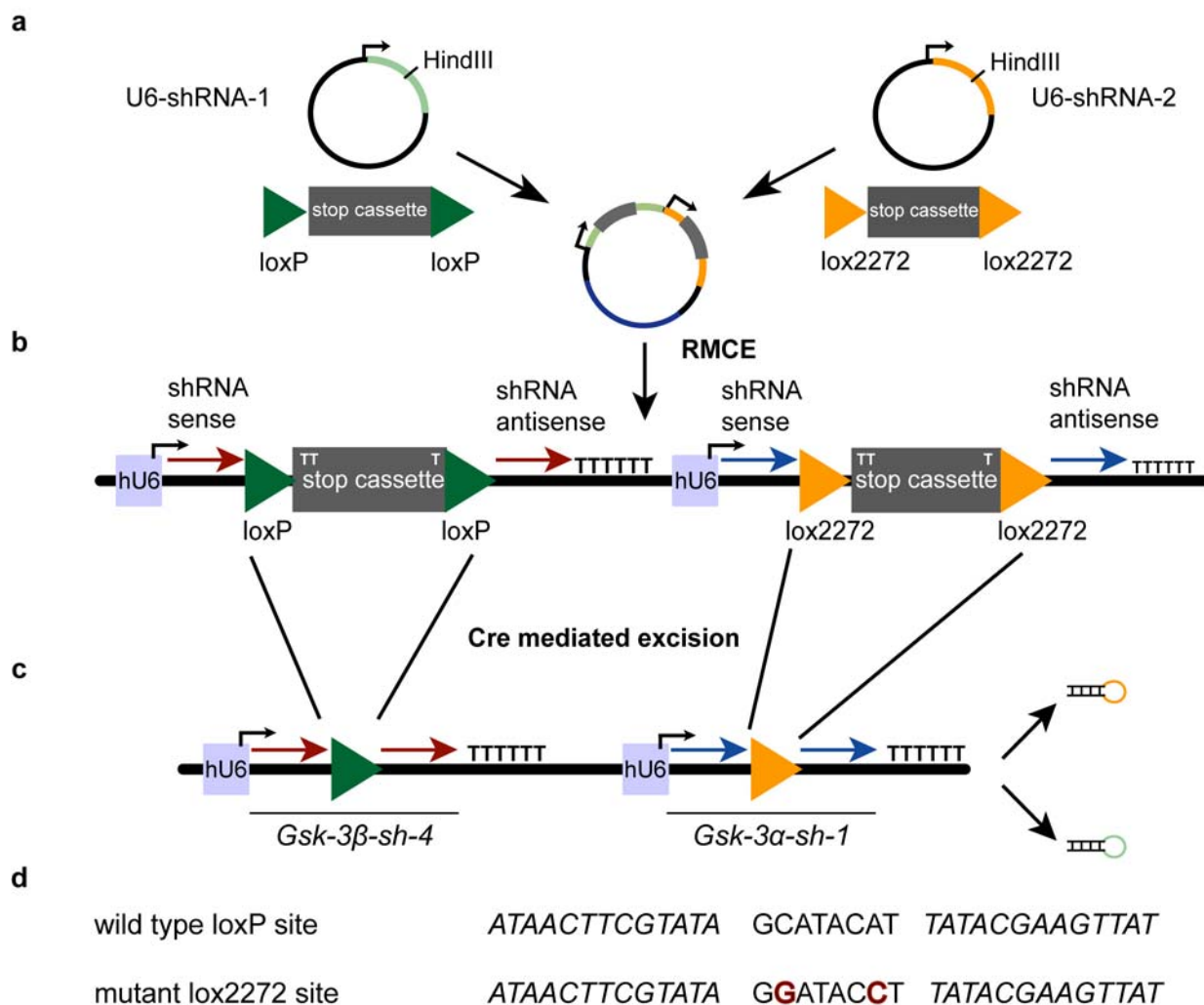


Fig. 19: Principle of double-conditional shRNA constructs. U6 promoter driven shRNA vectors are disrupted in the loop region by a transcriptional stop element (stop cassette), flanked by a pair of loxP or lox2272 sites, respectively. The conditional shRNA units are combined into a double shRNA vector that contains functions for RMCE by C31 Integrase (a). The double shRNA vector is integrated into the *Rosa26* locus of ES cells by RMCE (b). Upon Cre recombination of the double shRNA vector both stop cassettes are excised; one lox site remains within each shRNA loop region but does not interfere with shRNA activity (c). The sequence of loxP and lox2272 differs in two nucleotides of the spacer region. Inverted repeats are in italic and the mutant nucleotides of lox2272 site are shown in red (d).

5.3.6 Integration of shRNAs into ES cells by RMCE

On basis of the three efficiency tests, shRNA vectors for stable integration into ES cells and subsequent production of knockdown mice were selected. Since they performed best in all tests, the *Gsk-3β-sh2* and *Gsk-3β-sh4* shRNA vectors were chosen. Due to the high reproducibility in the efficiency tests, this shRNAs should enable sufficient knockdown *in vivo*. For the *Gsk-3α* gene one of the three candidates, *Gsk-3α-sh1*, *Gsk-3α-sh3*, and *Gsk-3α-sh4*, was chosen. The results from Real-time qRT-PCR and Western blot were very similar for the three shRNAs, but the

Gsk-3 α -sh1 performed best in the pScreeniT™ system. Therefore, it was selected for production of Gsk-3 α knockdown mice.

Conditional shRNA expression cassettes were integrated into the mouse genome via recombinase mediated cassette exchange (RMCE) into the *Rosa26* locus. A well characterized genomic location for the integration of transgenes is the *Rosa26* locus on mouse chromosome six. It was shown that a single copy integration of a shRNA vector in *Rosa26* triggers stable and effective body-wide gene silencing (Seibler et al., 2005; Yu and McMahon, 2006). The homozygous deletion of the *Rosa26* locus does not cause a phenotype in mice and offspring are viable and fertile. The *Rosa26* locus is active in ES cells and during embryonic development, which facilitates the use of shRNAs for gene silencing in the early embryo (Soriano, 1999). The directed integration of a single copy into a defined genomic locus is preferred to random integration of multiple copies, because of unpredictable Cre mediated recombination events, which could occur between multiple integration cassettes.

To insert the shRNA expression cassettes into ES cells by RMCE, the wild type *Rosa26* locus was modified into an acceptor allele (*Rosa26.10*). Attachment sites for integrase of phage Φ C31 (C31Int) were inserted into the *Rosa26* locus of IDG3.2 ES cells together with a pgk promoter driven hygromycin resistance gene (Fig. 20b). The hygromycin coding sequence and the polyA signal between these attP sites can be exchanged by C31Int with any sequence flanked by attB sites. Suitable pRMCE vectors carry a promoterless neomycin resistance gene with a polyA signal and the conditional shRNA expression cassette, flanked by attB sites (Fig. 20c). Upon co-transfection of the pRMCE vector with a C31Int expression plasmid into acceptor ES cells (IDG3.2-26.10-3), the exchange of flanked sequences occurs, shifting the hygromycin resistance to neomycin, which allows the selection of exchanged ES cell clones (Fig. 20d). During this recombination the attP and attB sites are transformed into incompatible attL and attR sites, leaving a stable integration in the genome. FRT sites flanking the pgk promoter and the neomycin resistance gene enable the deletion of this sequence by Flp recombinase in ES cells or in mice.

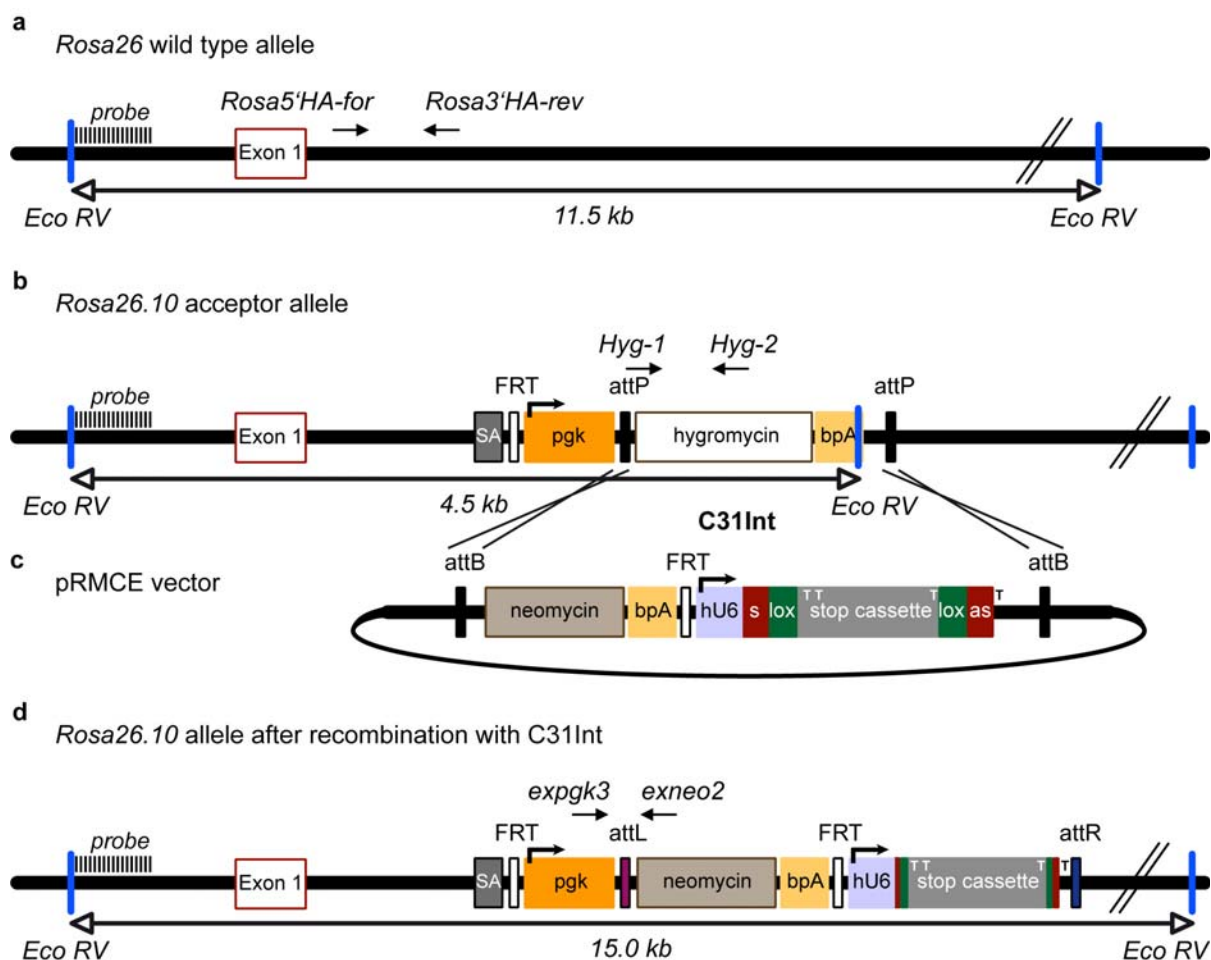


Fig. 20: Stable integration of shRNAs into ES cells via RMCE. For stable integration of shRNAs the *Rosa26* locus was used (a). First, attachment sites for C31Int (attP sites) were introduced into the genome, together with a *pgk* promoter and a hygromycin resistance gene to create an acceptor allele for RMCE (b). Second, a pRMCE vector, carrying a second type of attachment sites (attB sites), which flank a neomycin resistance gene and the shRNA expression cassette, was transfected together with a C31Int expression plasmid into acceptor ES cells (c). After the recombination event the attB flanked sequence with the shRNA expression cassette was stably integrated into the *Rosa26* locus and the recombined ES cell clones could be selected for their neomycin resistance. The attP and attB sites are recombined into attL and attR sites, which are no longer compatible with each other (d).

The single conditional pRMCE-shRNA vectors were constructed using the 3-fragment ligation technique (4.1.1.5). The pRMCE donor vector was opened with *Asi*I and *Sfi*I, and to enhance the cloning efficiency the vector was additionally digested with *Scal*. The 3.1 kb fragment of the *Asi*I/*Scal* digest and the 1.2 kb fragment of the *Sfi*I/*Scal* digest were ligated with the conditional shRNA expression cassette obtained with *Asi*I and *Sfi*I from the conditional shRNA vectors (5.3.2). The pRMCE-shRNA vectors were sequenced with M13 for and bpA primers. For the construction of the double pRMCE-shRNA vectors, the single pRMCE-shRNA vectors, containing the conditional *Gsk-3 β* shRNA, were opened with *Spe*I and

dephosphorylated. The conditional Gsk-3 α -sh1 expression cassette with lox2272 sites was isolated as an XbaI fragment and cloned into the single pRMCE-shRNA vector, containing one of the Gsk-3 β shRNAs. Recombinant colonies showed bands at 1.3 and 5.5 kb, and were recombined with Cre enzyme. Recombined clones showed after digestion with SacI a shift from 3.0 kb to a 1.4 kb band. These clones were sequenced and confirmed clones and parental vectors were used for further experiments.

5.3.7 Transfer of shRNAs into ES cells

To insert the conditional shRNA expression cassettes into the *Rosa26* locus by RMCE, the pRMCE-shRNA vector was electroporated into acceptor ES cells (IDG3.2-26.10-3) together with a C31Int expression plasmid. Since the correct recombination event occurs at a frequency of 40 to 60% among neomycin resistant ES cell colonies, I selected from each electroporation 24 neomycin resistant ES cell clones.

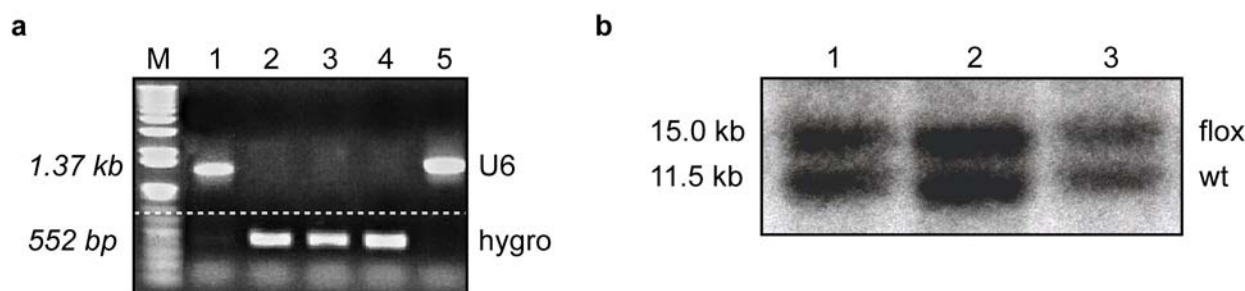


Fig. 21: Analysis of neomycin resistant ES cell clones by PCR and Southern blot. Resistant ES cell clones were screened first by PCR. After a successful exchange event the primer pair U6 for and Rosa3'HA-rev2 (U6) could amplify a 1.37 kb band in the resistant clones (lane 1 and 5) covering the sequence of the U6 promoter to the 3' integration site. Where no exchange took place the Hyg-1 and Hyg-2 (hygro) primer pair could still amplify the 552 bp band (lane 2 - 4) of the hygromycin resistance gene (a). ES cell clones positive for the exchange were confirmed by Southern blot. After digestion of the genomic DNA with EcoRV and detection with the Rosa5'probe, all clones displayed a 11.5 kb band for the wild type locus (wt). Correct integration of the pRMCE-shRNA vector was indicated by an additional 15.0 kb band (flox), which can be seen in lanes 1 - 3. Clones without integration would raise a 4.5 kb band and partial cassette exchange would give a 10.0 kb band (b).

These clones were screened by PCR and analyzed by Southern blotting for the correct integration into the *Rosa26* locus. Genomic DNA of selected ES cell clones was amplified with the primer pair U6-for and Rosa3'HA-rev2 to screen for clones with complete integration of the expression cassette. This PCR reaction amplifies the expression cassette from the U6 promoter to the 3' *Rosa26* integration site. Due to

the size of the stop cassette, the PCR amplifies a 1.37 kb band from the conditional vector. To confirm the loss of the hygromycin gene by RMCE, the primer pair Hyg-1 and Hyg-2 was used. The absence of the 552 bp band indicated the loss of the hygromycin resistance gene. Clones positive for the expgk3/exneo2 PCR and negative for the Hyg-1/Hyg-2 PCR were regarded to contain a correct cassette exchange event (Fig. 21a). As alternative to the U6 for/Rosa3'HA-rev2 PCR, the primer pair expgk3 and exneo2 could be used to screen for all clones with a successful integration of the expression cassette downstream of the pgk promoter (280 bp band). This PCR could give rise to an additional band of ~180 bp, amplified from residual feeder cells of the ES cell culture.

The genotype of recombined ES cell clones, identified by PCR, was confirmed by Southern blot analysis. Genomic DNA was digested with EcoRV and hybridized with the Rosa5'probe, a 448 bp fragment from the pCRII-Rosa5'probe vector (digested with EcoRI, see Fig. 20 for location of the probe and EcoRV restriction sites). All clones showed an 11.5 kb band of the wild type *Rosa26* locus and correct recombined clones displayed additionally a 15.0 kb band (double shRNAs 16.3 kb). Unrecombined clones, which still carry the hygromycin resistance, showed a 4.5 kb band derived from the acceptor allele. In case of partial recombination, that is the integration of the complete pRMCE-shRNA vector sequence, a 10.0 kb band would be seen (Fig. 21b) and the Hyg-1/Hyg-2 primer pair would amplify the 552 bp product. Confirmed ES cell clones were expanded and frozen in liquid nitrogen until injection into blastocysts.

5.3.8 Generation of conditional knockdown mice

Genetically modified ES cells were thawed, cultivated and injected into mouse blastocysts for the generation of chimeric mice. To increase injection efficiency, the ES cells were kept at least 48 h without antibiotic selection. Injected blastocysts were transferred into pseudo-pregnant foster mothers and after 17 days chimeras were born. Besides injection of ES cells into the blastocoel to let them contribute to the inner cell mass of the blastocyst, it is possible to generate complete ES cell-derived mice via tetraploid embryo aggregation (Nagy et al., 1993). Using this technique, mutations are transferred into the germline from beginning on and the tetraploid derived animals already represented the first animals of the newly established mouse

line. However, a problem is the low frequency (approximate 2%) of viable offspring, so this technique was used only in addition to blastocyst injection.

Tab. 2 shows ES cell clones used for blastocyst injections and tetraploid embryo aggregation, as well as the derived knockdown mouse lines. In nearly all cases, the ES cells were capable of generating germline chimeras or even tetraploid derived animals as for the lines *Gsk-3-flox-dh* and *Gsk-3-flox-dh2*, which are based on these founder animals.

mouse line	ES cell clones	no. of animals from aggregation	no. of animals from injection	germline transmission
<i>Gsk-3α-flox</i>	PS-31.B1	0	-	not tested
	PS-31.C2	-	16	yes
	PS-31.C6	-	0	-
	PS-31.D5	-	1	not tested
<i>Gsk-3β-sh</i>	PS-36.6	-	3	(yes)
	PS-36.8	-	8	(yes)
	PS-36.10	0	-	-
	PS-36.14	0	-	-
	PS-36.15	-	0	-
<i>Gsk-3β-flox-sh1</i>	PS 21.A2	-	2	yes
	PS 21.A4	-	8	yes
<i>Gsk-3β-flox-sh2</i>	PS-22.B1	-	0	-
	PS-22.B6	-	9	yes
	PS-22.C2	0	-	-
	PS-22.C6	-	5	yes
<i>Gsk-3-flox-dh</i>	PS-32.12	-	16	not tested
	PS-32.14	1	6	yes
	PS-32.19	14	-	yes
	PS-32.20	-	8	not tested
<i>Gsk-3-flox-dh2</i>	PS-34.6	-	3	yes
	PS-34.7	2	12	yes
	PS-34.20	-	3	not tested

Tab. 2: ES cell clones used for injection and tetraploid aggregation are listed here. The number of animals from tetraploid aggregation and the number of chimeras for each clone are given as well. Founder animals of each mouse line and respective ES cell clones are indicated bold.

Only in case of the non-conditional *Gsk-3 β -sh2* vector (*Gsk-3 β -sh* mouse line) mutant offspring was not obtained. However, three of the four mated chimeras were able to generate agouti pups, indicating that mutant ES cells populated the gonads in these chimeras. Since the knockout of *Gsk-3 β* leads to embryonic lethality (Hoefflich et al., 2000) and the *Gsk-3 β -sh2* was very effective in ES cell clones, reducing GSK-3 β protein nearly to the detection level (Fig. 22), it is likely that the knockdown embryos

died postnatal or during development. One indication for this assumption was the small litter size of one to five pups per litter. After four months of breeding, the three chimeras produced eleven black and eight agouti wild type animals. According to Mendel's laws, half of these animals should have carried the mutation, but since this was not the case, further breeding was abandoned and a mouse line for the non-conditional Gsk-3 β -sh2 could not be established.

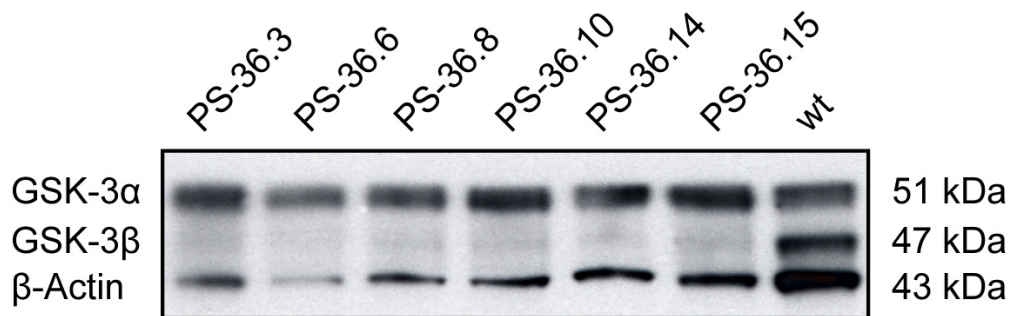


Fig. 22: Analysis of ES cell clones carrying the non-conditional Gsk-3 β -sh2. This Western blot shows ES cell clones with the non-conditional Gsk-3 β -sh2 in the *Rosa26* locus. The knockdown of GSK-3 β protein was very strong, indicating an effective shRNA. *wt: IDG3.2 wild type ES cells*

5.4 Characterization of used Cre mouse lines

The expression of shRNAs in conditional knockdown mice depends on the expression of Cre recombinase in the tissue. Multiple mouse lines are available that express Cre recombinase under the control of various promoters. For the expression of Cre recombinase in the nervous system, a lot of different mouse lines are available, targeting different brain regions or cell types (Gaveriaux-Ruff and Kieffer, 2007).

Since I was interested in the role of Gsk-3 in the brain, I chose the Cre expressing mouse lines *Nestin-cre* and *CamKII-cre*, which are characterized further in the following section.

5.4.1 The *Nestin-cre* mouse line

The *Nestin-cre* mouse strain was generated by injection of an expression vector into mouse oocytes by Tronche et al. in 1999. To express Cre recombinase in neuronal stem cells, CNS progenitors, and neuronal and glial cell precursors, the rat Nestin (*Nes*) promoter was used. The nervous system specific enhancer from the second intron of the rat *Nestin* gene (Zimmerman et al., 1994) was added to the promoter. Tronche et al. analyzed the mice by using a reporter strain, whose LacZ expression

was dependent on Cre mediated recombination. In newborn mice they detected extensive blue staining in the central and peripheral nervous system with occasional stained cells in heart and kidney. The expression of Cre recombinase under the control of the Nestin promoter was present from embryonic day eleven (E11.0) and the mice were kept on *C57Bl/6J* background.

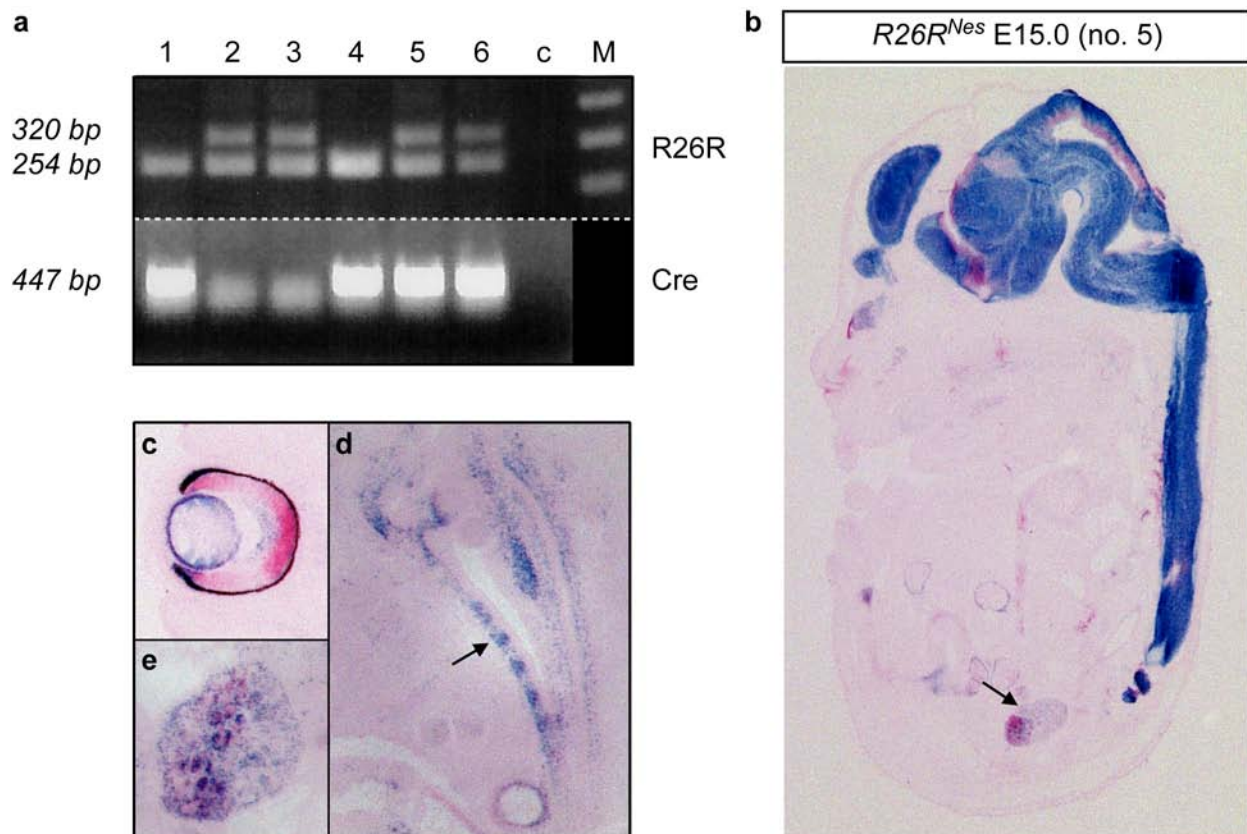


Fig. 23: Cre recombinase expression pattern in the *Nestin-cre* mouse line. Offspring of *R26R* and *Nestin-cre* breeding were genotyped by PCR using DNA of the yolk sac. The *R26R* allele was genotyped by triple PCR (*R26R*) using the following primer: *R26R-D1*, *R26R-R1*, and *R26R-Mt*. Wild type embryos displayed a band of 254 bp (lane 1 and 4), whereas heterozygous embryos were identified by an additional band of 320 bp (lane 2, 3, 5, and 6). To detect embryos carrying Cre recombinase, a Cre PCR (*Cre*) was performed with the primer *Cre1* and *Cre2* (447 bp). Four of the six embryos carried Cre recombinase (lane 1, 4, 5, and 6) and two double transgenic embryos could be identified (lane 5 and 6) and used for LacZ staining (a). Embryo no. 5 was cut in 30 μ m thick slices and stained for LacZ activity. The developing brain and the spinal cord are stained positively in clear blue (b). Additionally, I detected other areas of stronger staining in the eye (c), in the cartilage of the trachea (d), and in the kidney (e). c: water control

To confirm the expression pattern of Cre recombinase in *Nestin-cre* mice, they were crossed with the reporter strain *R26R* (Soriano, 1999), whose LacZ expression was dependent on Cre mediated recombination. *R26R* males were bred with *Nestin-cre* females and embryos were dissected on embryonic day 15 (E15.0). The *R26R* mice were genotyped by triple PCR using the primers *R26R-D1*, *R26R-R1*, and *R26R-Mt*. To identify double transgenic mice a Cre specific PCR was performed in addition

(Cre1 and Cre2 primer). Embryos positive for both PCRs were cut in sagittal sections (30 μ m), analyzed by LacZ staining overnight, and counterstained with eosin-red. As expected, the developing brain and the spinal cord displayed strong blue staining. In contrast to Tronche et al., I found additional areas of LacZ staining. The embryo showed a weak staining in every tissue and areas with stronger staining like in kidney, heart, trachea, eye, and lung were identified (Fig. 23). LacZ staining could not be detected in a non-recombined heterozygous *R26R* embryo (no. 2), used as negative control.

5.4.2 The *CamKII-cre* mouse line

To restrict the expression of the shRNAs to the forebrain, I used the *CamKII-cre* mouse line. This strain was generated by Minichiello et al. in 1999 via random integration of an expression vector consisting of the 8.5 kb CaMKII α promoter, the Cre coding sequence, a hybrid intron with a nuclear localization sequence, and a SV40 polyadenylation signal, into the mouse genome. The expression of Cre recombinase under the control of the CaMKII α promoter was tested via crosses with a lacZ reporter strain. Cre activity was present at or after postnatal day 20 (P20), specifically in excitatory neurons of the forebrain. Before postnatal day 15 (P15), no or little LacZ staining was detected in double transgenic animals. In detail, Cre recombination was observed in pyramidal neurons of the hippocampus (strong staining in CA1, lighter in CA3 and dentate gyrus), neocortex, striatum, and amygdala. Few cells were stained in the cerebellum, the olfactory bulbs, and the inferior colliculus. At the age of eight weeks, about 50% recombination was detected by Southern blot in hippocampus, cortex, and olfactory bulb of mice carrying a loxP flanked allele. No deletion was found in cerebellum, liver, kidney, spleen, or tail. The mice were kept on *C57Bl/6J* background (Minichiello et al., 1999).

To confirm this expression pattern, I crossed the *CamKII-cre* mice present in our colony to the *R26R* reporter strain. At the age of ten weeks, double transgenic mice were sacrificed and brains were dissected for analysis. The results of the LacZ staining are depicted in Fig. 24 and the observed pattern reflected the recombination as published by Minichiello et al. In addition, the observed pattern included the hypothalamus and the recombination in the olfactory bulbs increased in comparison

to the data of Minichiello et al. An increase in the occasional staining of inferior colliculus, cerebellum, and brain stem was detected as well.

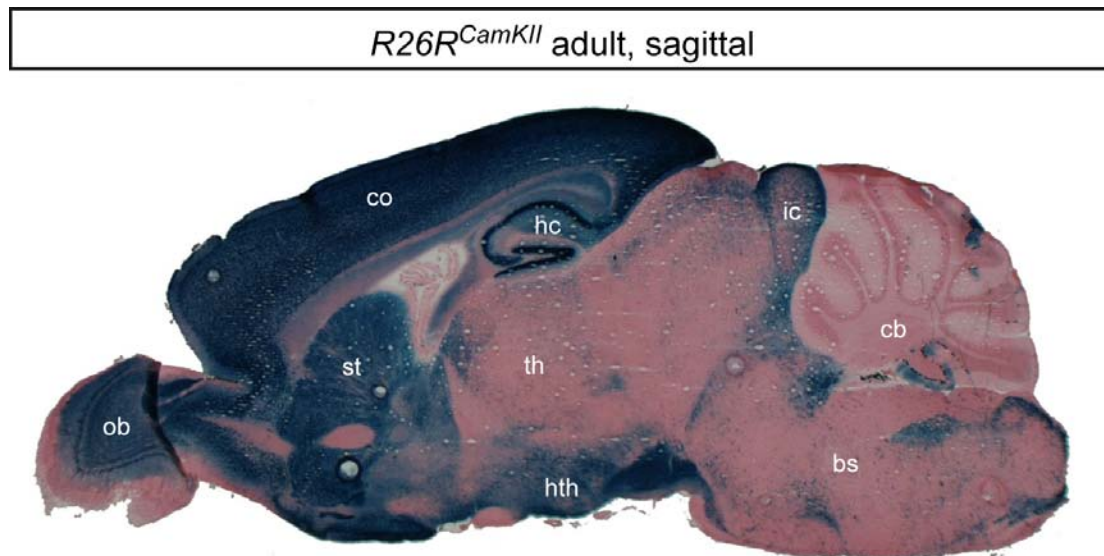


Fig. 24: Cre recombinase expression pattern in the *CamKII-cre* strain. Offspring of *R26R* and *CamKII-cre* breeding were genotyped by *R26R* and Cre PCR. At ten weeks, adult mice were sacrificed, perfused, and the brain was dissected. 50 μ m thick sagittal sections were stained for LacZ activity. Strong staining indicating complete recombination was detected in cortex (co), hippocampus (hc), and striatum (st). Partial staining was observed in olfactory bulbs (ob), hypothalamus (hth), and inferior colliculus (ic). No or occasional staining was found in cerebellum (cb), thalamus (th), and brain stem (bs).

5.5 Silencing of *Gsk-3* genes in mice

To address the function of *Gsk-3* in the adult mouse brain, I generated several conditional knockdown mouse lines. By activation of shRNA expression through deletion of a loxP flanked the stop cassette the *Gsk-3* mRNA(s) are silenced. By removal of the stop cassette, shRNAs are expressed from the U6 promoter in tissues that expressed Cre recombinase during development. In Fig. 25 the *Rosa26* locus is depicted after Cre mediated deletion of the stop cassette. The two 34 bp loxP sites are recombined, and the sequence in-between is deleted. This recombination step is irreversible, because it removes one loxP site permanently. The other loxP site remains in its position, but I showed already in ES cell culture that the function of the shRNA was not negatively influenced (see 5.3.4.2).

In the following, the various conditional knockdown mice were analyzed for gene silencing efficiency and their behavioral changes.

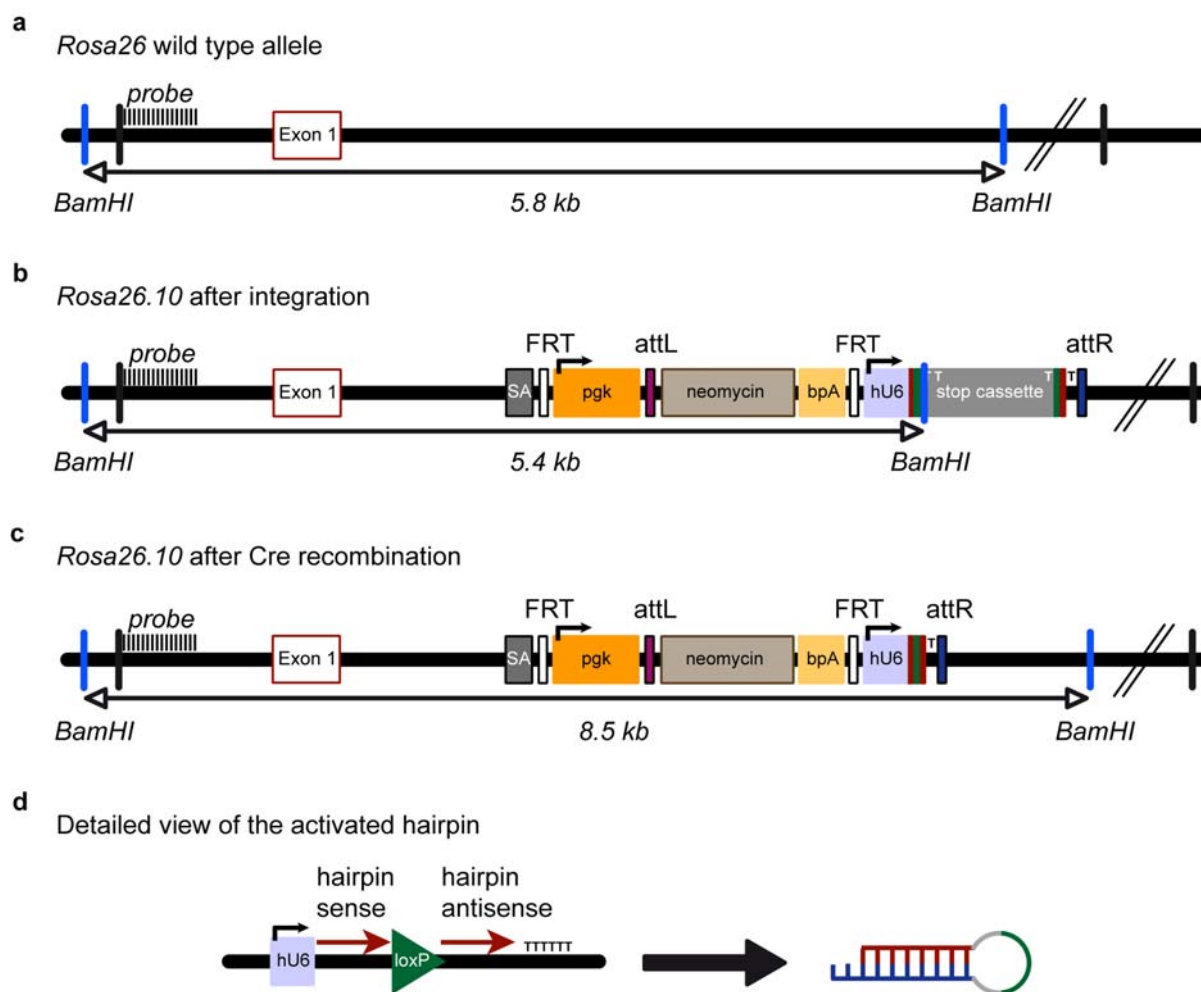


Fig. 25: Activation of the shRNAs by Cre recombinase. After integration of the shRNA expression cassette into the *Rosa26* locus (a, b), it can be activated by Cre recombinase. The inhibitory stop cassette is deleted, and the transcription of the shRNAs can take place (c). The recombination leaves one loxP site in the loop region of the shRNA, which does not interfere with its function (d).

5.5.1 Breeding of *Gsk-3* knockdown mice

The knockdown of *Gsk-3* was activated in mice by breeding the conditional strains to *CamKII-cre* and *Nestin-cre* mice (Tab. 3). The chimeras or animals from tetraploid aggregation were bred to *C57Bl/6J* females to obtain heterozygous floxed (+/flox) animals. These mice were intercrossed to get homozygous floxed (flox/flox) animals, which were bred with Cre expressing transgenic mice. The heterozygous and homozygous floxed (+/flox; flox/flox) mice without Cre transgene were viable, fertile, and displayed no obvious phenotype.

Since the F1 ES cells used for mouse production are derived from the mouse strains *C57Bl/6J* and *129SvEv/Tac*, they contained already 50% of *C57Bl/6J* background. After crossing to the Cre strains, which were on *C57Bl/6J* background as well, the

genetic constitution of mice for phenotype analysis included a mean of 87.5% of the *C57Bl/6J* genome.

mouse line	parental mouse lines	expressed shRNA(s)
<i>Gsk-3α-flox^{Nes}</i>	<i>Gsk3α-flox</i> x <i>Nestin-cre</i>	Gsk-3 α -sh1
<i>Gsk-3α-flox^{CamKII}</i>	<i>Gsk3α-flox</i> x <i>CamKII-cre</i>	Gsk-3 α -sh1
<i>Gsk-3β-flox-sh1^{Nes}</i>	<i>Gsk3β-flox-sh1</i> x <i>Nestin-cre</i>	Gsk-3 β -sh2
<i>Gsk-3β-flox-sh2^{Nes}</i>	<i>Gsk3β-flox-sh2</i> x <i>Nestin-cre</i>	Gsk-3 β -sh4
<i>Gsk-3β-flox-sh2^{CamKII}</i>	<i>Gsk3β-flox-sh2</i> x <i>CamKII-cre</i>	Gsk-3 β -sh4
<i>Gsk-3-flox-dh^{Nes}</i>	<i>Gsk3-flox-dh</i> x <i>Nestin-cre</i>	Gsk-3 β -sh2 and Gsk-3 α -sh1
<i>Gsk-3-flox-dh2^{Nes}</i>	<i>Gsk3-flox-dh2</i> x <i>Nestin-cre</i>	Gsk-3 β -sh4 and Gsk-3 α -sh1
<i>Gsk-3-flox-dh2^{CamKII}</i>	<i>Gsk3-flox-dh2</i> x <i>CamKII-cre</i>	Gsk-3 β -sh4 and Gsk-3 α -sh1

Tab. 3: Mouse lines generated by breeding with *Nestin-cre* and *CamKII-cre* mice. The parental mouse lines and the expressed shRNAs are given, too.

For the analysis of mutant strains in the German Mouse Clinic (GMC), 10 to 15 animals per sex and genotype were required. To obtain this number of animals with a maximum age difference of 14 days, 13 to 15 breeding cages were set up, each with two females and one male. After two weeks the males were removed from the cages to prevent contact with the newborns and to avoid further litters. By breeding homozygous floxed animals with Cre transgenic mice, the offspring was split into a mutant group, consisting of heterozygous animals carrying the Cre transgene (+/ Δ) and heterozygous floxed littermate controls (+/flox). Pups were weaned at the age of three weeks and genotyped using tail clip DNA.

5.5.2 Analysis of knockdown efficiency in *Gsk-3/Nestin-cre* mice

Although the shRNAs were tested for efficiency *in vitro*, it was necessary to confirm their functionality *in vivo*. Various techniques were used to assess the shRNA expression in the brain, their knockdown efficiency *in vivo* at the mRNA and protein level, and the efficiency of Cre mediated stop cassette deletion.

5.5.2.1 Activation of the shRNAs in the adult brain

The activation and expression of shRNAs is crucial for gene silencing *in vivo*. To show the expression of shRNAs in mice, I performed Northern blot analysis of

small RNAs. Small RNA was extracted from one brain half (separated sagittally) of *Gsk-3/Nestin-cre* knockdown mice, and 2 μ g each were loaded onto a Urea-TBE gel. As internal controls for the labeling reaction, the respective antisense oligonucleotides were loaded. The sense oligonucleotides were labeled radioactively with γ - 32 P-dATP. In *Gsk-3 β -flox-sh2^{Nes}* mice, the Gsk-3 β -sh4 was detected as 21 nt band. In *Gsk-3-flox-dh^{Nes}* mice, the Gsk-3 α -sh1 was visible, but the Gsk-3 β -sh2 was not detectable (Fig. 26a). The expression of Gsk-3 α -sh1 in *Gsk-3 α -flox^{Nes}* mice was detected as well (data not shown).

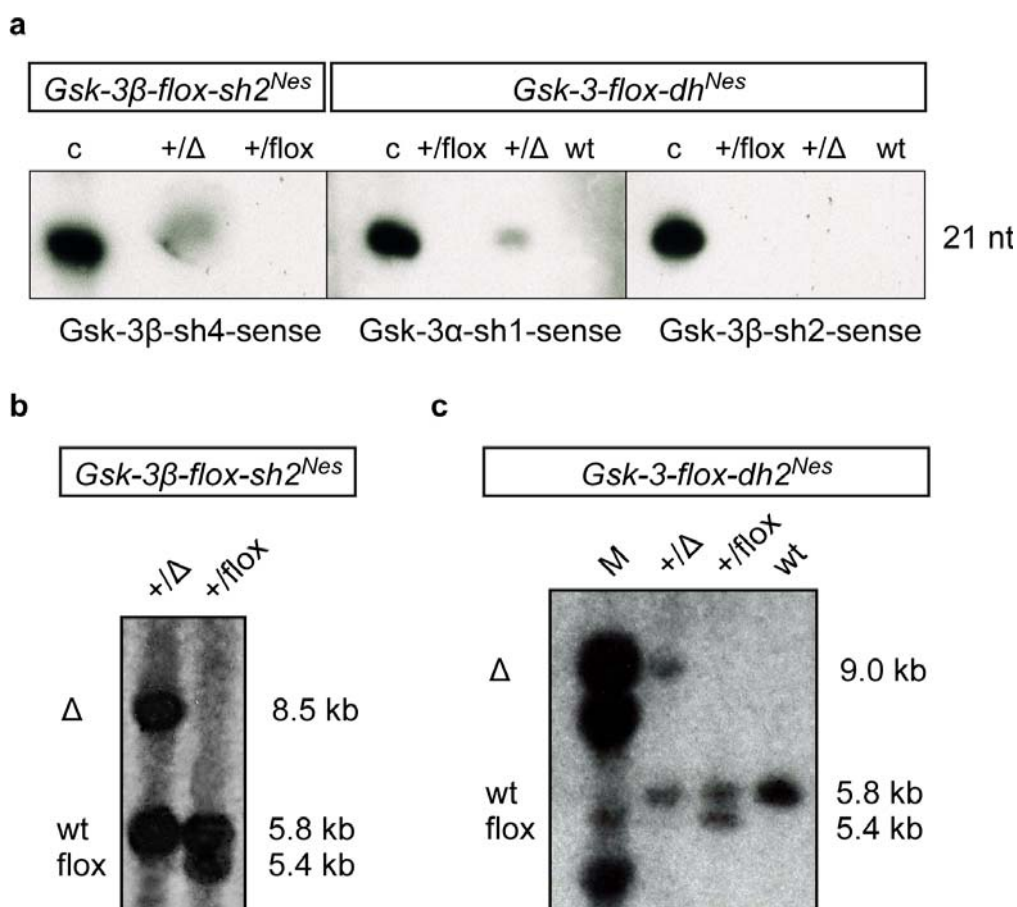


Fig. 26: ShRNA expression and recombination efficiency in brain of adult *Gsk-3/Nestin-cre* mice. Small RNA was extracted from one brain half and 2 μ g each were loaded onto a Urea-TBE gel. As positive controls (c), the respective antisense oligonucleotides were loaded and the shRNAs were detected by radioactively labeled sense oligonucleotides. In *Gsk-3 β -flox-sh2^{Nes}* mice, the Gsk-3 β -sh4 was detected as 21 nt band. In *Gsk-3-flox-dh^{Nes}* mice, the Gsk-3 α -sh1 was found, but the Gsk-3 β -sh2 was not detectable (a). To check the recombination efficiency, Southern blot analysis was performed on brain DNA of adult mice. After digestion with BamHI and detection with the Rosa5'probe, the wild type *Rosa26* locus displayed a 5.8 kb band (wt). A 5.4 kb band was found for the floxed allele (flox) and an 8.5 kb (9.0 kb for double shRNA) was observed after recombination (Δ). In *Gsk-3 β -flox-sh2^{Nes}* mice, complete recombination took place, because the floxed band is not detectable anymore (b). The same was true in the *Gsk-3-flox-dh2^{Nes}* mice (c).

In *Gsk-3 β -flox-sh1^{Nes}* mice, also carrying the *Gsk-3 β -sh2*, the shRNA was not detectable either. It seemed that the expression of the *Gsk-3 β -sh2* was blocked. A possible reason could be a mutation in the U6 promoter. To analyze the promoter and shRNA sequence, I amplified the segment including the U6 promoter and the shRNA termination signal using brain DNA of *Gsk-3 β -flox-sh1^{Nes}* and *Gsk-3-flox-dh^{Nes} +/Δ* mice with the primers bpA and RMCE-rev. In floxed littermates, the primers bpA and StopK1-rev were used to amplify the segment from the U6 promoter to the 5' end of the stop cassette. PCR products were sequenced with the bpA primer and all sequences were found to be correct. In conclusion, the expression cassette of the *Gsk-3 β -sh2* is intact, but since a clear explanation for the malfunction of the shRNA vector was not found, the mouse lines *Gsk-3 β -flox-sh1^{Nes}* and *Gsk-3-flox-dh^{Nes}* were terminated.

5.5.2.2 Cre recombination efficiency in mice

The recombination efficiency of Cre recombinase in mouse tissue is crucial for the expression of shRNAs *in vivo*. I performed Southern blot analysis to determine the extend of recombination in various organs. First, brain DNA of adult mice was digested with BamHI and hybridized with the Rosa5'probe. The wild type *Rosa26* locus displayed a 5.8 kb band. A 5.4 kb band was derived for the floxed allele (flox) and an 8.5 kb (9.0 kb for double shRNA) was observed after recombination (Δ) (see Fig. 25 for location of restriction sites). In *Gsk-3 β -flox-sh2^{Nes}* and *Gsk-3 α -flox^{Nes}* mice, complete recombination took place, because the floxed band is not detectable anymore (Fig. 26b). The same was seen in the double shRNA mice (Fig. 26c).

The analysis of *Nestin-cre* mice, revealed a broad LacZ staining pattern in the embryo (see 5.4.1), therefore I decided to analyze the recombination efficiency of Cre recombinase in selected organs of knockdown mice. For this analysis the *Gsk-3 β -flox-sh2^{Nes}* mouse line was used, and two male and two female +/Δ mice were tested. As expected, the recombination in the brain was complete, but unexpectedly I detected nearly complete recombination in the pancreas as well. Moderate recombination was detected in the kidney, but in heart, skeletal muscle, and lung the recombination was low. Liver and spleen showed no vector recombination at all (Fig. 27). Besides the CNS, *Gsk-3* silencing is induced also in other organs at varying extend.

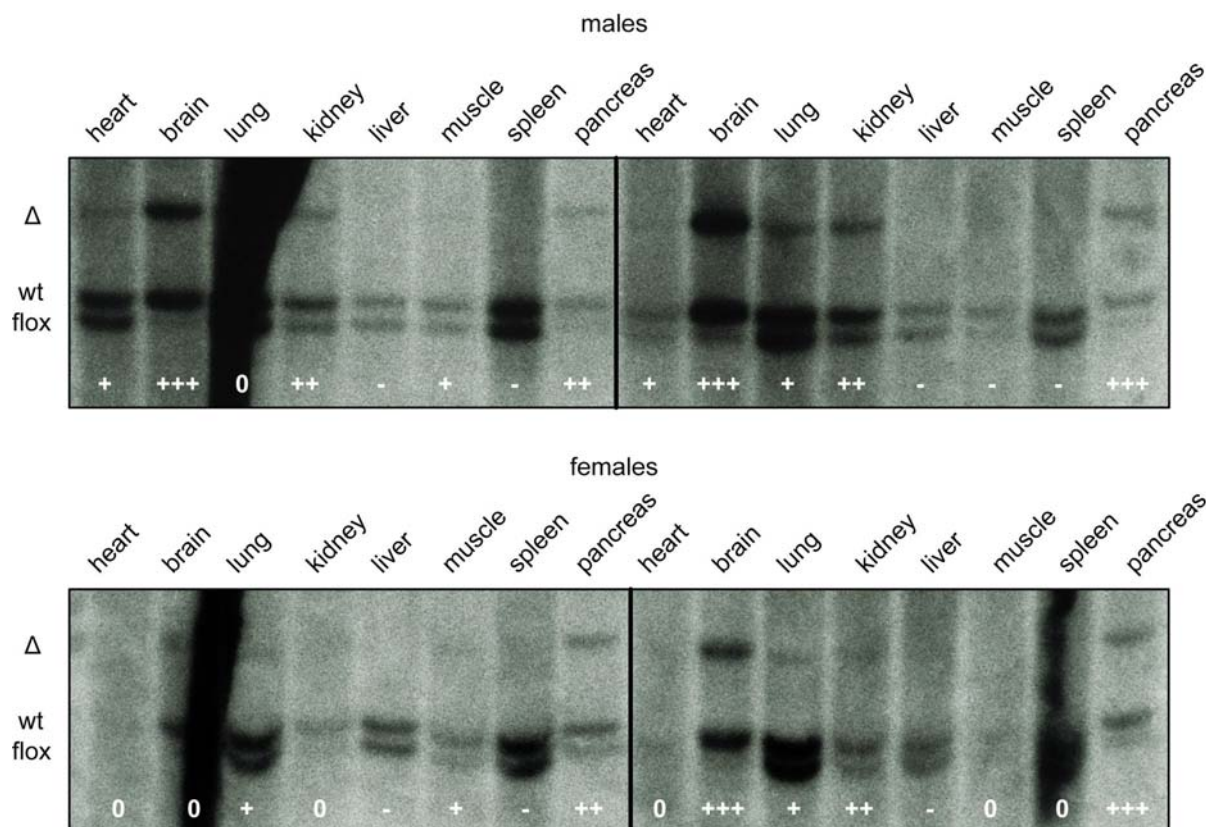


Fig. 27: Analysis of Cre recombination in *Gsk-3β-flox-sh2^{Nes}* male and female mice. Southern blot analysis was performed with DNA of different tissues from two male and two female adult *Gsk-3β-flox-sh2^{Nes}* mice. The genomic DNA was digested with BamHI resulting in the following band sizes: 5.8 kb for wild type *Rosa26* locus (wt), 5.4 kb for the conditional shRNA (flox), and 8.5 kb for the recombined shRNA (Δ). Near complete recombination took place in the brain and surprisingly in the pancreas. +: weak recombination, ++: moderate recombination, +++: high recombination, -: no detectable recombination, 0: not analyzable

5.5.2.3 Reduction of *Gsk-3* mRNA in the adult brain

To analyze the knockdown of *Gsk-3* mRNA in the brain of adult mice, Northern blot analysis was performed. Total RNA was extracted from one sagittal brain half and 20 μ g of total RNA were applied to a 1% agarose gel. The ISH probes for *Gsk-3 α* and *Gsk-3 β* were used for detection of the mRNA, and labeled with α -³²P-dCTP. The blots showed a clear reduction of *Gsk-3* mRNA in the mutant +/ Δ animals compared to their floxed (+/flox) littermate controls (Fig. 28).

For normalization of *Gsk-3* signals, the blots were stripped and β -Actin was used for standardization. The signal intensities were measured by exposure of membranes to an Imaging Plate, which enables signal quantification with a FLA-3000 image analyzer. Signal intensities were corrected for background and normalized to β -Actin. After this, the +/flox and +/ Δ values were compared to a dilution series of control

mRNA. This technique does not allow exact quantification, but only estimation of approximate knockdown levels. In *Gsk-3 α* and *Gsk-3 β* mice knockdown levels were similar, but not comparable to the achieved knockdown in ES cells. The mRNA reduction in *Gsk-3 α -flox^{Nes}* mice was estimated to 60% and in *Gsk-3 β -flox-sh2^{Nes}* mice to 55%. A similar knockdown level was confirmed in the *Gsk-3-flox-dh2^{Nes}* mice.

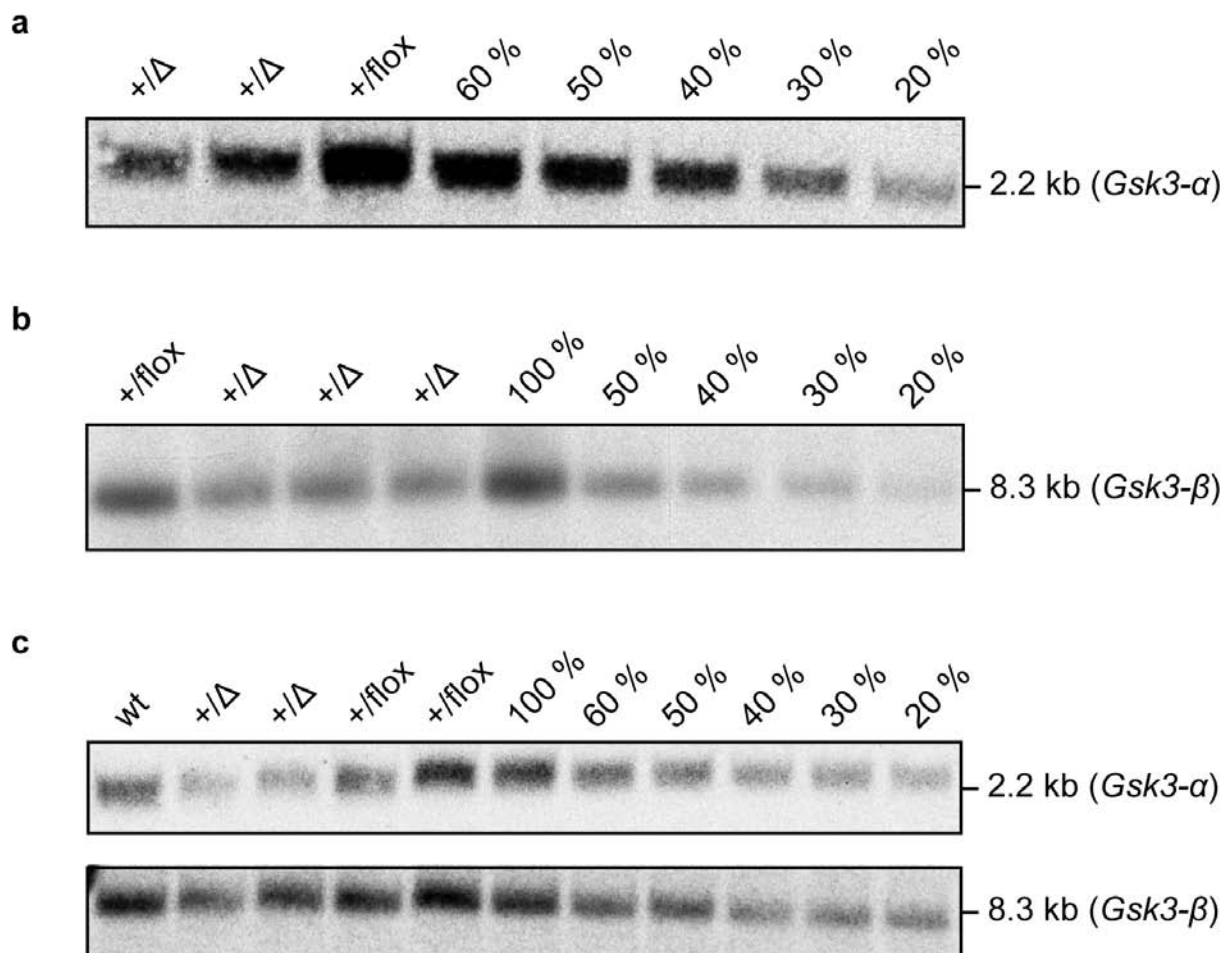


Fig. 28: Quantification of *Gsk-3* mRNA knockdown. Northern blot analysis was performed on brain RNA of adult mice. +/Δ samples were applied in duplicate. In *Gsk-3 α -flox^{Nes}* mice (a) and *Gsk-3 β -flox-sh2^{Nes}* mice (b) the dilution series is based on the +/flox samples. The mRNA reduction was estimated to approximate 60% in the *Gsk-3 α -flox^{Nes}* mice and to approximate 55% in *Gsk-3 β -flox-sh2^{Nes}* mice. A similar knockdown level was confirmed in the *Gsk-3-flox-dh2^{Nes}* mice (c).

In addition to Northern blot analysis, I checked for *Gsk-3* mRNA expression by ISH on adult brain slices (Fig. 29). In *Gsk-3 β -flox-sh2^{Nes}* mice, I found a clear reduction of the *Gsk-3 β* signal, especially in the Purkinje cell layer of the cerebellum. *Gsk-3 β* mRNA could not be detected anymore. The same was true for the *Gsk-3 α* signals in *Gsk-3 α -flox^{Nes}* mice, although the reduction seemed to be less prominent.

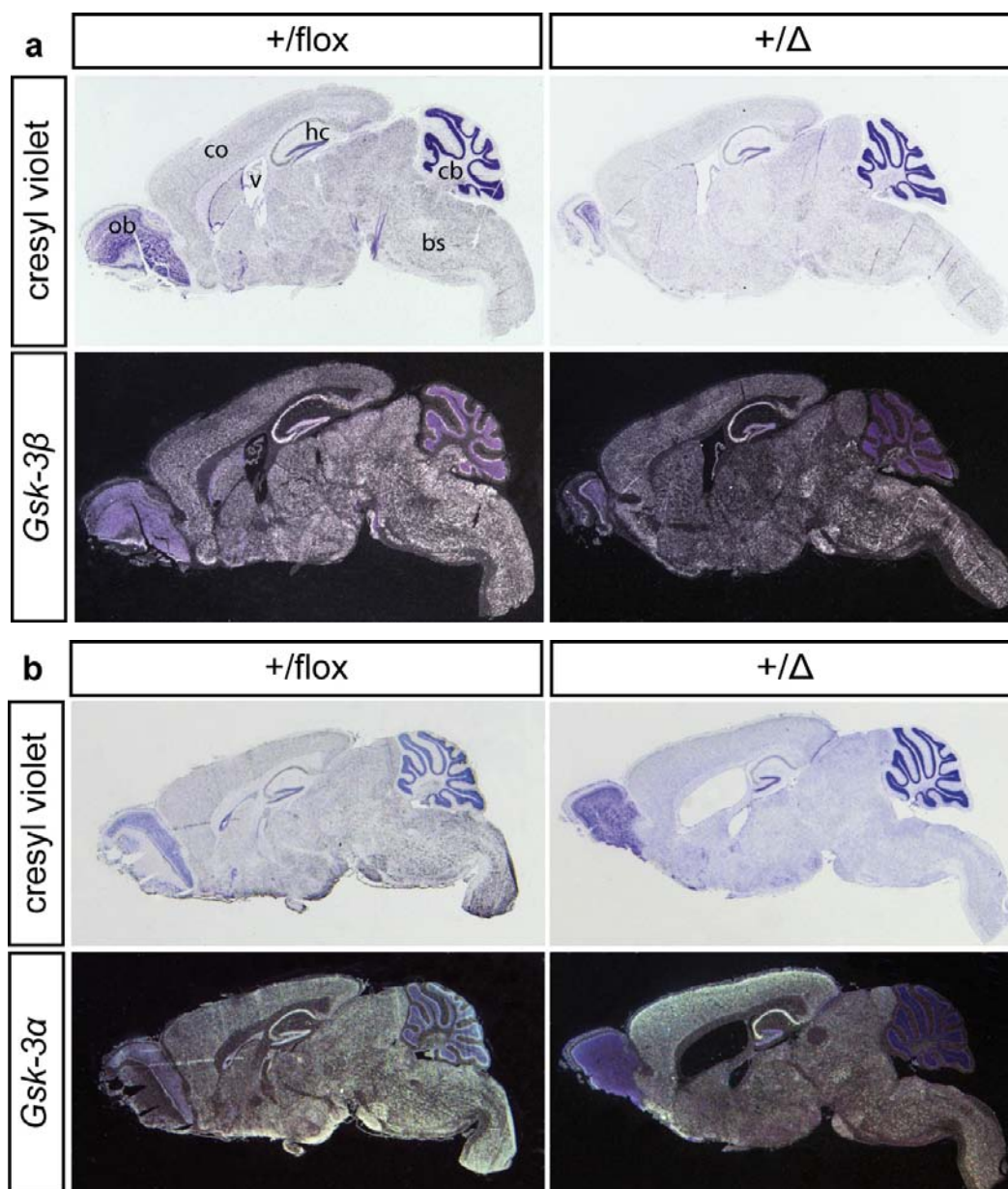


Fig. 29: Reduction of *Gsk-3* mRNA in brain sections of adult knockdown mice. This figure shows radioactive ISH on sagittal brain sections of *Gsk-3 α -flox^{Nes}* and *Gsk-3 β -flox-sh2^{Nes}* mice. In *Gsk-3 β -flox-sh2^{Nes}* mice (a) the reduction of *Gsk-3 β* mRNA was clearly visible all over the brain, especially in the Purkinje cell layer of the cerebellum (cb). Also in the *Gsk-3 α -flox^{Nes}* mice (b) reduction of *Gsk-3 α* mRNA was detected. ob: olfactory bulbs, co: cortex, hc: hippocampus, cb: cerebellum, bs: brainstem, v: ventricle

In conclusion, the mRNA reduction of *Gsk-3 α* and *Gsk-3 β* in *Gsk-3 α -flox^{Nes}* and *Gsk-3 β -flox-sh2^{Nes}* mice was estimated to 60% and 55% respectively, and could be confirmed by a clear reduction of signals in the ISH.

5.5.2.4 Knockdown of GSK-3 proteins in the adult brain

Finally, I analyzed the reduction of GSK-3 proteins in the brain of adult *Gsk-3/Nestin-cre* mice in Western blot analysis. In *Gsk-3 α -flox^{Nes}* and *Gsk-3 β -flox-sh2^{Nes}* single knockdown mice, I detected a clear reduction of the targeted GSK-3 proteins. A similar reduction was seen in the *Gsk-3-flox-dh2^{Nes}* mice (Fig. 30).

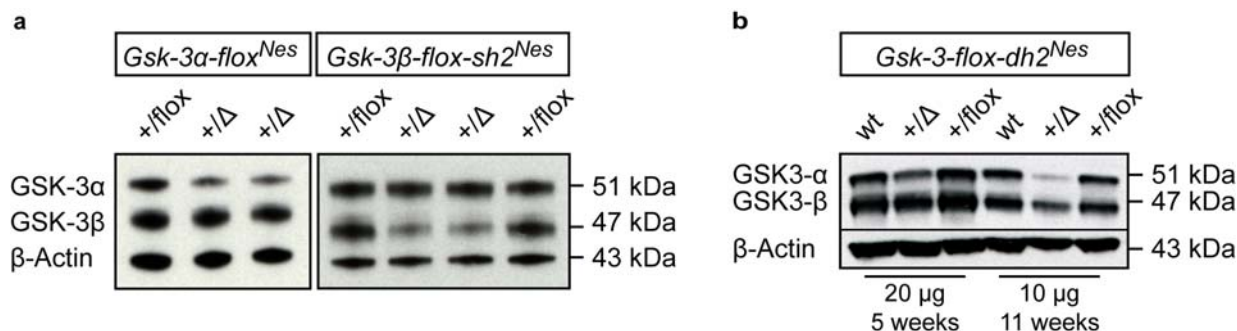


Fig. 30: Reduction of GSK-3 protein in the brain of knockdown mice. Total brain protein (5 μ g) of adult mice was applied to a 10% SDS polyacrylamide gel and detected with a GSK-3 specific antibody. As loading control, a β -Actin antibody was used. GSK-3 α , or respectively GSK-3 β , was visibly reduced in single knockdown mice (a). In double knockdown mice, a clear reduction of GSK-3 protein was observed, too (b).

Although the quantification of Western blot films is only approximate due to the non-linear light exposure of the chemiluminescence reaction, I quantified the signals using the ImageJ software (Abramoff et al., 2004). The signals were corrected for the background in each lane and normalized to the β -Actin signal. The protein reduction of GSK-3 α in *Gsk-3 α -flox^{Nes}* mice was calculated to be 51% and the reduction of GSK-3 β in *Gsk-3 β -flox-sh2^{Nes}* mice was quantified to be 49%. These results were comparable to the mRNA reduction seen in the Northern blot analysis.

Taken together, the conditional RNAi system in mice was confirmed to be functional and the knockdown mutants were further analyzed for gene specific, phenotypic alterations.

5.5.3 General analysis of *Gsk-3* knockdown mice

In the first mutants of the *Gsk-3 β -flox-sh2^{Nes}* mouse line, I detected early some obvious differences to the floxed littermates. At weaning, the mutant mice were smaller than their floxed siblings. This difference remained until adulthood, getting even more obvious, since the mutants gained less weight (Fig. 31).

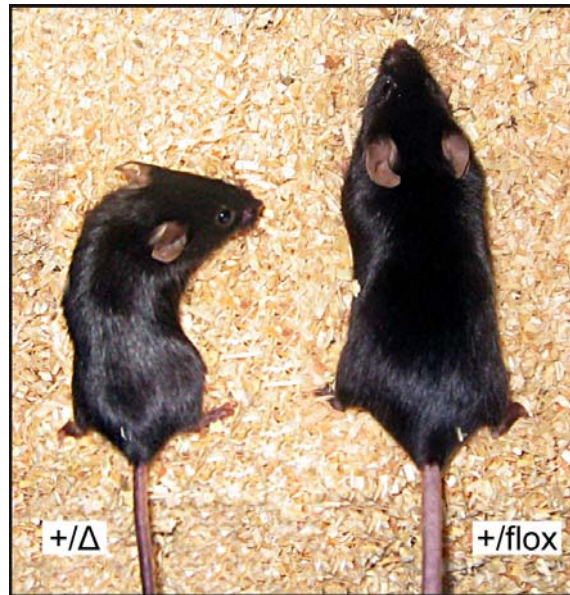


Fig. 31: Appearance of adult *Gsk-3β-flox-sh2^{Nes}* female mice. Two adult female mice are shown. The mutant mouse (+/Δ) is smaller than the littermate (+/flox), the tail is thinner and body weight is reduced.

To confirm this observation, I started to document the body weight of the *Gsk-3/Nestin-cre* mice at different ages, starting at weaning. The difference in body weight was already detectable at the age of three weeks and increased throughout adulthood. The GMC confirmed the significant reduction in body size and weight for *Gsk-3α-flox^{Nes}* and *Gsk-3β-flox-sh2^{Nes}* mice during the primary screen. Fig. 32 shows the body weight for two single knockdown mouse lines. These weights were documented during the accelerating rotarod test. The difference is obvious in the *Gsk-3β-flox-sh2^{Nes}* mutants. Here, the females displayed a reduction of 25%, whereas in males the body weight was reduced by 26%. The reduction of body weight was less prominent in the *Gsk-3α-flox^{Nes}* mutants, but still significant. In female mutants the body weight was reduced by 18% and in males it was reduced by 19%. Since the *Gsk-3-flox-dh2^{Nes}* mice were not bred in larger numbers for the GMC, a more detailed analysis of the body weight was not performed. The mutants of this strain were smaller in size and displayed a clear body weight reduction within the small number of analyzed animals. The respective *Gsk-3/CamKII-cre* mutant mice did not show a body weight phenotype at all.

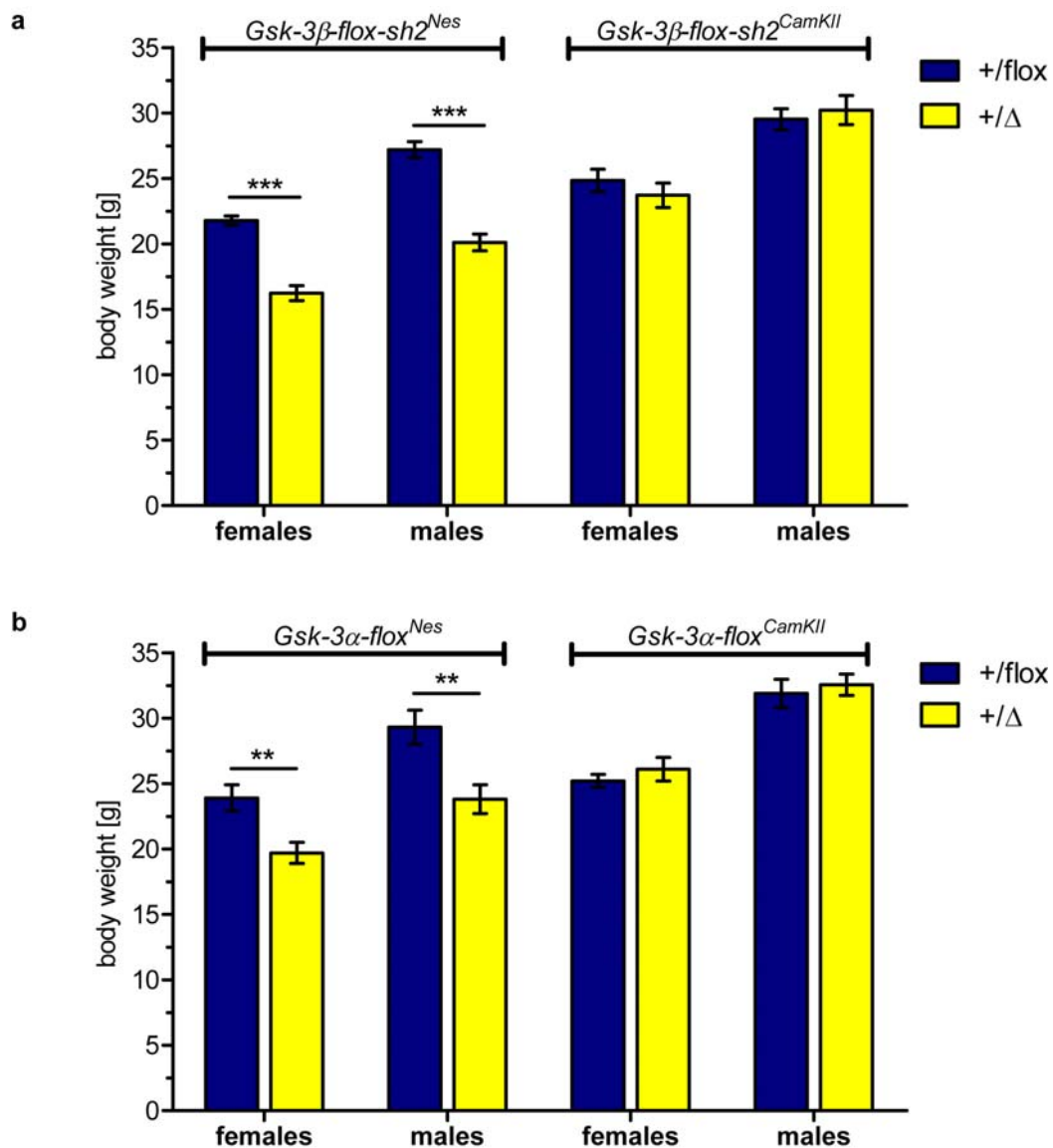


Fig. 32: Body weight of *Gsk-3α-flox* and *Gsk-3β-flox-sh2* mice. Body weight was measured in the GMC during the accelerating rotarod test. In *Gsk-3β-flox-sh2^{Nes}* mutants the body weight was reduced by 25% in the female and by 26% in the male mice ($p < 0.0001$; unpaired t-test with Welch's correction). In the *Gsk-3β-flox-sh2^{CamKII}* mice the body weight was not altered (a). The reduction in body weight was less in the *Gsk-3α-flox^{Nes}* mutants. Here, the females exhibited a reduction of 18%, whereas in the males the body weight was reduced by 19% ($p < 0.005$; unpaired t-test with Welch's correction). Again, in the *Gsk-3α-flox^{CamKII}* mice the body weight was unchanged (b). Error bars represent the SEM.

In mutant *Gsk-3β-flox-sh2^{Nes}* mice on a background of 75% *C57Bl/6J* another anomaly was observed. When mice were disturbed during the day by handling or opening the home cage, they leave immediately the sleeping or resting place and start to explore or change their position in the cage. But many of these *Gsk-3β-flox-sh2^{Nes}* mutants displayed a different behavior. Upon disturbance, they tried to leave their resting place as well, but instead they were frozen stiff in their position for approximate 10 sec. During this period, they were just able to move

slowly their tail or to stabilize their position with their fore limbs. In more severe cases, they toppled to one side and could not manage to reach an upright position. After this paralysis, they slowly regained their coordination ability and started moving, but instead of a straight walk, they mostly tumbled from one side to another. Their movements normalized after some time, although they were quite slow compared to their floxed cage mates. This phenotype was not observed in *Gsk-3 β -flox-sh2^{Nes}* mutant mice with 87.5% *C57Bl/6J* background.

During the tests for knockdown efficiency, mutant (+/ Δ) *Gsk-3/Nestin-cre* mice were bred with homozygous flox (flox/flox) mice to obtain homozygous mutants (Δ/Δ). But only for the *Gsk-3 α -flox^{Nes}* mice homozygous mutants were obtained. So, heterozygous mutant *Gsk-3 β -flox-sh2^{Nes}* mice were analyzed for their fertility and therefore male and female mutants were bred to *C57Bl/6J* wild type mice. After six months of breeding, no pups were obtained. To exclude organic defects, mutant animals were analyzed with the help of Dr. A. Boersma from the GMC. Two male and two female mutants were dissected and the gonads were inspected. In the males, the testis and the epididymis seemed to be smaller and supplied with less blood. In the females, the ovaries were smaller and atrophic and displayed no follicles or corpora lutea. The sperms of the males were analyzed for motility and morphology. The percentage of motile sperm was reduced in the mutant males, as was the percentage of progressive sperm. The same was found for the concentration and all measured speed parameters. Taken together, the sperms of mutant males swam slower, with less force and not as straight as the sperm of the control male. The morphological analysis revealed for the mutant males a higher percentage of abnormal, damaged sperm. The sperm of one mutant male was used for *in vitro* fertilization, but only ten embryos developed and were transferred into foster mothers. No pups were born. These first results indicate that organic defects may cause the observed infertility of *Gsk-3 β -flox-sh2^{Nes}* mutant mice.

5.5.4 Viability of *Gsk-3/Nestin-cre* knockdown mice

In general, mutant (+/ Δ) mice were viable, but in *Gsk-3-flox-dh2^{Nes}* mice the number of viable mutants was reduced. The founder animals of the *Gsk-3-flox-dh2* line, derived from tetraploid aggregation, were bred directly to *Nestin-cre* mice to get mutant offspring. From 12 litters, 96 animals were obtained. Referring to Mendel's laws the following genotypes should be obtained at a frequency of 25% each: wild

type mice, *Nestin-cre* mice, floxed (+/flox), and mutant mice. The results are depicted in Fig. 33a. Only 13% of the weaned pups were mutants, instead of the estimated 25%. So the question emerged, if in this mouse line the mutants suffer from increased mortality.

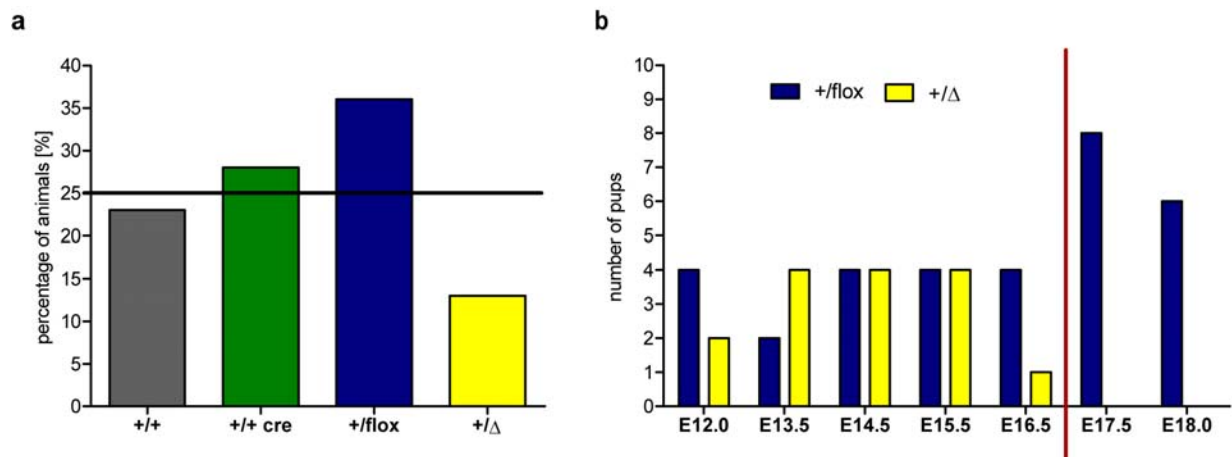


Fig. 33: Numbers of obtained mutants in the *Gsk-3-flox-dh2^{Nes}* strain. Tetraploid *Gsk-3-flox-dh2* males were bred to *Nestin-cre* females and the genotypes of the obtained offspring are depicted. Referring to Mendel's laws, 25% of mutants should be obtained, but this percentage was reduced to 13% at weaning age (a). So, various developmental stages were analyzed. Homozygous floxed males were bred to *Nestin-cre* females and for each stage one female was dissected (47 embryos in total). Up to stage E15.5 the estimated genotypes were distributed equally. But at stage E16.5, the number of mutant embryos was already reduced. Finally, at stage E17.5 and E18.0, no mutant embryos were detected at all (b).

To study this question further, homozygous floxed males were bred to *Nestin-cre* females and embryos were dissected at various developmental stages. From stage E12.0 to E15.5, the distribution of mutant and floxed embryos was as expected (50% each). At stage E16.5, the number of mutant embryos was already reduced. In final developmental stages (E17.5, E18.0) mutant embryos were not present (Fig. 33b). In conclusion, it seems to be possible that the combined reduction of *Gsk-3α* and *Gsk-3β* results in increased embryonic lethality of mutant *Gsk-3-flox-dh2^{Nes}* mice.

5.5.5 Analysis of brain morphology in *Gsk-3* knockdown mice

Since some of the mutant mice already showed obvious phenotypes regarding body size and weight, fertility, and occasional occurring paralysis, I analyzed the brain morphology to exclude defects in the brain development as cause of these phenotypes.

5.5.5.1 Gsk-3/Nestin-cre knockdown mice

To analyze the expression of key neuronal marker genes, I used Digoxigenin (DIG) labeled *in situ* hybridization. This non-radioactive ISH was performed using the Genesis RSP 200 robot from TECAN.

probe	target mRNA	expressed in
GAD2	glutamic acid decarboxylase 2	GABAergic neurons
Sert	Serotonin transporter	serotonergic neurons
TH	Tyrosine hydroxylase	catecholaminergic neurons
VACHT	vesicular acetylcholine transporter	cholinergic neurons

Tab. 4: Neuronal markers used for DIG labeled ISH. The name of the probe, the target mRNA and the marked neuronal population are given here. Catecholaminergic neurons include adrenergic, noradrenergic, and dopaminergic neurons.

All three *Gsk-3/Nestin-cre* mouse lines were analyzed for different neuronal populations, using the markers shown in Tab. 4. In none of the knockdown lines a difference in the expression pattern of the neuronal markers was detected.

On sagittal sections used here and in the radioactive ISH (Fig. 29), I observed an increase in ventricle size in mutant mice. Since this observation was made in all *Gsk-3/Nestin-cre* mouse lines, the ventricle volume in one of the single knockdown mouse lines, namely in the *Gsk-3 α -flox^{Nes}* mice, was analyzed in detail.

Five mutant males and five littermate controls (approximate 14 months old) were sacrificed, and the brains were cut coronally with the cryostat in 40 μ m thick sections. The free floating slices were mounted to slides and stained with cresyl violet. The ventricle volume was measured using a stereomicroscope. The results are depicted in a box & whiskers blot in Fig. 34. The whiskers represent the minimum and maximum values. In coronal sections, it was obvious that the ventricle volume is increased in mutant animals. This analysis confirmed a significant difference in ventricle size of mutant mice. Interestingly, the GMC did not detect any difference in total brain size. Additionally, the body weight of the mice could not be related to the ventricle volume.

Taken together, the brain morphology in mutant *Gsk-3/Nestin-cre* mice was found unchanged, since the analyzed neuronal populations could be detected and were not obviously altered. The only outstanding anomaly was the significant increase in ventricle size, which was observed in all of the *Gsk-3/Nestin-cre* lines.

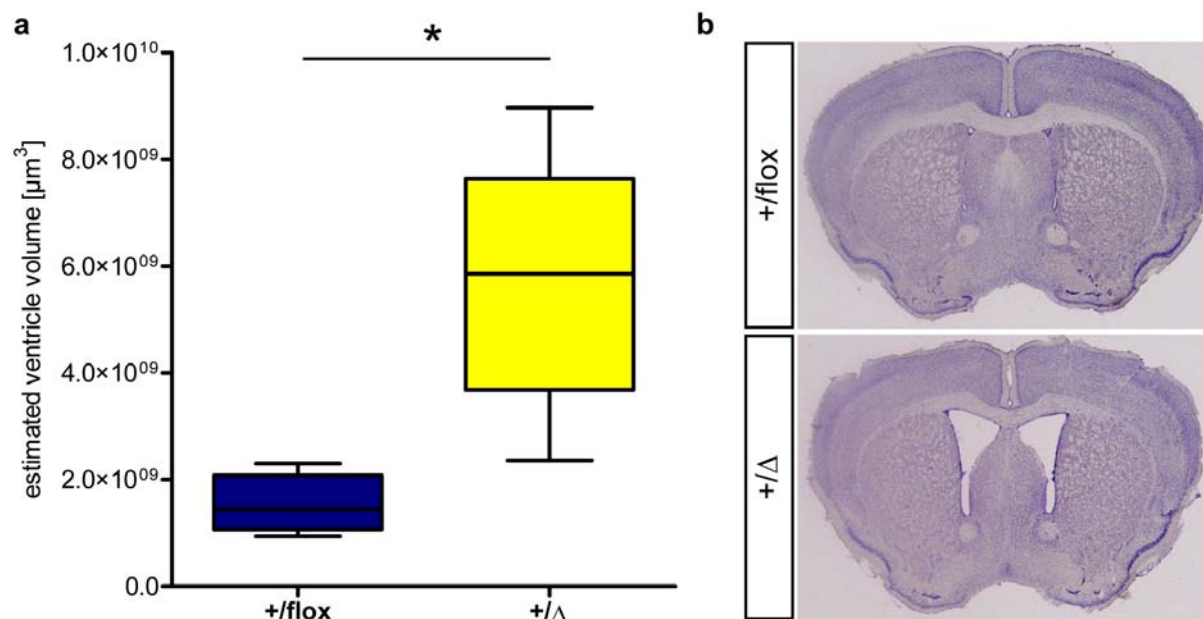


Fig. 34: Analysis of ventricle size in *Gsk-3α-flox^{Nes}* mice. Coronal sections of adult *Gsk-3α-flox^{Nes}* mice were stained with cresyl violet and the volume of the ventricles was measured using a stereomicroscope. The results are depicted in a box & whiskers blot (min; max) and were analyzed by an unpaired t-test with Welch's correction. Compared to littermate controls (+/flox) the ventricle volume is significantly increased in mutant (+/Δ) mice ($p=0.019$) (a). Already in the sections stained by cresyl violet, the increase in ventricle volume is obvious (b).

5.5.5.2 Gsk-3/CamKII-cre knockdown mice

Since the *Gsk-3/CamKII-cre* mice did not show an obvious phenotype, I did not expect any differences in their brain structure. To obtain an overview of brain morphology in these mice, I performed Nissl staining of sagittal brain sections of adult mice.

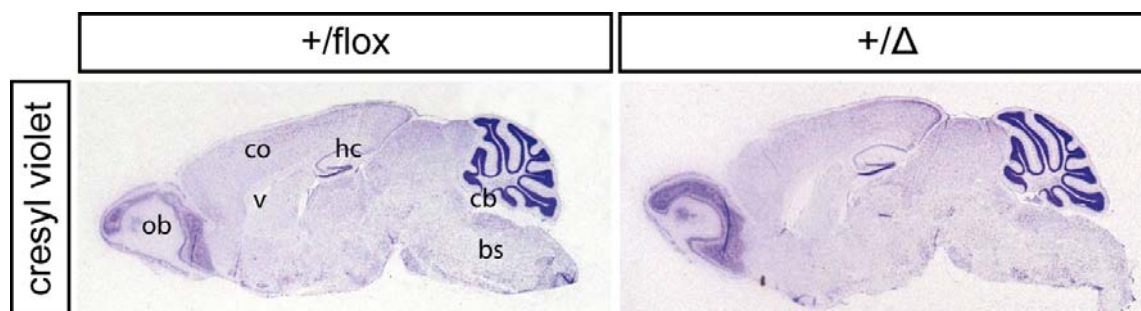


Fig. 35: Nissl staining of sagittal brain sections of adult *Gsk-3-flox-dh2^{Nes}* mice. Male *Gsk-3-flox-dh2^{Nes}* mice were perfused at the age of 16 weeks; brains were dissected and embedded in paraffin. The 8 μm thin slices were stained with cresyl violet and no difference was detected between mutant (+/Δ) and littermate control mice (+/flox). ob: olfactory bulbs, co: cortex, hc: hippocampus, cb: cerebellum, bs: brainstem, v: ventricle

In all *Gsk-3/CamKII-cre* mouse lines, the mutant animals were indistinguishable from their littermate controls and the ventricle size was normal as well (Fig. 35).

5.5.5.3 Influence of *Gsk-3* silencing on apoptosis

Since earlier findings link *Gsk-3* inhibition with an increase of neuronal apoptosis (Gomez-Sintes et al., 2007), I performed immunohistochemical stainings for caspase-3. In Fig. 36 brain sections from adult *Gsk-3-flox-dh2* mice are shown. Neither the *Gsk-3-flox-dh2^{Nes}* nor the *Gsk-3-flox-dh2^{CamKII}* mutants displayed any differences in comparison to their littermate control mice. The same result was found for *Gsk-3 β -flox-sh2^{Nes}* mutant mice.

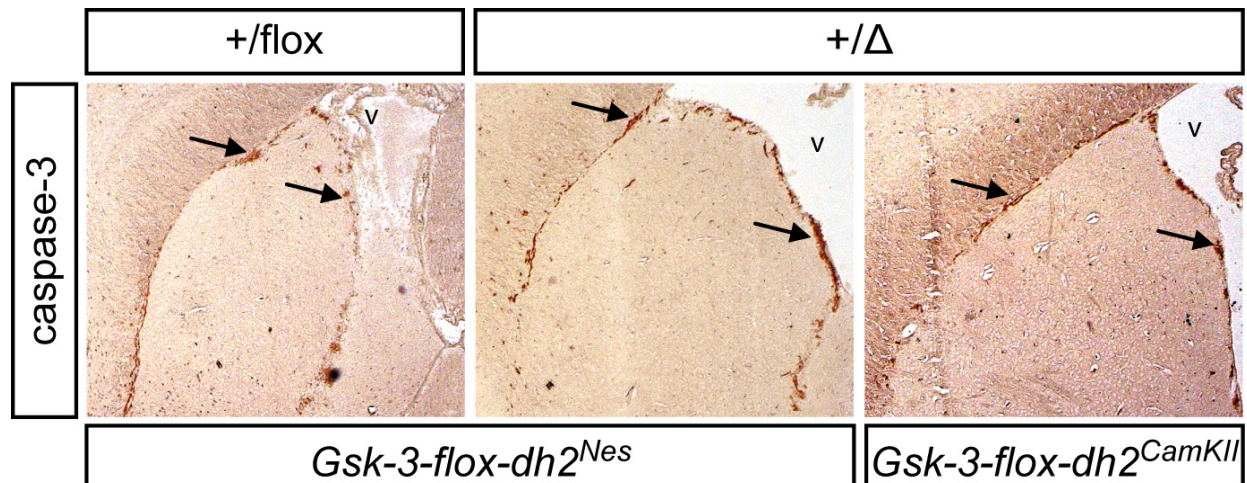


Fig. 36: Immunohistochemical staining for caspase-3 in adult brain slices. Sagittal brain sections of *Gsk-3-flox-dh2^{Nes}* and *Gsk-3-flox-dh2^{CamKII}* mice were stained with an antibody against caspase-3. Arrows indicate stained cells. No difference was detected between mutant (+/Δ) and littermate control mice (+/flox). v: ventricle

5.5.6 Phenotypic analysis in the German Mouse Clinic

The German Mouse Clinic (GMC) at the HelmholtzZentrum München offers a standardized phenotypic analysis in the areas of behavior, bone and cartilage development, neurology, clinical chemistry, eye development, immunology, allergy, steroid metabolism, energy metabolism, lung function, vision and pain perception, molecular phenotyping, cardiovascular and pathology. All these modules are passed during the primary screen. After evaluation of the results from the primary screen, the facility offered a secondary screen for further confirmation and more detailed analysis.

Since I observed some unexpected defects in the mouse strains *Gsk-3 β -flox-sh2^{Nes}* and *Gsk-3 α -flox^{Nes}* regarding the body weight and size (5.5.3), these mice were analyzed in the GMC to obtain a more complete overview of their constitution. For these strains the complete GMC primary screen was performed with some modifications regarding the age and the behavior module.

5.5.6.1 Behavioral analysis of *Gsk-3/Nestin-cre* knockdown mice

Previous publications connect the loss or inhibition of *Gsk-3* to modified anxiety and depression related behavior and motor coordination deficits (Gomez-Sintes et al., 2007; O'Brien et al., 2004). To gain information about the behavior of *Gsk-3* knockdown mice, the following behavioral tests were performed: modified Hole Board test (mHB), light-dark box (LD), accelerating rotarod (Rota), and forced swim test (FST). The measured parameters of each test are listed in the appendix (8.3).

In the mHB a whole set of parameters is analyzed. This test measures the spontaneous behavior of mice in a novel environment. Additionally, signs of anxiety related endophenotypes can be detected.

Comparing the mouse strains *Gsk-3 α -flox^{Nes}* and *Gsk-3 β -flox-sh2^{Nes}* in the mHB, the results for all locomotion parameters were nearly the same: all mutants exhibited a straighter path shape (reduced mean turn angles $p < 0.01$, angular velocity $p < 0.001$, and absolute meander $p < 0.05$) than the littermate controls. This might be due to the fact that those mutants kept only a very short distance to the wall. This phenotype was even stronger in the *Gsk-3 α -flox^{Nes}* mice and indicated that these mutants show an increased anxiety in novel environment. Additionally, in the *Gsk-3 α -flox^{Nes}* animals, other parameters, which support this observation, were altered, namely the time on board and the entries on board were significantly decreased and the latency to first board entry was significantly increased ($p < 0.05$). This phenotype was also detected in the *Gsk-3 β -flox-sh2^{Nes}* mutants, although it lacked significance (Fig. 37). The *Gsk-3 α -flox^{Nes}* mutants also spent more time in social contact with the group ($p < 0.05$) and with grooming ($p < 0.05$) than the control animals. This indicated an increased emotionality in the mutants. The horizontal exploratory behavior was also altered, because these animals explored significantly less holes ($p < 0.01$) than the control animals. No difference in horizontal exploration was detected in the *Gsk-3 β -flox-sh2^{Nes}* mutants, they just started later with hole exploration ($p < 0.05$).

Besides the general locomotion and exploration behaviors, anxiety related behavior is measured in the light-dark box by observing the time spent by the animals in the different compartments. This test was first performed with the *Gsk-3 β -flox-sh2^{Nes}* mouse line, but no alterations in the behavior were detected. Since behavior tests are time consuming, the *Gsk-3 α -flox^{Nes}* mice were not tested.

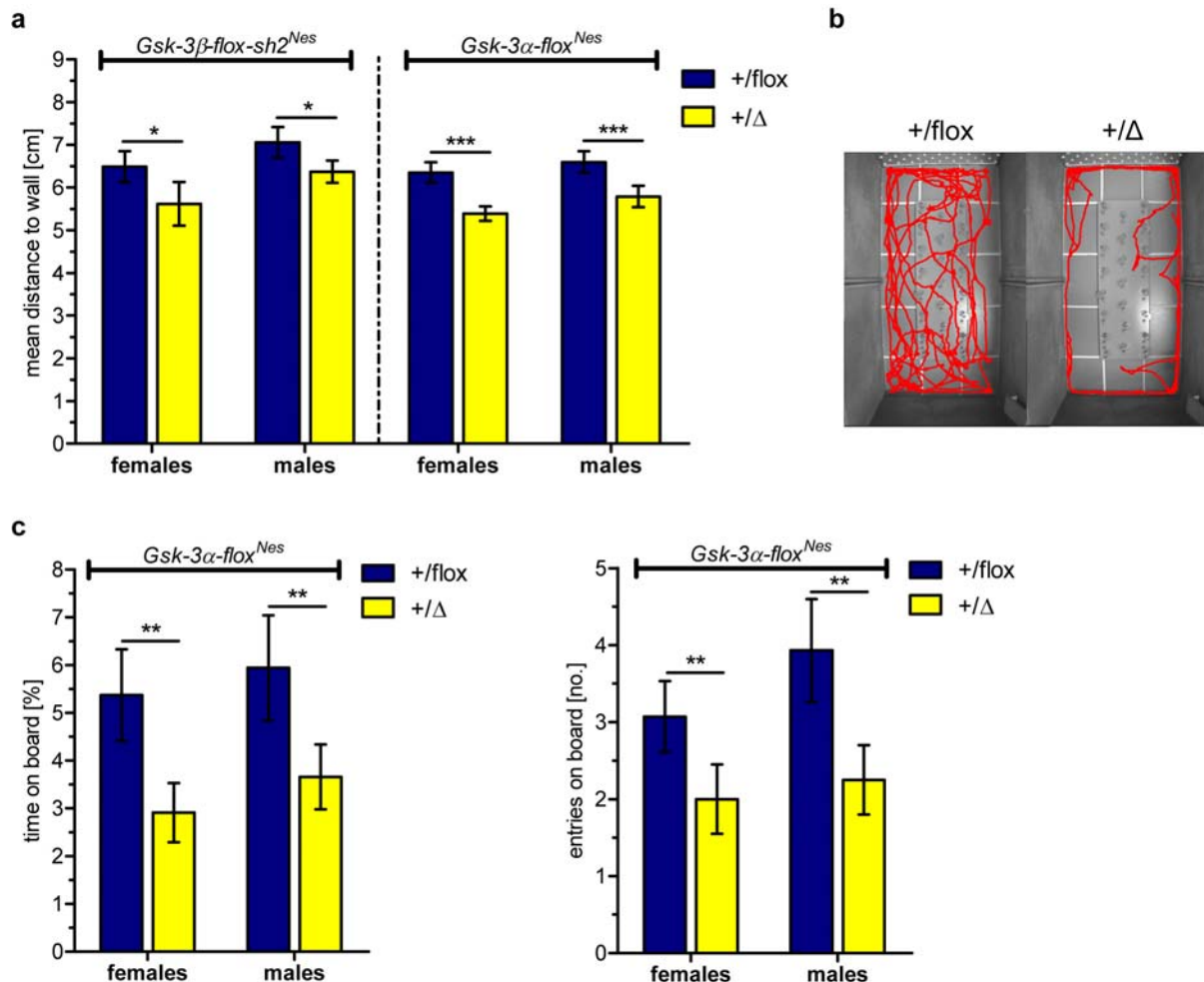


Fig. 37: Modified Hole Board behavior results of $Gsk-3/Nestin-cre$ mice. Mutant $Gsk-3\beta-flox-sh2^{Nes}$ and $Gsk-3\alpha-flox^{Nes}$ mice kept a significantly shorter distance to the wall, indicating increased anxiety in novel environment (a). A concrete example for the straightened path shape is depicted in the right panel (b). Additionally, $Gsk-3\alpha-flox^{Nes}$ mutants showed a decrease in time and entries on board, supporting the picture of an increased anxiety related behaviour in these mice (c). Error bars represent the SEM. *: $p < 0.05$, **: $p < 0.01$, ***: $p < 0.001$

In the accelerating rotarod the motor coordination of mice is measured. Impairments of motor coordination were not detected in $Gsk-3\alpha-flox^{Nes}$ mice. In the $Gsk-3\beta-flox-sh2^{Nes}$ mice the females displayed a subtle phenotype. In general, the mice improved coordination during the three trials and were able to stay longer on the rod with each trial. This was not the case in female mutants. No improvement during the trials was detected.

The forced swim test is an indicator for stress and motivation related behavior. Alterations were not detected in $Gsk-3\alpha-flox^{Nes}$ mice, but only 30 instead of 60 animals were tested due to a changed workflow in the GMC. Only the $Gsk-3\beta-flox-sh2^{Nes}$ mutant females showed some alterations in the FST. They spend significantly less time swimming and more time floating than the control animals

($p < 0.01$). Since the mutants decreased their swimming effort over time, a reasonable explanation, regarding the decreased body weight and size, could be that the mutant females had less muscle strength to keep up swimming during the trial.

5.5.6.2 Behavioral analysis of *Gsk-3/CamKII-cre* knockdown mice

Initially, the behavior of *Gsk-3/Nestin-cre* knockdown mice should be compared to the behavior of *Gsk-3/CamKII-cre* mutants, so the same set of behavior tests was performed with these two mouse lines. But since all *Gsk-3/Nestin-cre* knockdown mice suffered from physical impairment, it was not possible to compare the results of the behavior tests with the results of the *Gsk-3/CamKII-cre* knockdown mice, because of the strong influence of the physical ability in these tests.

In the mHB test the behavior of the *Gsk-3/CamKII-cre* knockdown mice was the opposite of the *Gsk-3/Nestin-cre* knockdown mice. Basically, the mutants of the mouse lines *Gsk-3 α -flox^{CamKII}* and *Gsk-3 β -flox-sh2^{CamKII}* displayed highly significant increased locomotion and activity parameters, comprising the following values: line crossing frequency, total distance traveled, and mean velocity (Fig. 38). Due to increased locomotion, their path shape was slightly straightened, indicated by decrease in absolute meander ($p < 0.05$). In general, these parameters were altered in the *Gsk-3-flox-dh2^{CamKII}* mouse line as well, but only in female mutants. The male mutants spent less time in group contact and showed increased defecation. Together with their tendency to increased grooming, which started significantly ($p < 0.05$) earlier in both sexes, I assumed higher emotionality in male *Gsk-3-flox-dh2^{CamKII}* mutants. Taken together, the *Gsk-3/CamKII-cre* knockdown mice showed a hyperactive behavior in the novel environment of the mHB.

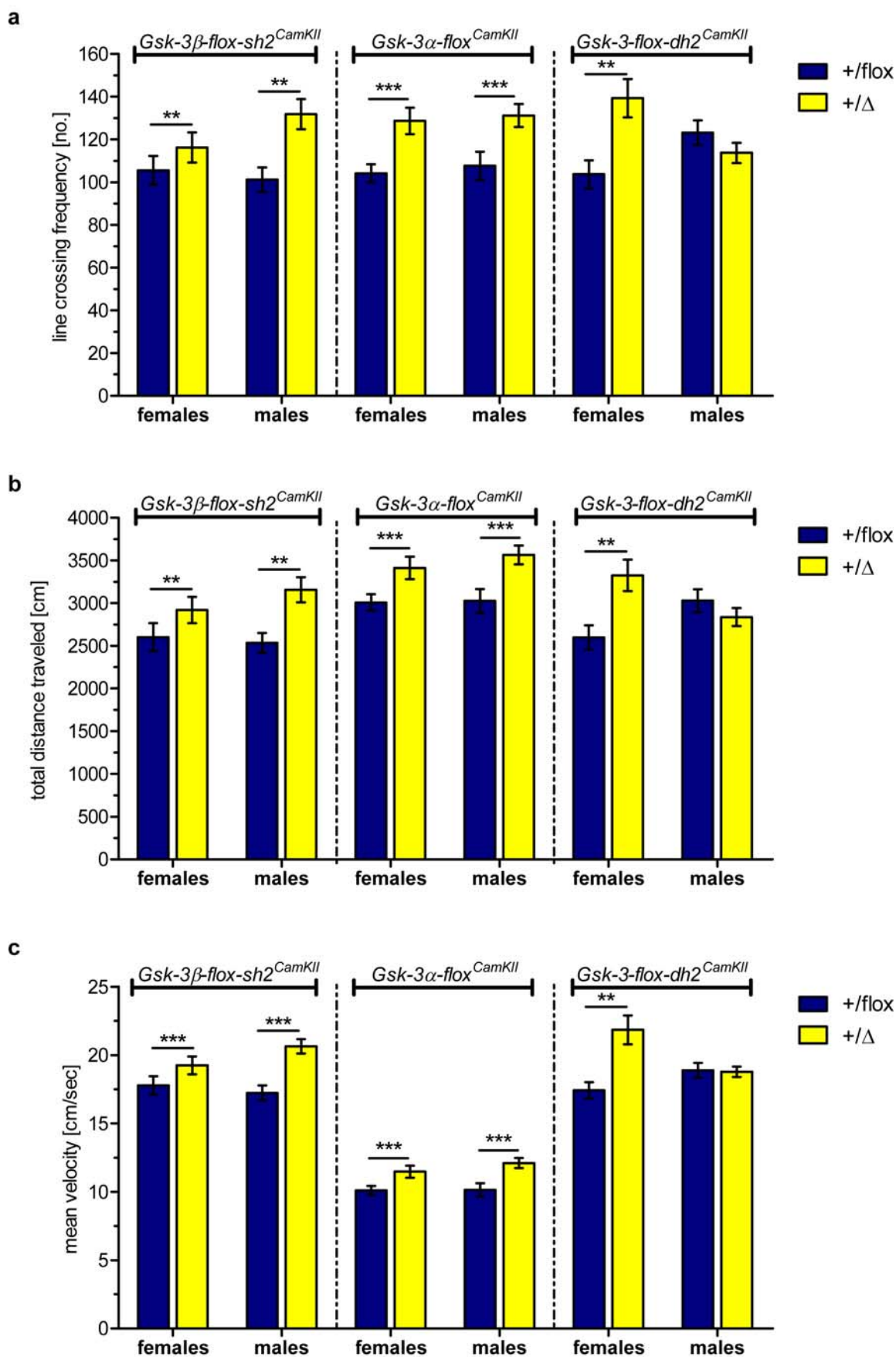


Fig. 38: Modified Hole Board behavior results of *Gsk-3/CamKII-cre* mice. In *Gsk-3α-flox^{CamKII}*, *Gsk-3β-flox-sh2^{CamKII}*, and female *Gsk-3-flox-dh2^{CamKII}* mutant mice activity and forward locomotion parameters were altered. An increase in line crossing

frequency indicated higher activity in mutant mice (a). The total distance traveled was also significantly increased (b). Additionally, the mutants moved with higher speed than the control mice. The general decrease in mean velocity in $Gsk-3\alpha-flox^{CamKII}$ mutants can be explained by a higher age at the test time (c). Error bars represent the SEM. **: $p < 0.01$, ***: $p < 0.001$

Although the behavior of the $Gsk-3\beta-flox-sh2^{Nes}$ mouse line was not altered in the light-dark box test, some alterations were detected in the behavior of $Gsk-3\beta-flox-sh2^{CamKII}$ mutant mice. The total time spent in the light compartment, like the performed rearings there, was significantly increased. To exclude vision defects, the mice were tested in the optical drum and no difference to control mice was detected. These changes indicate less anxiety related behavior in the $Gsk-3\beta-flox-sh2^{CamKII}$ mutants (Fig. 39). In $Gsk-3\alpha-flox^{CamKII}$ and $Gsk-3-flox-dh2^{CamKII}$ mutants only a subtle increase in some locomotion and speed parameters was detected.

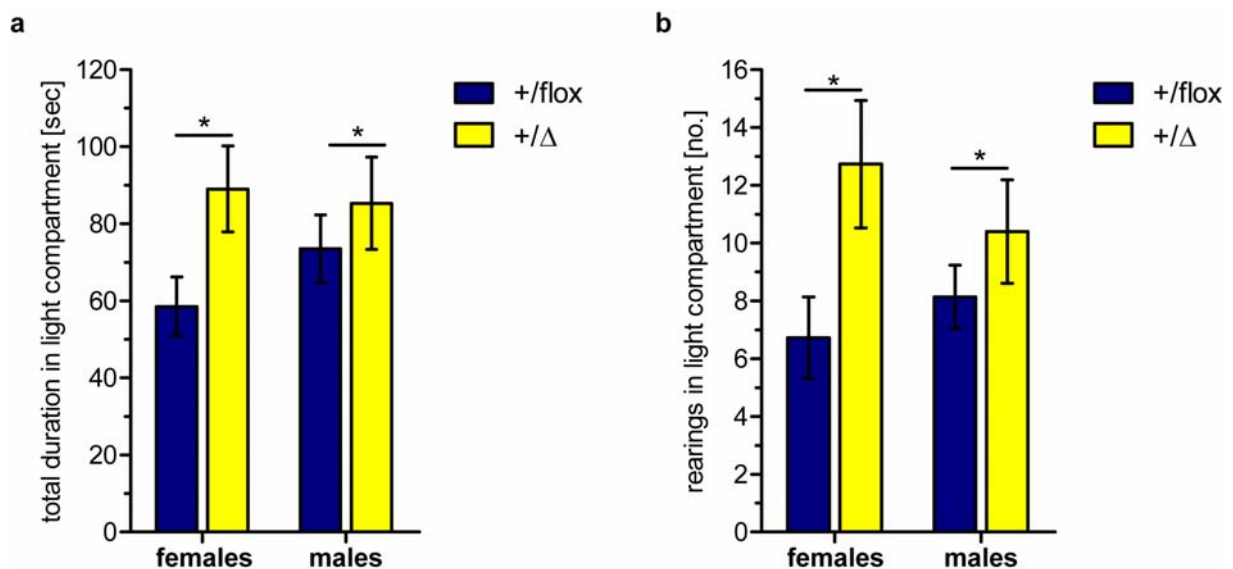


Fig. 39: Light-dark box behavior results of $Gsk-3\beta-flox-sh2^{CamKII}$ mice. $Gsk-3\beta-flox-sh2^{CamKII}$ mutant mice displayed less anxiety related behavior. This was measured by the total time spent in the light compartment (a) and the increased vertical exploration behavior measured in total number of rearings in the light compartment (b). Error bars represent the SEM. *: $p < 0.05$

Motor coordination, measured in the accelerating rotarod, of $Gsk-3\beta-flox-sh2^{CamKII}$ and $Gsk-3\alpha-flox^{CamKII}$ mutants was unchanged. $Gsk-3-flox-dh2^{CamKII}$ mutant animals fell significantly later from the rod than their littermate controls and tend to have an increased number of passive rotations, which means that the test was not stopped by the mouse falling off, but by the observer. Interestingly, from the very beginning the male mutants performed better in this test than the controls (Fig. 40).

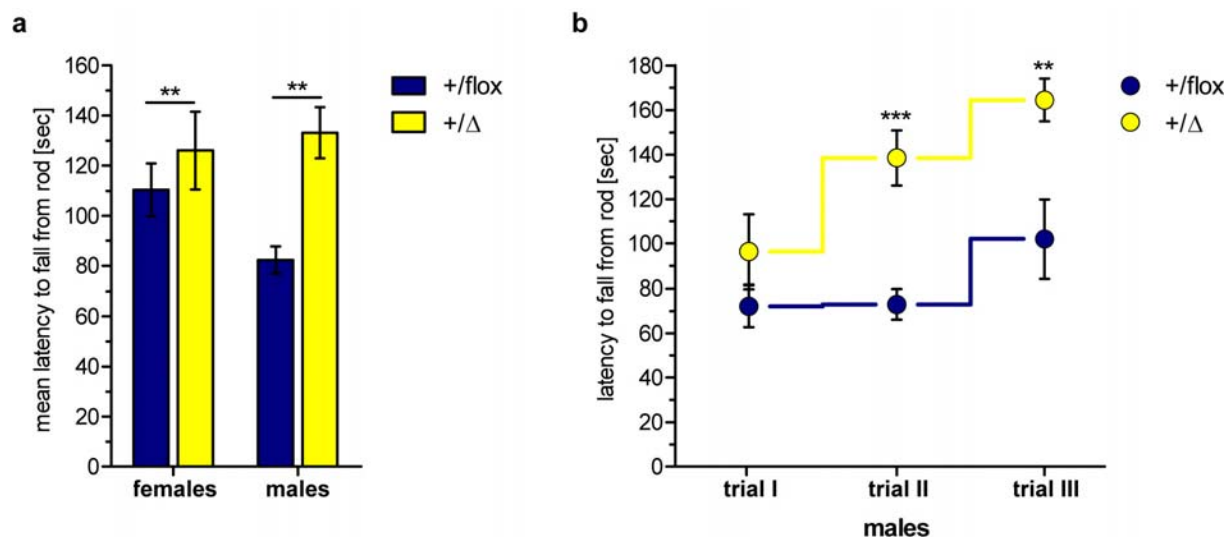


Fig. 40: Behavior results of *Gsk-3-flox-dh2^{CamKII}* mice in the accelerating rotarod. The mean latency to fall from the rod was significantly increased in *Gsk-3-flox-dh2^{CamKII}* mutant mice (a). Especially the mutant males performed, from the very beginning, much better on the rod than the littermate controls (b). Error bars represent the SEM. **: $p < 0.01$, ***: $p < 0.001$

During the forced swim test, the *Gsk-3β-flox-sh2^{CamKII}* mutants spent less time struggling, which indicates a less active stress coping behavior. This was not confirmed in the *Gsk-3α-flox^{CamKII}*. Here, the mutant animals spent significantly more time swimming and less time floating, which is connected to a more active stress coping behavior (Fig. 41). The *Gsk-3-flox-dh2^{CamKII}* mutant females spent less time struggling during the first three minutes. Besides, the swimming and floating parameters are unchanged in both sexes. Only in the last minute of the trial, the mutant males showed a significant decrease in the time spent floating ($p < 0.01$) and a correlating increase in the time spent swimming ($p < 0.05$). Perhaps the increased activity detected in this mouse line enables the mutants to a last physical effort.

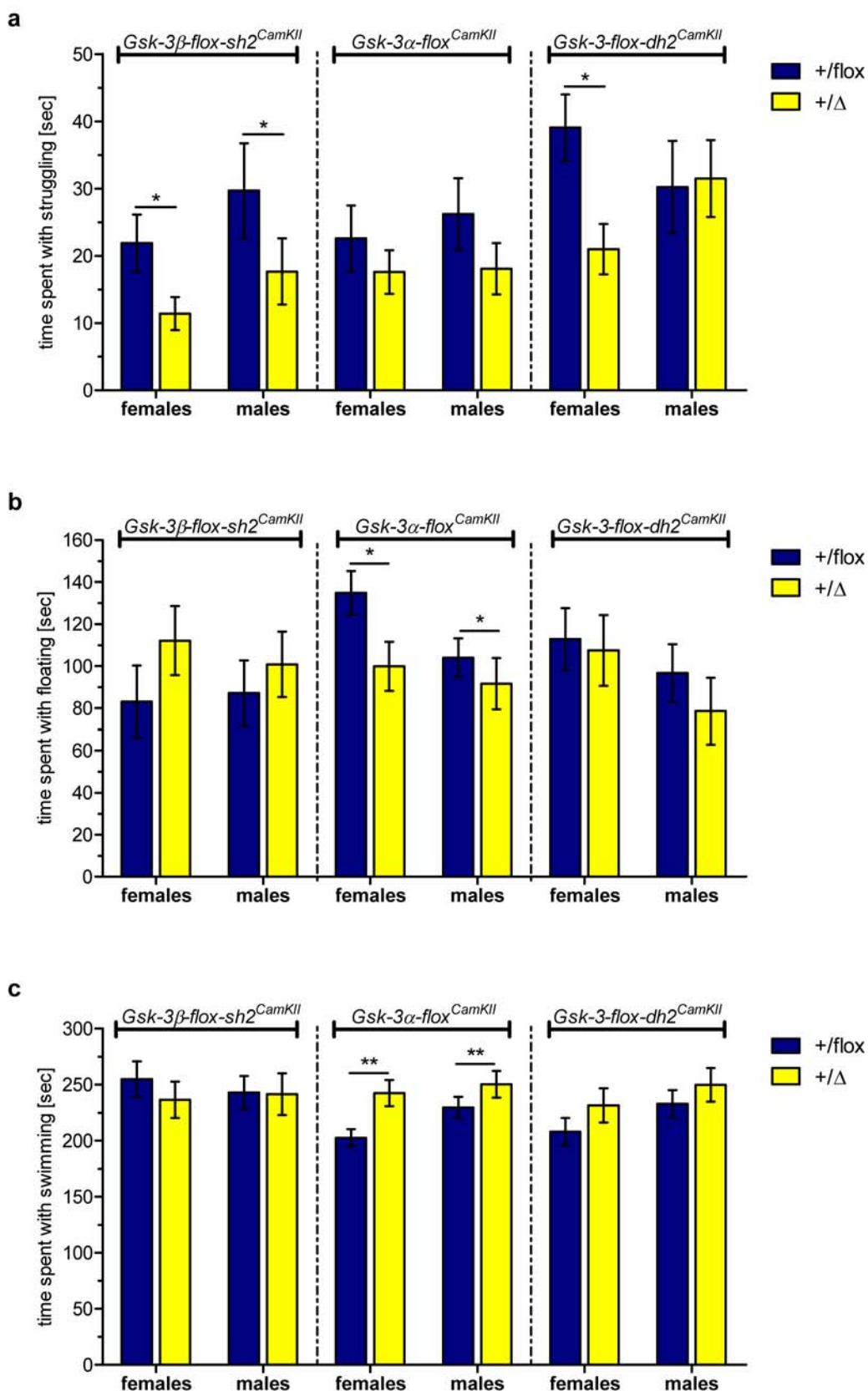


Fig. 41: Forced swim test behavior results of *Gsk-3/CamKII-cre* mice. In the FST the time the mice spent struggling (a), floating (b), and swimming (c) is measured. *Gsk-3β-flox-sh2^{CamKII}* mutants struggled less than the control animals, which indicated a less active stress coping behavior. The female *Gsk-3-flox-dh2^{CamKII}* mutant mice also spent less time with struggling, mainly during the first three minutes. Only in the *Gsk-3α-flox^{CamKII}* mutants, changes in the time spent swimming and floating were

detected. These animals swam more and floated less than the respective control animals. These changes indicated a more active stress coping behavior. *Error bars represent the SEM. *: $p < 0.05$, **: $p < 0.01$*

5.5.6.3 Influence of *Gsk-3* silencing on blood pressure

During the GMC primary screen, one of the most significant and surprising results was found in the cardiovascular module. Here, the blood pressure was measured and electrocardiogram (ECG) was performed.

Blood pressure analysis provides insights into functions of the vascular system including the regulation of vascular tone and left ventricular pump function. Blood pressure is strongly influenced by defects in many organ systems (heart, kidney, lung, liver) and metabolic or (neuro)endocrine pathways. Imbalances in one or, usually several organs and pathways, result in changes of this sensitive global parameter (Deschepper et al., 2004; Krege et al., 1995; Lorenz, 2002). The ECG measures the electrical activity, rate and rhythm of the heart beat, supplying information about the conductive properties (function of ion channels), the excitable myocardial mass and the propagation of excitation within the heart tissue. Almost all types of cardiac pathologies will eventually cause also distinct ECG changes. Therefore, the ECG provides a comprehensive overview on cardiac function (Doevendans et al., 1998; Ehmke, 2003; Royer et al., 2005).

In the *Gsk-3 β -flox-sh2^{Nes}* mice, mutants of both sexes showed a significant decrease of pulse rate, systolic, diastolic, and mean arterial pressure. The ECG was not significantly altered. In *Gsk-3 α -flox^{Nes}* mice a similar phenotype was confirmed. Interestingly, in this mouse line, only the female mutants displayed a significant decrease in systolic, diastolic, and mean arterial pressure. The pulse rate was again significantly decreased in both sexes (Fig. 42). The *Gsk-3 β -flox-sh2^{CamKII}* mice were tested as well, but alterations of blood pressure parameters were not detected.

Since both *Gsk-3/Nestin-cre* knockdown mouse lines displayed a similar blood pressure phenotype, I decided to perform an inhibitor experiment in the cardiovascular module. The inhibitor SB216763, an anilino maleimide and ATP competitor for GSK-3, was injected into *C57Bl/6J* wild type female mice (17 weeks of age) for five consecutive days and blood pressure parameters were measured each day. The mice were split into three groups: one control group with 12 animals and two test groups with 11 animals each. The first test group and the control group were

injected one hour before the measurement of blood pressure. The second test group was injected with the inhibitor five hours before measurement. As described, 10 $\mu\text{g/g}$ of the inhibitor (in max. 200 μl DMSO) were injected intraperitoneally (Beaulieu et al., 2004; Shakoori et al., 2007). The control group was injected with pure DMSO. Measurement started at 2:00 PM, and four mice were measured in parallel.

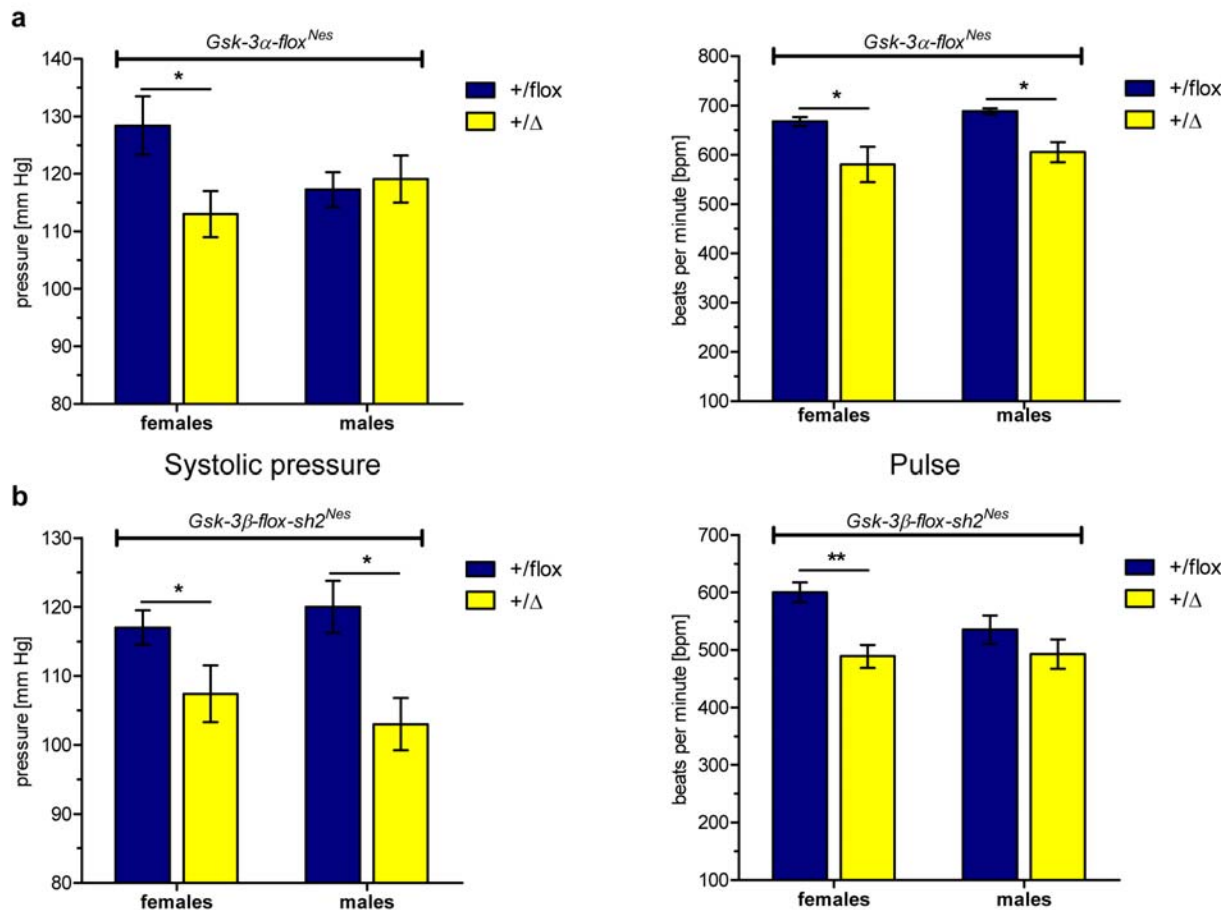


Fig. 42: Systolic pressure and pulse rate of *Gsk-3 β -flox-sh2^{Nes}* and *Gsk-3 α -flox^{Nes}* mice. The left graphs display the measured systolic pressure and pulse rate of *Gsk-3 α -flox^{Nes}* (a) and *Gsk-3 β -flox-sh2^{Nes}* mice (b). In the *Gsk-3 β -flox-sh2^{Nes}* mice the pressure was decreased in both sexes ($p < 0.05$), whereas in the *Gsk-3 α -flox^{Nes}* mice only female mutants showed a pressure decrease. In the right graphs the pulse rate is depicted. Here, both sexes were affected in the *Gsk-3 α -flox^{Nes}* mice, and only the mutant females of the *Gsk-3 β -flox-sh2^{Nes}* mice. Error bars represent the SEM.

During the test week, the mice lost weight (approximately 22 g before to 19 g after the experiment) and six mice, with the highest weight loss, died (in total, from all groups). It seemed that the DMSO influenced the health of the animals *per se*. Dead mice were excluded from the analysis, leaving ten animals in the control and the first test group (1 h) and eight animals in the second test group (5 h). Data were analyzed using an unpaired t-test with Welch's correction and are depicted in Fig. 43 as box & whiskers plot. The whiskers represent the minimum and maximum values.

No significant differences were detected between the groups; only the pulse rate in the first test group (1 h) was decreased, however not reaching significance level. In general, the control and the second test group (5 h) showed very similar results, indicating the decrease of inhibitory function after five hours.

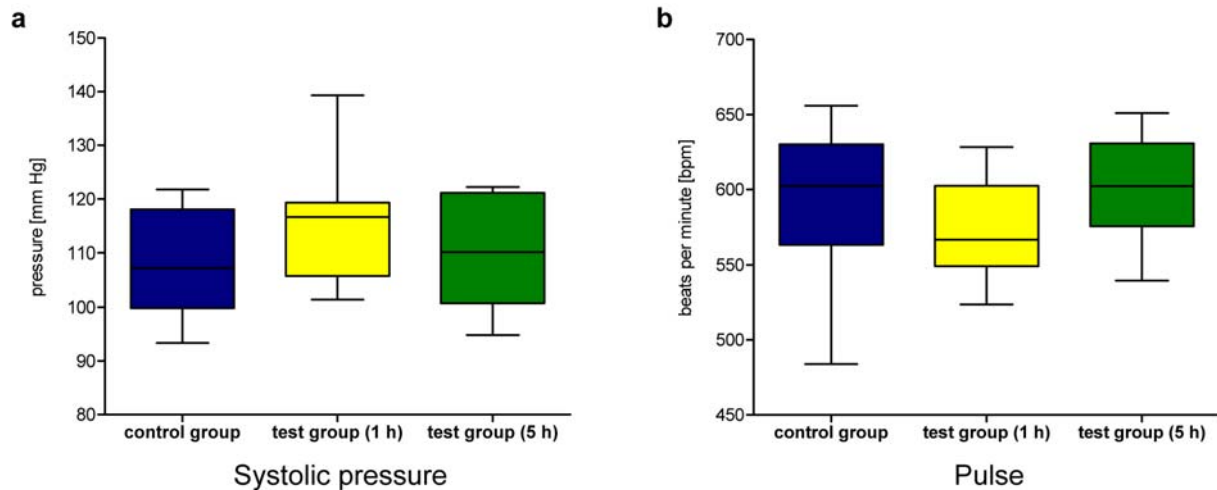


Fig. 43: Influence of GSK-inhibitor on blood pressure parameters. The results are depicted as box & whiskers plot (min; max) and were analyzed using an unpaired t-test with Welch's correction. The systolic pressure was not altered between the groups (a), but there was a slight tendency that the pulse rate was reduced in the animals of the first test group (b).

5.5.6.4 Analysis of myelin in the central nervous system

The *Gsk-3 β -flox-sh2^{Nes}* mice were analyzed first in the GMC primary screen. During the pathology screening an increased vacuolization in the brain of mutant animals was detected (Fig. 44). Vacuoles were found in 15 of 25 analyzed mutants (seven males and eight females) with different severity in cerebrum, particularly substantia nigra, dorsal fornix, cingulum, truncus corporis callosi, and medulla oblongata. One possible reason for this vacuolization was a deficit in myelination. Interestingly, no increase of vacuolization was detected in the *Gsk-3 α -flox^{Nes}* mice.

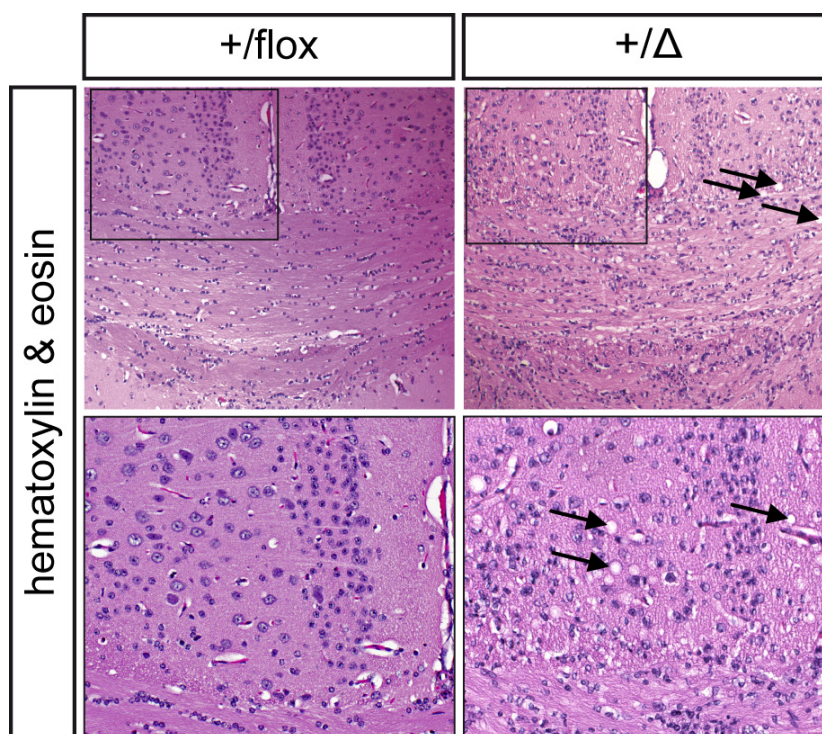


Fig. 44: HE staining of coronal brain sections of adult *Gsk-3β-flox-sh2^{Nes}* mice. In the pathology, coronal sections were cut and stained with hematoxylin and eosin (HE). While the littermate control mice (+/flox) were without pathological findings, in mutant (+/Δ) mice an increased vacuolization (arrows) in the cingulum was detected. The lower panel shows a higher magnification of the marked box.

As secondary analysis, the pathology performed luxol fast blue staining to analyze the state of myelin in the affected mice. This analysis showed a severe loss of myelin in the brain of mutant animals. In Fig. 45, exemplary luxol fast blue staining of coronal brain sections from *Gsk-3β-flox-sh2^{Nes}* and *Gsk-3α-flox^{Nes}* mice is seen. In this staining myelin sheaths appear in a clear blue color, whereas grey matter is colored in aquamarine, and nuclei are shown in deep purple-blue. In +/flox littermate controls, the myelin showed a distinct staining pattern, mainly in the corpus callosum and in the caudate putamen. Additionally, the ventral fiber tracts, like the fornix and the mammillothalamic tract, are clearly distinguishable. The optic tract was also stained strongly. The degree of demyelination was differentiated into none, mild, moderate, and severe loss of myelin. Severe demyelination was only detected in the mutant *Gsk-3β-flox-sh2^{Nes}* mice. In *Gsk-3α-flox^{Nes}* mice, only mutants with a moderate loss of myelin were found. In general, the demyelination is easy detectable in the corpus callosum. Higher magnifications of this brain region are shown in Fig. 46.

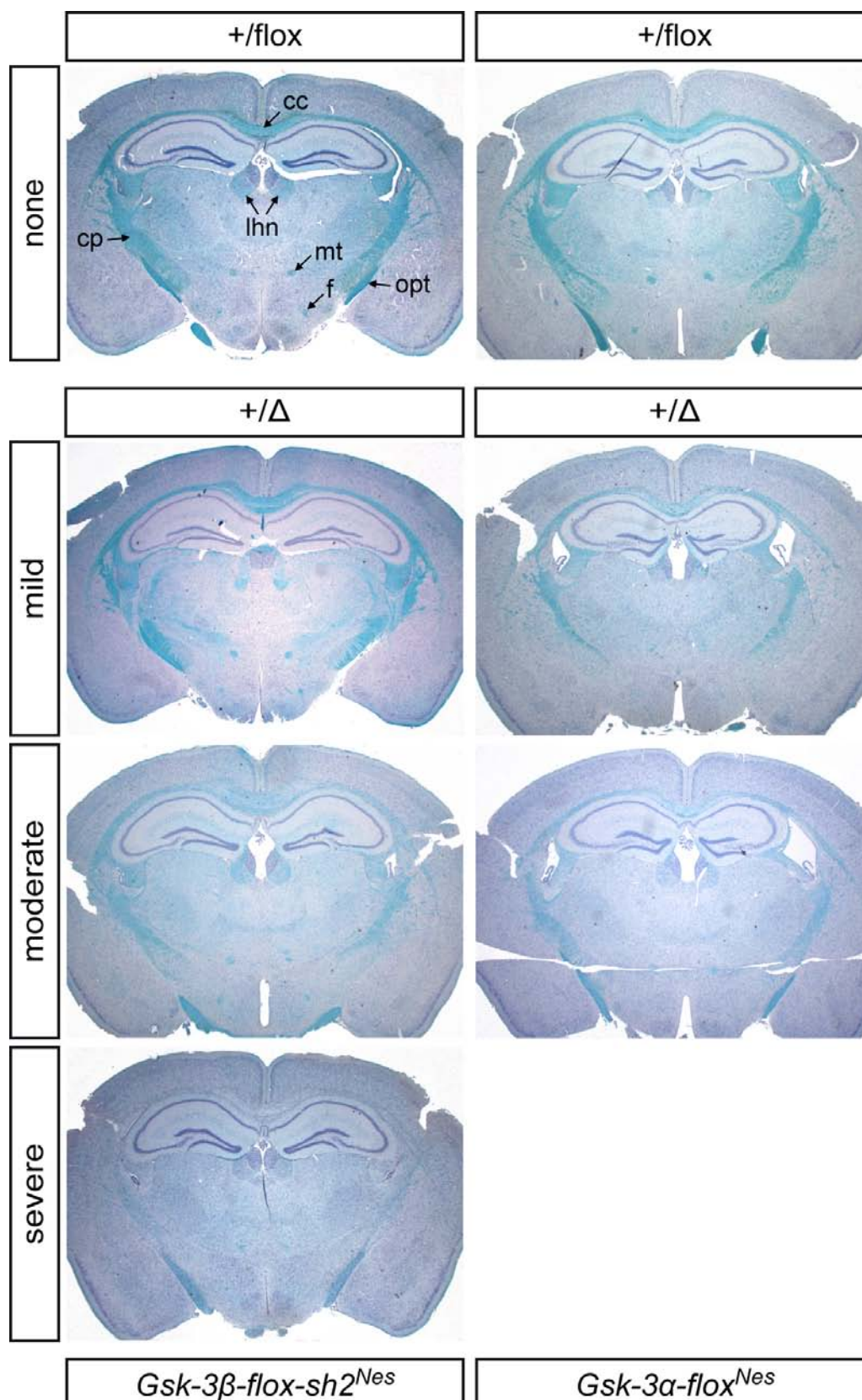


Fig. 45: Luxol fast blue staining of *Gsk-3β-flox-sh2*^{Nes} and *Gsk-3α-flox*^{Nes} mice brain sections. As secondary analysis luxol fast blue staining was performed by the pathology and the loss of myelin was differentiated into the following degrees: none, mild, moderate, and severe demyelination. The loss of myelin was strongest in the *Gsk-3β-flox-sh2*^{Nes} mice, because some mutants (+/Δ) showed a nearly complete loss of myelin (lowest panel). cc: corpus callosum, cp: caudate putamen, f: fornix, lhn: lateral habenular nucleus, mt: mammillothalamic tract, opt: optic tract

In total, all mutants of the *Gsk-3 β -flox-sh2^{Nes}* and *Gsk-3 α -flox^{Nes}* mice were analyzed for the degree of demyelination. Additionally, the mouse lines *Gsk-3-flox-dh2^{Nes}* and *Gsk-3-flox-dh2^{CamKII}* were included in the analysis. The age of the analyzed mice varied from 24 to 47 weeks and the numbers of analyzed mutant animals are given in Tab. 5.

analyzed mouse lines	total number of mutant animals (+/ Δ)	Degree of demyelination			
		<i>none</i>	<i>mild</i>	<i>moderate</i>	<i>severe</i>
<i>Gsk-3α-flox^{Nes}</i>	16	7	5	4	-
<i>Gsk-3β-flox-sh2^{Nes}</i>	25	5	7	7	6
<i>Gsk-3-flox-dh2^{Nes}</i>	6	2	4	-	-
<i>Gsk-3-flox-dh2^{CamKII}</i>	6	6	-	-	-

Tab. 5: Mouse lines analyzed with luxol fast blue staining are listed here. The degree of myelin loss and the total numbers of stained mutant animals are given, too.

In 80% (48% in females; 32% in males) of the mutant *Gsk-3 β -flox-sh2^{Nes}* mice, a loss of myelin was detected. The distribution of different demyelination classes was: 24% showed severe and 28% mild or moderate loss of myelin. In the *Gsk-3 α -flox^{Nes}* mice the penetrance of this phenotype was lower with 56% (31% in females; 25% in males) of mutant animals suffering from myelin loss. In contrast to *Gsk-3 β -flox-sh2^{Nes}* mutants, only cases of moderate demyelination were detected in *Gsk-3 α -flox^{Nes}* mutants (25%). In the remaining 31% of mutant animals showing demyelination, a mild loss of myelin was detected. Finally, *Gsk-3-flox-dh2^{Nes}* and *Gsk-3-flox-dh2^{CamKII}* mutant mice were analyzed, too. In the first, 67% (50% in females; 17% in males) of mutant animals showed only a mild loss of myelin, and in the latter no demyelination was detected at all.

No demyelination was observed in floxed littermate controls. Since it is known for certain Cre recombinase expressing mouse strains to suffer from side effects of high Cre recombinase expression, the so called Cre toxicity (Forni et al., 2006; Schmidt-Supprian and Rajewsky, 2007; Schmidt et al., 2000), *Nestin-cre* mice were included in this analysis. In the brains of five *Nestin-cre* mice no signs of myelin loss were detected.

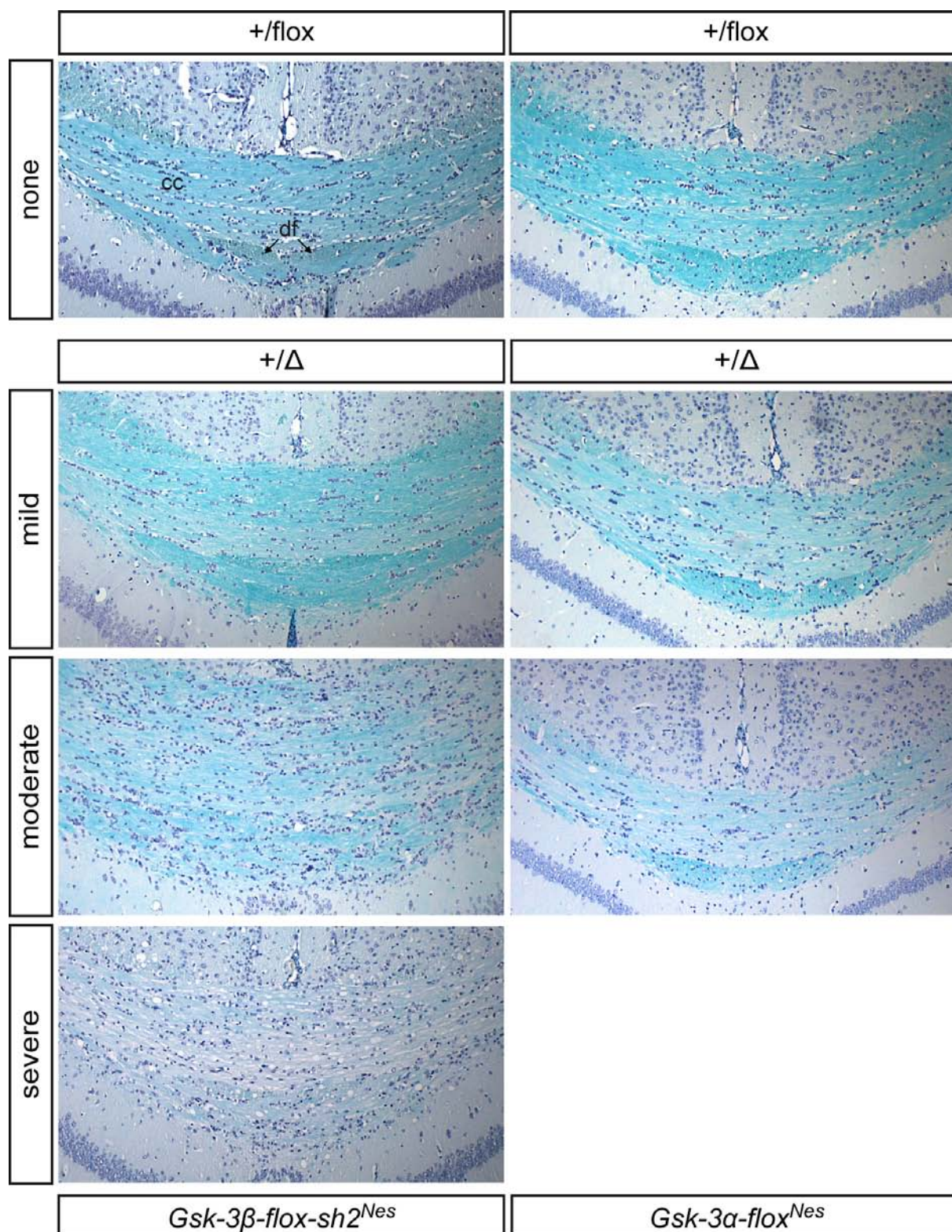


Fig. 46: Loss of myelin in the corpus callosum of *Gsk-3β-flox-sh2^{Nes}* and *Gsk-3α-flox^{Nes}* mice. In the corpus callosum the loss of myelin is very strong. Especially in mutant (+/Δ) *Gsk-3β-flox-sh2^{Nes}* mice, the dorsal fornix can no longer be distinguished in moderate and severe stages, due to the increased loss of staining. *cc*: corpus callosum, *df*: dorsal fornix

6 DISCUSSION

6.1 Generation of *Gsk-3 α* knockout mice by gene trapping

Since *Gsk-3 α* knockout mice were not described at the beginning of this work, I decided to generate such knockout mice from a gene trap ES cell clone. In general, gene trapping is a fast and easy approach to achieve mutagenesis in the genome, since direct manipulation of the target locus is not necessary. Additionally, it is applicable to high-throughput analysis and can be refined for conditional mutagenesis (Turksen, 2001).

Although the ES cell clone RRK111 was confirmed for the trapping of the *Gsk-3 α* locus and correct splicing of the gene trap vector to exon one, loss of GSK-3 α protein was not detected in homozygous gene trap mice. To analyze this problem, lacZ stainings of spleen, liver, and kidney of gene trap mice were performed to assure the correct function of the reporter construct. Surprisingly these samples stained red instead of the expected blue color, with a more intense staining in homozygous mice. Since the positive control stained blue, it might be that the reporter LacZ was damaged in the construct, only able to produce the reduced red form of the desired blue indigo dye.

It is known that in some cases gene trap vectors are not fully mutagenic, because of integration into intron sequences and the possibility of alternative splicing resulting in low levels of wild type transcript or hypomorphic alleles (Stanford et al., 2001; Turksen, 2001). To clarify this issue, I performed RT-PCR analysis using cDNA from homozygous gene trap mice and I could directly show the presence of *Gsk-3 α* wild type transcript (Fig. 12). This unexpected finding clearly indicated that the gene trap vector in the ES cell clone RRK111 was spliced out as part of the first *Gsk-3 α* intron. To analyze the efficiency of this splice event, Northern blot analysis of brain RNA was performed. Besides the expected fusion transcript of the gene trap vector, the *Gsk-3 α* wild type transcript was detected and quantified to represent 85.5% of total *Gsk-3 α* transcripts. Therefore, it was obvious that the gene trap vector in these mice did not work properly. There is no clearly identified cause for this malfunction, but Southern blot analysis with a neo probe displayed several bands in genomic DNA of gene trap mice, indicating multiple integrations of the gene trap vector into the

Gsk-3 α locus. Additionally, this locus was difficult to analyze by PCR, since two different PCR approaches were able to detect the *Gsk-3 α* wild type genomic sequence in homozygous gene trap mice. In conclusion, these findings suggest an inaccurate, rearranged vector integration into the *Gsk-3 α* gene of the ES cell clone RRK111 and subsequent ignorance of the gene trap vector by the splicing machinery of the cell.

6.2 Comparison of knockdown efficiency of shRNAs *in vitro* and *in vivo*

RNA polymerase III promoters, like the H1 promoter and the human U6 promoter, are commonly used for the expression of shRNAs (Brummelkamp et al., 2002; Dykxhoorn et al., 2003; Paddison et al., 2004). In our group the use of the human U6 promoter was established and confirmed to be functional in combination with a transcriptional stop element within the loop region of the shRNA (Hitz et al., 2007).

Besides the strength of the used promoter, the knockdown efficiency of shRNAs depends on their specific target sequence. The key elements for effective shRNA design are low G/C content, low internal stability at the 5' antisense strand, lack of inverted repeats, and sense strand base preferences at positions 3, 10, 13, and 19. These and other criteria were incorporated into algorithms used for prediction of effective target sequences (Mittal, 2004; Reynolds et al., 2004; Vermeulen et al., 2005). Three different public available selection tools were used to predict five shRNA target sequences for each *Gsk-3* gene (Tab. 1). One shRNA for *Gsk-3 β* (*Gsk-3 β -sh5*) was chosen from a recent publication (Yu et al., 2003). To target all known splice variants of *Gsk-3*, alternative exons were excluded from shRNA targeting. Furthermore, the mismatches between the two isoforms were taken into account to prevent unspecific targeting of both *Gsk-3* genes with a single shRNA.

Before the production of transgenic mice, the selected shRNAs were tested in ES cell culture for their knockdown efficiency on mRNA and protein level in three different test systems. First, shRNAs were tested by real-time qRT-PCR (Fig. 14) and it turned out that all shRNAs against *Gsk-3 α* , except *Gsk-3 α -sh2*, induced more than 70% mRNA knockdown. The results for *Gsk-3 β* were more divergent. Three shRNAs reached the threshold: *Gsk-3 β -sh1*, *Gsk-3 β -sh2*, and *Gsk-3 β -sh4*, but the other two, especially *Gsk-3 β -sh3*, showed high error variation and low mean knockdown

efficiency. Surprisingly also the Gsk-3 β -sh5 shRNA published by Yu et al. was ineffective. In accordance with a published report, I confirmed that this shRNA was not able to mediate a strong knockdown of Gsk-3 β (Kim et al., 2006).

Second, the knockdown efficiency of the target mRNA was tested with the pScreen-iT™ system from Invitrogen, based on the degradation of a *lacZ-Gsk-3* fusion transcript (Fig. 16/17). As in the real-time qRT-PCR, all Gsk-3 α shRNAs induced efficient knockdown in the pScreen-iT™ system. For the Gsk-3 β shRNAs, the results were again more divergent, but comparable to the real-time qRT-PCR results. Using this approach, I checked also the Cre recombined shRNA vectors with the remaining lox site in the loop region and showed that the knockdown efficiency was not diminished by the presence of a loxP or lox2272 site.

Finally, the knockdown efficiency of shRNA vectors on the target protein was measured by transient transfection of ES cells and subsequent quantification of Western blot signals. Taking the results of all three efficiency tests together, I selected the Gsk-3 β -sh2 and Gsk-3 β -sh4 shRNAs for the generation of Gsk-3 β knockdown mice. For silencing of the Gsk-3 α gene, Gsk-3 α -sh1 was chosen, since it was the only one standing out in the pScreeniT™ system, besides similar results in the other tests. The reproducibility of knockdown in all tests *in vitro* would hopefully lead to a sufficient knockdown *in vivo*. In general, all these tests rely on a transfection efficiency of ES cells near 100%, but this efficiency is definitely not reached in each test and one reason for the high variability between replicates. Only the pScreeniT™ system offers the possibility of correcting the data for transfected cells by cotransfection of the firefly luciferase expression vector. However, this system suffers from the disadvantage that the silencing efficiency is measured on a fusion transcript of *lacZ* with the target gene cDNA. The structural difference of this fusion transcript to the wild type mRNA target may expose target sequences differentially to the RISC complex and thereby alter the efficiency of gene silencing.

The Gsk-3/*Nestin-cre* mice were analyzed for their protein and mRNA knockdown in the brain. The mRNA reduction of Gsk-3 α and Gsk-3 β in the brain was estimated to a value of 60% and 55% respectively, and could be confirmed by a clear reduction of ISH signals in brain sections. The reduction of GSK-3 α protein was calculated to a value of 51% and the reduction of GSK-3 β was quantified to 49%. Taking multiple

sources of error in the quantification procedure into account, the results of protein and mRNA knockdown obtained *in vivo* were quite comparable. However, the knockdown levels in mice were not comparable to the levels determined *in vitro*, which was for the Gsk-3 β -sh4 98% in the pScreeniT™ system compared to 55% in the Northern blot *in vivo*. Surprisingly, the efficiency of protein knockdown *in vitro* was comparable to the results *in vivo* (Tab. 6).

shRNA	knockdown level <i>in vitro</i>		knockdown level <i>in vivo</i>	
	mRNA [%]	protein [%]	mRNA [%]	protein [%]
Gsk-3 α -sh1	97	41	60	51
Gsk-3 β -sh2	98	68	-	below detection
Gsk-3 β -sh4	98	64	55	49

Tab. 6: Comparison of knockdown levels *in vitro* and *in vivo*, measured by the pScreen-iT™ system and Northern blot or by Western blot. For the Gsk-3 β -sh2, the *in vivo* data was measured in tetraploid embryos with random integration of the non-conditional shRNA.

These differences are perhaps caused by the use of single shRNA vector copies in transgenic mice as compared to multiple copies transfected into ES cells for the *in vitro* efficiency tests. The number of non-transfected cells might balance this difference *in vitro*. So, regarding the potential of the shRNAs, the pScreeniT™ system gives a good overview, but since the efficiency of the shRNA in single copy is crucial for the knockdown *in vivo*, the system is only useful to exclude shRNAs with a very low potential even in high copy number. The measurement in the Western blot gave more reasonable numbers, but was not able to differentiate properly *in vitro* between functional and high effective shRNAs. Both Gsk-3 β shRNAs displayed in Tab. 6 gave similar protein knockdown of 68 and 64% in ES cells, but *in vivo* they varied from 49% to a reduction below the detection limit in tetraploid embryos carrying the Gsk-3 β -sh2. The latter embryos were generated from ES cells containing a randomly integrated shRNA vector, which may result in multiple genomic copies, but in Fig. 22 the protein knockdown in single integrated ES cells is depicted and again GSK-3 β is reduced nearly to the detection limit. Although it is experimentally not most straightforward, the accurate way for measuring shRNA efficiency is to stably integrate single copies of the expression cassette into ES cells by RMCE and to subsequently quantify mRNA and protein knockdown by Northern and Western blot analysis.

6.3 The Cre recombinase expression pattern in transgenic Cre mice

Since Cre recombinase expressing mouse lines are essential for the restriction of gene silencing to specific cell types and tissues, I checked the expression pattern for the used mouse lines, expressing Cre recombinase under the control of the Nestin and the CaMKII α promoter. To confirm the published expression patterns, the Cre recombinase expressing mouse lines were crossed to the reporter strain *R26R*, whose LacZ expression was dependent on Cre mediated recombination.

The pattern in the *CamKII-cre* mice was only slightly different to the pattern published by Minichiello et al. (1999). I found additional recombination in hypothalamus, olfactory bulbs, inferior colliculus, cerebellum, and brain stem, although the increase in the last three regions was only occasional (Fig. 24).

In contrast, a broad shift of Cre activity was detected in the *Nestin-cre* mouse line. The rat Nestin promoter combined with the nervous system specific enhancer from the second intron of the rat *Nestin* gene (Zimmerman et al., 1994) should restrict the Cre recombinase expression to neuronal stem cells, CNS progenitors, and neuronal and glial cell precursors. Although, it has been reported that the expression is restricted to the CNS, I observed in embryos obtained from crossings with the *R26R* reporter strain, lacZ staining in multiple organs and tissue additionally to staining of the CNS (Fig. 23). Since it is hard to determine recombination efficiency in tissues just based on staining results, I measured recombination as well via Southern blot analysis in the *Gsk-3 β -flox-sh2^{Nes}* mouse line (Fig. 27). Besides the brain, the analysis revealed high recombination in the pancreas, and moderate recombination in kidney. It is likely that in these organs knockdown of Gsk-3 takes place, which may alter the metabolism in *Gsk-3/Nestin-cre* knockdown mice, regarding the involvement of GSK-3 in metabolic pathways. Although recombination levels in other tested organs like heart, skeletal muscle, and lung was low, a disturbance of GSK-3 functions in these tissues cannot be excluded. For all phenotypic findings in these mice, it is important to note that some alterations may not be caused by the reduction of GSK-3 in the brain, but in other organs.

Working with Cre recombinase, its specific features have to be taken into account (Forni et al., 2006; Schmidt-Supprian and Rajewsky, 2007; Schmidt et al., 2000). Besides the desired recombination between loxP sites, Cre recombinase can cause

chromosome abnormalities like chromatid breaks, dicentric chromosomes, exchange figures, and ringshaped chromosomes. This cellular toxicity of Cre depends on the concentration of recombinase in the nucleus. Below a certain threshold, alterations are not detected, but with increasing concentration, the toxicity of Cre becomes obvious. Another factor is the timing of Cre expression. During mitosis, the uncondensed chromatin is quite sensitive to Cre, whereas in resting, postmitotic cells alterations are rare. To avoid recombination in the germline, it is necessary to inherit the loxP flanked and the Cre containing transgenes separately. The work with Cre recombinase in mice requires strict control over the time points and expression levels of Cre and a constant awareness of unwanted side effects, which may be caused by Cre recombinase. Because of this, wherever possible, knockdown mice were compared to their floxed littermates and Cre expressing wild type mice.

6.4 Gene silencing in mice via RNAi

For the generation of knockdown mice, I used recombinase mediated cassette exchange to integrate a single copy of shRNA expression cassettes into the *Rosa26* locus of mouse ES cells. Since the first description of RMCE (Seibler et al., 1998), the high efficiency and reproducibility of this approach was shown by different research groups and also applied to RNAi in mice (Hitz et al., 2007; Seibler et al., 2005). An alternative to this single integration approach is the random, multicopy integration of shRNA expression vectors into the genome by electroporation or pronuclear injection (Coumoul et al., 2005; Kunath et al., 2003). Although it is known that the U6 promoter is ubiquitously active, the local chromatin environment may alter the promoter activity such that several clones or mouse lines have to be screened for promoter activity and knockdown efficiency. These screenings are time and resources intense and an obvious disadvantage as compared to the integration into a well defined, ubiquitously active locus like *Rosa26* (Yu and McMahon, 2006). I could also confirm the high efficiency of RMCE during this project, because all shRNA constructs were successfully integrated into ES cells.

For the production of mice from ES cells, mainly blastocyst injection was used and as shown in Tab. 2, chimeras were born for every injected construct. Only for two mouse lines, transgenic mice were successfully generated by tetraploid aggregation (Nagy et al., 1993). One major problem of this technique is the low efficiency

(approximate 2%) of viable offspring, but if transgenic mice are obtained, the time saving can be immense, since the conditional transgenic mice can be bred directly to Cre recombinase expressing mouse lines.

As compared to the production of conditional knockout mice by gene targeting, the use of single or double conditional knockdown mice is less time and space consuming. By the combination of RMCE and tetraploid aggregation, the first conditional mutants can be obtained within four months from the transfection into ES cells (*Gsk-3-flox-dh2*^{Nes} mice), as compared to at least 12 month necessary to generate a classical non-conditional knockout strain.

A specific strength of RNAi is its flexibility that allows the gradual inhibition of gene function to model hypomorphic disease alleles or target inhibition upon pharmacological intervention. As compared to transgenic mice expressing mutant, dominant negative proteins, available only for a limited number of enzymes, RNAi can be readily applied to any protein coding gene.

6.4.1 Simultaneous gene silencing of two genes in mice

By the use of shRNA vectors multiple genes of a signaling pathway can be targeted at once (Jazag et al., 2005). I refined this technique by implementation of the Cre/loxP recombination system to restrict gene inactivation to specific tissues or cell types (Minichiello et al., 1999; van der Neut, 1997) and thereby circumvent occasional embryonic lethality, which can be caused already by the loss of a single gene. The Cre/loxP recombination system became even more versatile by the discovery that certain mutant lox sites are recombined by Cre independently of wild type loxP (Schnutgen et al., 2003; Siegel et al., 2001). Here, I adapted the system by the use of loxP and mutant lox2272 sites to control two conditional shRNAs that allow independent silencing of *Gsk-3 α* and *Gsk-3 β* (Steuber-Buchberger et al., 2008).

Since Jazag et al. showed that the U6 promoter is able to drive the expression of shRNAs in close proximity, I used the single shRNA expression cassettes for the simultaneous targeting of both *Gsk-3* isoforms. Cre mediated recombination between lox2272 sites was successful *in vitro* and the cell culture tests displayed full silencing efficiency of the recombined lox2272 shRNA as compared to the recombined loxP shRNA (5.3.4.2, Fig. 16/17). Therefore, I cloned one shRNA against *Gsk-3 β* with the

loxP flanked stop cassette and another shRNA targeting *Gsk-3 α* interrupted by the lox2272 stop cassette into a single pRMCE vector for the production of double knockdown mice. Because the sequence of loxP and lox2272 differs in two base pairs at position 2 and 7 of the spacer region (Fig. 19), each of these lox sites is recombined only with its own type, and is incompatible for recombination with the other type (Siegel et al., 2001). This technology allows the independent control of two conditional shRNAs using Cre recombinase.

As shown in 5.5.2, the simultaneous knockdown of *Gsk-3 α* and *Gsk-3 β* in the mouse brain was successful and the knockdown efficiency was comparable to that achieved in single knockdown mice, indicating that the combination of both vectors, as such, does not diminish the efficiency of gene silencing. For this mouse line, I analyzed the protein knockdown in recombinant ES cells after Cre mediated recombination. Compared to non-recombined parental ES cells, the level of GSK-3 α and GSK-3 β was reduced by 84% and 52%, respectively (Steuber-Buchberger et al., 2008). In the brains of double transgenic mice (*Gsk-3-flox-dh2^{Nes}*), I measured a reduction of 60% for the *Gsk-3 α* mRNA and of 50% for the *Gsk-3 β* mRNA.

The recombination efficiency of the double shRNA constructs was analyzed by Southern blot in the brains of *Gsk-3-flox-dh2^{Nes}* mice. Like for the single knockdown mice, the complete recombination was successful, indicated by a shift from the 5.4 kb BamHI fragment to the 9.0 kb band, representing the recombined allele (5.5.2.2, Fig. 26). I did not detect an 8.5 kb band that would result in case that the loxP and lox2272 sites are recombined with each other. To determine the frequency of single recombined alleles that still contain either the loxP or the lox2272 flanked stop cassette, I used Southern blot probes that detect the recombination status of each shRNA unit. The frequency of these events was below the detection limit of the analysis (5 to 10%; Data not shown), indicating that both lox flanked stop cassettes were recombined independently.

In contrast to single knockdown mice, I observed increased mortality in *Gsk-3-flox-dh2^{Nes}* mutants, which was not found in *Gsk-3-flox-dh2^{CamKII}* mutants. More detailed analysis revealed that the number of mutant embryos was reduced from E16.5. Only 50% of the expected mutants reached the weaning age and adulthood, and no further increase in mortality was observed with age. It is known

that the loss of both *Gsk-3 β* genes causes embryonic or postnatal lethality (Hoefflich et al., 2000; Kim et al., 2006), but the complete loss of *Gsk-3 α* does not influence viability (MacAulay et al., 2007). My results are the first hint that moderate, brain-specific loss of both *Gsk-3* isoforms leads to defects in embryonic development, diminishing the survival of affected embryos.

Exemplified by the *Gsk-3 α/β* gene pair, I showed *in vitro* and *in vivo* that it is possible to silence two independent genes simultaneously using conditional shRNA vectors activated through deletion of stop elements flanked by independent lox sites. This approach allows the conditional knockdown of gene pairs by two alternative vector configurations. In the first configuration, used in the present study, two conditional shRNA vectors are combined into a single unit. This configuration is most straightforward if only one specific gene pair is of interest. Alternatively, if more than two genes and several gene combinations are required, shRNA mice with single conditional shRNA vectors, disrupted by the loxP or lox2272 stop cassette, can be generated and two shRNA alleles of interest can be combined by breeding. For this combinatorial approach, stop cassettes flanked by incompatible lox sites will exclude interallelic Cre mediated recombination. Since additional incompatible lox site mutants have been described (Lee and Saito, 1998; Siegel et al., 2001), it may be possible to further extend the simultaneous knockdown approach to four genes by the combination of two *Rosa26* alleles, each containing a conditional double knockdown vector. Taken together, the described conditional double-knockdown approach greatly simplifies the functional analysis of two independent or redundant genes and should contribute to the further understanding of the genetic network in mice.

6.4.2 Mouse lines based on the *Gsk-3 β -sh2* shRNA

During the test for the activation of shRNAs in the brain (5.5.2.1), in two mouse lines, *Gsk-3 β -flox-sh1^{Nes}* and *Gsk-3-flox-dh^{Nes}*, the expression of *Gsk-3 β -sh2* could not be detected. Additionally, the mice were analyzed for knockdown of GSK-3 β protein. Since neither the shRNA was detected, nor a reduction in protein levels was observed, the sequence of the shRNA vector within the *Rosa26* locus was checked. PCR and subsequent sequencing in floxed littermates and mutant animals could exclude mutations in the shRNA expression cassette, including the U6 promoter,

the shRNA, and the termination signal. This indicated that the locus was successfully targeted by Cre recombinase and the recombination took place as planned.

In all performed tests to measure shRNA efficiency, no hints for transcription problems were seen. In ES cell culture, the Gsk-3 β -sh2 was transcribed from the pBluescript vector and caused sufficient protein and mRNA knockdown as non-conditional shRNA and also as activated conditional shRNA (Fig. 17/18). So, it is very unlikely that the remaining loxP site in the loop region of the shRNA is responsible for the failed transcription.

Another possibility might be a sequence specific problem of this shRNA in the *Rosa26* locus. So, I generated a non-conditional mouse line expressing the Gsk-3 β -sh2. Although three of the four mated chimeras were able to generate brown-colored pups, I could not detect any mutant offspring. But since the knockout of Gsk-3 β leads to embryonic lethality (Hoeflich et al., 2000) and the Gsk-3 β -sh2 was very effective in ES cell clones, reducing GSK-3 β protein nearly to the detection level (Fig. 22), there was still the possibility that the knockdown embryos died postnatal or during gestation. It seems that Gsk-3 β -sh2 was functional in the non-conditional state in the *Rosa26* locus. I could confirm the function of the non-conditional shRNA also by random integration of the expression cassette into mouse ES cells. Via tetraploid aggregation transgenic embryos were generated and analyzed for their protein knockdown and, as in ES cells generated via RMCE, I observed a reduction of GSK-3 β protein close to the detection level (Data not shown).

It is not clear whether the integration site in combination with the recombined shRNA is responsible for the failure of transcription from the Gsk-3 β -sh2 vector, but this remains the only reasonable explanation. Besides the fact that I could demonstrate that a nearly complete loss of target protein can be achieved by the RNAi technique, the results of these mouse lines point to the importance of a detailed analysis of shRNA activation and knockdown level *in vivo*.

6.5 Redundancy of GSK-3 isoforms

Little is known about the functional redundancy of the two GSK-3 isoforms in multiple signaling pathways, since much research on GSK-3 was done using inhibitor studies. All known GSK-3 inhibitors share a common disadvantage: Besides the fact that most of them inhibit also a range of other kinases (Forde and Dale, 2007), they cannot discriminate between GSK-3 α and GSK-3 β through their mode of inhibition (2.1.1). The possibility to analyze the functional redundancy of the two GSK-3 isoforms in signaling pathways is given only by genetic targeting of the *Gsk-3* loci or by the use of RNAi, like in this work, because only these approaches can guarantee a specific silencing of GSK-3 α or GSK-3 β .

The early lethality of *Gsk-3 β* knockout mice (2.1.2) prevents the *in vivo* analysis of GSK-3 α redundancy in adult homozygous knockout animals. Only the use of conditional *Gsk-3 β* knockout or knockdown mice can answer this question.

6.5.1 The role of GSK-3 in the Wnt signaling pathway

One main function of GSK-3 is its role in canonical Wnt signaling, so the question emerged if the generated knockdown mice display any alterations in this pathway. In publications concerning the Wnt pathway mainly the GSK-3 β isoform is mentioned, but at a closer look most studies reveal the use of inhibitors or methods, which are unable to distinguish between the two isoforms and therefore affect the functions of both molecules. This preference for GSK-3 β has evolved from rescue experiments with both mammalian isoforms in *Drosophila* mutants lacking the GSK-3 homologue *zeste-white3*. In these experiments, only the GSK-3 β isoform can substitute for the loss of the *Drosophila* kinase, so the focus in Wnt literature concentrated on GSK-3 β (Frame and Cohen, 2001; Woodgett, 2001).

The function of GSK-3 in the Wnt pathway is isolated from its other tasks and the key role of the Axin complex is the recruitment of a fraction of the total cellular GSK-3 pool for regulation of β -catenin (Woodgett, 2001). The fact that both isoforms participate in the Wnt pathway is supported by the phenotypes of the *Gsk-3* knockout mice. Neither the *Gsk-3 β* nor the *Gsk-3 α* knockout mice show alteration of Wnt signaling or evidence for subsequent β -catenin accumulation (Hoeflich et al., 2000; MacAulay et al., 2007). Additionally, the *Gsk-3 β* knockout cells do not

compensate by increasing levels of GSK-3 α . Recent work in ES cells clearly demonstrated that only the loss of three or all of the *Gsk-3* alleles results in a dosage effect on β -catenin (Doble et al., 2007). Therefore, only the loss of at least 75% of total GSK-3 activity will result in changes in the Wnt signaling pathway.

In accordance with these facts, I could not detect any differences in the protein levels of β -catenin (Data not shown) in the *Gsk-3/Nestin-cre* mice thereby supporting the fact that the Wnt pathway is insensitive to the GSK-3 isoforms.

6.5.2 The role of GSK-3 in neurogenesis

Like in the Wnt literature, other research fields also preferred the GSK-3 β isoform in their experimental plans, but recently the use of RNAi in GSK-3 related studies was established and allowed the first insights into the specific functions of the isoforms. One of these research fields is the role of GSK-3 in neurogenesis and axon specification, since the targets of GSK-3 include cytoskeleton related proteins including tau, neurofilament, and CRMP-2. For correct axon specification and neuronal organization, the polarization of the developing neuron is essential. A single axon has to be established by the promotion of only one neurite, while others have to be inhibited and promoted to dendrites (Wiggin et al., 2005). Altering levels of GSK-3 activity, resulting in morphological changes in axons, like growth retardation and branching initiation, has shown the involvement of GSK-3 in this sensitive process. It was shown that GSK-3 is involved in establishing and maintaining neuronal polarity and that GSK-3 inhibition causes multiple long axon formation with concomitant reduction of dendrite formation (Gartner et al., 2006; Jiang et al., 2005; Yoshimura et al., 2005). In contrast, other studies report robust dendrite initiation (Naska et al., 2006) or decreased axon elongation (Lucas et al., 1998) after GSK-3 inhibition. So far from the published results, it is still unclear if GSK-3 enhances or inhibits axon growth.

Studies in hippocampal neuronal cultures have shown that inhibition of GSK-3 by inhibitors or shRNAs impairs axon formation, and that the inhibition of GSK-3 α or GSK-3 β leads to reduced number of developed axons in transfected neurons (Garrido et al., 2007). In contrast, *Gsk-3 β* null mice show no gross morphology abnormalities in their nervous system or of axon formation in hippocampal neuronal

cultures, indicating the redundancy of both isoforms regarding the regulation of axon morphology (Kim et al., 2006). Additionally, Kim et al. (2006) could show that the combined inhibition of GSK-3 by one shRNA or inhibitors reduced axon growth *in vitro*. These different findings in *Gsk-3 β* knockout mice and *in vitro* experiments by Garrido et al. (2007) might be a consequence of adaptation in the *Gsk-3 β* null mice to the early and permanent loss of GSK-3 β . Perhaps *in vivo* GSK-3 α is able to compensate the functions of GSK-3 β in these animals in this specific pathway.

It would be interesting for further research to analyze the axon morphology in the *Gsk-3/Nestin-cre* mice since no differences in axon morphology in these mice might indicate a general ability of the two isoforms to replace each others functions in axon development *in vivo*.

6.6 Phenotypic changes in *Gsk-3* knockdown mice

The knockdown of *Gsk-3* in the brain of conditional shRNA mice is comparable to hypomorphic mutations for these genes. The limited levels of gene silencing can be explained by the use of RNAi target sequences that activate the RISC complex at varying efficiency (Reynolds et al., 2004). Higher levels of gene silencing were obtained using the *Gsk-3 β -sh2* shRNA.

Besides the analysis of *Gsk-3* basic gene functions, the moderate, simultaneous inhibition of these protein kinases can serve as a model for the beneficial as well as the side effects of chronic administration of small molecule inhibitors interfering with both kinase isoforms. For GSK-3, small molecule inhibitors have been developed for the treatment of diseases associated with increased GSK-3 activity in the brain, like AD and mood disorders (Bhat et al., 2004; Jope and Roh, 2006). Therefore, it is of interest to determine which inhibition level of normal GSK-3 activity results in phenotypic alterations.

The levels of GSK-3 kinase activity seem to be tightly controlled *in vivo*, since a behavioral phenotype has already been found in heterozygous *Gsk-3 β* knockout mice (O'Brien et al., 2004). Another example is the role of GSK-3 in neuronal development. Although the inhibition of GSK-3 by inhibitors with different efficiencies results in alterations of axonal development, homozygous loss of *Gsk-3 β* in the knockout mice has no effects on axonal morphology (Kim et al., 2006).

In addition, mice expressing a dominant negative *Gsk-3* transgene in forebrain neurons with a reduced GSK-3 kinase activity of only 25% to 50%, display increased neuronal apoptosis and deficits in motor coordination (Gomez-Sintes et al., 2007). These mice are considered as a model for the inhibition of GSK-3 by drugs. Due to these facts, I could expect multiple phenotypic changes in knockdown mice despite the moderate levels of *Gsk-3* silencing.

6.6.1 CNS unrelated phenotypes of *Gsk-3/Nestin-cre* knockdown mice

Due to the various functions of GSK-3 and the enlarged expression pattern of the *Nestin-cre* mice to non-neuronal tissues (see 5.4.1 and 6.3), it was likely that phenotypic alterations would be detectable outside of the CNS.

6.6.1.1 Systemic defects

The difference in body weight and size observed in mutant *Gsk-3/Nestin-cre* mice was an unexpected finding. This phenotype seems to be unique to the knockdown mice, since neither the *Gsk-3 α* knockouts (MacAulay et al., 2007), nor the heterozygous *Gsk-3 β* knockout mice demonstrate any alterations in body weight (personal communication with J. Woodgett). A possible reason for this discrepancy could be the difference in genetic background. The mutant *Gsk-3 β -flox-sh2^{Nes}* mice on a more hybrid background (75% *C57Bl/6J*) suffer from an even more explicit weight reduction than the mutants finally analyzed in the GMC primary screen with 87.5% *C57Bl/6J*. They displayed a mean weight reduction of 40% in female and 45% in male mutant mice, compared to a reduction of 25% and 26% in mutants with the increased *C57Bl/6J* background. In *Gsk-3 α -flox^{Nes}* on this hybrid background, I observed a similar difference. Here, the mutants demonstrated a mean weight reduction of 24% in females and of 32% in male mice, whereas the analyzed mutants of the primary screen displayed a reduction of 18% and 19%, respectively. This is a strong indication that changes in the genetic background influence the observed phenotype and this might also be the reason why such differences were not detected in *Gsk-3 α* knockouts, which were generated from G4 ES cells on 129/B6 background (George et al., 2007). Similar variations were observed in the *Gsk-3 β* knockout mice, where the time point of lethality varied from E 13.5 to postnatal age and additional variances were reported regarding the other published defects, which could not be

confirmed by other research groups (Hoeflich et al., 2000; Kim et al., 2006; Liu et al., 2007; Stankunas et al., 2003).

Another reason for the difference between *Gsk-3* knockout and knockdown mice might be the role of Cre toxicity on metabolism and it has been reported that mouse lines expressing Cre recombinase under the *Nestin* promoter display reduced body size and hydrocephalus (Forni et al., 2006). But first, these mice show the described phenotypes only in the homozygous state, which fits to the observation that Cre toxicity is linked to increased Cre recombinase expression (Schmidt-Suppran and Rajewsky, 2007), and second other *Nestin-cre* mutant mouse lines generated in our group did not show alterations in body weight. The same is true for *Nestin-cre* and control shRNA transgenic mice as such (Hitz et al., 2007). In addition, if Cre toxicity would be responsible for this phenotype, I would expect the same amount of reduction in both *Gsk-3* knockdown lines. Since this was not the case, it seems that GSK-3 β has a stronger influence on the respective pathways than GSK-3 α .

The observed infertility in mutant *Gsk-3 β -flox-sh2^{Nes}* mice might be influenced by Cre toxicity, too (5.5.3). It was already published that Cre can cause chromosome rearrangements in mouse spermatids (Schmidt et al., 2000), but if the monitored infertility here is caused by Cre toxicity, there is no explanation why it was not observed in *Gsk-3 α -flox^{Nes}* mutants or why it also affected the females. Besides, it is known that GSK-3 α is highly phosphorylated in motile caudal sperm compared to immotile caput epididymal sperm (Vijayaraghavan et al., 2000), which indicates a role for GSK-3 in motility initiation and mature sperm function. To gain insight into the infertility phenotype of the mutant *Gsk-3 β -flox-sh2^{Nes}* mice, it will be necessary to analyze the amount of Cre recombination in the testis and to repeat the sperm measurements with an increased number of animals. Apart from a functional difference between the two GSK-3 kinases, a reason for the divergent observations could be the different physiological state of the animals. Although the reduction of GSK-3 is higher in the *Gsk-3 α -flox^{Nes}* mutants, the *Gsk-3 β -flox-sh2^{Nes}* mutant mice seem to suffer from more severe defects. As the production and development of spermatids need high amounts of energy (Miki, 2007), the *Gsk-3 β -flox-sh2^{Nes}* mutants may not be able to invest this much, because of their low body weight and probably impaired metabolism. Additionally, round spermatids prefer lactate as substrate for ATP production (Mita and Hall, 1982) and in accordance to this the

mean blood lactate concentration is significantly ($p < 0.05$) reduced in male *Gsk-3 β -flox-sh2^{Nes}* mutants (Data from GMC primary screen). Taken together, there might also be an involvement of GSK-3 β in sperm development and motility initiation.

6.6.1.2 Hypotension of *Gsk-3* knockdown mice

The alterations in blood pressure of *Gsk-3/Nestin-cre* mutants (Fig. 42), measured in the GMC primary screen in the cardiovascular module, were unexpected. The measurement of blood pressure in the body is dependent on pressure receptors in the great arteries and the heart, which signal pressure alterations to the hypothalamus and the medulla, where the pressure is adjusted by multiple regulation factors, like hormones and vascular muscle contraction induced by the autonomic nervous system.

In the *Gsk-3 β -flox-sh2^{Nes}* mice, mutants of both sexes showed a significant decrease of pulse rate, systolic, diastolic, and mean arterial pressure. A similar phenotype was found in *Gsk-3 α -flox^{Nes}* mice, although only the female mutants showed a significant decrease in systolic, diastolic, and mean arterial pressure, whereas the pulse rate was significantly decreased in both sexes.

Several functions of GSK-3 might influence the systemic blood pressure. One is its role in antigen-specific T-cell responses in the immune system. It was shown that the inactivation of GSK-3 is required for maximal proliferation and interleukin 2 (IL-2) production. Experiments with lithium demonstrated that inhibition of GSK-3 resulted in dramatically increase of IL-2 production (Ohteki et al., 2000). The link with hypotension was made by an experiment injecting high doses of IL-2 into mice over five days, which resulted in a time-dependent decrease in systolic blood pressure with severe hypotension on day four and five (Samlowski et al., 2000-2005).

Another connection between GSK-3 and hypotension is its involvement in neurological disorders and diabetes. Diabetes and neurological disorders like Parkinson's disease can lead to polyneuropathies in the autonomic nervous system and to insufficiency of neurohormonal regulatory mechanisms, including the hypothalamus-pituitary-axis. These lesions can cause the so-called orthostatic hypotension, which is defined in humans as the decrease in systolic pressure by at

least 20 mmHg while standing in three minutes after getting up compared to the pressure when lying down (Braune and Lücking, 1997).

To analyze whether the hypotension of *Gsk-3/Nestin-cre* mutants is caused by a developmental response to the reduction of GSK-3 activity or if it is an acute regulatory mechanism, I treated wild type *C57Bl/6J* females with the GSK-3 inhibitor SB216763 for five consecutive days. With regard to the blood pressure, no significant differences were detected between the inhibitor and control groups. Only a slight decrease in the pulse rate of inhibitor injected animals was detected. These results indicated that the influence of GSK-3 reduction on the blood pressure is not reproducible by short term GSK-3 inhibition, but it may play a role in long term administration of GSK-3 inhibitors during the treatment of mental disorders like BPD, schizophrenia, or depression.

6.6.2 Alterations in ventricle size in *Gsk-3/Nestin-cre* knockdown mice

Because of the known functions of GSK-3 in neurons, phenotypic changes the brain of *Gsk-3/Nestin-cre* knockdown mice were expected. In contrast to Gomez-Sintes et al. (2007), I could not detect an increase in neuronal apoptosis in the brain (Fig. 36), but the role for GSK-3 in mediating apoptosis is already known to be divergent. Other research groups have shown that inhibition of GSK-3 induces neuronal differentiation and neurogenesis instead of apoptosis and that this phenomenon positively contributes to the therapeutic effects of antidepressants (Chen et al., 2000; Kim et al., 2004; Maurer et al., 2007).

Although the brain size of *Gsk-3/Nestin-cre* mutants was not altered (Data from GMC primary screen), I found a significant increase of the lateral ventricle volume. An increase in ventricle volume together with communicating hydrocephalus was reported as a result of Cre toxicity in different *Nestin-cre* lines (Forni et al., 2006), but in our case the *Nestin-cre* wild type animals did not display any differences in ventricle volume (Data not shown) and hydrocephalus was not observed. In addition, no correlation with the reduction in body weight and the increase in ventricle volume could be detected.

But an increase in ventricle volume was linked with the pathology of mood disorders and schizophrenia (Chen et al., 2000; Elkis et al., 1995). It is unclear now if these

changes in brain morphology are part of the natural pathology of these disorders, or caused by long term treatment with antidepressant and GSK-3 inhibiting drugs. Further research should include the analysis of different brain developmental stages to determine the onset of this phenotype and rescue experiments by re-inducible full GSK-3 expression.

6.6.3 Influence of *Gsk-3* silencing on myelination

Subtypes of glia cells, the oligodendrocytes, form the insulating myelin sheaths of the axons in the CNS. In the peripheral nervous system (PNS) Schwann cells are responsible for the myelin wrap of the axons. In both cases, the reason of the interactions between neurons and oligodendrocytes or Schwann cells for myelination is the increase of conduction velocity, but the regulatory mechanisms involved in this event differ between the PNS and the CNS (Colello and Pott, 1997).

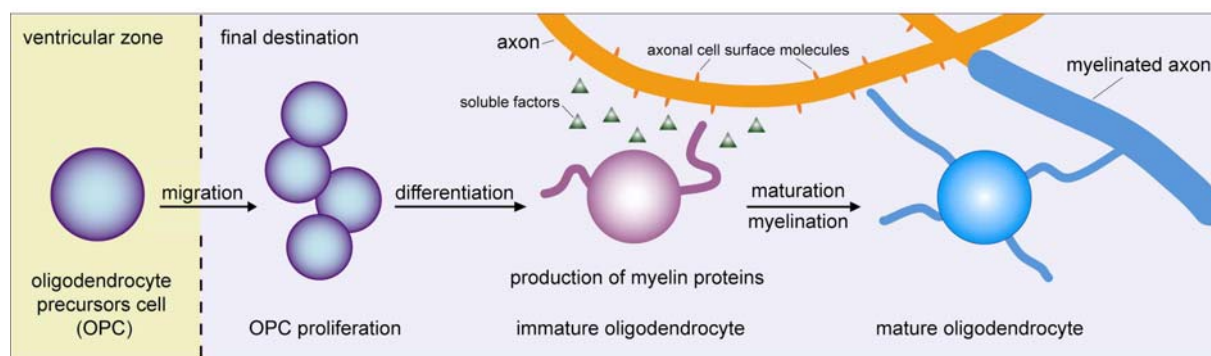


Fig. 47: The myelination process in the CNS. OPCs migrate from the ventricular zone to their final destination in the CNS, where they proliferate and differentiate into immature oligodendrocytes. Nearby axons induce maturation into myelinating oligodendrocytes by soluble factors (FGF, thyroid hormone) and cell surface molecules (NCAM, L1, MAG, N-cadherin).

The process of myelination consists of several steps (Fig. 47). During development oligodendrocyte precursor cells (OPCs) are induced from cells of the neuroepithelium and migrate from specific loci in the ventricular zone throughout the CNS to axons in the brain and the spinal cord. At their final destination, OPCs proliferate and differentiate into immature oligodendrocytes, which transcribe and translate the genes encoding for myelin proteins (Miller, 2002). Although they do not myelinate the nearby axons at this time point, they already fulfill other functions in the CNS like the clustering of proteins at nodal domains or the *de novo* synthesis of cholesterol. Additionally, they may play a role in maintaining axonal integrity that is independent of myelin formation (Rosenberg et al., 2007). Finally, signals from the axon induce

maturation and contact of oligodendrocyte processes with the nearby axons and subsequent formation of the myelin sheath (Miller, 2002). Oligodendrocyte differentiation and subsequent myelination starts short time after birth in the PNS, but is delayed in the CNS, where myelination can start between two days until two weeks postnatally (Rosenberg et al., 2007). In general, the peak of myelination is reached at P23 (Foran and Peterson, 1992).

During the analysis in the GMC primary screen, loss of myelin was detected in 80% of the mutant *Gsk-3 β -flox-sh2^{Nes}* mice and a milder phenotype with less penetrance was also detected in the other *Gsk-3/Nestin-cre* knockdown lines (5.5.6.4). A reason for the mild appearance in *Gsk-3-flox-dh2^{Nes}* could be the loss of severely affected mutants during gestation. Perhaps the resulting defects in brain development are too severe, so that only mutants with a milder phenotype are able to survive until adulthood.

6.6.3.1 OPC development

During development and until P20, GSK-3 expression in wild type mice was observed in the white matter and in oligodendrocytes of the forming brain (5.1.2). Since Cre recombinase expression in *Nestin-cre* mice starts at E11.0 and concerns also glia cell precursors, the time and spatial requirements are given that GSK-3 loss might influence the development, migration or proliferation of OPCs.

In *Gsk-3/CamKII α -cre* mice, the neuronal CaMKII α promoter is activated after OPC development, migration, and proliferation, and since in these mutants no myelin alterations were detected, these early states of the myelination process might be altered in *Gsk-3/Nestin-cre* knockdown mice. To confirm this early alteration of the myelination process, it is necessary to determine the myelination in the CNS of postnatal mice. Identification of OPCs by detection of PDGF- α R or the transcription factors *Olig 1* and *Olig 2* (Miller, 2002) and analysis of OPC numbers in the brain of postnatal *Gsk-3/Nestin-cre* knockdown mice may give more hints for alterations in the early myelination steps.

6.6.3.2 Oligodendrocyte maturation

Although GSK-3 is not expressed in oligodendrocytes in the adult brain, there is still the possibility that it influences pathways in not myelinated adjacent neurons, which normally induce oligodendrocyte maturation and myelination by diffusible and membrane-associated molecules (Foran and Peterson, 1992). Candidates for such axonal signals include FGFs and thyroid hormone as soluble factors and axonal cell surface molecules such as L1, MAG, NCAM, and N-cadherin. Oligodendrocyte maturation is also influenced by neuregulins that are expressed on many axons and in the absence of their receptor ErbB2, only few oligodendrocytes mature and those that do not, fail to interact with axons and the production of myelin (Miller, 2002).

A possible interaction molecule of GSK-3 is one of the major myelin components, the myelin basic protein (MBP) (Yu and Yang, 1994). Another known GSK-3 target and participant in oligodendrocyte maturation is NCAM (Grimes and Jope, 2001). In cultures of cerebral hemispheres the treatment with an anti-NCAM antibody resulted in an increase in the number of myelinated axons. The number of MBP-expressing oligodendrocytes was found unchanged, indicating that this effect is specific to the final myelination (Rosenberg et al., 2007). Therefore, an unchanged number of OPCs or mature oligodendrocytes can nevertheless result in altered myelination.

Besides the possible alteration of the early myelination, target proteins of GSK-3 involved in the final myelination step, make it worthwhile to analyze the interactions between axons and maturing oligodendrocytes further. Problems in this step might display the penetrance and the gradual loss of myelin in affected *Gsk-3/Nestin-cre* mutants better than the hypothesis of OPC loss or reduction, since in HE staining (Fig. 44) no obvious hints for a drastic change in cell number of mutant animals were found. However, it is known that the myelination process can fail although oligodendrocytes are present in the CNS and despite correct signals from surrounding axons, like in *Olig1*-Null mice, which exhibit severe neurological deficits, including tremors and seizures, and die around P14 (Xin et al., 2005).

The most interesting questions in this situation should be: Why are some *Gsk-3/Nestin-cre* mutants able to form correct myelin sheaths and is the difference

observed in the myelin status of affected mutants a result of active demyelination or a deficit in initial myelination?

Active demyelination and oligodendrocyte apoptosis can be caused by TNF, which is a potent inflammatory mediator strongly implicated in the pathogenesis of neuroinflammatory and demyelinating diseases. TNF and its receptors are up-regulated in tissues of multiple sclerosis patients and TNF levels in the cerebrospinal fluid correlate with the disease severity (Akassoglou et al., 1998). From knockout studies, GSK-3 β exerts a putative protective role from TNF cytotoxicity (2.1.2), so the partial loss of GSK-3 might increase the vulnerability of oligodendrocytes to TNF induced apoptosis.

Obviously many questions have to be answered before the role of GSK-3 in the myelination process can be elucidated, but the GSK-3 knockdown mice show for the first time that subtle alterations of GSK-3 levels result in unexpected morphological changes of the neuronal environment.

6.6.3.3 Myelination in the PNS

The mentioned divergence between knockdown level and severity of phenotype is also reflected in the paralysis of the *Gsk-3 β -flox-sh2^{Nes}* mutants with an increased hybrid background (75% *C57Bl/6J*) after sudden disturbance of the animals in their home cage (5.5.3). This paralysis could be influenced by loss of myelin in peripheral nerves and the penetrance for loss of myelin in these mutants might be even higher than in the analyzed mutants with 87.5% *C57Bl/6J* background.

Since neuropathies and myelin lesions can cause orthostatic hypotension (6.6.1.2), another reason for the paralysis phenotype might be the inability to adjust the blood pressure immediately to the acute stress caused by handling of the cage. In humans, orthostatic hypotension can result in weakness, dizziness, or even absence, so perhaps the affected mice suffer from these symptoms and therefore display this drowsiness and difficulties in movement. Myelination defects in the PNS could even be the reason for the lowered systolic blood pressure observed in the analyzed *Gsk-3/Nestin-cre* mutants and might be the reason why we could not reproduce the cardiovascular phenotype by use of inhibitors. Therefore, the myelination status in the PNS should be determined in further studies.

6.6.3.4 Remyelination

In the adult brain, remyelination follows the pathological loss of myelin in diseases like multiple sclerosis (MS). Remyelination can restore the conduction properties of axons and is believed to exert a neuroprotective role. So far, it is known that remyelination occurs in two major steps: first, the lesions are colonized by OPCs and second, the precursors differentiate into mature oligodendrocytes that contact the demyelinated axons to generate the myelin sheaths new. But the reasons why this process can fail, like in MS, are not yet elucidated (Chari, 2007). For example the depletion of OPCs during the disease, inhibition within the glial scar, or damage of the affected neurons could prevent remyelination (Levine et al., 2001).

Apparently, in affected *Gsk-3/Nestin-cre* mutants this remyelination does not take place. However, it is not clear if in these mice the myelin sheaths were ever properly formed, so no statements can be given if remyelination is also affected in these mutants. The *CaMKII α* promoter of the *Gsk-3/CamKII-cre* mutants is only activated in neurons shortly before the peak of myelination, so in these mice most of the myelin should already be formed and accordingly these mutants show no differences in myelination. To analyze the influence of GSK-3 loss on remyelination, it would be interesting to monitor remyelination processes after caused injuries in the *Gsk-3/CamKII-cre* mice.

6.6.4 Behavior alterations induced by *Gsk-3* silencing in the brain

The identification of genes involved in psychiatric disorders is a difficult task, and those genes that have been suggested as candidates show only weak association. The expectation to model the whole complexity of these phenotypes in rodents is certainly unrealistic, but however partial or intermediate phenotypes have been successfully modeled and studied in mice, including physiological or anatomical brain changes and behavioral traits (Seong et al., 2002).

The behavioral tests performed with the *Gsk-3* knockdown mice were chosen to analyze the anxiety and depression related behavior. In the mHB a whole set of different parameters can be analyzed, but mainly the spontaneous behavior of mice in a novel environment is observed. Additionally, hints for anxiety related endophenotypes could be detected. Anxiety related behavior is measured in the light-

dark box by observing the entries of the animals in the different compartments. The forced swim test is an indicator for stress and motivation related behavior, whereas in the accelerating rotarod general motor coordination deficits can be measured. An overview about the main results of the behavior tests is given in Tab. 7.

Behavior test	<i>Gsk-3/Nestin-cre</i> mice		<i>Gsk-3/CamKII-cre</i> mice		
	<i>Gsk-3β-flox-sh2^{Nes}</i>	<i>Gsk-3α-flox^{Nes}</i>	<i>Gsk-3β-flox-sh2^{CamKII}</i>	<i>Gsk-3α-flox^{CamKII}</i>	<i>Gsk-3-flox-dh2^{CamKII}</i>
mHB	dec. locomot., dec. distance to wall	dec. locomot., dec. distance to wall, dec. on board, inc. social contact	inc. locomot., inc. activity	inc. locomot., inc. activity	f: inc. locomot., inc. activity, m: dec. social contact
LD box	no alterations	not tested	inc. time/ rearing in light	inc. locomot.	inc. locomot.
FST	f: dec. swimming, inc. floating	no alterations	dec. struggling	inc. swimming, dec. floating	f: dec. struggling
Rotarod	f: don't improve over the trials	no alterations	no alterations	no alterations	inc. mean latency to fall

Tab. 7: Summary of behavior results of mutant *Gsk-3* knockdown mice. *f*: females, *m*: males, *dec*: decreased, *inc*: increased, *locomot*: locomotion

6.6.4.1 Silencing of *Gsk-3* in the central nervous system

The *Gsk-3/Nestin-cre* knockdown mice performed in the behavioral tests almost like wild type mice despite their reduced body weight and size. For the interpretation of these results, this difference has to be regarded, since it could alter the behavior of the mutants. For example, reduced locomotion and the adjacency to the wall might indicate an increased anxiety related behavior of these mutants in the novel environment of the mHB. Likewise the mutants might be socially deprived in their home cage regarding the hierarchy and therefore develop an increased anxiety related behavior independent from the genetic background. Supporting an influence of the genetic alterations is the fact that the phenotype is more defined in the *Gsk-3 α -flox^{Nes}* mice, which suffer from less physical restrictions. In addition, these mutants displayed alterations in the time and entries on board, which indicate again an increased anxiety related behavior.

In the FST and the Rotarod, an influence of the body weight is reasonable and likely this physical impairment is the cause for the observed behavior of the female *Gsk-3 β -flox-sh2^{Nes}* mutants. This assumption is supported by decreased forelimb grip

strength in mutants of this mouse line (Data from GMC primary screen). Differences in forelimb grip strength were not found in the less physically affected *Gsk-3 α -flox^{Nes}* mice. The observed divergence between knockdown level and severity of physical phenotype is not confirmed by the behavior results. Here, the more defined phenotype is obviously observed in the *Gsk-3 α -flox^{Nes}* mice.

Heterozygous *Gsk-3 β* knockout mice were tested for their behavior and compared to lithium treated mice (O'Brien et al., 2004). They observed a markedly decreased time immobile in the FST, but no alterations in total activity, righting response, grip strength or on the Rotarod. Interestingly, after treatment of these mice with lithium, which further inhibited the activity of GSK-3 β , these mice displayed more marked responses in the FST, but also decreased overall activity in the hole board and reduced grip strength similar to the knockdown mice. These facts indicate an increased inhibition of GSK-3 β activity in the *Gsk-3 β -flox-sh2^{Nes}* knockdown mice than in the heterozygous *Gsk-3 β* knockouts.

6.6.4.2 Silencing of *Gsk-3* in forebrain neurons

In contrast to *Gsk-3/Nestin-cre* knockdown mice, the locomotion and activity parameters in *Gsk-3/CamKII-cre* knockdown mice were significantly increased, indicating a hyperactive behavior in the novel environment of the mHB. The observation of increased general locomotor activity, including total distance traveled and velocity, in transgenic mice overexpressing GSK-3 β (Prickaerts et al., 2006) is contradictory to the findings in the *Gsk-3* knockdown mice. Perhaps disturbance of the tight regulation of GSK-3 *in vivo* in both directions causes similar behavior alterations.

A specific anxiety related behavior was only observed in the *Gsk-3 β -flox-sh2^{CamKII}* mutant mice in the LD box test. The rearings and the time spent in the light compartment were significantly increased. This phenotype could not be confirmed in the *Gsk-3 α -flox^{CamKII}* and *Gsk-3-flox-dh2^{CamKII}* mutants, therefore the test should be repeated. The results of the FST were also not consistent. In *Gsk-3 β -flox-sh2^{CamKII}* and female *Gsk-3-flox-dh2^{CamKII}* mutants the time spent struggling was decreased, which indicates a less active stress coping behavior, whereas the *Gsk-3 α -flox^{CamKII}* mutants spent significantly more time swimming and less time floating, which is connected to a increased active stress coping behavior. The reduced time spent with

floating is comparable to the feature time spent immobile, and therefore this result is consistent with GSK-3 inhibitor studies in the FST (Gould et al., 2004).

6.6.4.3 GSK-3 and lithium in depression and anxiety

A famous inhibitor of GSK-3 is lithium. For 50 years, this simple drug has been the main treatment for bipolar disorder patients. Many biochemical actions of lithium have been identified, but the mechanisms of its therapeutic actions are still unclear, especially since the therapeutic effects of lithium only become evident after several weeks of treatment at a low plasma concentration of 1 mM (Jope, 2003).

Besides its ability to inhibit other kinases (Zhang et al., 2003), lithium is one of the main inhibitors of GSK-3, so GSK-3 became the putative target of the therapeutic actions of lithium in BPD (2.1.4). In conclusion, mouse models with altered GSK-3 levels were analyzed for their depression and anxiety related behavior. The results of these studies varied. In heterozygous *Gsk-3 β* knockout animals a markedly decreased time immobile in the FST was observed. After treatment of these mice with lithium, these mice displayed more marked responses in the FST, but also decreased overall activity in the hole board and reduced grip strength (O'Brien et al., 2004). This decreased immobility was also observed during GSK-3 inhibitor studies in the FST (Gould et al., 2004). I could not confirm this finding in the GSK-3 knockdown mice, only the *Gsk-3 α -flox^{CamKII}* mutants spent less time floating, which is comparable to the feature time spent immobile, and therefore only in these mutants this result is consistent with previous studies. Another research group could also not confirm the reported behavior phenotype of the *Gsk-3 β* heterozygote knockout mice in the FST (Bersudsky et al., 2008b). This work used a different genetic background than in the studies of O'Brien et al. (2004) and these changes of genetic background might be the reason why this phenotype was not reproduced in the GSK-3 knockdown mice. However, it seems that the behavior phenotype, as well as the molecular phenotype (2.1.2) of the *Gsk-3 β* knockout mice, is not very robust, and this fact seems to be true for the knockdown mice as well.

Findings in β -catenin overexpressing mice indicate that lithium could mediate its therapeutic actions via this transcription factor (Gould et al., 2007). It was reported that heterozygous *Gsk-3 β* knockout mice display a similar behavior phenotype (O'Brien et al., 2004), but this is contradictory to the fact that in *Gsk-3 β* knockout mice no alterations of the β -catenin levels were found (Hoefflich et al., 2000). Interestingly, also *Gsk-3 β* overexpressing mice display a reduced immobility in the FST, which is contributed by the authors to the hyperactivity of the animals (Prickaerts et al., 2006). In contrast, recent studies in rats showed an increased immobility time in the FST after lithium administration and a reduced immobility time after administration of another GSK-3 inhibitor (Silva et al., 2008).

In general, the final link between GSK-3, lithium, and its therapeutic actions in BPD is not clarified so far. The varying behavior results in mouse models inhibiting GSK-3 were not able to elucidate the therapeutic actions of lithium so far, leaving the possibility that there are additional or other GSK-3 independent pathways which mediate the improvement of BPD patients after lithium treatment (Bersudsky et al., 2008a; Yanagita et al., 2007).

6.7 Conclusion

In this work, I successfully implemented conditional vector-based RNAi in mice using the Cre/loxP recombination system. A further refinement of this technology enabled the simultaneous conditional knockdown of two genes in the brain of mice by the combined use of wild type and mutant loxP sites.

The various mouse lines generated with this technique during the project targeted specifically the isoforms of GSK-3 via RNAi in the CNS or adult forebrain neurons. The limited knockdown of GSK-3 α by 60% in *Gsk-3 α* knockdown mice and of GSK-3 β by 55% in *Gsk-3 β* knockdown mice was nevertheless sufficient to elicit distinct phenotypic effects.

Besides general physical impairments in *Gsk-3/Nestin-cre* knockdown mice regarding the body weight and size, infertility, hypotension, and defects in brain morphology were observed. The loss of myelin in the brain of *Gsk-3/Nestin-cre* knockdown mice link GSK-3 for the first time to the myelination process and oligodendrocyte precursor function, differentiation and development.

The behavioral analysis of *Gsk-3/CamKII-cre* knockdown mice for anxiety and depression related behavior raised questions about the just partial conformance to previous results from genetic and inhibitor studies. Further detailed research with these mice might allow specifying the distinct roles of GSK-3 α and GSK-3 β in the complex regulation of behavior in mood disorders. In addition, the knockdown mice facilitate the analysis of gradual and long term GSK-3 loss and can serve as a model of sustained, GSK-3 inhibiting drug administration in humans.

7 LITERATURE

- Abramoff MD, Magelhaes PJ, Ram SJ.** (2004): Image Processing with ImageJ. *Biophotonics International* 11(7):36-42.
- Acevedo N, Wang X, Dunn RL, Smith GD.** (2007): Glycogen synthase kinase-3 regulation of chromatin segregation and cytokinesis in mouse preimplantation embryos. *Mol Reprod Dev* 74(2):178-188.
- Akassoglou K, Bauer J, Kassiotis G, Pasparakis M, Lassmann H, Kollias G, Probert L.** (1998): Oligodendrocyte apoptosis and primary demyelination induced by local TNF/p55TNF receptor signaling in the central nervous system of transgenic mice: models for multiple sclerosis with primary oligodendroglialopathy. *Am J Pathol* 153(3):801-813.
- Ali A, Hoeflich KP, Woodgett JR.** (2001): Glycogen synthase kinase-3: properties, functions, and regulation. *Chem Rev* 101(8):2527-2540.
- Beaulieu JM, Sotnikova TD, Yao WD, Kockeritz L, Woodgett JR, Gainetdinov RR, Caron MG.** (2004): Lithium antagonizes dopamine-dependent behaviors mediated by an AKT/glycogen synthase kinase 3 signaling cascade. *Proc Natl Acad Sci U S A* 101(14):5099-5104.
- Bersudsky Y, Shaldubina A, Agam G, Berry GT, Belmaker RH.** (2008a): Homozygote inositol transporter knockout mice show a lithium-like phenotype. *Bipolar Disord* 10(4):453-459.
- Bersudsky Y, Shaldubina A, Kozlovsky N, Woodgett JR, Agam G, Belmaker RH.** (2008b): Glycogen synthase kinase-3beta heterozygote knockout mice as a model of findings in postmortem schizophrenia brain or as a model of behaviors mimicking lithium action: negative results. *Behav Pharmacol* 19(3):217-224.
- Bhat RV, Budd Haeberlein SL, Avila J.** (2004): Glycogen synthase kinase 3: a drug target for CNS therapies. *J Neurochem* 89(6):1313-1317.
- Braune S, Lücking CH.** (1997): Orthostatische Hypotonie: Pathophysiologie, Differentialdiagnose und Therapie. *Dtsch Arztebl* 94(50):A-3413-3418.
- Brummelkamp TR, Bernards R, Agami R.** (2002): A system for stable expression of short interfering RNAs in mammalian cells. *Science* 296(5567):550-553.
- Chari DM.** (2007): Remyelination in multiple sclerosis. *Int Rev Neurobiol* 79:589-620.
- Chen G, Rajkowska G, Du F, Seraji-Bozorgzad N, Manji HK.** (2000): Enhancement of hippocampal neurogenesis by lithium. *J Neurochem* 75(4):1729-1734.
- Cohen P, Frame S.** (2001): The renaissance of GSK3. *Nat Rev Mol Cell Biol* 2(10):769-776.

- Colello RJ, Pott U.** (1997): Signals that initiate myelination in the developing mammalian nervous system. *Mol Neurobiol* 15(1):83-100.
- Coumoul X, Shukla V, Li C, Wang RH, Deng CX.** (2005): Conditional knockdown of *Fgfr2* in mice using Cre-LoxP induced RNA interference. *Nucleic Acids Res* 33(11):e102.
- Dajani R, Fraser E, Roe SM, Young N, Good V, Dale TC, Pearl LH.** (2001): Crystal structure of glycogen synthase kinase 3 beta: structural basis for phosphate-primed substrate specificity and autoinhibition. *Cell* 105(6):721-732.
- Deschepper CF, Olson JL, Otis M, Gallo-Payet N.** (2004): Characterization of blood pressure and morphological traits in cardiovascular-related organs in 13 different inbred mouse strains. *J Appl Physiol* 97(1):369-376.
- Doble BW, Patel S, Wood GA, Kockeritz LK, Woodgett JR.** (2007): Functional redundancy of GSK-3alpha and GSK-3beta in Wnt/beta-catenin signaling shown by using an allelic series of embryonic stem cell lines. *Dev Cell* 12(6):957-971.
- Doble BW, Woodgett JR.** (2003): GSK-3: tricks of the trade for a multi-tasking kinase. *J Cell Sci* 116(Pt 7):1175-1186.
- Doevendans PA, Daemen MJ, de Muinck ED, Smits JF.** (1998): Cardiovascular phenotyping in mice. *Cardiovasc Res* 39(1):34-49.
- Dykxhoorn DM, Novina CD, Sharp PA.** (2003): Killing the messenger: short RNAs that silence gene expression. *Nat Rev Mol Cell Biol* 4(6):457-467.
- Ehmke H.** (2003): Mouse gene targeting in cardiovascular physiology. *Am J Physiol Regul Integr Comp Physiol* 284(1):R28-30.
- Eldar-Finkelman H, Krebs EG.** (1997): Phosphorylation of insulin receptor substrate 1 by glycogen synthase kinase 3 impairs insulin action. *Proc Natl Acad Sci U S A* 94(18):9660-9664.
- Eldar-Finkelman H, Schreyer SA, Shinohara MM, LeBoeuf RC, Krebs EG.** (1999): Increased glycogen synthase kinase-3 activity in diabetes- and obesity-prone C57BL/6J mice. *Diabetes* 48(8):1662-1666.
- Elkis H, Friedman L, Wise A, Meltzer HY.** (1995): Meta-analyses of studies of ventricular enlargement and cortical sulcal prominence in mood disorders. Comparisons with controls or patients with schizophrenia. *Arch Gen Psychiatry* 52(9):735-746.
- Fire A, Xu S, Montgomery MK, Kostas SA, Driver SE, Mello CC.** (1998): Potent and specific genetic interference by double-stranded RNA in *Caenorhabditis elegans*. *Nature* 391(6669):806-811.

- Foran DR, Peterson AC.** (1992): Myelin acquisition in the central nervous system of the mouse revealed by an MBP-Lac Z transgene. *J Neurosci* 12(12):4890-4897.
- Forde JE, Dale TC.** (2007): Glycogen synthase kinase 3: a key regulator of cellular fate. *Cell Mol Life Sci* 64(15):1930-1944.
- Forni PE, Scuoppo C, Imayoshi I, Taulli R, Dastru W, Sala V, Betz UA, Muzzi P, Martinuzzi D, Vercelli AE, Kageyama R, Ponzetto C.** (2006): High levels of Cre expression in neuronal progenitors cause defects in brain development leading to microencephaly and hydrocephaly. *J Neurosci* 26(37):9593-9602.
- Frame S, Cohen P.** (2001): GSK3 takes centre stage more than 20 years after its discovery. *Biochem J* 359(Pt 1):1-16.
- Garrido JJ, Simon D, Varea O, Wandosell F.** (2007): GSK3 alpha and GSK3 beta are necessary for axon formation. *FEBS Lett* 581(8):1579-1586.
- Gartner A, Huang X, Hall A.** (2006): Neuronal polarity is regulated by glycogen synthase kinase-3 (GSK-3beta) independently of Akt/PKB serine phosphorylation. *J Cell Sci* 119(Pt 19):3927-3934.
- Gaveriaux-Ruff C, Kieffer BL.** (2007): Conditional gene targeting in the mouse nervous system: Insights into brain function and diseases. *Pharmacol Ther* 113(3):619-634.
- George SH, Gertsenstein M, Vintersten K, Korets-Smith E, Murphy J, Stevens ME, Haigh JJ, Nagy A.** (2007): Developmental and adult phenotyping directly from mutant embryonic stem cells. *Proc Natl Acad Sci U S A* 104(11):4455-4460.
- Gomez-Sintes R, Hernandez F, Bortolozzi A, Artigas F, Avila J, Zaratini P, Gotteland JP, Lucas JJ.** (2007): Neuronal apoptosis and reversible motor deficit in dominant-negative GSK-3 conditional transgenic mice. *EMBO J* 26(11):2743-2754.
- Gould TD, Einat H, Bhat R, Manji HK.** (2004): AR-A014418, a selective GSK-3 inhibitor, produces antidepressant-like effects in the forced swim test. *Int J Neuropsychopharmacol* 7(4):387-390.
- Gould TD, Einat H, O'Donnell KC, Picchini AM, Schloesser RJ, Manji HK.** (2007): Beta-catenin overexpression in the mouse brain phenocopies lithium-sensitive behaviors. *Neuropsychopharmacology* 32(10):2173-2183.
- Grimes CA, Jope RS.** (2001): The multifaceted roles of glycogen synthase kinase 3beta in cellular signaling. *Prog Neurobiol* 65(4):391-426.
- Hitz C, Wurst W, Kühn R.** (2007): Conditional brain-specific knockdown of MAPK using Cre/loxP regulated RNA interference. *Nucleic Acids Res* 35(12):e90.

- Hoeflich KP, Luo J, Rubie EA, Tsao MS, Jin O, Woodgett JR.** (2000): Requirement for glycogen synthase kinase-3 β in cell survival and NF- κ B activation. *Nature* 406(6791):86-90.
- Ishiguro K, Takamatsu M, Tomizawa K, Omori A, Takahashi M, Arioka M, Uchida T, Imahori K.** (1992): Tau protein kinase I converts normal tau protein into A68-like component of paired helical filaments. *J Biol Chem* 267(15):10897-10901.
- Jazag A, Kanai F, Ijichi H, Tateishi K, Ikenoue T, Tanaka Y, Ohta M, Imamura J, Guleng B, Asaoka Y, Kawabe T, Miyagishi M, Taira K, Omata M.** (2005): Single small-interfering RNA expression vector for silencing multiple transforming growth factor- β pathway components. *Nucleic Acids Res* 33(15):e131.
- Jiang H, Guo W, Liang X, Rao Y.** (2005): Both the establishment and the maintenance of neuronal polarity require active mechanisms: critical roles of GSK-3 β and its upstream regulators. *Cell* 120(1):123-135.
- Jope RS.** (2003): Lithium and GSK-3: one inhibitor, two inhibitory actions, multiple outcomes. *Trends Pharmacol Sci* 24(9):441-443.
- Jope RS, Roh MS.** (2006): Glycogen synthase kinase-3 (GSK3) in psychiatric diseases and therapeutic interventions. *Curr Drug Targets* 7(11):1421-1434.
- Kaladchibachi SA, Doble B, Anthopoulos N, Woodgett JR, Manoukian AS.** (2007): Glycogen synthase kinase 3, circadian rhythms, and bipolar disorder: a molecular link in the therapeutic action of lithium. *J Circadian Rhythms* 5:3.
- Ketting R, Plasterk, R.** (2005): RNAi and its applications. *Nature Reviews Genetics* 6(12):poster.
- Kim JS, Chang MY, Yu IT, Kim JH, Lee SH, Lee YS, Son H.** (2004): Lithium selectively increases neuronal differentiation of hippocampal neural progenitor cells both in vitro and in vivo. *J Neurochem* 89(2):324-336.
- Kim WY, Zhou FQ, Zhou J, Yokota Y, Wang YM, Yoshimura T, Kaibuchi K, Woodgett JR, Anton ES, Snider WD.** (2006): Essential roles for GSK-3s and GSK-3-primed substrates in neurotrophin-induced and hippocampal axon growth. *Neuron* 52(6):981-996.
- Koivisto L, Jiang G, Hakkinen L, Chan B, Larjava H.** (2006): HaCaT keratinocyte migration is dependent on epidermal growth factor receptor signaling and glycogen synthase kinase-3 α . *Exp Cell Res* 312(15):2791-2805.
- Krege JH, Hodgins JB, Hagaman JR, Smithies O.** (1995): A noninvasive computerized tail-cuff system for measuring blood pressure in mice. *Hypertension* 25(5):1111-1115.

- Kunath T, Gish G, Lickert H, Jones N, Pawson T, Rossant J.** (2003): Transgenic RNA interference in ES cell-derived embryos recapitulates a genetic null phenotype. *Nat Biotechnol* 21(5):559-561.
- Laemmli UK.** (1970): Cleavage of structural proteins during the assembly of the head of bacteriophage T4. *Nature* 227(5259):680-685.
- Lee G, Saito I.** (1998): Role of nucleotide sequences of loxP spacer region in Cre-mediated recombination. *Gene* 216(1):55-65.
- Leroy K, Brion JP.** (1999): Developmental expression and localization of glycogen synthase kinase-3beta in rat brain. *J Chem Neuroanat* 16(4):279-293.
- Levine JM, Reynolds R, Fawcett JW.** (2001): The oligodendrocyte precursor cell in health and disease. *Trends Neurosci* 24(1):39-47.
- Liu KJ, Arron JR, Stankunas K, Crabtree GR, Longaker MT.** (2007): Chemical rescue of cleft palate and midline defects in conditional GSK-3beta mice. *Nature* 446(7131):79-82.
- Lorenz JN.** (2002): A practical guide to evaluating cardiovascular, renal, and pulmonary function in mice. *Am J Physiol Regul Integr Comp Physiol* 282(6):R1565-1582.
- Lovestone S, Killick R, Di Forti M, Murray R.** (2007): Schizophrenia as a GSK-3 dysregulation disorder. *Trends Neurosci* 30(4):142-149.
- Lucas FR, Goold RG, Gordon-Weeks PR, Salinas PC.** (1998): Inhibition of GSK-3beta leading to the loss of phosphorylated MAP-1B is an early event in axonal remodelling induced by WNT-7a or lithium. *J Cell Sci* 111 (Pt 10):1351-1361.
- MacAulay K, Doble BW, Patel S, Hansotia T, Sinclair EM, Drucker DJ, Nagy A, Woodgett JR.** (2007): Glycogen synthase kinase 3alpha-specific regulation of murine hepatic glycogen metabolism. *Cell Metab* 6(4):329-337.
- Martin M, Rehani K, Jope RS, Michalek SM.** (2005): Toll-like receptor-mediated cytokine production is differentially regulated by glycogen synthase kinase 3. *Nat Immunol* 6(8):777-784.
- Maurer MH, Bromme JO, Feldmann RE, Jr., Jarve A, Sabouri F, Burgers HF, Schelshorn DW, Kruger C, Schneider A, Kuschinsky W.** (2007): Glycogen synthase kinase 3beta (GSK3beta) regulates differentiation and proliferation in neural stem cells from the rat subventricular zone. *J Proteome Res* 6(3):1198-1208.
- Meister G, Tuschl T.** (2004): Mechanisms of gene silencing by double-stranded RNA. *Nature* 431(7006):343-349.
- Mello CC, Conte D, Jr.** (2004): Revealing the world of RNA interference. *Nature* 431(7006):338-342.

- Metzlaff M, O'Dell M, Cluster PD, Flavell RB.** (1997): RNA-mediated RNA degradation and chalcone synthase A silencing in petunia. *Cell* 88(6):845-854.
- Miki K.** (2007): Energy metabolism and sperm function. *Soc Reprod Fertil Suppl* 65:309-325.
- Miller RH.** (2002): Regulation of oligodendrocyte development in the vertebrate CNS. *Prog Neurobiol* 67(6):451-467.
- Minichiello L, Korte M, Wolfer D, Kuhn R, Unsicker K, Cestari V, Rossi-Arnaud C, Lipp HP, Bonhoeffer T, Klein R.** (1999): Essential role for TrkB receptors in hippocampus-mediated learning. *Neuron* 24(2):401-414.
- Mita M, Hall PF.** (1982): Metabolism of round spermatids from rats: lactate as the preferred substrate. *Biol Reprod* 26(3):445-455.
- Mittal V.** (2004): Improving the efficiency of RNA interference in mammals. *Nat Rev Genet* 5(5):355-365.
- Mukai F, Ishiguro K, Sano Y, Fujita SC.** (2002): Alternative splicing isoform of tau protein kinase I/glycogen synthase kinase 3beta. *J Neurochem* 81(5):1073-1083.
- Muyllaert D, Kremer A, Jaworski T, Borghgraef P, Devijver H, Croes S, Dewachter I, Van Leuven F.** (2008): Glycogen synthase kinase-3beta, or a link between amyloid and tau pathology? *Genes Brain Behav* 7 Suppl 1:57-66.
- Nagy A, Rossant J, Nagy R, Abramow-Newerly W, Roder JC.** (1993): Derivation of completely cell culture-derived mice from early-passage embryonic stem cells. *Proc Natl Acad Sci U S A* 90(18):8424-8428.
- Naska S, Park KJ, Hannigan GE, Dedhar S, Miller FD, Kaplan DR.** (2006): An essential role for the integrin-linked kinase-glycogen synthase kinase-3 beta pathway during dendrite initiation and growth. *J Neurosci* 26(51):13344-13356.
- O'Brien WT, Harper AD, Jove F, Woodgett JR, Maretto S, Piccolo S, Klein PS.** (2004): Glycogen synthase kinase-3beta haploinsufficiency mimics the behavioral and molecular effects of lithium. *J Neurosci* 24(30):6791-6798.
- Ohl F, Sillaber I, Binder E, Keck ME, Holsboer F.** (2001): Differential analysis of behavior and diazepam-induced alterations in C57BL/6N and BALB/c mice using the modified hole board test. *J Psychiatr Res* 35(3):147-154.
- Ohteki T, Parsons M, Zakarian A, Jones RG, Nguyen LT, Woodgett JR, Ohashi PS.** (2000): Negative regulation of T cell proliferation and interleukin 2 production by the serine threonine kinase GSK-3. *J Exp Med* 192(1):99-104.
- Paddison PJ, Cleary M, Silva JM, Chang K, Sheth N, Sachidanandam R, Hannon GJ.** (2004): Cloning of short hairpin RNAs for gene knockdown in mammalian cells. *Nat Methods* 1(2):163-167.

- Patel S, Doble B, Woodgett JR.** (2004): Glycogen synthase kinase-3 in insulin and Wnt signalling: a double-edged sword? *Biochem Soc Trans* 32(Pt 5):803-808.
- Phiel CJ, Wilson CA, Lee VM, Klein PS.** (2003): GSK-3alpha regulates production of Alzheimer's disease amyloid-beta peptides. *Nature* 423(6938):435-439.
- Prickaerts J, Moechars D, Cryns K, Lenaerts I, van Craenendonck H, Goris I, Daneels G, Bouwknecht JA, Steckler T.** (2006): Transgenic mice overexpressing glycogen synthase kinase 3beta: a putative model of hyperactivity and mania. *J Neurosci* 26(35):9022-9029.
- Reynolds A, Leake D, Boese Q, Scaringe S, Marshall WS, Khvorova A.** (2004): Rational siRNA design for RNA interference. *Nat Biotechnol* 22(3):326-330.
- Rosenberg SS, Powell BL, Chan JR.** (2007): Receiving mixed signals: uncoupling oligodendrocyte differentiation and myelination. *Cell Mol Life Sci* 64(23):3059-3068.
- Royer A, van Veen TA, Le Bouter S, Marionneau C, Griol-Charhbil V, Leoni AL, Steenman M, van Rijen HV, Demolombe S, Goddard CA, Richer C, Escoubet B, Jarry-Guichard T, Colledge WH, Gros D, de Bakker JM, Grace AA, Escande D, Charpentier F.** (2005): Mouse model of SCN5A-linked hereditary Lenegre's disease: age-related conduction slowing and myocardial fibrosis. *Circulation* 111(14):1738-1746.
- Samlowski WE, Petersen R, McGregor JM, Kondapaneni M, Salvemini D.** (2000-2005): Evaluation of a Superoxide Dismutase Mimetic as an Adjunct to Interleukin 2 Based Cancer Therapy. *Landes Bioscience (Eurekah) Ischemia-Reperfusion*.
- Schmidt-Supprian M, Rajewsky K.** (2007): Vagaries of conditional gene targeting. *Nat Immunol* 8(7):665-668.
- Schmidt EE, Taylor DS, Prigge JR, Barnett S, Capecchi MR.** (2000): Illegitimate Cre-dependent chromosome rearrangements in transgenic mouse spermatids. *Proc Natl Acad Sci U S A* 97(25):13702-13707.
- Schnutgen F, Doerflinger N, Calleja C, Wendling O, Chambon P, Ghyselinck NB.** (2003): A directional strategy for monitoring Cre-mediated recombination at the cellular level in the mouse. *Nat Biotechnol* 21(5):562-565.
- Seibler J, Kuter-Luks B, Kern H, Streu S, Plum L, Mauer J, Kuhn R, Bruning JC, Schwenk F.** (2005): Single copy shRNA configuration for ubiquitous gene knockdown in mice. *Nucleic Acids Res* 33(7):e67.
- Seibler J, Schubeler D, Fiering S, Groudine M, Bode J.** (1998): DNA cassette exchange in ES cells mediated by Flp recombinase: an efficient strategy for repeated modification of tagged loci by marker-free constructs. *Biochemistry* 37(18):6229-6234.

- Seong E, Seasholtz AF, Burmeister M.** (2002): Mouse models for psychiatric disorders. *Trends Genet* 18(12):643-650.
- Shakoori A, Mai W, Miyashita K, Yasumoto K, Takahashi Y, Ooi A, Kawakami K, Minamoto T.** (2007): Inhibition of GSK-3 beta activity attenuates proliferation of human colon cancer cells in rodents. *Cancer Sci* 98(9):1388-1393.
- Siegel RW, Jain R, Bradbury A.** (2001): Using an in vivo phagemid system to identify non-compatible loxP sequences. *FEBS Lett* 499(1-2):147-153.
- Silva R, Mesquita AR, Bessa J, Sousa JC, Sotiropoulos I, Leao P, Almeida OF, Sousa N.** (2008): Lithium blocks stress-induced changes in depressive-like behavior and hippocampal cell fate: the role of glycogen-synthase-kinase-3beta. *Neuroscience* 152(3):656-669.
- Siolas D, Lerner C, Burchard J, Ge W, Linsley PS, Paddison PJ, Hannon GJ, Cleary MA.** (2005): Synthetic shRNAs as potent RNAi triggers. *Nat Biotechnol* 23(2):227-231.
- Smith AG, Heath JK, Donaldson DD, Wong GG, Moreau J, Stahl M, Rogers D.** (1988): Inhibition of pluripotential embryonic stem cell differentiation by purified polypeptides. *Nature* 336(6200):688-690.
- Soriano P.** (1999): Generalized lacZ expression with the ROSA26 Cre reporter strain. *Nat Genet* 21(1):70-71.
- Stanford WL, Cohn JB, Cordes SP.** (2001): Gene-trap mutagenesis: past, present and beyond. *Nat Rev Genet* 2(10):756-768.
- Stankunas K, Bayle JH, Gestwicki JE, Lin YM, Wandless TJ, Crabtree GR.** (2003): Conditional protein alleles using knockin mice and a chemical inducer of dimerization. *Mol Cell* 12(6):1615-1624.
- Sternberg N, Sauer B, Hoess R, Abremski K.** (1986): Bacteriophage P1 cre gene and its regulatory region. Evidence for multiple promoters and for regulation by DNA methylation. *J Mol Biol* 187(2):197-212.
- Steuber-Buchberger P, Wurst W, Kühn R.** (2008): Simultaneous Cre-mediated conditional knockdown of two genes in mice. *Genesis* 46(3):144-151.
- Takahashi M, Tomizawa K, Ishiguro K.** (2000): Distribution of tau protein kinase I/glycogen synthase kinase-3beta, phosphatases 2A and 2B, and phosphorylated tau in the developing rat brain. *Brain Res* 857(1-2):193-206.
- Takahashi M, Tomizawa K, Kato R, Sato K, Uchida T, Fujita SC, Imahori K.** (1994): Localization and developmental changes of tau protein kinase I/glycogen synthase kinase-3 beta in rat brain. *J Neurochem* 63(1):245-255.
- Tronche F, Kellendonk C, Kretz O, Gass P, Anlag K, Orban PC, Bock R, Klein R, Schutz G.** (1999): Disruption of the glucocorticoid receptor gene in the nervous system results in reduced anxiety. *Nat Genet* 23(1):99-103.

- Turksen K.** (2001): Embryonic Stem Cells: Methods and Protocols. *Humana Press* 185:350.
- van der Neut R.** (1997): Targeted gene disruption: applications in neurobiology. *J Neurosci Methods* 71(1):19-27.
- Vermeulen A, Behlen L, Reynolds A, Wolfson A, Marshall WS, Karpilow J, Khvorova A.** (2005): The contributions of dsRNA structure to Dicer specificity and efficiency. *Rna* 11(5):674-682.
- Vijayaraghavan S, Mohan J, Gray H, Khatra B, Carr DW.** (2000): A role for phosphorylation of glycogen synthase kinase-3alpha in bovine sperm motility regulation. *Biol Reprod* 62(6):1647-1654.
- Wiggin GR, Fawcett JP, Pawson T.** (2005): Polarity proteins in axon specification and synaptogenesis. *Dev Cell* 8(6):803-816.
- Williams RL, Hilton DJ, Pease S, Willson TA, Stewart CL, Gearing DP, Wagner EF, Metcalf D, Nicola NA, Gough NM.** (1988): Myeloid leukaemia inhibitory factor maintains the developmental potential of embryonic stem cells. *Nature* 336(6200):684-687.
- Woodgett JR.** (2001): Judging a protein by more than its name: GSK-3. *Sci STKE* 2001(100):RE12.
- Woodgett JR, Ohashi PS.** (2005): GSK3: an in-Toll-erant protein kinase? *Nat Immunol* 6(8):751-752.
- Xin M, Yue T, Ma Z, Wu FF, Gow A, Lu QR.** (2005): Myelinogenesis and axonal recognition by oligodendrocytes in brain are uncoupled in Olig1-null mice. *J Neurosci* 25(6):1354-1365.
- Yanagita T, Maruta T, Uezono Y, Satoh S, Yoshikawa N, Nemoto T, Kobayashi H, Wada A.** (2007): Lithium inhibits function of voltage-dependent sodium channels and catecholamine secretion independent of glycogen synthase kinase-3 in adrenal chromaffin cells. *Neuropharmacology* 53(7):881-889.
- Yao HB, Shaw PC, Wong CC, Wan DC.** (2002): Expression of glycogen synthase kinase-3 isoforms in mouse tissues and their transcription in the brain. *J Chem Neuroanat* 23(4):291-297.
- Yoshimura T, Kawano Y, Arimura N, Kawabata S, Kikuchi A, Kaibuchi K.** (2005): GSK-3beta regulates phosphorylation of CRMP-2 and neuronal polarity. *Cell* 120(1):137-149.
- Yu J, McMahon AP.** (2006): Reproducible and inducible knockdown of gene expression in mice. *Genesis* 44(5):252-261.

- Yu JS, Yang SD.** (1994): Protein kinase FA/glycogen synthase kinase-3 predominantly phosphorylates the in vivo site Thr97-Pro in brain myelin basic protein: evidence for Thr-Pro and Ser-Arg-X-X-Ser as consensus sequence motifs. *J Neurochem* 62(4):1596-1603.
- Yu JY, Taylor J, DeRuiter SL, Vojtek AB, Turner DL.** (2003): Simultaneous inhibition of GSK3alpha and GSK3beta using hairpin siRNA expression vectors. *Mol Ther* 7(2):228-236.
- Yuan B, Latek R, Hossbach M, Tuschl T, Lewitter F.** (2004): siRNA Selection Server: an automated siRNA oligonucleotide prediction server. *Nucleic Acids Res* 32(Web Server issue):W130-134.
- Zhang F, Phiel CJ, Spece L, Gurvich N, Klein PS.** (2003): Inhibitory phosphorylation of glycogen synthase kinase-3 (GSK-3) in response to lithium. Evidence for autoregulation of GSK-3. *J Biol Chem* 278(35):33067-33077.
- Zimmerman L, Parr B, Lendahl U, Cunningham M, McKay R, Gavin B, Mann J, Vassileva G, McMahon A.** (1994): Independent regulatory elements in the nestin gene direct transgene expression to neural stem cells or muscle precursors. *Neuron* 12(1):11-24.

8 APPENDIX

8.1 Abbreviations

A	purine base adenine
Ac	acetate
AD	Alzheimer's disease
Ago	argonaute
APC	adenomatous polyposis coli
ATP	adenosine triphosphate
attB	attachment site in the donor vector (RMCE)
attP	attachment site in the acceptor sequence (RMCE)
BCA	bicinchoninic acid
bp	basepair
BPD	bipolar disorder
BSA	bovine serum albumin
°C	degree Celsius
c	centi (10^{-2})
C	pyrimidine base cytosine
<i>C. elegans</i>	<i>Caenorhabditis elegans</i>
C31Int	integrase from phage Φ C31
CaCl ₂	calcium chloride
CDK2	cyclin-dependent kinase 2
cDNA	copyDNA
Ci	Curie; 1 Ci = 3.7 x 10 ¹⁰ Bq
CNS	central nervous system
CO ₂	carbon dioxide
cpm	counts per minute
CREB	cAMP response element-binding
CRMP-2	collapsin response mediator protein-2
CTP	cytosine triphosphate
Da	Dalton
DAB	3,3'-diaminobenzidine
DEPC	diethylpyrocarbonate
DH5 α	E.coli strain
DIG	Digoxigenin
DMSO	dimethylsulfoxide
DNA	desoxyribonucleic acid
dNTP	desoxyribonucleotide triphosphate
dsRNA	double stranded RNA
DTT	1,4-dithiothreitol

DVL	Dishevelled
E	embryonic day
<i>E.coli</i>	<i>Escherichia coli</i>
e.g.	exempli gratia, for example
EDTA	ethylenediaminetetraacetate
EGTA	ethyleneglycol-bis-(b-aminoethylether)-N,N,N',N'-tetraacetate
ES cells	embryonic stem cells
EtOH	ethanol
F	Farad
FCS	fetal calf serum
FGF	fibroblast growth factor
Fig.	figure
FRAT	frequently rearranged in advanced T-cell lymphomas
g	acceleration of gravity (9.81 m/s ²)
g	gramme
G	purinbase guanine
G418	geneticin
GMC	German Mouse Clinic
GSK-3	glycogen synthase kinase 3
GSP1	gene-specific antisense oligonucleotide primer
GSP2	nested gene specific primer
h	hour(s)
hc	humid chamber
hCG	human chorion gonadotropin
HCl	hydrochloric acid
HPRT	hypoxanthine phosphoribosyltransferase
i.p.	intraperitoneally
IHC	immunohistochemistry
IL-2, IL-10	interleukin -2; -10
IRS-1	Insulin receptor substrate-1
ISH	in situ hybridization
ITI	intertrial interval
IVC	individually ventilated cages
kb	kilobasepairs
kD	kilodalton
Klenow	Large fragment of <i>E.coli</i> DNA polymerase I
knockdown	organism, in which a gene is silenced by RNAi
knockout	organism, in which one gene is completely switched off
l	liter
LacZ	β-Galactosidase
LB	Luria Broth
Li	lithium

LIF	leukemia inhibiting factor
LPS	lipopolysaccharide
Luc	firefly-luciferase
m	milli (10^{-3})
M	molar (mol/l)
MAG	myelin associated glycoprotein
MgCl ₂	magnesium chloride
mHB	modified Holeboard
min	minute(s)
miRNA	micro RNA
mRNA	messenger ribonucleic acid
MS	multiple sclerosis
mut	mutant
MBP	myelin basic protein
n	nano (10^{-9})
n	sample size
NaCl	sodium chloride
NaOAc	sodium acetate
neo	neomycin
NH ₄ OAc	ammonium acetate
nm	nanometer
no.	number
NP-40	Nonidet P-40
nt	nucleotides
OD	optical density
ORF	open reading frame
p	pico (10^{-12})
p	p-value for statistical analysis
P	postnatal day
P body	processing body
PAZ	piwi-argonaute-zwille
PBS	phosphate buffered saline
PCR	polymerase chain reaction
PDGF- α R	platelet-derived growth factor receptor alpha
PFA	paraformaldehyde
PI3K	phosphoinositide 3-kinases
PKB	protein kinase B
PMSG	pregnant mare's serum gonadotropin
PNK	polynucleotide kinase
PNS	peripheral nervous system
RIPA	protein lysis buffer
RISC	RNA-inducing silencing complex

RMCE	recombinase mediated cassette exchange
RNA	ribonucleic acid
RNAi	RNA interference
rpm	rounds per minute
RT	room temperature
RT-PCR	reverse transcription PCR
SAP	shrimp alkaline phosphatase
SDS	sodium dodecyl sulfate
sec or s	second(s)
SEM	standard error of the mean
Ser (S)	Serine
shRNA	short hairpin RNA
siRNA	small interfering RNA
SSC	sodium saline citrate
T	pyrimidine base thymine
Tab.	table
TAE	tris acetate with EDTA
TBE	tris borate with EDTA
TBS	tris buffered saline
TBS(T)	tris buffered saline (with Tween)
TE	tris-EDTA
temp.	temperature
TLRs	Toll-like receptors
TNF- α	tumor necrosis factor α
Tris	trishydroxymethyl-aminoethane
tRNA	transfer ribonucleic acid
U	unit(s)
UTP	uracil triphosphate
UTR	untranscribed region of a gene
UV	ultraviolet
V	volt
Vol.	volume or volumetric content
wt	wild type
x	Symbol for crosses between mouse lines
μ	micro (10 ⁻⁶)

8.2 Index of figures and tables

Figures

Fig. 1:	Scheme of mammalian GSK-3 α and GSK-3 β	3
Fig. 2:	Regulation of GSK-3 by phosphorylation of the regulatory serine residue.....	4
Fig. 3:	Regulation of GSK-3 in the canonical Wnt signaling pathway.....	5
Fig. 4:	Influence of inhibitors on GSK-3 activity.....	6
Fig. 5:	Substrates of mammalian GSK-3.....	9
Fig. 6:	The RNAi pathway in the cell.....	13
Fig. 7:	Expression of <i>Gsk-3</i> mRNA in the embryo.....	68
Fig. 8:	Expression of <i>Gsk-3β</i> mRNA in the adult mouse brain (coronal view).....	69
Fig. 9:	Expression of <i>Gsk-3</i> mRNA in the adult mouse brain (sagittal view).....	70
Fig. 10:	Trapping of a gene with a conventional gene trap vector.....	71
Fig. 11:	Integration of the gene trap vector in the RRK111 ES cell clone.....	72
Fig. 12:	Analysis of <i>Gsk-3α</i> gene trap mice.....	73
Fig. 13:	Location of shRNA target sequences in the corresponding <i>Gsk-3</i> cDNA.....	75
Fig. 14:	Real-time qRT-PCR for <i>Gsk-3</i> shRNAs upon transfection into ES cells.....	79
Fig. 15:	Cloning of the pScreeniT™ <i>Gsk-3α</i> cDNA vector.....	80
Fig. 16:	ShRNA efficiency for <i>Gsk-3α</i> in the pScreeniT™ system.....	81
Fig. 17:	ShRNA efficiency for <i>Gsk-3β</i> in the pScreeniT™ system.....	83
Fig. 18:	Knockdown of GSK-3 proteins in the Western blot of shRNA transfected ES cells.....	84
Fig. 19:	Principle of double-conditional shRNA constructs.....	86
Fig. 20:	Stable integration of shRNAs into ES cells via RMCE.....	88
Fig. 21:	Analysis of neomycin resistant ES cell clones by PCR and Southern blot.....	89
Fig. 22:	Analysis of ES cell clones carrying the non-conditional <i>Gsk-3β-sh2</i>	92
Fig. 23:	Cre recombinase expression pattern in the <i>Nestin-cre</i> mouse line.....	93
Fig. 24:	Cre recombinase expression pattern in the <i>CamKII-cre</i> strain.....	95
Fig. 25:	Activation of the shRNAs by Cre recombinase.....	96
Fig. 26:	ShRNA expression and recombination efficiency in brain of <i>Gsk-3/Nestin-cre</i> mice.....	98
Fig. 27:	Analysis of Cre recombination in <i>Gsk-3β-flox-sh2^{Nes}</i> male and female mice.....	100
Fig. 28:	Quantification of <i>Gsk-3</i> mRNA knockdown.....	101
Fig. 29:	Reduction of <i>Gsk-3</i> mRNA in brain sections of adult knockdown mice.....	102
Fig. 30:	Reduction of GSK-3 protein in the brain of knockdown mice.....	103
Fig. 31:	Appearance of adult <i>Gsk-3β-flox-sh2^{Nes}</i> female mice.....	104
Fig. 32:	Body weight of <i>Gsk-3α-flox</i> and <i>Gsk-3β-flox-sh2</i> mice.....	105
Fig. 33:	Numbers of obtained mutants in the <i>Gsk-3-flox-dh2^{Nes}</i> strain.....	107
Fig. 34:	Analysis of ventricle size in <i>Gsk-3α-flox^{Nes}</i> mice.....	109
Fig. 35:	Nissl staining of sagittal brain sections of adult <i>Gsk-3-flox-dh2^{Nes}</i> mice.....	109
Fig. 36:	Immunohistochemical staining for caspase-3 in adult brain slices.....	110
Fig. 37:	Modified Hole Board behavior results of <i>Gsk-3/Nestin-cre</i> mice.....	112
Fig. 38:	Modified Hole Board behavior results of <i>Gsk-3/CamKII-cre</i> mice.....	114
Fig. 39:	Light-dark box behavior results of <i>Gsk-3β-flox-sh2^{CamKII}</i> mice.....	115
Fig. 40:	Behavior results of <i>Gsk-3-flox-dh2^{CamKII}</i> mice in the accelerating rotarod.....	116
Fig. 41:	Forced swim test behavior results of <i>Gsk-3/CamKII-cre</i> mice.....	117
Fig. 42:	Systolic pressure and pulse rate of <i>Gsk-3β-flox-sh2^{Nes}</i> and <i>Gsk-3α-flox^{Nes}</i> mice.....	119
Fig. 43:	Influence of GSK-inhibitor on blood pressure parameters.....	120
Fig. 44:	HE staining of coronal brain sections of adult <i>Gsk-3β-flox-sh2^{Nes}</i> mice.....	121
Fig. 45:	Luxol fast blue staining of <i>Gsk-3β-flox-sh2^{Nes}</i> and <i>Gsk-3α-flox^{Nes}</i> mice brain sections..	122

Fig. 46:	Loss of myelin in the corpus callosum of <i>Gsk-3β-flox-sh2^{Nes}</i> and <i>Gsk-3α-flox^{Nes}</i> mice..	124
Fig. 47:	The myelination process in the CNS.	142

Tables

Tab. 1:	ShRNAs against <i>Gsk-3α</i> and <i>Gsk-3β</i>	76
Tab. 2:	ES cell clones used for injection and tetraploid aggregation.....	91
Tab. 3:	Mouse lines generated by breeding with <i>Nestin-cre</i> and <i>CamKII-cre</i> mice.....	97
Tab. 4:	Neuronal markers used for DIG labeled ISH.....	108
Tab. 5:	Mouse lines analyzed with luxol fast blue staining..	123
Tab. 6:	Comparison of knockdown levels <i>in vitro</i> and <i>in vivo</i>	128
Tab. 7:	Summary of behavior results of mutant <i>Gsk-3</i> knockdown mice.....	147

8.3 Measured parameters in the behavior tests

8.3.1 Modified Hole Board test

Behavior	Parameters
forward locomotion	distance moved, line crossings (latency, frequency)
speed of movement	velocity (mean, maximum, angular)
exploration	vertical: rearings (box, board; latency, frequency) horizontal: holes (latency, frequency), objects (novel, familiar; latency, frequency, duration)
risk assessment	stretched attends (latency, frequency)
anxiety-related	board entries (latency, frequency, duration); distance to the wall
grooming	grooming (latency, frequency, duration)
defecation	boli (latency, frequency)
social affinity	exploration of the partition (latency, frequency, duration)
object memory	object recognition index

8.3.2 Light-dark box

Behavior	Parameters
forward locomotion	distance moved (total), turn angle (number, mean), meander
speed of movement	velocity (mean, maximum, angular)
exploration	rearings in compartments (latency, frequency)
grooming	grooming in compartments (frequency, duration)
anxiety-related	compartment entries (latency, frequency, duration)

8.3.3 Accelerating rotarod

Behavior	Parameters
forward locomotion	latency to fall from rod (per trials, mean), passive rotations
speed of movement	speed of rotating rod
general	body weight

8.3.4 Forced swim test

Behavior	Parameters
forward locomotion/ stress-related	swimming, floating (total duration, per min)
anxiety-related	struggling (total duration, per min)

Patricia Mareike Steuber-Buchberger

Diplom-Biologin Univ.

Ziegelhöbach 10
85298 Scheyern

Telefon privat (08441) 786760
Telefon mobil (0177) 874 5235
E-Mail p.steubuch@yahoo.de



PERSÖNLICHE DATEN

Geburtsdatum, -ort 11. April 1980 in Frechen (NRW)
Familienstand verheiratet, geb. Steuber
Staatsangehörigkeit deutsch

AUSBILDUNG

1986 – 1989 Grundschule Fürstenfeldbruck
1989 – 1990 Grundschule Scheyern
1990 – 1999 Schyregymnasium Pfaffenhofen a.d. Ilm
mathematisch – naturwissenschaftlicher Zweig
allgemeine Hochschulreife mit der Gesamtnote 2,2

STUDIUM

Studiengang Diplom-Biologie an der Technischen Universität München,

Außenstelle Wissenschaftszentrum Weihenstephan (WZW) in Freising

10/1999 Studienbeginn
09/2001 Vordiplomsprüfung
10/2003 Diplomprüfung in den Bereichen:
Technische Biologie Prüfungsnote 1,3
Botanik Prüfungsnote 1,0
Immunologie Prüfungsnote 1,0
12/2003 – 06/2004 Diplomarbeit am Lehrstuhl für Zellbiologie (Prof. Dr. B. Hock) zum
Thema: "Genexpressionsmuster-Analyse mit DNA-Microarrays zum
Nachweis von endokrinen Effekten beim Zebraärbling (Danio
rerio)", Note 1,0
15.07.2004 Abschluss des Studiums mit der Gesamtnote 1,1
– Prädikat „mit Auszeichnung bestanden“

11/2004 – jetzt Promotion am Helmholtz Zentrum München, Institut für Entwicklungsgenetik, zum Thema: „Genetische Analyse von Glykogen Synthase Kinase-3 im adulten Gehirn der Maus“

STUDIENBEGLEITENDE TÄTIGKEITEN

1996 – 1998 Siemens AG (München) als Ferienaushilfe

1999 – 2004 Infineon Technologies AG (München) als Werkstudentin im Mask House in der Abteilung Customer Support & Sales mit folgenden Aufgaben:

- Management Präsentationsdesign (deutsch / englisch)
- Teamassistentin mit Verwaltungs- und administrativen Tätigkeiten (Bestellung, Reisebuchung und Abrechnung)
- Dokumentenmanagement im Quality Management nach EN ISO 9001:2000 / ISO TS 16949:1999

07/2004 – 10/2004 MANPOWER GmbH Personaldienstleistungen (Aichach) als Abteilungsleiterin mit folgenden Aufgaben:

- Rekrutierung neuer Zeitmitarbeiter
- Betreuung und Disposition bestehender Zeitmitarbeiter
- Akquirierung neuer Kunden im Verkaufsgebiet und Mitbetreuung bestehender Kunden
- Erfüllung von Kundenaufträgen
- Verwaltung und Pflege der Akten und Datensätze der Zeitmitarbeiter und Kunden

ZUSATZQUALIFIKATIONEN

2005 Fortbildung „Schutz und Vermarktung von Forschungsergebnissen in der GSF“

2006 Fortbildung Rhetorik „Sicher auftreten – frei reden“

2006/2007 Fortbildung Betriebswirtschaft für Naturwissenschaftler
Baustein I: Einführung, Bilanz, Kosten- und Leistungsrechnung
Baustein III: Projektmanagement und Führung
von der RKW Bayern GmbH

2007 Fortbildung „Clear Writing for Science Publications“

AUSZEICHNUNGEN & VERÖFFENTLICHUNGEN

- 2005 Auszeichnung der Stadt Freising für die Diplomarbeit
- 2008 Steuber-Buchberger P., Wurst W., Kühn R.:
Simultaneous Cre-mediated conditional knockdown of two genes in mice. *Genesis* 46(3):144-151.

EDV-KENNTNISSE UND SPRACHEN

EDV

Sehr gute Kenntnisse: MS Windows, MS Office inklusive PowerPoint und MS Outlook

Gute Kenntnisse: Adobe Acrobat, Illustrator, Photoshop, EndNote, Vector NTI

Sprachen Deutsch (Muttersprache), Englisch (verhandlungssicher),
Französisch (Grundkenntnisse)

INTERESSEN UND AKTIVITÄTEN

Taekwon-Do nach Großmeister Kwon, Jae-Hwa

Haustiere und Garten

Computer

Lesen

Scheyern, den 04.06.2008

Patricia M. Steuber-Buchberger